1755

MARCH 1981 PPPL-1755

CONF-791225--

MASTER

PROCEEDINGS OF THE US-JAPAN JOINT SYMPOSIUM ON COMPACT TORUSES AND ENERGETIC PARTICLE INJECTION, PRINCETON, NEW JERSEY, 12/12-14/79

PLASMA PHYSICS LABORATORY

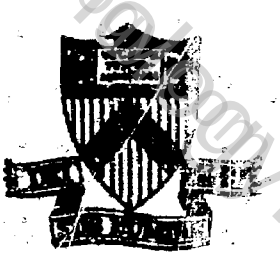

PRINCETON UNIVERSITY
PRINCETON, NEW JERSEY

This work was supported by the U.S. Department of Energy Contract No. DE-AC02-76-CHO 3073. Reproduction, translation, publication, use and disposal, in whole or in part, by or for the United States government is permitted.

PROCEEDINGS OF THE US-JAPAN JOINT SYMPOSIUM ON COMPACT TORUSES AND ENERGETIC PARTICLE INJECTION

HOSTED BY

PLASMA PHYSICS LABORATORY
PRINCETON UNIVERSITY
PRINCETON, NEW JERSEY 08544

ON

12-14 DECEMBER 1979

PREFACE

The sixty papers contained in these Proceedings serve to convey some idea of the highly original and diversified discussions that took place at the US-Japan Joint Symposium on Compact Toruses and Energetic Particle Injection.

Perhaps the most striking feature of the Symposium, however, was not its diversity, but its essential unity. Researchers from such seemingly disparate fields as tokamaks, mirrors, theta pinches, zed-pinches, and relativistic-beam injection found themselves confronting identical problems of physics and converging towards a similar reactor goal.

The participants were also pleased to experience a second form of convergence: the joining of the Japanese and United States fusion programs in a collaborative effort. This collaboration promises to be particularly fruitful in the area of compact toruses and energetic particle injection — where so much depends on the emergence of new ideas and new experimental techniques.

Harold P. Furth
21 January 1980

TABLE OF CONTENTS

INTRODUCTORY REMARKS

John F. Clarke, Deputy Director, Office of Fusion Energy, Department of Energy, Washington, D.C. 20545

I wish to add my welcome and that of the Department of Energy to Mel's. Exchange visits of the past have proven to be valuable to the participants from both countries, and it is gratifying that this is the first to be held under the newly inaugurated series with the Government of Japan.

It may not be coincidental that the topic for this conference is in the area of alternative concepts. The diversity of our national program is probably matched only by the Japanese program among the several national fusion programs worldwide. Further, the focus of the meeting, what we call compact toroids, is indicative of the readiness of the worldwide fusion community to deal with worthy, innovative ideas.

In the U.S. program we continuously evaluate alternate confinement approaches for development as fusion power systems. How do we arrive at a decision to launch development of an approach such as compact toroids and neglect others?

This is a difficult technical management issue that we are frequently asked to address. The answer is not simple and ultimately must rely on professional judgments. The process for selecting concepts has evolved as technical successes were obtained in the development of the mainline confinement concepts. That introduces a key element in the selection process; we examine and select alternate confinement approaches by taking full account of the status of the principle confinement approaches, and we do not undertake selection of alternate fusion confinement as an abstract exercise.

Historically, the mainline confinement approaches, the tokamak and mirror, have reached a prominent role in the development program because of demonstrated experimental success in confining hot, fusion-quality plasma earlier than other approaches. However, the flexibility implicit in the physical principles that unite all confinement concepts has permitted a great variety of feasible fusion approaches to be conceived and proposed for development. These are collectively identified as alternate concepts. Any number of them might be chosen for development and ultimately lead to successful fusion power systems. It is taken as an imperative by the Office of Fusion Energy that any attempt to develop all of them with equal emphasis would be detrimental to the eventual technical success of the most promising and an irresponsible utilization of valuable resources.

Several courses of action are conceivable in order to optimize the development of the highest potential of fusion for commercial application. The one approach that is clearly unsound is to ignore potential advantages that can come to the development program from ideas outside the mainline effort. It is precisely this factor that is employed in the review and selection process for alternate concepts.

The selection of alternate confinement approaches for development involves three factors: potential reactor advantages with respect to the mainline

approaches, technical feasibility, and the readiness (or timeliness) of undertaking the development with respect to the status of worldwide fusion development. The analysis of these factors is a continuing process; the level of performance by which the concepts are evaluated becomes increasingly more demanding as the concepts mature (and as the successes of the mainline effort elevate the general standard for all fusion development). Novel alternate concepts such as compact toroids must be perceived by the fusion community as having the potential of significant reactor advantages with respect to the mainline concepts. As the concept matures and becomes ready for proof-of-principle level tests, the perception must be replaced by quantitative studies supporting the reactor advantages. The compact toroid concept is clearly in an embryonic state. As the research we will hear about during the next several days evolves, this concept will be submitted to this scrutiny also.

We wish the research success for it is equally clear that this approach has significant potential benefits for users. Despite the enthusiasm for such a fusion system it still takes the dedicated work of the fusion community to make the promise of it a reality.

THE COMPACT TORUS CONCEPT AND THE SPHEROMAK

H. P. Furth, Plasma Physics Laboratory, Princeton University, Princeton, New Jersey 08544

Photographs of solar activity, using polarized filters [1], have provided indirect evidence of the emission of long-lived toroidal plasma configurations confined by linked poloidal and toroidal magnetic fluxes. Plasma configurations of this sort were first produced in the laboratory by H. Alfvén [2] and his coworkers (cf. Fig. 1) and reported at the Second International Conference on Peaceful Uses of Atomic Energy in 1958.

The injection of a current layer of highly energetic electrons (an "E-layer") to produce a steady-state toroidal plasma confined by poloidal field was proposed at the same conference by N. Christofilos [3]. A modern variant of this idea, using a neutral-beam-injected, medium-energy ion current [4], is shown in Fig. 2. Reversed-poloidal-field configurations of the same form have long been produced successfully by means of ordinary plasma currents in theta pinches — both with and without toroidal magnetic field component [5,6] (Fig. 3).

The common feature of all these plasma confinement schemes is that the magnetic field lines are closed, yet the field generating coil system is not required to link the plasma toroid. The principal variants of this "compact torus" concept are tabulated in Fig. 4. The present paper is concerned mainly with a brief review of the case $\rho_{pol} < a_{plasma}$, where the current carriers have poloidal-field gyroradii that are smaller than the scale height of the plasma.

Experimental theta-pinch plasmas with essentially null toroidal-field component ($B_{pol} \gg B_{tor}$) have exhibited remarkable longevity in terms of the characteristic time scale for MHD instability [7,8]. While the ideal MHD theory for this configuration does not actually allow all modes to be stabilized, the elimination of the strongest instabilities by axial elongation, combined with the finiteness of the plasma ion gyroradius ($\rho_{pol} < a_{plasma}$) may be providing effective stability in the experiments. For the reactor application, the null-B_t variant has the obvious advantage of very high beta-value ($\langle\beta\rangle \leq 1$), but the possible drawback of insufficiently stable confinement, since there may be a contradiction between the requirements for stability against gross modes and microinstabilities. The fast time scales and high voltages of the field-reversed theta-pinch formation method (Fig. 2) could be avoided in the beam-injected field-reversed mirror approach (Fig. 3), provided that the problem of ion-current cancelation by the electron-drag current can be resolved satisfactorily [4].

The compact torus with comparable toroidal and poloidal field components (Fig. 1), which has lately come to be called the "spheromak," has long received theoretical attention [9,10,11]. The toroidal field is supported by poloidal currents flowing inside the plasma and must, of course, vanish outside the plasma boundary. Ideal MHD stability is achievable when the plasma

entity is somewhat oblate, as in Fig. 5, and is surrounded by a moderately close-fitting conducting shell [12]. Under these conditions, the stability limit for $\beta_\delta^* \equiv 8\pi(\langle p^2\rangle)^{1/2}/B_0^2$ (where B_0 is the field strength on the magnetic axis) is typically of order 2-5%, but it can be several times greater in highly optimized configurations [13]. The basic advantage of the finite-B_{tor} regime is that stability against all ideal MHD modes can be ensured even for the case $\rho_{pol} \ll a_{plasma}$, which is congenial to good microstability properties. The main drawbacks are that special provision must be made for generating the toroidal flux and that beta must remain well below unity. It should be noted, however, that a limiting value of β_δ^* in the 5-10% range for the spheromak gives as much $(\langle p^2\rangle)^{1/2}$ as a tokamak β_δ^*-value of 50-100%, if the maximum field strength at the magnet coils is the same in the two cases. This is because the spheromak field is maximal at the plasma center (Fig. 5) while the tokamak field is maximal at the coils.

The spheromak is closely related to the conventional reversed-field Z-pinch (RFP) [14]: it corresponds to the particular case of null field-reversal and fairly low aspect ratio. The RFP has more shear, and thus is able to tolerate somewhat higher limiting beta values, but has the drawback of requiring plasma linkage by external toroidal-field coils. Experimentally [15], the null-field case of the RFP is found to lie precisely at the transition point between the "quiescent" state that is achieved with external $B_{tor} \leq 0$ and the turbulent state that prevails for external $B_{tor} > 0$.

The finite-resistivity MHD kink modes of the spheromak have been studied for large aspect ratio: stability is found to be realizable with optimal current profiles and very close-fitting shells [16] — quite comparable to the case of the conventional RFP. The low-aspect-ratio limit appears to have similar resistive instability characteristics [12], but has not yet been treated for optimized profiles. The stabilization of the resistive interchange mode in the spheromak depends mainly on collisionlessness and moderation of the beta value [17]. (For the $B_{tor} = 0$ version of the compact torus, the resistive MHD analysis has been carried out thus far only for the special case of axisymmetric modes [18].)

The experimental study of spheromak plasmas began with Alfvén [2]. It has been resumed recently, by means of the same coaxial-gun technique [19, 20] (Fig. 1), as well as by means of a theta-pinch formation process (Fig. 3) that includes toroidal-field generation [21]. References 22-24 describe a new type of "quasi-static" spheromak-formation technique that is aimed at avoiding the high pulsed powers associated with a dynamic forming process in plasmas of reactor size.

The degree of gross stability observed during the limited pulse time of the theta-pinch spheromak experiment [21] has been excellent — or even too good, since the ideal MHD theory clearly predicts a tilting mode [12] for prolate plasmas of the type of Fig. 3, whether a toroidal field component is present or absent. The antitheoretical stability against tilting has also been noted experimentally in the $B_{pol} \gg B_{tor}$ case [7,8]. Very recently, however, the injection of a gun-produced spheromak plasma into a prolate conducting shell has exhibited the predicted tilting [20].

The suppression of the tilting mode, as well as of higher surface modes, may be a consequence of the presence of hot plasma at the separatrix (cf. Fig. 3) and just outside it. An effect might be expected when the ion gyroradii are large or when the field outside the separatrix retains finite shear, due to the presence of external axial plasma currents or helical windings [12]. External-plasma stabilization could turn out to be very important for the compact-torus reactor application, since stabilization by close-fitting conducting shells would be inconveniently restrictive. As is shown in several reactor studies [25-27], one of the attractions of the compact torus is its potential ability to undergo compression, expansion, or displacement, free of mechanical constraints.

ACKNOWLEDGMENT

This work supported by US Department of Energy Contract No. EY-76-C-02-3073.

REFERENCES

[1] RIDDLE, A. C., Solar Physics 13 (1970) 448-457.
[2] ALFVEN, H., Proc. 2nd Int. Conf. on Peaceful Uses of Atomic Energy 31 (1958) 3.
[3] CHRISTOFILOS, N., Proc. 2nd Int. Conf. on Peaceful Uses of Atomic Energy 32 (1958) 279.
[4] COHEN, B. I., BRENGLE, T. A., Particle-Fluid Hybrid Simulation of Field Reversal in a Mirror Plasma, this conference.
[5] KOLB, A. C., DOBBIE, C. B., GRIEM, H. R., Phys. Rev. Lett. 3 (1959) 5.
[6] KOLB, A., et al., in Plasma Physics and Controlled Nuclear Fusion Research (Proc. 3rd Int. Conf., Novosibirsk, 1968) II (IAEA, Vienna, 1968) 567.
[7] ES'KOV, A. G., et al., in Controlled Fusion and Plasma Physics (Proc. 7th European Conf., Lausanne, 1975) I, 55.
[8] LINFORD, R. K., and CT Staff, The LASL Compact Torus Program, this conference.
[9] LÜST, R., SCHLÜTER, A., Z. Astrophys. 34 (1954) 263.
[10] CHANDRASEKHAR, S., in Proc. of the National Academy of Sciences 42 (1956) 1.
[11] MORIKAWA, G. K., et al., Phys. Fluids 12 (1969) 1648.
[12] BUSSAC, M. N., et al., in Plasma Physics and Controlled Nuclear Fusion Research (Proc. 7th Int. Conf., Innsbruck, 1978) III (IAEA, Vienna, 1979) 249.
[13] GAUTIER, P., et al., in Controlled Fusion and Plasma Physics (Proc. 9th European Conf., Oxford, 1979) paper EP 30, to be published.
[14] BAKER, D. A., Toroidal Reversed Field-Pinch Experiments, this conference.
[15] ORTOLANI, S., Some Properties of the Heating and Confinement in the RFP Configuration, this conference.
[16] GLASSER, A., SELBERG, H., to be published.
[17] BUSSAC, M. N., Bull. Am. Phys. Soc. 23 (1979) 872.
[18] BERK, H. L., et al., Tearing-Mode Stability Analysis of a Cylindrical Plasma, this conference.

[19] TURNER, W. C., et al., Initial Results of Field Reversed Plasma Gun Experiment, this conference.
[20] JARBOE, T. R., et al., Magnetized Gun Experiments, this conference.
[21] GOLDENBAUM, G. C., et al., Dynamically Formed Spheromak Plasma (PS-1), this conference.
[22] OKABAYASHI, M., et al., Spheromak Equilibrium and Stability and Numerical Studies of a Spheromak Formation Scheme, this conference.
[23] YAMADA, M., et al., Design and Fabrication of the S-1 Spheromak Device, this conference.
[24] AYDEMIR, A., et al., Two-Dimensional Simulation of the Formation of the PPPL Spheromak, this conference.
[25] MILEY, G. H., Field-Reversed Configurations: Theoretical Considerations and Reactor Applications, this conference.
[26] KATSURAI, M., YAMADA, M., Preliminary Studies of Spheromak Reactors, this conference.
[27] SMITH, A. C., Jr., et al., The Moving-Ring Field-Reversed Mirror Reactor Concept, this conference.

FIGURES

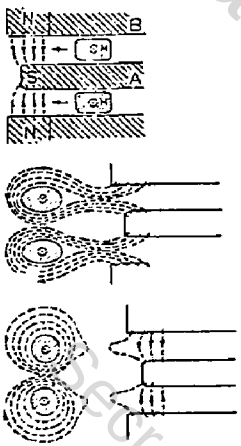

Fig. 1. Spheromak generation, using a coaxial plasma gun with poloidal field at the muzzle.

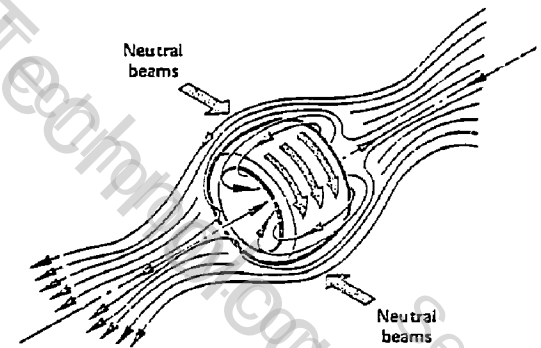

Fig. 2. Neutral-beam-driven field-reversed mirror machine.

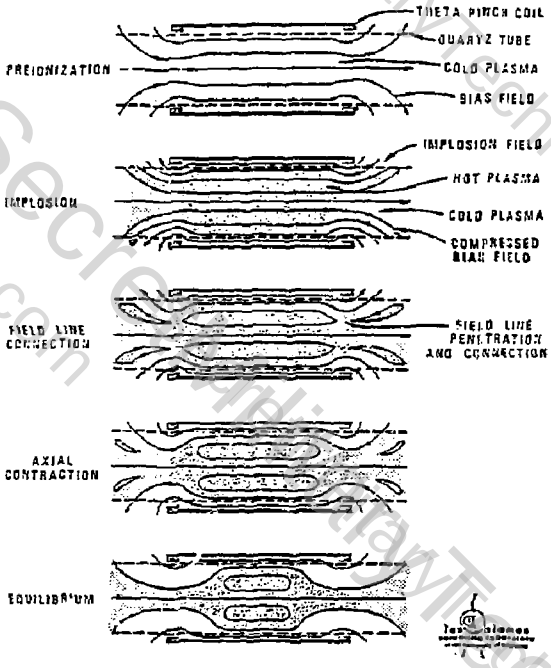

Fig. 3. Field-reversed theta pinch.

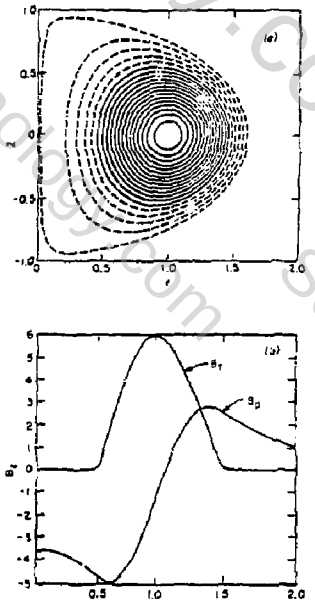

Fig. 5. Oblate spheromak. Plasma current is localized within the solid-field-line region. (PPL 786431)

	$\rho_{POL} < a_{PLASMA}$	$\rho_{POL} > a_{PLASMA}$
$B_{POL} >> B_{TOR}$	FIELD-REVERSED MIRROR OR θ-PINCH	E-LAYERS P-LAYERS
$B_{POL} \sim B_{TOR}$	SPHEROMAK OR "NULL-FIELD Z-PINCH"	REB-INJECTED TORUSES

Fig. 4. Tabulation of compact toruses.

INJECTION OF RELATIVISTIC ELECTRON BEAM INTO TOROIDAL SYSTEMS

Akihiro Mohri, Kazunari Narihara, Yukihiro Tomita
Institute of Plasma Physics, Nagoya University
Nagoya 464, JAPAN

In recent years, the injection of high current relativistic electron beams into toroidal systems has been a subject of absorbing interest in connection with compact torus and OH assist startup for large tokamak. Injection methods tried up to the present are surveyed here and a method using Plasma Anode, which is adopted for REB injection into SPAC, is reviewed.

The first question we have is whether an electron ring is suited for confinement of fusion plasma in the practical sense. The electron energy of E-layer of Astron should be so high as the relativistic factor $\gamma > 100$ in order to produce a strong magnetic field and a sufficient volume for confinement. The resultant strong synchrotron radiation brings a serious problem concerning the energy loss. However, if we use an appropriate mechanism to keep the ring radius large enough at lower γ in the strong external field for equilibrium, such a problem will not be fatal. When a high current REB ring closely in a force-free state is formed, its major radius can be controlled with an applied vertical field like Astron-Spherator. We do not need the use of ion-ring in this case. Besides, generator of 1~10 MeV REB is now at the commercial base. When the main toroidal current is generated by REB injection from outside, we can neglect any other current-driving equipment and, thereby, toroidal configurations of very small aspect ratio are realizable.

The concept mentioned above much depends on the success of REB injection into toroidal systems. Methods examined up to the present are summarized as follows;

* ASTRON (LLL), RECE-BERTA and RECE-CHRISTA (Cornell Univ.) inject REB obliquely to the mirror axis and stop the axial motion by dissipation.
* Cornell Univ.(Gilad, Kusse, Lockner) divert toroidal field lines to the cathode of a diode by using self-field of the diode current.
* Physics International (Benford, Ecker, Bailey) use a guiding field and the drift motion of REB.
* Cornell Univ. and Maryland Univ. use a cusp field.

All of above methods are for injection into neutral gas. However, adjustment of the initial density of plasma at the time of the injection becomes necessary so as to control the β value of thus confined plasma for stability. In the case of the injection into neutral gas, the range of the gas pressure should be chosen from the condition of space charge neutrality. Usually, the pressure is 0.1 to 1 torr. For the reason, REB injection into a plasma of appropriate density is required, where ions of the plasma easily cancel the space charge of the injected beam electrons.

In order to catch a ring immediately after its formation in an equilibrium position, we have to suppress the induced return currents which mask the poloidal field of the ring. Besides, we can not change the vertical field within a time comparable with the pulse duration of injection. These difficult points can be solved if we use Plasma Anode instead of usual foil anode. Figure 1 shows a schematic explanation of the function of plasma anode.

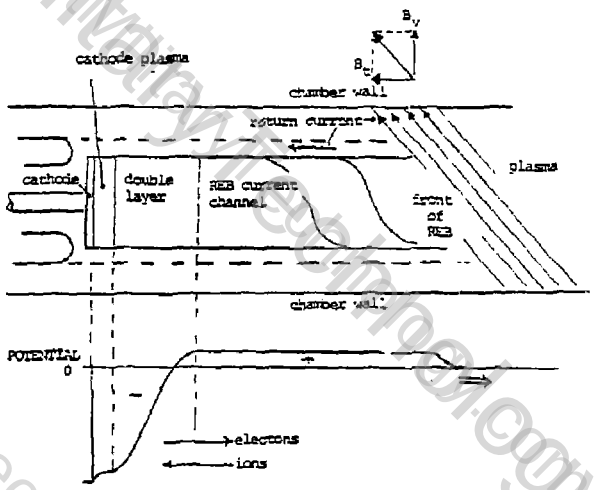

Fig. 1

A cathode is set inside the toroidal chamber so that its face is directed parallel to the toroidal field. The toroidal and the vertical fields are applied before REB injection and then the chamber is filled with a plasma. The plasma contacts both the cathode and the chamber wall. When a negative-pulse voltage is applied on the cathode, ions of the plasma are accelerated towards the cathode and bombard the cathode surface where multi-layers of gas molecules are present. Thus, a high density plasma is produced on the surface. There appears a plasma sheath of double layer type and the electrons of the cathode plasma are accelerated in the sheath. The plasma-anode is very superior to the conventional

foil anode in that there is no need to exchange foils and thus a repetitive operation becomes possible. Owing to the thin sheath, fairly high current density is obtainable for REB without causing a pinch, and the beam electrons are ejected in the same direction. The induced return current can not flow towards the cathode, and the current is forced to take its path towards the chamber wall along the magnetic field lines. Inside the beam channel there exists a strong self-magnetic field due to the beam and the resultant magnetic field becomes helix because of the presense of the toroidal magnetic field. The channel winds round the toroidal major axis. Another possible path of the return current is on the just outside of the beam channel as shown in Fig.1. This return current wraps the beam channel like a thin sleeve and masks the self-field of the beam. Since the skin time of the sleeve is very short, neighboring paths of the beam channel merge themselves as the self-field appears out of the sleeve. Finally, an axially symmetric REB ring with a single magnetic axis is formed. The rise time of the poloidal field is therefore very short. The time is about 150 ns in the case of SPAC-V, as shown in Fig.2. Strong plasma heating could be expected

Fig. 2

Rises of poloidal fields on the upper and the lower sides of a REB ring in SPAC-V.

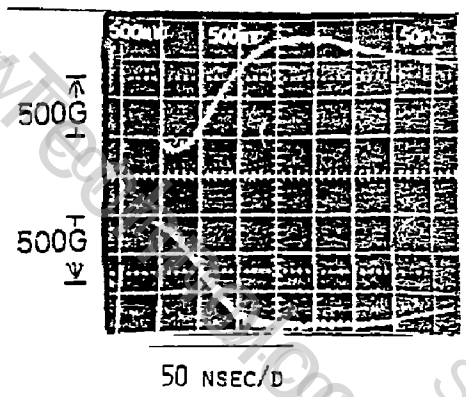

during this merging phase.

While the plasma-anode is working, the cathode is subject to ion bombardment. During the time, the material of the cathode is evaporated or sputtered and may enter the confined plasma region as impurities. Figure 3 presents photographs of the cathode surface, taken with an electron-scanning-microscope. Damage of the surface like chunks are observed. Materials stronger against the ion bombardment should be used such as Mo. In this injection of REB, the cathode plasma is easily produced by ionizing attached molecules on the cathode surface. The density of the molecules is more than 10^{14} cm^{-2} which is sufficient for the purpose. It does not need to use the plasma of the cathode material itself.

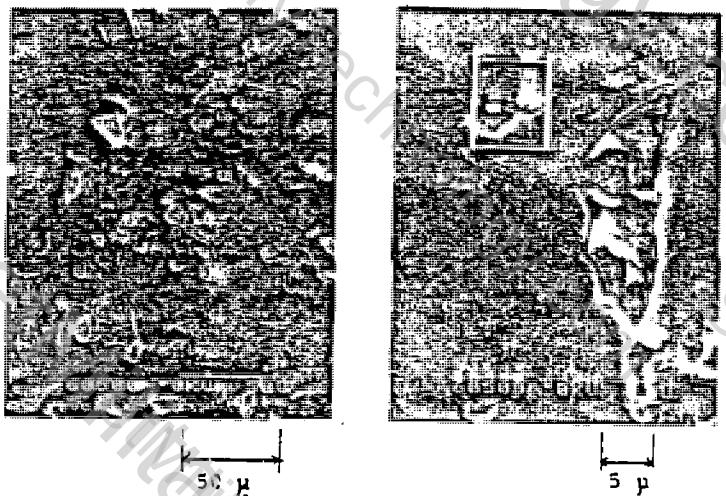

Fig. 3 Damage of the cathode surface.
Irradiation power of protons: 10^7 W/cm^2,
Number of irradiation : 85 shots,
Total irradiated energy : 30 J/cm^2.
Cathode : SUS-304

THE LASL COMPACT TORUS PROGRAM*

R. K. Linford and CT Staff**, Los Alamos Scientific Laboratory, Los Alamos, New Mexico 87545

INTRODUCTION

The Compact Torus (CT) concept includes any axisymmetric toroidal plasma configuration, which does not require the linking of any material through the hole in the torus. Thus, the magnet coils, vacuum vessel, etc., have a simple cylindrical or spherical geometry instead of the toroidal geometry required for Tokamaks and RFP's. This simplified geometry results in substantial engineering advantages in CT reactor embodiments while retaining the good confinement properties afforded by an axisymmetric toroidal plasma-field geometry. The cross section in Fig. 1 of a prolate CT shows the essential features of the B-fields and plasma dimensions. CT's can be classified into three major types by using the ion gyro radius ρ_i and the magnitude of the maximum toroidal field B_{tm}. The well-known Astron configuration is a CT with large ρ_i, or as is defined in this paper $\rho_i/a > 1$ (see Fig. 1). The two other classes of CT's, Sheromaks and Field Reversed Configurations (FRC's), both have $\rho_i/a < 1$. However, $B_{tm} = 0$ for an FRC in contrast to $B_{tm} = B_{pm}$ (maximum poloidal field) for a Spheromak.

PROGRAM OUTLINE

The LASL CT Program is focused on the study of the physical properties of Spheromaks and FRC's in order to develop viable reactor embodiments. The main facility for this study (Fig. 2) is under construction. The two types of CT's

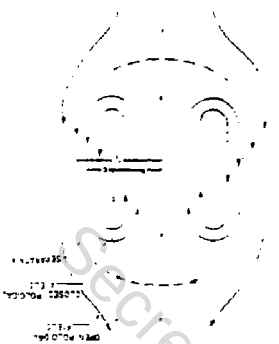

Figure 1. CT Cross Section

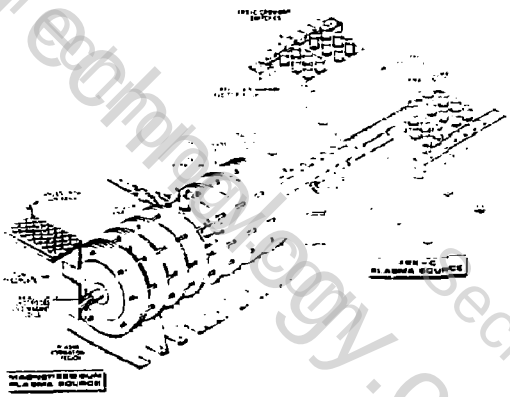

Figure 2. CTX Facility

*Work performed under the auspicies of the U. S. Department of Energy.
**W. T. Armstrong, R. R. Bartsch, R. J. Commisso, G. A. Ekdahl, E. Henins, H. W. Hoida, T. R. Jarboe, J. Libson, J. Marshall, Jr., K. F. McKenna, D. A. Platts, A. R. Sherwood, E. G. Sherwood, R. E. Siemon

will be produced by the Magnetized Gun (Spheromak) and the FRX-C (FRC). Eventually, both sources will be able to inject CT's into the central CTX tank where they will be trapped in a dc mirror field of up to 10 kG. Stability, transport, and heating studies will be carried out on these single cell configurations. Stability and transport studies of multiple cell configurations will also be carried out in a modified version of the 5 m long Scylla IV-P theta pinch.

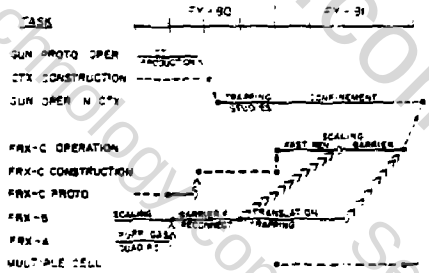

Figure 3. CT Program Plan

In preparation for these experiments, Spheromaks are being produced in a Gun Prototype facility and FRC's are being studied in two 1 m long theta pinch systems, FRX-A and FRX-B. Figure 3 shows the time scales for these experiments. As indicated, the Gun will be the first plasma source tested in the CTX tank. The FRX-C will be operated as a separate facility during FY 81. At the end of that fiscal year, the transition section will be added to allow the translation of the FRC plasma into the CTX tank. The significance of the planned experiments on FRX-B systems is discussed later. The remainder of the paper is devoted to a brief status report on the Gun, CTX, and FRX experiments. Companion papers in these proceedings[1,2,3,4] describe in more detail the experimental and theoretical results and future plans for these systems.

GUN PROTOTYPE

A 70 cm long Marshall-type coaxial plasma gun has been constructed with electrode radii of 15 cm and 10 cm. Slow risetime magnet coils have been placed inside the inner electrode and outside the outer electrode. These coils produce a radial field across the muzzle of the gun, which is stretched by the emerging plasma and eventually forms the poloidal field of the Spheromak. In addition, these coils produce a bias field in the gun barrel (between the electrodes) which allows repeatable operation of the gun at much lower fill pressures than otherwise possible. Initial fill densities of 3×10^{14} to 2×10^{15} cm^{-3} have been used successfully with bank energies of about 30 kJ. Magnetic field probes indicate that Spheromaks have been formed by the gun and stopped in a 45 cm diameter stainless steel flux conserver with no guide field[1].

CTX

The main CTX tank is installed and has been pumped down to 1×10^{-7} mtorr with one of the three cryo pumps. The dc magnets have also been installed but are not yet connected to the power supply. The 10 kV bank for the gun magnets and the 60 kV main gun bank are in place awaiting power supply and control system installation.

FRX SYSTEMS

The large body of experimental and theoretical data available from the FRC research cannot be summarized here. However, three important FRC issues are discussed, which include some of these results and also provide some of the motivation for the experiments outlined in Fig. 3.

(1) Gross Stability

The observed gross stability in the experiments for more than 100 Alfven transit times appears at odds with simple MHD estimates. Note that as a result of the absence of toroidal field in the FRC, the β is high, the safety factor $q = 0$, and there is no shear. However, detailed ideal MHD calculations[4], which include the proper geometry effects (high elongation b/a, and low aspect ratio R/a) yield results that are consistent with the observed gross stability.

In contrast to this ideal MHD stability, the FRC is usually terminated by a rotationally driven $n = 2$ (toroidal mode number) mode. The exceptions are the Kurtmullaev results[2] and a few non-repeatable shots on FRX-B. Although these observations are not completely understood, they are largely consistent with the following theoretical results[4]. The mode is stable if the ion rotational frequency Ω_i is kept below the threshold of $\Omega_i/\Omega^* \approx 1.4$, where Ω^* is the ion diamagnetic frequency. The source of rotation, which drives Ω_i beyond this limit, is dominated by particle loss although there are other effects associated with geometry, flux annihilation, and electron-ion energy equilibration. The most important result, however, is that the mode does not limit the energy confinement of the FRC. This result, which is supported by experiments[2], predicts that about half the energy is lost by transport before the mode goes unstable.

(2) Transport Scaling

The transport, which limits the plasma lifetime appears to be anomalous. MHD turbulance does not appear important because decreasing λ_i for fixed R and decreases a Finite-Larmor-Radius (FLR) stabilization but increases observed lifetime. However, the observed scaling is consistent with the results of a 1-1/4 D transport code with the lower-hybrid-drift (LHD) instability dominating the transport coefficient[6].

There are several important transport scaling parameters. Variations in R result in the usual surface-to-volume effects. The density scale length λ_n is very important because λ_n/λ_i strongly affects the LHD transport. In turn, λ_n/λ_i is controlled by the density n, R, and r_s/r_w where r_w is the radius of the conducting wall. In particular, as $r_s/r_w \to 1$, $\lambda_n/\lambda_i \to a/\lambda_i$, which is the largest and most favorable value possible.[5] Thus fat plasmas ($r_s/r_w \to 1$) are favorable not only because of wall stabilization, but because it results in slower transport. As a consequence, the angular acceleration is decreased and the onset of the rotational mode is delayed.

A major purpose of the planned FRX experiments is to examine techniques for producing fat plasmas ($r_s/r_w \to 1$) and thus extending the plasma lifetime. The production of fat plasmas requires the trapping of more bias flux in the theta pinch during the field reversal. Two techniques for trapping more flux will be

tested. (1) reversing the field more rapidly and (2) trapping the bias flux with an octapole barrier field during reversal.[2] The fast reversal technique will be tried first on the FRX-C using its 250 kV loop voltage. The FRX-B is being modified to test the barrier field and reconnection techniques of Kurtmullaev.[2] If these prove superior to fast reversal, FRX-C will be modified accordingly.

The Multiple Cell experiment is designed to test transport and stability in the multiple cell geometry. In particular, a study will be made of the effects of increasing ℓ_n/ρ_i by multiple-mirror confinement of plasma on the open field field lines."

(3) Translation and Trapping

Translation and trapping are necessary if the FRC plasma is to be studied in the dc field of the CTX tank. The formation and translation have already been demonstrated in FRX-A. However, it is important to use a puffed gas fill instead of a static fill so that the FRC can be translated into a vacuum. This technique is being studied in conjunction with a quadrapole preionization scheme on FRX-A (see Fig. 3). The results will be incorporated in the translation and trapping experiment on FRX-B. These experiments should produce all of the necessary data for the successful translation of FRX-C plasmas into the CTX in FY 82.

REFERENCES

1. T. R. Jarboe et al., "Magnetized Gun Experiments," these proceedings.
2. W. T. Armstrong et al., "Field Reversal Experiments, and FRX-A and FRX-B Results," these proceedings
3. R. E. Siemon and LASL Compact Torus Staff, "FRX-C and Multiple Cell Experiments," these proceedings.
4. D. C. Barnes et al., "Compact Torus Theory--MHD Equilibrium and Stability," these proceedings.
5. A. G. Es'kov et al., "Principles of Plasma Heating and Confinement in a Compact Toroidal Configuration," Plasma Phys. and Contr. Nucl. Fusion Research, Innsbruck, Vol. II (1978) 187.
6. S. Hamasaki and R. K. Linford, Bull. Am. Phys. Soc. 24 (1979) 1081.

INITIAL RESULTS OF FIELD REVERSED PLASMA GUN EXPERIMENT*

W. C. Turner, C. W. Hartman, and J. Taska
Lawrence Livermore Laboratory, Livermore, California 94550

A. C. Smith, Jr.
Pacific Gas and Electric Company, San Francisco, California 94106

We have begun experiments using a magnetized co-axial plasma gun to produce field reversed plasma.[1][2] The gun injects axially into the Beta II facility at Livermore. The experimental program consists of three stages: (1) formation, (2) translation and magnetic mirror trapping and (3) neutral beam heating of field reversed plasma. Experiments to date pertain to the first stage and have demonstrated production of field reversed plasma.

The experimental apparatus is shown in Figure 1. The co-axial gun electrodes are 1.5 m long. The diameter of the inner (outer) electrode is .15 m (.30 m). The electrodes are fitted with solenoid coils that, together with the guide coils of the Beta II device, form a magnetic cusp at the gun muzzle. The inner electrode solenoid provides magnetic flux that is opposite the guide field (field reversed flux). The outer electrode solenoid is used to control the bias field between electrodes.

Diagnostics include an array of magnetic loop probes and a Cu calorimeter. The external magnetic loops consist of four single turn diamagnetic flux loops, two Rogowski belts and a loop that measures the azimuthally averaged component of radial magnetic field at one axial location. An axial magnetic probe can be scanned vertically through the interior of the plasma and contains small loop probes to measure local components of magnetic field. The magnetic probes shown in Figure 1 are center tapped for differential readout, stainless steel jacketed, and compensated with passive RC networks. The probes are calibrated with pulsed solenoid and Helmholtz coils.

The data in this paper were obtained by choosing a guide field strength 4.8 kG, a net inner solenoid flux 0.90 kG - cm^2, a plenum gas fill of 50 atm - cm^3 D_2, and then scanning the gun bank charge voltage (V_G) and bias field between electrodes (B_{bias}) to find optimum values for production of field reversal. These values turned out to be V_G = 35 kV and B_{bias} = 2.25 kG in the same direction as the guide field, opposite the field inside the inner electrode.

Gun discharge voltage and current are shown in Figure 2. The gun current peaks at 940 kA, producing a magnetic field of 25 kG at the surface of the inner electrode that is accelerating plasma out of the gun. The time integral of voltage and current shown at the bottom of Figure 2 gives 130 kJ energy input to the gun terminals.

Time of flight data from the four diamagnetic flux loops show an initial plasma front velocity in the range 82 to 130 x 10^6 cm/sec, filling the region between the gun and calorimeter with plasma in approximately 2 microseconds. Thereafter signals on the diamagnetic loops persist for about 25 μsec. For the conditions described above the Rogowski belts measure zero net axial current drawn from the gun to the calorimeter and returning in the vacuum chamber walls. Figure 3 shows an axial magnetic probe signal giving

*Work performed by LLL for USDOE under contract W-7405-Eng-48.

a peak change in axial magnetic field strength ΔB_z = 18.9 kG and field reversal factor $\Delta B_z/B_0$ = 4.2 in the 4.5 kG guide field. The bottom half of Figure 3 shows separately signals from each half of the center tapped probe. The two components are equal in magnitude, opposite in sign, verifying their magnetic origin. This verification is equivalent to flipping probe orientation or changing sign of all magnetic fields and observing opposite polarity probe signals. Electrostatic signals would have the same sign for each half of the probe and obviously have been reduced to negligible proportions by shielding and isolation. Typically a time integrated energy deposition of 15 kJ is recorded on the calorimeter.

A radial scan of the axial component of magnetic field strength is shown in Figure 4. Data are plotted on successive shots, moving the probe between shots. Each data point plotted is a five microsecond average over the peak of the recorded waveform. A multi-channel radial probe has been constructed to verify the profile in Figure 4 on a single shot but no data have been taken yet with this probe. Several points can be made from Figure 4. First, a field reversed region with B_z = -10 kG, corresponding to $\Delta B_z/B_0$ = 3.1, extends out to a radius 0.10 m. Second the radius of the axial field null is 0.15 m. Third, the magnetic flux inside the null is 4.9×10^3 kG - cm^2, a factor 5.4 times the net flux inside the inner electrode. A flux amplification effect has been noted earlier by Alfvén and his co-workers.[2][3] Fourth, the radius enclosing zero flux is 0.23 m. Fifth, the radial profile in Figure 4 conserves the vacuum flux out to the wall at 0.75 m. Sixth, the axial magnetic field energy inside the separatrix is 28 kJ/m. Equilibrium of the profile in Figure 4 requires existence of a toroidal field component since the axial field pressure inside exceeds that outside the plasma by a factor of four. Toroidal field components have been observed but a radial profile verifying the equilibrium has not been obtained yet.

A scan of ΔB_z on axis versus net flux in the inner gun electrode is shown in Figure 5. For negative values of net flux the inner electrode solenoid is not pulsed strongly enough to reverse the guide field flux, and the plasma produced does not reverse the guide field. Once the net flux is positive large field reversals are readily produced, but if the net flux is too large, field reversed plasma does not emerge from the gun.

(1) H. Alfvén, Proc. Second Int'l. Conf. on Peaceful Uses of Atomic Energy, 31, 145 (1958).
(2) H. Alfvén, L. Lindberg, P. Mitlid, J. Nucl. Energy, 1, 116 (1960).
(3) L. Lindberg, C. Jacobsen, Astro. J., 133, 1043 (1961).

Figure 1. BETA II PLASMA GUN DIAGNOSTIC SET-UP

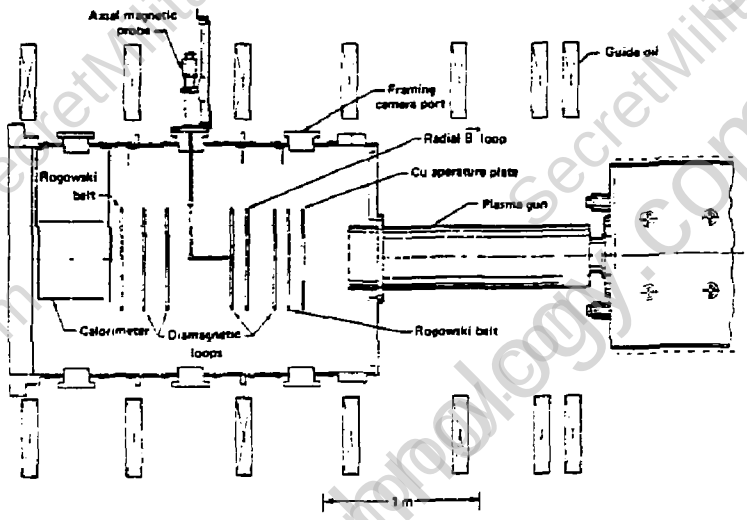

Figure 2

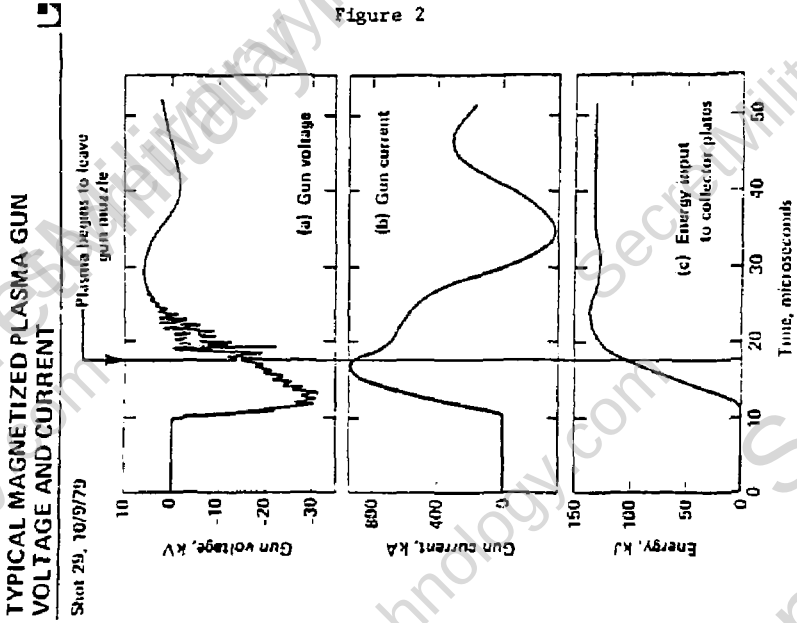

Figure 3

TYPICAL FIELD REVERSAL SIGNAL FROM BALANCED MAGNETIC PROBE

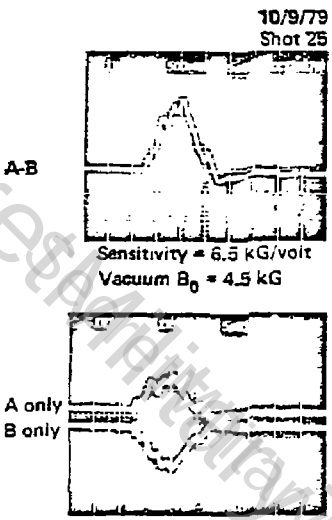

Figure 4

RADIAL SCAN OF AXIAL MAGNETIC FIELD

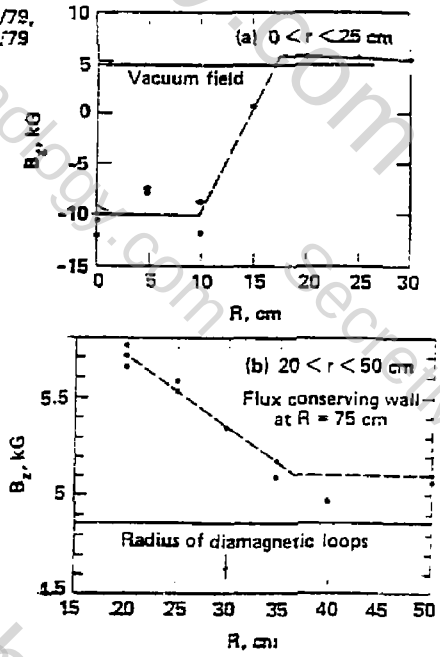

Figure 5

AXIAL MAGNETIC FIELD PROBE SIGNAL VERSUS PLASMA GUN INNER ELECTRODE FLUX

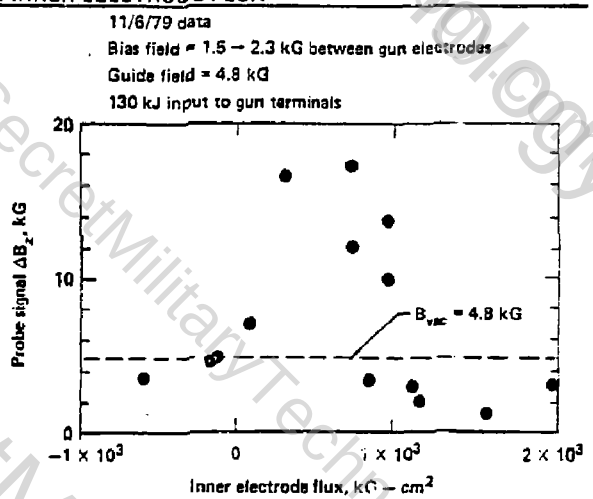

EXPERIMENT ON PLASMA CONFINEMENT BY INTENSE RELATIVISTIC ELECTRON BEAM RING

Y. Tomita, K. Narihara, T. Tsuzuki, M. Hasegawa, K. Ikuta, and A. Mohri, Institute of Plasma Physics, Nagoya University, Nagoya 464, Japan

1. INTRODUCTION

Toroidal magnetic configurations formed by injection of intense relativistic electron beams (REB) have many benefits for plasma confinement. The formation time is so short that the state can pass over to a final stable one, quickly going through dangerous, unstable regions. When a beam is injected into a preformed plasma, the plasma is effectively heated in a short time. Since no equipment to generate toroidal currents is necessary around the major axis, compact toroidal configurations are realizable.

An experimental program named SPAC has been conducted to investigate the possibilities mentioned above [1-3]. In SPAC-V, REB rings with a current of 30 kA and milliseconds life were successfully formed using a new injection method in which plasma acts as anode and no anode foil is needed. Encouraged by the results from the SPAC-V experiments, we have constructed a scale-up toroidal device SPAC-VI which was designed aiming at longer life and higher current of REB rings. In the new toroidal device SPAC-VI, the strong adiabatic compression is easily applicable, when the beam electrons and the plasma are both energized.

In the next section (Section 2) a summary of the results of the SPAC-V experiment is given. In Section 3 the design and experimental results from SPAC-VI are presented.

2. SPAC-V EXPERIMENT

Experimental setup is schematically shown in Fig. 1. The end of the magnetically insulated transmission line (MITL), which is connected to pulsed high voltage generators PHOEBUS II or III, is inserted inside the vacuum vessel where the cathode is set with the surface towards the toroidal direction. After applying the magnetic fields, the vacuum vessel is filled with a prepared plasma. The plasma contacts with the surfaces of the cathode and the vessel. On the application of the voltage, a plasma sheath forms in front of the cathode. Across this sheath, electrons are accelerated to the applied voltage and enter into the plasma. This method of beam injection, which we call "Plasma-Anode Method," is superior to the conventional foil anode in the following points: (1) There is no need for exchanging foils and highly repetitive operation is possible. (2) Electrons are

scarcely momentum scattered by the anode material. (3) By changing the plasma density and the area of cathode, the diode impedance is easily changed. (4) The small thickness of sheath enables fairly high current density beam emission without causing a pinch. In the experiment, the cathode was 4-6 cm in diameter and the plasma density around the cathode was 10^{12}-10^{13} cm^{-3}.

Features of the REB rings thus formed depend largely on the external magnetic field strengths and on the plasma density before REB injection. When REB are injected into the denser plasma, a ring current as high as 150 kA was obtained. The lifetime, however, was as short as 20 microseconds.

The lifetime of the REB ring has been prolonged up to 1.6 msec. Figure 2(a) presents time dependences of the ring current I_R, poloidal magnetic fields at the center B_{pC} and the major radius of the ring R_R. The ring current reached 42 kA 300 nsec after the injection, and it decayed fairly quickly for 200 microseconds. Then, the current decayed slowly until a final large disruption occurred. The major radius decreased in the rising phase of B_V and then the radius was nearly constant for about 1 msec. A train of stepwise damps of current were observed during the fast decay of the ring current in the early stage. At the final large disruption, intense x-ray flash emitted from the central region and a positive spike appeared in the poloidal field at the center. These facts suggest that the collapse of the ring was accompanied with the fast shrinkage of the major radius. Figure 2(b) presents the case where the toroidal magnetic field was adjusted to decay faster. In this case, disruption occurred at a faster time than in the previous case. This fact suggests that the life of the ring is determined by the decay of the toroidal magnetic fields.

The vertical magnetic field necessary for the equilibrium is

$$B_V = \frac{\mu_o I_R}{4\pi R_R}\left(\ln\frac{8R_R}{a} - 1.5 + \frac{l_i}{2} + \beta_{peff}\right),$$

$$\beta_{peff} = \beta_p + (\gamma^2 - 1)^{1/2}\frac{I_A}{I_R}, \quad I_A = \text{Alfvén current},$$

where a is the minor radius of the ring, l_i the internal inductance, and β_{peff} is the effective poloidal beta which includes the centrifugal force effect of the circulating electrons. From the experimentally measured values of B_V, I_R, R_R and the roughly estimated value of a, we can estimate β_{peff}. In the

case of Fig. 2(a), β_{peff} increased from 0.8 at t = 0.4 msec to 1.6 at t = 1.2 msec. This increment could be caused by the heating of plasma due to beam plasma interaction and/or the acceleration of the beam electrons embedded in the plasma.

From a micro-wave interferometry, the averaged density of the confined plasma was estimated to range around several times 10^{13} cm^{-3}.

From the Doppler broadening of impurity lines ion temperature was estimated to be about 100 ev at the early phase of the ring current evolution.

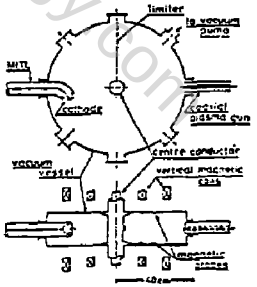

Fig. 1. Schematic diagram of the toroidal device SPAC-V.

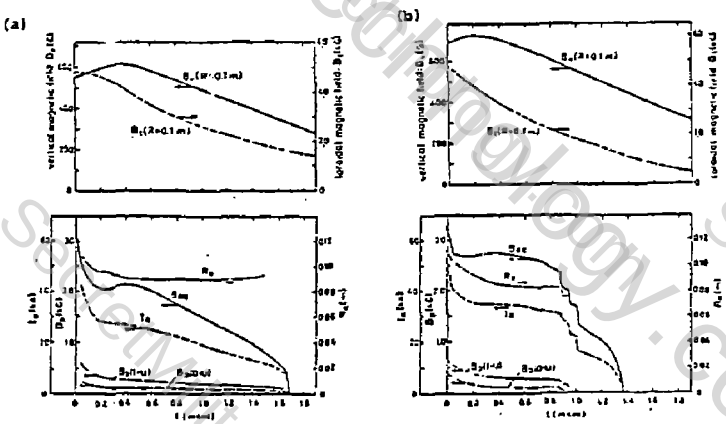

Fig. 2. Time variations of the external magnetic fields(B_V,B_t) and the net current(I_R), the poloidal magnetic field(B_p), and the major radius(R_R) in the case of (a) slower decay and (b) faster decay of B_t.

3. Design and Experimental Results of SPAC-VI

A new toroidal device SPAC-VI was constructed continuously from previous experiments : SPAC-V. This new toroidal device was designed with aiming at plasma confinement by REB rings of longer life and higher current and stronger major radial adiabatic compression. For this purpose, the vacuum chamber was made larger and vertical magnetic field coils were distributed radially.

Figure 3 shows the schematic structure of SPAC-VI. The toroidal field B_t is generated by the current(1.2MA maximum) in a single center conductor set along the major axis of the torus and its flat top time within ±7% change is 20msec. The vertical magnetic field coils are installed to keep the decay index less than 1.1 for stabilizing the positional instability of REB rings extending the whole space of plasma confiment and a maximum vertical magnetic field is generated 12kG. For the purpose

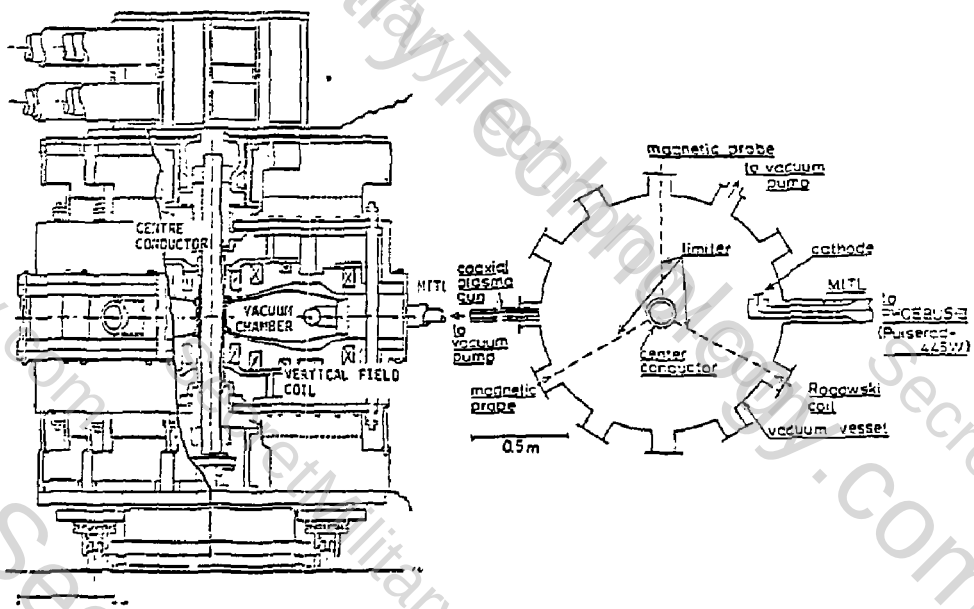

Fig. 3 Schematic structure of SPAC-VI

of major radial compression of plasma, the wave form of the vertical magnetic field B_V is able to be adjusted. The vacuum vessel for plasma confinement is made of thin stainless steel with a shell effect. This vessel 1.28m in outer diameter does not have a flat lid aiming at adiabatic compression of confined plasma. In this experiment, for REB injection "The Plasma Anode Method" was adopted to form REB rings. Pulse of negatively high voltage delivered from a Marx generator PHOEBUS-III (Pulserad-445W; 1.8MV,370kA,50kJ) is sent to a cathode through a magnetically insulated transmission line(MITL). This cathode is inserted inside the vacuum vessel and is set with the surface towards the toroidal direction. The MITL can be operated in ultra high vacuum and the transmission efficiency is more than 80% at the pulse strength of 1.6MV and 190kA of 80nsec duration. A partially ionized cold hydrogen plasma, which is prepared by a coaxial plasma gun, serves for the plasma-anode.

The experiment of plasma confinement by REB rings using SPAC-VI and PHOEBUS-III (Pulserad-445W) was firstly carried out to have a long lifetime. The external magnetic fields of SPAC-VI can be maintained ten times as long as in the case of SPAC-V where the lifetime of REB rings had been determined by that of the external magnetic fields. In a high q mode operation ($q \geq 2$), the ring current I_R continued for 10msec which was ten times the previous record of SPAC-V(Fig.4). The peak ring

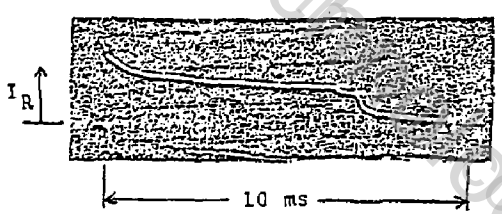

Fig. 4 Wave form of a REB ring current

current was 43kA and the major radius of REB rings, which was decided from measurement of poloidal field near the wall using magnetic probes, was 23cm, where the toroidal magnetic field B_t was 5.4kG. In this case, the slowest decay time $[dI_R/(I_R \cdot dt)]^{-1}$ was 50msec. The injected REB had the particle energy of ~1MeV and the current of ~80kA. However, highly repetitive short bursts of both x-rays and impurity lines appeared during the decay of the ring current. Origin of the phenomena is now in full pursuit.

The major subject of this experiment using the toroidal device SPAC-VI is to form long-lived REB rings with very low q-value and to apply a strong adiabatic compression on them, because this would lead to a compact torus reactor. Compression ratio of 2.5 with respect to the major radius is possible in SPAC-VI. Experimental results in these operations will be reported. Diagnostic instruments which can work in strong x-ray environments are under commission, so that detailed parameters of confined plasma will be found out.

REFERENCES

[1] MOHRI, A., MASUZAKI, M., NARIHARA, K., YAMANAKA, K., IKUTA, K., in Plasma Physics and Controlled Nuclear Fusion Research (Proceedings 6th International Conference, Berchtesgaden, 1976) Vol. III, IAEA, Vienna (1977) 395.

[2] MOHRI, A., NARIHARA, K., TSUZUKI, T., KUBOTA, Y., TOMITA, Y., IKUTA, K., MASUZAKI, M., in Plasma Physics and Controlled Nuclear Fusion Research (Proceedings 7th International Conference, Innsbruck, 1978) Vol. III, IAEA, Vienna (1979) 311.

[3] NARIHARA, K., TOMITA, Y., TSUZUKI, T., MOHRI, A., in Proceedings 3rd International Topical Conference on High-Power Elect. and Ion Beam Research and Technology (Novosibirsk, 1979) to be published.

INTENSE RELATIVISTIC ELECTRON BEAMS IN TOROIDAL MAGNETIC GEOMETRIES

V. Bailey, J. Benford, R. Cooper, B. Ecker, and H. Helava,
Physics International Company, San Leandro, CA. 94577

Intense relativistic beams (REBs) can perform important functions in toroidal fusion devices. Among these are: (1) starting up and/or maintaining the current in a steady-state toroidal reactor,[1,2] (2) producing the confining magnetic fields for the plasma,[3-6] (3) rapidly heating the plasma to ignition conditions,[7] (4) providing start-up plasma heating and current maintenance for a steady-state, compact, high β torus.[8,9]

The REB is injected parallel to the toroidal magnetic field and trapped in the toroidal plasma column by drift-injection, energy loss trapping.[10-13] This technique, which has been demonstrated experimentally,[13] allows multi-turn injection, whereby the injection time is many times the single transit time of electrons around the torus, and has been shown experimentally to be efficient. This method uses toroidal-plus-betatron-type field geometry with trapping resulting from partial beam energy loss by self-magnetic field generation and/or by heating of the plasma.

The increase in the net toroidal current caused by the REB is an increasing function of the kinetic energy of the injected REB and is inversely proportional to the inductance per unit length of the beam-plasma system. The predicted scaling of the increase in net toroidal current compares well with recent experimental data. The time scale for this increase is significantly shorter than the normal L/R decay time of the plasma. The fraction of the injected REB energy that is initially converted to poloidal magnetic field energy or plasma thermal energy can be adjusted by changing the parameters of the injected beam. This allows a great deal of flexibility in using the REB for plasma heating and current-drive.

The average ~ 3 power level required to maintain the toroidal current in a steady-state toroidal reactor is only slightly larger than the ohmically dissipated power and is significantly less than that required by rf current drive. For a typical tokamak reactor the ratio of the toroidal current to the average REB power required to maintain that current is 10 A/W. The generally accepted value of this ratio for rf current drive is 0.1 A/W.[14] Injection of a 6.6 MV REB having an average power of 1.5 MW could maintain a toroidal current of 15.6 MA in a tokamak reactor, while 150 MW would be required if rf current drive were used. In this example approximately 80 percent of the injected beam energy is converted to increased poloidal magnetic field energy. The higher efficiency of the REB current drive permits the larger reactor

Q-value (Q_{max} = fusion power/current drive power) for a steady-state reactor.

Stable beta of tokamaks can be increased by either lowering the aspect ratio A or by intensive heating during the formative stages of the discharge to control the growth of the ballooning modes.[15,16] Jassby[17] used the small-aspect-ratio technique in his design for "SMARTOR" and PITR, and Peng[9] achieved similar results by compressing a large-aspect-ratio plasma. The intense heating technique is used at Columbia in TORUS II and at Nagoya in SPAC-V to obtain a high-beta (> 10 percent) stable equilibrium. These high-beta configurations may best be realized by repetitive injection and trapping of a REB in a torus. Starting with a cold plasma and no toroidal current, a pulse sequence can be defined to bring the reactor to ignition at constant poloidal beta, without ohmic heating coils. In principle, this beta can be chosen large enough to be in the stable regime for the ballooning modes.

Using the high-beta equilibrium of Peng and Dory, we have selected a compact steady-state toroidal reactor driven by REBs.[8] The reactor has a low aspect ratio (2.0), high beta (0.18), a 1.6 m major radius, and 250 MWe net output. It is started with 225 pulses of a 1 MV, 0.4 MA, 2 μs beam at 100 Hz, and current is sustained by the same beam operating at 0.33 Hz.

REFERENCES

1. K. Ikuta, Jap. J. Appl. Phys., II, 1684 (1972).

2. V. Bailey, Steady-State Current Drive in Tokamaks, Workshop Summary, DOE/ET-0077, National Technical Information Service (NTIS), Springfield, Virginia (February 1979).

3. S. Yoshikawa, Phys. Rev. Letters, 26, 295 (1971).

4. S. Yoshikawa and N. Christofilos, Proceedings of the Fourth International Conference on Plasma Physics and Controlled Nuclear Fusion Research, Vol. 2, p. 357 held in Madison, Wisconsin (1971); published by International Atomic Energy Agency, Vienna, Austria (1972).

5. C. W. Hartman, Phys. Rev. Letters, 267, 14, 826 (1971).

6. S. Yoshikawa, Bull. Am. Phys. Socl, p. 996 (November 1971).

7. J. Hammer and K. Papadopoulos, Nuclear Fusion, 15, 977 (1975).

8. V. Bailey, R. Cooper, and T.S.T. Young, Third International Topical Conference on High Power Electron and Ion Beam Research and Technology, Novosibirsk, USSR (July 3-6, 1979).

REFERENCES (Cont.)

9. Y-K. M. Peng and R. A. Dory, ORNL/TM-6535, Oak Ridge National Laboratory (October 1978).

10. J. Benford, B. Ecker, and V. Bailey, Phys. Rev. Letters, 33, 574 (1974).

11. M. Masuzaki et al., Jap. J. Appl. Phys., 14, 1413 (1975).

12. V. Bailey, Proceedings of the International Conference on Synchrotron Radiation and Runaway Electrons in Tokamaks, held in College Park, Maryland (1977).

13. A. Mohri et al., Proceedings of the Fifth International Conference on Plasma Physics and Controlled Fusion Research, IAEA-CN-37-X-5, held in Innsbruck, Austria (1978).

14. A. Bers, Steady-State Current Drive in Tokamaks, Workshop Summary, DOE/ET-0077, National Technical Information Service (NTIS), Springfield, Virginia (February 1979)

15. B. Coppi et al., Nucl. Fusion 19, 715 (1979).

16. H. Strauss et al., PPPL-1535 (1979), Princeton Plasma Physics Laboratory.

17. D. L. Jassby et al., PPPL-1371 (1977) and PPPL-1453 (1978), Princeton Plasma Physics Laboratory.

COMPACT TORUS RESEARCH AT U.C.I.

A. Fisher, S. Robertson, and N. Rostoker
Department of Physics, University of California, Irvine, California 92717

Compact torus research at U.C.I. consists of several experimental and theoretical programs involving intense electron and ion beams, field-reversed mirrors, and toroidal confinement systems. These programs are based upon an earlier program of research into field reversal and heating with intense electron beams.[1]

I. Spheromak Generation by Beam Induced Currents.[2]

In this experiment a closed, field-reversed magnetic configuration is created by return currents induced in initially neutral gas by a rotating relativistic electron beam. The electron beam (1 MV, 100 kA, 50 nsec) is made to rotate by locating the cathode at the end of a helically wound supporting shank which generates a cusp-like field only during the beam pulse. Initially, a cylindrical metal vacuum chamber (20 cm dia × 40 cm) is filled with 200 mTorr neutral hydrogen gas. One end of the chamber is made of thin, low resistivity aluminum foil. All of the walls conserve flux, i.e., the magnetic diffusion time through the walls is longer than the time scale of the experiment. Therefore no field lines may pass through the container during the course of the experiment. This elementary property of conductors assures that any magnetic field lines created within the container must close upon themselves. The electron beam is injected through the metal foil into the gas causing it to become ionized and conducting. The magnetic fields due to the beam current are then "frozen in" to the plasma which then carries a return current induced by the decay of the beam current (Fig. 1). The present experimental parameters are: peak toroidal field ≅ 1.5 kG, peak poloidal field ≅ 1 kG, decay constant = 5 μsec, and lifetime = 15 μsec. In an earlier version of the experiment the plasma parameters were found to be $n_e \cong 10^{14}\,cm^{-3}$, $T_e \cong 3 - 17$ eV.

If $\vec{J}$ is parallel to $\vec{B}$ at the boundaries then no currents should flow to the walls, i.e., the plasma current (like the B field) should close upon itself. Measurement of the current profile indicates that 32 kA flows "up" the major axis with 16 kA returning in the walls and 16 kA returning along closed current loops within the plasma. Detailed profiles of B_θ and B_z have been obtained and are being compared to theoretically derived force-free equilibria with cylindrical boundary conditions. In future experiments the cylindrical container will be replaced by oblate and prolate spherical containers in order to investigate the equilibria and stability of spheromaks of various elongations.

II. Spheromak Generation by Relativistic Electrons.[3]

In this experiment the risetime of the rotating electron beam (600 kV, 18 kA, 1 μsec) is longer than the Alfvén time of the target plasma ($n_e = 10^{12} - 10^{14}\,cm^{-3}$, $B_z = 1$ kG) so that, unlike the previous experiment, no return currents are generated. A reversal of the field by a factor of

two is observed; however, the lifetime is limited to the 1 μsec beam duration if the electrons are not confined. At the downstream end of the 1 m long plasma the electrons have been successfully contained by a 3:1 magnetic mirror. Reflection of the electron beam is observed. A fast pulsed gate coil is being tested to reduce the loss of electrons at the upstream end.

III. Intense Ion Beam Injection.

Neutral atomic beams have proved effective as a means of heating tokamaks and minimum B mirrors; however, their efficiency decreases as they are scaled to the higher voltages required by reactor-sized devices. Recently experiments at three laboratories (University of California, Irvine,[4] Naval Research Laboratory,[5] University of Tsukuba[6]) have shown that a sufficiently intense beam of ions that is space-charge neutralized by electrons will penetrate into a magnetic field. Our experiment in progress is to determine whether or not such beams can be efficiently trapped in a target plasma. The experiment is performed with a magnetically insulated diode ion source (100 kV, 15 A/cm^2, 1 μsec) and the *U.C.I. Tokamak* (R = 60 cm, a = 15 cm, B = 6 kG).

Intense ion beams are space-charge neutralized by electrons and thus may be created as plasma describable by the usual parameters of Debye length, plasma frequency, drift velocity, and thermal velocity. The beam plasma enters the magnetic field by self-polarization and E × B drift.[7] The transition to collective behavior occurs where there is more than sufficient beam energy density to set up the required field:

$$\frac{1}{2} n m_i V^2 > > E^2/8\pi \quad . \tag{1}$$

This expression may also be written

$$4\pi n m_i c^2/B^2 = \varepsilon - 1 = \omega_{pi}^2/\Omega_i^2 > > 1 \quad , \tag{2}$$

where ε is the plasma dielectric constant. At a field of 5 T (a typical value for conceptual reactor designs) the critical beam density at 100 kV corresponds to a current density of 9.2 A/cm^2 which is well within the capabilities of intense ion diodes.

In our experiment the ion beam is injected radially through a 15 cm × 30 cm injection port into the tokamak with only the toroidal field operated. Beam propagation is measured by Faraday cups, calorimeters, and floating potential probes. At the peak field of 6 kG, $\omega_{pi}^2/\Omega_i^2 \approx 10$ and 10 - 40% of the beam is detected calorimetrically at a point four Larmor radii into the field. Propagation is reduced when a shorting conductor is placed across the field lines near the injection port. Floating potential probes indicate potentials of + 60 - 100 kV within the field. One dimensional[8] and two dimensional[9] theoretical models have been developed which describe cross-field propagation. A parallel program of ion source development has demonstrated repetitive operation[10] and impurity control.[11]

IV. Electron Injection Into Closed Confinement Systems.

If an electron beam is used to sustain currents or to heat a fusion reactor with closed magnetic surfaces, the electron injector must be located outside the region of hot plasma and the beam must move into the plasma across magnetic surfaces by means of some collective or nonlinear effect, such as by means of image currents in the walls of the reactor. If the beam is entirely charge and current neutralized within the beam channel (as in Section I above), there will be no currents induced in the walls. We are therefore considering injection of a long pulse beam (as in Section II above) or a beam of variable rise and fall time into a tokamak or field reversed pinch. If the beam electrons carry angular momentum the stability properties of the field reversed pinch may be improved.[12]

The U.C.I. research staff includes G. Endo, W. Peter, G. Saenz, J. Schneider, and F. Wessel.

This research is supported by the United States Department of Energy.

References

1. K. Molvig and N. Rostoker, Phys. Fluids 20, 494 (1977); C. W. Roberson et al., Appl. Phys. Lett. 32, 214 (1978); C. W. Roberson, Nucl. Fusion 18, 1693 (1978); S. Robertson et al., Phys. Fluids, to appear.

2. G. Endo and S. Robertson, Bull. Am. Phys. Soc. 24, 1021 (1979).

3. G. Saenz and C. W. Roberson, Bull. Am. Phys. Soc. 23, 764 (1978); G. Saenz and A. Fisher, Bull. Am. Phys. Soc. 24, 1070 (1979).

4. S. Robertson et al., Bull. Am. Phys. Soc. 24, 1098 (1979).

5. J. A. Pasour et al., Bull. Am. Phys. Soc. 23, 816 (1978).

6. K. Kamada et al., J. Phys. Soc., Japan 46, 1693 (1979).

7. E. Ott and W. Manheimer, Nucl. Fusion 17, 1057 (1977).

8. W. Peter et al., Phys. Fluids 22, 1471 (1979).

9. W. Peter and N. Rostoker, Bull. Am. Phys. Soc. 24, 1098 (1979).

10. F. Wessel and S. Robertson, Appl. Phys. Lett. 34, 7 (1979).

11. G. Endo and S. Robertson, Appl. Phys. Lett. 35, 849 (1979).

12. N. Rostoker and A. C. Kolb, Phys. Rev. 124, 965 (1961).

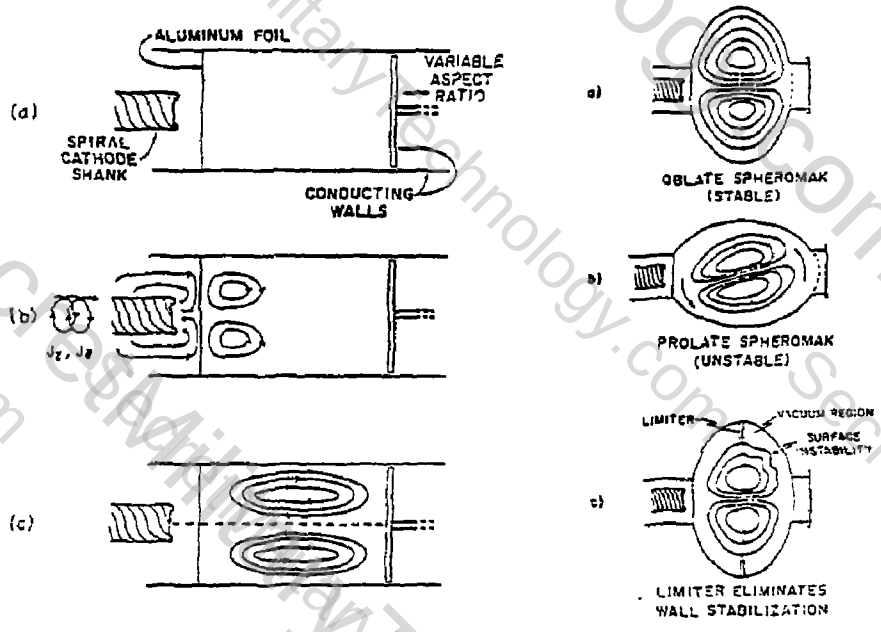

Figure 1.

Left: Spheromak start-up technique

(a) Before beam is fired no field lines are present.

(b) Rotating beam propagates through flux-conserving conducting walls.

(c) Beam leaves behind circulating return currents in plasma.

Right: Illustration of three experiments to examine spheromak equilibria and stability.

THE LONGSHOT INJECTOR: A 5/4 kJ, 120 keV PULSED SOURCE OF 3×10^{16} IONS FOR ION RING FORMATION

J. B. Greenly, D. A. Hammer, and R. N. Sudan

Laboratory of Plasma Studies, Cornell University, Ithaca, New York

Formation of a compact toroidal magnetic configuration using the diamagnetic current of large Larmor radius ions to produce a field-reversed ion ring was first suggested many years ago [1]. Experimental programs in ion ring formation have been undertaken at Cornell [2] and the Naval Research Laboratory [3], and diamagnetic proton layers have been formed, their propagation in magnetic mirror systems studied [4], and transient field reversal by a rotating proton beam observed [5]. Nevertheless, the goal of a trapped, field-reversed ion ring is far from being attained in these experiments because they are limited by the ion sources which have been available to them.

The short-pulse (100 nsec) magnetically insulated source used in the IREX experiments at Cornell produces only ~1.5 mcoul of protons per pulse, limiting the diamagnetism of the rotating beam (δB) to a few percent of the applied field (B_0) [4]. Also, the short-pulse beam does not propagate well across the strong cusp magnetic field which induces diamagnetic rotation, unless neutral gas (>30 mtorr) is introduced into the cusp region. The gas is needed to produce plasma in the beam channel which can respond to and neutralize the space potential that would disrupt an unneutralized proton beam.

The NRL experiment, using a reflex-type ion source and a much larger pulse power generator (Gamble II), is able to produce, and transport through a weak cusp, enough protons (~10 mcoul) to produce transient reversal ($\delta B/B_0 \sim 1.2$) of the weak guide field downstream of the cusp [5]. The pulse length of this beam is shorter than in the IREX experiment, and it seems likely that in using a strong cusp to slow the axial motion of the beam, as in IREX, beam propagation problems will appear. If neutral gas is required, it must either be isolated in the cusp or will, as in IREX, limit the ring lifetime to a few microseconds by ion-neutral collisions.

To overcome these limitations, we are developing at Cornell a new long pulse intense ion beam source, LONGSHOT, based on the "Pulselac" injector built at Sandia Laboratories [6]. The present LONGSHOT injector produces 5 mcoul at 100-150 keV (0.5-0.75 kJ) of ions in a 600 nsec pulse, with a pulse power generator considerably smaller than either the IREX or NRL experiment, and this long-pulse beam propagates well across a strong cusp in vacuum, without injection of neutral gas or provision of any active electron sources by charge neutralization.

The LONGSHOT injector is shown schematically in Fig. 1. It is an annular, magnetically insulated diode, with radial insulating field produced by coils in the grounded cathode structure. The insulating field is shaped by flux-excluding surfaces behind the anode, which is of the surface-flashover

type. A virtual cathode is formed by electrons emitted along the insulating field lines connecting the shaped cathode-defining surfaces. The annular ion beam passes between concentric drift tubes and exits the injector 15 cm from the anode-cathode gap. The injector is driven directly by a low inductance (0.6 μH) Marx Generator.

Typical diode voltage and current waveforms, and current of the extracted ion beam, are shown in Fig. 2. The current rises throughout the pulse, reaching >13 kA at the end of the voltage pulse. The ion current density 15 cm from the gap reaches >100 A/cm^2, a factor of 30 above Child-Langmuir space charge limited flow. This ion current density over the 140 cm^2 anode area accounts for essentially all the diode current, indicating very low electron current losses. The long pulse is made possible by good confinement of electrons in the gap, which also allows the large enhancement of ion current over Child-Langmuir flow.

Preliminary results of injection of the LONGSHOT beam across a cusp ($v_\perp/v \sim .5$) into a solenoid to form a diamagnetic layer are shown in Fig. 3. The observed beam diamagnetism, as well as the beam shape seen with damage targets, indicate that nearly all of the beam propagates across the cusp in vacuum (2×10^{-5} torr) without space-charge disruption. The mechanism proposed [6] for the observed charge neutralization is that electrons emitted from surfaces provided outside the beam channel are able to equilibrate in the beam by some dissipation mechanism, and to depress the space potential to near zero on a time scale of ~100 nsec. Thus, a small amount of the beginning of the long-pulse beam is lost to these surfaces, secondary electrons are emitted, and the rest of the beam propagates undisturbed in the resulting charge-neutral channel. The time required to reach neutralization is apparently too long to allow complete neutralization of short pulse (<100 nsec) beams.

The loss of the head of the long-pulse beam can be seen in the current density trace of Fig. 2, which (offset to eliminate time-of-flight) lags behind the rising diode current for the first ~100 nsec. Further beam loss in traversing the cusp appears to be small since the observed diamagnetic signal requires >75% of the total diode current in the rotating beam. Also the damage targets show the expected radial convergence of the beam indicating insignificant residual space charge. Once through the cusp, electrons can travel along field lines with the beam, which thus can remain charge-neutral as in the IREX experiments, without further losses [4].

The present LONGSHOT beam consists of ≥50% protons and ≤50% C^+ ions from the "flashboard" anode, and is of 1.5 m axial length in the downstream solenoid, giving $\delta B/B$ of ~5%. Experiments are underway to axially compress the diamagnetic layer in a downstream mirror, and $\delta B/B > 20\%$ would be expected if the present 5 mcoul pulse can be shortened axially to a length comparable to its 10 cm radius.

It appears practical, by straightforward scaling up of the present injector, to produce the 20-30 mcoul necessary for a fully field-reversed ring, ($\delta B/B_0 > 1$) with a relatively small and inexpensive device. Of equal importance are the superior propagation characteristics of the long pulse

beam. Furthermore, the LONGSHOT injector configuration is compatible with a long life, single ion species plasma gun anode source [6], and thus has the basic features necessary for development to a high efficiency, high repetition rate source of a pure proton or deuteron beam. Since the physics of the injection and ring formation process is dependent on the source characteristics (e.g., pulse length, as we have described), it is important to study ion ring formation with a source type that is compatible with the lifetime and repetition rate requirements of future applications.

This work supported by the U.S. Department of Energy.

References

1. N. C. Christofilos, Progress in Nuclear Energy; Series XI - Plasma Physics and Controlled Nuclear Fusion 1, 576 (1959).

2. P. L. Dreike, D. A. Hammer, R. N. Sudan, and L. G. Wiley, Phys. Rev. Lett. 41, 1328 (1978).

3. J. Golden, Bull. Am. Phys. Soc. 24, 966 (1979).

4. P. L. Dreike, J. B. Greenly, D. A. Hammer, and R. N. Sudan, Bull. Am. Phys. Soc. 24, 1032 (1979).

5. C. Kapetanakos, Proceedings this conference.

6. S. Humphries, Jr., J. R. Freeman, J. Greenly, G. W. Kuswa, C. W. Mendel, J. W. Poukey, and D. W. Woodall, Sandia Laboratories Report 79-1675 (August 1979).

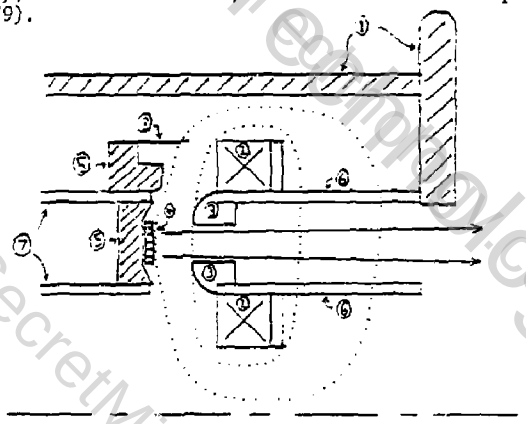

Figure 1. The LONGSHOT injector: 1) outer flux excluding vacuum vessel, 2) insulating field coils, 3) virtual cathode-defining electrodes, 4) "flashboard" anode, 5) field-shaping flux excluders, 6) stainless steel drift tubes, 7) anode support and connection to pulse power generator, 8) barrier blocking external breakdown path. Insulating field shown by dots. End flange is 15 cm from virtual cathode.

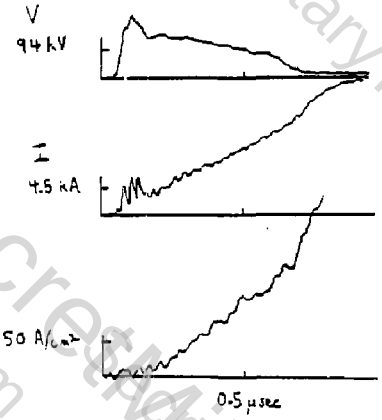

Figure 2. Typical diode voltage and current, and current density measured by biased charge collector 15 cm from gap. Current density trace has been offset to eliminate 50 nsec time-of-flight between gap and charge collector.

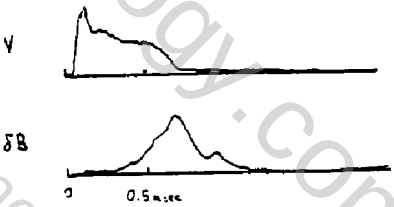

Figure 3(a). Diamagnetic signal at flux-excluding wall, showing time delay after diode voltage pulse due to time-of-flight, and peaks due to protons and carbon.

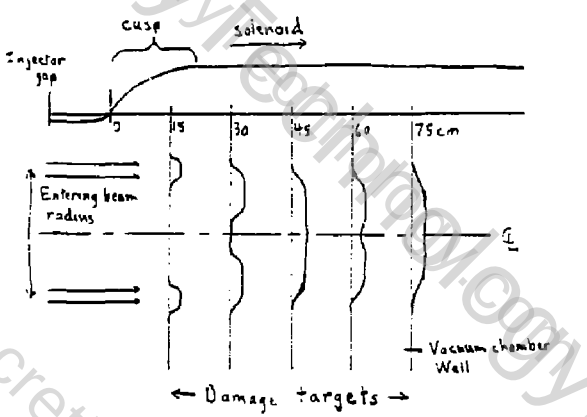

Figure 3(b). Qualitative damage patterns showing propagation of rotating beam. Canonical angular momentum is nearly zero, so ion orbits move inward, barely encircling the axis. Protons should be closest to axis at ~50 cm, C^+ moves inward slightly over this length. Velocity spread in entering beam mixes orbit phases by 75 cm.

REVERSED-FIELD CONFIGURATION WITH ROTATING RELATIVISITIC ELECTRON BEAMS

J.D. Sethian, K.A. Gerber, D.N. Spector and A.E. Robson
Naval Research Laboratory, Washington, D.C. 20375

The use of rotating relativistic electron beams to produce a field reversed configuration was first proposed by Christofilos.[1] In his Astron concept, the field-reversing currents were provided by the relativistic electrons. This paper describes a different method of achieving a reversed field geometry, in which the beam has been used to induce plasma currents, in originally neutral hydrogen gas, which then maintain the fields long after the beam has left the system.[2] Because the beam has both azimuthal and axial components, both axial (poloidal) and azimuthal (toroidal) fields are induced, and thus the configuration can be topologically similar to a Compact Toroid.

In this experiment, the rotating beam is produced by first forming an annular beam ($V \approx 900$ kV, $I \approx 80$ kA, $\tau \approx 100$ nsec.) in a field-emission diode immersed in a uniform axial magnetic field, and then passing this beam through a "half cusp" in which the field is brought to zero in a distance short compared to the electron Larmor radius. When injected into neutral hydrogen at a pressure of about 150 mTorr, the plasma produced by the beam is sufficiently dense to neutralize the beam charge, but not sufficiently dense to neutralize the beam current. As there is no applied magnetic field, the radial equilibrium of the beam is determined solely by the axial and azimuthal self-magnetic fields and by currents induced in the tube wall. Since the total axial flux inside the tube must be zero at all times, the axial fields inside and outside the beam are anti-parallel, automatically forming the reversed field configuration. The passage of the beam increases the plasma electron temperature. Thus, the induced magnetic fields must be frozen in the plasma, and, when the beam leaves the system, they are maintained by the induced plasma currents.

After the beam transits the system, the initial hydrogen gas is fully ionized and the electron temperature is typically 5 eV, as measured by Thomson scattering. The efficiency of conversion of beam energy to magnetic energy has been measured to be as high as 50%. That the configuration is maintained by plasma currents (rather than trapped beam electrons) has been shown by x-ray studies. The system decays over a period of 20μsec. During the first 5μsec the system re-arranges itself, converting toroidal magnetic field along its length into poloidal magnetic field at one

end. This is similar to the manner of a coil tending to maximize its inductance by axially contracting. After the re-arrangement process is stopped (presumably due to axial pressure gradients), the entire configuration decays uniformly with a time constant of about 8usec, which is consistent with classical resistive dissipation of the plasma currents, at the electron temperature of 7 eV measured by Thomson scattering. (The dissipation of the currents tends to heat the electrons, and in similar experiments an increase in electron temperature was observed several microseconds after the beam had left the system.)

In order to understand how the configuration is formed, a model which uses conservation of flux, particles, and canonical angular momentum to describe the beam propagation has been developed and experimentally verified.[3] Particles emitted from the diode are reflected at the beam head, giving a small fraction of their energy to the self-magnetic field. The axial motion of the beam front is retarded by the "inductive load" of the reversed field configuration, and, therefore, the beam front velocity, $v_f \sim .04c$, which is much less than the individual beam particle velocity ($\sim c$). As the particles return to the diode they are reflected by the electrostatic mirror in the anode-cathode gap, and are sent back into the beam. Because of the multiple reflection process, the beam density, and hence ν/γ, is increased to a value of approximately $c/v_f \sim 25$. Conservation of canonical angular momentum through the cusp shows that the axial flux enclosed by the beam is conserved to the order of (ν/γ). Furthermore, the beam current pitch angle and radius equal those of the plasma to the same approximation.

The configuration, in its present form, is not a genuine Compact Toroid, even though it contains both a poloidal and a toroidal field. This is because a net poloidal current flows from one end wall, through the plasma, to the other end wall, and returns along the side wall of the system. (See Fig. 1.) Because the system is maintained by plasma currents, this flow of current to the wall represents a loss mechanism. In contrast, a Compact Toroid would have the poloidal current completely enclosing the plasma, as shown in Fig. 1b. (Note that what differentiates the present system from the desired configuration is that the poloidal current lines, not the poloidal field lines, are not closed in the plasma.) The reason for the existence of this net poloidal current can be seen by considering how the configuration is formed: As the electron beam propagates from one end of the system to the other, it carries a net axial current. Because the current must eventually return back to the electron beam generator, preferably by the lowest inductance path available, it chooses to flow radially outward from the beam head (carried by secondary electrons) and then back along the drift tube wall. This produces a net toroidal field between the beam, and after it passes, the plasma, and the tube wall.

To eliminate the net current, then, would require the elimination of this large net toroidal field. This cannot be achieved through simple interruption of the poloidal current path or reflection of the beam electrons, as large inductive voltages will arise to drive plasma currents that maintain the field.

It is possible, however, that the current lines can be closed with two counterstreaming beams. (Equilibrium for the two beams has been predicted by extrapolating the single beam model.) This process is envisaged schematically in Fig. 2. Initially, a reversed field configuration identical to the present one is formed with one beam. After the beam has passed out of the system, a second rotating beam, whose net poloidal current is equal to that flowing in the plasma, is injected at a larger radius and from the opposite end of the tube. As this beam is rotating in the same sense of the first, the poloidal field is amplified. The opposing net poloidal current, however, nulls the toroidal field external to the plasma. As the poloidal current now flows along one beam path and returns on the other, the configuration is free to contract axially without interrupting any current paths. Such a contraction is expected to take place as it is energetically favorable. Moreover, axial contractions have been observed in previous reversed field configurations such as reversed field theta pinches. In addition to closing the field lines, if the current of the second beam exceeds that of the first, it could also be used to heat the plasma. By adjusting the plasma density so that the second beam current is completely neutralized, save that necessary to cancel the initial poloidal current, the un-neutralized portion of the current will complete the configuration, and the return currents neutralizing the remainder will heat the plasma as they are dissipated. Experiments to test these concepts are currently underway.

References

1. N.C. Christofilos, Proc. 2nd Int. Conf. on Peaceful Use of Atomic Energy (United Nations, Geneva 1958) Vol. 32, p. 279.

2. J.D. Sethian, K.A. Gerber, D.N. Spector, and A.E. Robson, Phys. Rev. Lett. 41, 798 (1978).

3. J.D. Sethian, K.A. Gerber, D.N. Spector, and A.E. Robson, submitted to Phys. Fluids.

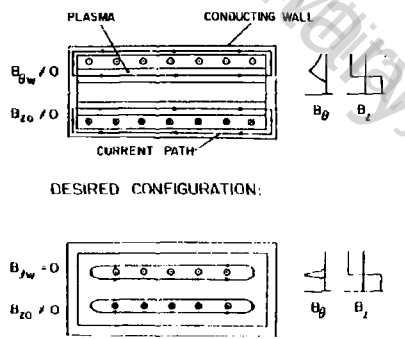

FIGURE 1

Present Configuration (UPPER)
Compact Toroid Configuration (LOWER)

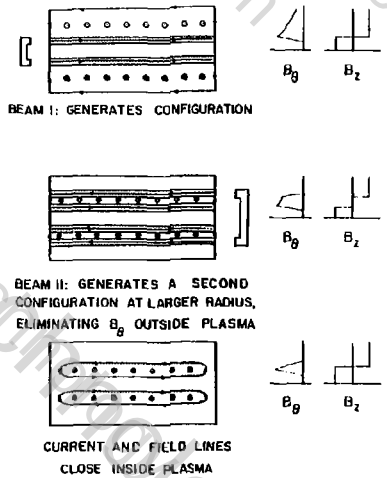

FIGURE 2

Closure of Poloidal Current Lines with two Counterstreaming Electron Beams

RESULTS AND PRESENT STATUS OF THE RELATIVISTIC ELECTRON RING EXPERIMENTS AND THEIR APPLICATION TO SPHEROMAK PROBLEMS*

H. H. Fleischmann
School of Applied and Engineering Physics, Cornell University, Ithaca, NY 14853

This paper is to summarize briefly the results and present status of the Cornell RECE program on field-reversing electron rings in particular with regard to potential applications of these results to other Compact Toroid concepts. Since its initiation in the early 70's, this program is aimed mainly at testing various physics questions related to the use of field-reversing fast-particle rings for the confinement and/or heating of a fusion plasma as envisioned by various authors (e.g., Refs. 1-3). In the related experiments, fast-electron rings are generated by injection of intense relativistic electron beams; their radius R normally is comparable to Larmor radius R_L of an electron having the maximum accelerator energy[4] in the applied magnetic field, as it had been envisioned in the original Astron[1] and the Ion Ring Compressor[2] concepts. Correspondingly, they may be considered as a large-orbit limit of the normal Field-Reversed Mirror (FRM)[5] scheme; they differ, however, in this regard from the similar SPAC-experiments[6] at Nagoya for which R/R_L=(a few). With field-reversal times of up to 1 msec, these rings, together with the SPAC rings,[6] constitute the longest-living Compact Toroid rings at this time. We envision, also, a number of related future applications of fast-electron and/or ions in the Compact Toroid area including (i) the injection of relativistic electrons into Spheromak[7] rings either for providing and/or maintaining the poloidal surface currents that otherwise may lead to a rapid resistive decay of these rings or (and) for help in the stabilization of the predicted[7] tilting modes, which may result through a change in coupling between the tilting motion and the internal deformation of the rings, as well as from the angular momentum of the fast particles. (ii) In addition, our estimates indicate that such electron or ion rings also may become useful for the generation of other CT rings in present experiments as well as for reactor applications.

RECE experiments have been performed and field-reversing rings have been obtained so far in three separate devices: (i) RECE-Christa[8] [see Fig. 1, tangential injection, nominal beam energy presently 3 MeV-5 MeV available, B_z≈500(1000) Gauss, toroidal field B_θ=(1-2)B_z, R=7-15 cm, ring current $I_z \lesssim$ 20 kA, field-reversal time ≤ 1.1 msec]; (ii) RECE-Berta[9] (tangent. inj., 0.4 MeV, 200 Gauss, no B_θ, 8-10 cm, ≲5 kA, few usec, respectively); and (iii) CHIP[10] (cusp inj., 0.4 MeV, 600 Gauss, 3-4 cm, no B_θ, ≲ 3 kA, few usec, respectively).

In all devices and under a wide variety of conditions, the observed electron ring behavior in most cases is now well understood and consistent with relatively simple theoretical analyses. Generally interesting are, in particular, the following results:

(i) Electron rings with field-reversals of up to 190% (RECE-Berta), 170% (RECE-Christa), and 120% (CHIP) have been obtained, and these rings generally show a smooth, stable decay well consistent with a purely collisional decay due to multiple scattering of the fast electrons in the background gas. In particular, we have not observed so far any tilting or wobbling instability. We feel that this is due to a specific coupling of the tilting motion with a widening of the minor ring cross section (due

to the large orbitals of the fast electrons) so that the energy balance becomes unfavorable for this mode. It appears that a similar effect may still be exploited in mixed systems with fast-electron and plasma currents.

(ii) The precessional mode[11] of the rings could be stabilized in RECE-Berta[12] either by conducting walls, toroidal fields or multipole/Ioffe fields with the stability limits in all cases agreeing well (10-20%) with theoretical analyses (including also significant increases due to partial flux penetration). In addition, studies with vertical field gradients[13] showed stable ring equilibria with the rings leaning against the conducting wall which open the possibility to provide radial feedback stabilization in reactor-type CT rings.

(iii) The application of weak Ioffe fields in RECE-Berta[14] generated anomalous fast-particle losses which are explained in full detail by a breakage of the normal fast-particle confinement due to conservation of the canonical angular momentum P_θ. This breakage becomes particularly serious for some resonant particle orbit. Quite importantly, the related theory predicts similar effects to occur quite strongly around the field-reversal point for ring geometries of the 2XIIB type. Such particle effects clearly will need careful examination in any non-symmetric system.

(iv) In RECE-Christa, field-reversing rings were moved successfully[15] and in good agreement with theory axially over distances of up to 1.5 m in a constant gas density as well as out of a high-density gas puff into low-density gas. Axial ring movement as it is planned in some reactor projections clearly will not constitute a serious obstacle.

(v) Field-reversing rings have also been compressed[16] in RECE-Christa without the occurrence of instabilities and in good agreement with theoretical calculations. Also, it was observed [17] that rings of roughly equal strength would readily combine, "stack," to produce a field single field-reversing ring.

(vi) Strong electron rings in RECE-Christa also have been observed in low-density gas (~1-2 mTorr) without indications of microinstabilities. In this case, the collisional rate of plasma electrons with gas molecules is considerably smaller than the collision rate with plasma particles, although gas collisions still will maintain a low plasma temperature.

Overall, these results clearly indicate good prospects for the usage of large-orbit particles either alone or in combination with plasma currents as envisioned in various CT schemes. On a reactor scale where the ring lifetimes will be larger than the flux conservation times of conducting walls, the radial ring stability will have to be provided either by feedback (recent calculations[18] indicate that this could be done quite easily on field penetration time scales) or by a rapid axial movement of the rings.

Regarding the trapping of fast particles in plasma rings like Spheromaks it will be important to provide some means for a change of the magnetic field configuration. In the RECE experiments, normally this is done by providing gas densities of 0.1-1 Torr in the trapping region. In this case, measurements[19] indicate that beam trapping occurs via fast field changes both before ionization of the gas and subsequently resulting from the high resistivity of the weakly ionized plasma. Alternate experiments were performed in RECE-Berta with beam injection into a gun-injected plasma.[20] In this case, detailed measurements and analyses showed the generation of large-amplitude Alfvén waves with the electrons being trapped and separated from the injector by

these waves. In agreement with this analysis, best results were obtained for the lowest useful plasma densities, $n=10^{11}cm^{-3}$, which were comparable to the beam density at injection. Unfortunately, Alfvén transit times across the ring still were longer than beam injection times, and only rings with $\delta \leq 30\%$ could be obtained. Estimates, however, indicate that a similar trapping mechanism may be possible for beam injection into Spheromaks.

The main open question presently concerns the plasma confinement characteristics of the field-reversing rings, and the effort of the RECE program now mostly is directed at this point. For this purpose, various changes were and are being incorporated into the RECE-Christa device to obtain for at least a few msec, the low gas density ($3x10^{-4}$ Torr) around the ring and the high energy input into the ring plasma required to overcome the radiation barrier. These changes include (see Fig. 2): (i) a change to puffing of ethane which both is slower and has a sufficiently low vapor pressure at liquid nitrogen temperatures, (ii) the addition of an LN cooled cryopump along the tank wall, (iii) a lengthening of the tank by 1.5 m, and (iv) the addition of a small axial heating coil which is to induce low-frequency plasma currents $I_{p_z} \leq 0.1\ I_\theta$ in the ring. Assuming full success and good plasma confinement, the plasma and ring parameters shown in Table I are expected.

Preliminary experiments were performed at the present beam energy to test various subquestions. In these quite successful tests, very strong layers with $\delta=2$ have been trapped in ethane clouds, and rings with $\delta=1$ have been moved into the downstream well. In further preliminary tests, weak plasma currents (few percent of I_θ) have been induced in the rings without serious deterioration of the ring stability and lifetimes; also, some heating of the plasma electrons is indicated by optical line observations. Further experiments will be performed after completion of the present reconstruction phase in the next months.

Table I
Anticipated Plasma Confinement Experiments

Electron Ring Parameters (Full accelerator energy and compression)		Plasma Parameters	
E_e	$\sim$ 5-10 MeV	n_p	$\sim 3x10^{13}cm^{-3}$
R	$\sim$ 8-10 cm	$T_i = T_e$	$\sim$ 50-100 eV
δ	$\sim$ 1.5-2.0	I_p	$\sim 1/10\ I_{ring} \leq 10$ kA
B_z	$\sim$ 3-4 kG	P_{ohmic}	$\leq$ 100 kW
B_{tor}	$\sim$ 5-8 kG	τ_{Ei}	$\sim$ 400 usec
I_{ring}	$\sim$ 50-80 kA		
τ	$\sim$ 2-5 msec		

*Work performed under DOE Contract EY-76-S-02-2319.A001.

1) N. C. Christofilos, 2nd United Nat. Intern. Conf. Peaceful Uses of Atomic Energy (Geneva 1958), Vol. 32, p. 279.
2) H. H. Fleischmann, Conf. on Electrost. and Electromag. Confinement of Plasmas and Phenomenology of Relativ. Electron Beams (New York, March 1975), Ann. N.Y. Acad. Sci. 251, 472 (1975).
3) S. Yoshikawa, Phys. Rev. Lett. 26, 705 (1971).
4) The typical energy of the actually trapped electrons is poorly known so far and is expected considerably smaller.
5) W. C. Condit, Jr., et al., UCRL 52008 (February 1976).
6) E.g., A. Mohri, this conference.
7) M. N. Bussac et al., IAEA Conference (Innsbruck 1978), Vol. II, p.249.
8) E.g., H. A. Davis et al., Phys. Rev. Lett. 37, 542 (1976).
9) E.g., D. A. Phelps et al., Phys. Fluids 17, 2226 (1974).
10) R. E. Kribel et al., Plasma Phys. 16, 113 (1974).
11) E.g., H. P. Furth, Phys. Fluids 8, 2020 (1965).
12) E.g., D. M. Woodall, Ph.D. thesis, Cornell University, 1975.
13) R. A. Meger et al., Phys. Fluids 17, 2100 (1974).
14) E.g., S. C. Luckhardt, Ph.D. thesis, Cornell University, 1979.
15) D. J. Rej et al., Appl. Phys. Lett. 33, 910 (1978).
16) M. Tuszewski et al., Phys. Rev. Lett. 43, 449 (1979).
17) H. A. Davis et al., Phys. Rev. Lett. 39, 744 (1977).
18) R. E. Kribel et al., Bull. Am. Phys. Soc. 24, 928 (1979).
19) A. C. Smith, Jr., Ph.D. thesis, Cornell University, 1977.
20) A. C. Smith, Jr., et al., Appl. Phys. Lett. 32, 133 (1978).

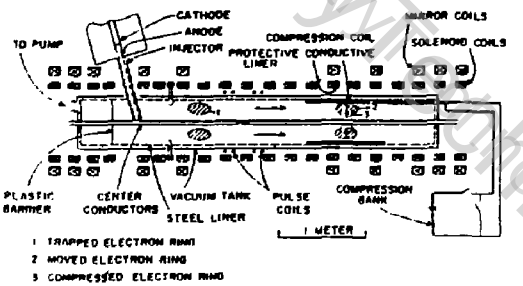

Fig. 1. Basic Schematic of RECE-Christa Device

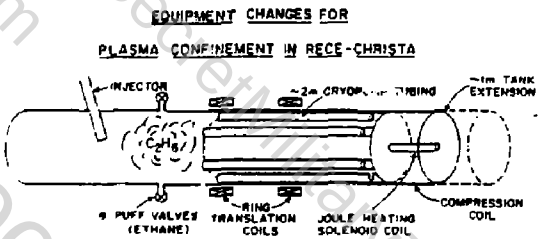

Fig. 2. Recent Changes in RECE-Christa for Plasma Confinement Experiments

REVERSED FIELD CONFIGURATIONS GENERATED BY PROTON PULSES*

J. A. Pasour, J. Golden, J. Marsh† and C. A. Kapetanakos, Naval Research Laboratory, Washington, D. C. 20375

I. Introduction

Magnetic field configurations with closed field lines are very promising for confining plasmas for thermonuclear applications because: (i) the plasma confinement time is considerably enhanced since the trapped plasma would have to cross the closed magnetic field lines in order to escape, (ii) the closed minimum -B magnetic field configuration provides hydrodynamic stability to the plasma, and (iii) the beta of the plasma can exceed unity resulting in high power density reactors.

Magnetic field configurations with closed field lines generated by energetic ion rings or layers have the additional advantage that the gyrating particles of the ring serve as an internal energy source for heating the confined plasma. The objective of the Ion Ring Program at NRL is to test the feasibility of forming strong ion rings that reverse the applied magnetic field by trapping about 10^{17} protons of 1-2 MeV energy inside a magnetic mirror.

II. Description of the Experiment and Results

A schematic of the experiment is shown in Fig. 1. The 5 meter long system consists of a low inductance inverse reflex tetrode (IRT), a magnetic cusp, a compressing magnetic field, a gate field and a magnetic mirror. In recent experiments the applied magnetic field has temporarily been modified by replacing the compressing field with a uniform field that is terminated in a single mirror. The proton source has been described previously.[2] In our best shots the total number of protons measured with the resonant reaction[3] $^{12}C(p,\gamma)^{13}N(\beta^+)^{13}C$ using carbon targets that are located 15 cm from the anode is in excess of 8×10^{18} per pulse. This number must be considered as a lower bound since protons with energy less than 470 keV do not activate the target and the number of counts is not corrected for target blowoff. The peak proton current is ~ 500 kA when the ramp shaped (corrected) voltage that is applied to the anode of the IRT increases from 0.6 MV to 1.7 MV within ~ 50 nsec. As a result of the ramp shaped voltage and the somersault effect[3], the ion pulse bunches axially. Magnetic probes that are located in the 1.5 kG, 75 cm long field plateau along the axis of the system show that the rotating ion pulse reverses the external field. The field reversal factor exceeds 120%. In addition, the signals of magnetic probes show that the ion pulse propagates with an axial speed v_z which is ~ 1.1 - 1.2 cm/nsec. The velocity of rotation v_θ is only 1/5 of v_z. The ratio v_θ/v_z is sensitive to the ratio of the magnetic field at the cusp B_c to the critical field of the cusp B_{cr}. The parameter $\alpha = B_c/B_{cr}$ was kept small, and so the ratio v_θ/v_z, in order to avoid excessive losses at the exit of the cusp. It appears that these losses are related to the long transition width δ of the cusp. In the present series of experiments δ is greater than the proton gyroradius because the cusp sharpening ferromagnetic disc has been removed.

This was necessary because of the substantial reduction in the inner and outer beam radii between the anode and the cusp. The radial profile of the beam and thus the change of its inner and outer radii is determined by individually counting small segments of a carbon target after it is activated by the beam. The dashed line in figure 2 shows the radial profile of the proton beam 15 cm from the anode. It is apparent that the thickness of the beam is appreciably greater than that of the anode foil. The observed "filling-in" of the proton beam is due mainly to the $qv_z B_\theta$ pinching force that acts on the ions inside the anode-cathode gap. The azimuthal magnetic field B_θ is generated by the ion current and the net electron current in the gap. It is estimated from the equations of motion, neglecting the radial electric field that at the cathode the protons have a radial velocity $v_r = v \sin\theta$, where v is the velocity corresponding to the applied voltage and

$$\sin\theta \approx (d/\tau V_o) \int_o^d B_\theta \, dz. \qquad (1)$$

In Eq. (1) d is anode-cathode gap, τ is the transit time of the ions, V_o the applied voltage on the anode and the integral is along the particle orbit. For d = 2 cm, $B_\theta = 10^4$ Gauss = const., $V_o = 1$ MV, Eq. (1) gives $\theta \approx 16°$.

In very recent experiments the "filling-in" of the beam has been substantially reduced by tilting both the cathode and anode with respect to a vertical plane in such a way that the protons obtain an outward directed radial velocity, which compensates the inward radial velocity of the pinching force. The solid line in Fig. 2 shows the radial profile of the beam at 15 cm from the anode for a tilting angle of 10°.

III. Conclusions

The elimination of the "filling-in" will make possible the operation of the system in higher magnetic fields, thus achieving higher velocity ratio v_θ/v_z without appreciable losses at the cusp. Trapping studies of the proton pulse using the magnetic field configuration of Fig. 1 will start in the near future.

IV. References

* Work is supported by ONR and DOE.

+ Sachs-Freeman Associates, Inc. Bladensburg, MD 20710.

1. C. A. Kapetanakos, J. Golden, J. A. Pasour, S. J. Marsh and R. A. Mahaffey, NRL Memorandum Report # 4135, 1979.
2. F. C. Young, J. Golden, and C. A. Kapetanakos, Rev. Sci. Instrum. 48, 432(1977).
3. S. J. Marsh, A. T. Drobot, J. Golden, and C. A. Kapetanakos, Phys. Rev. Lett. 39, 705(1977).

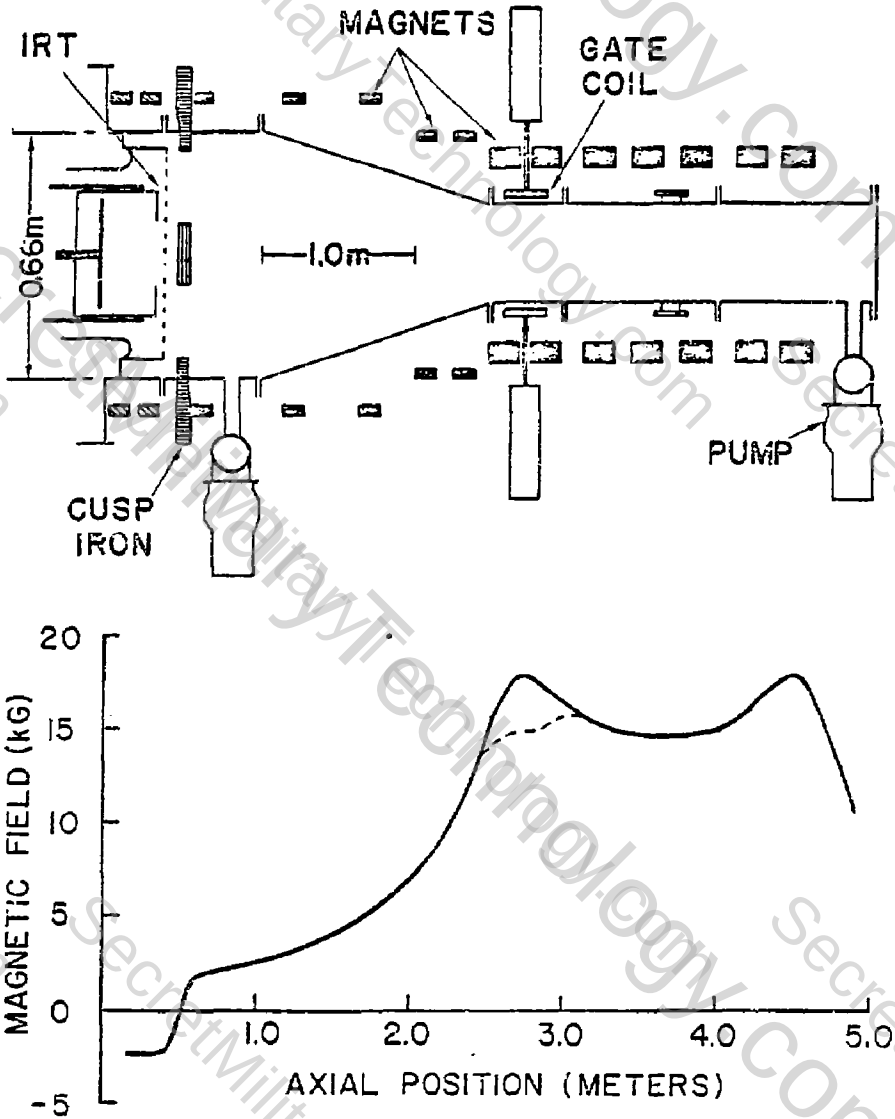

Fig. 1. Schematic of the experiment (top) and applied magnetic field configuration (bottom).

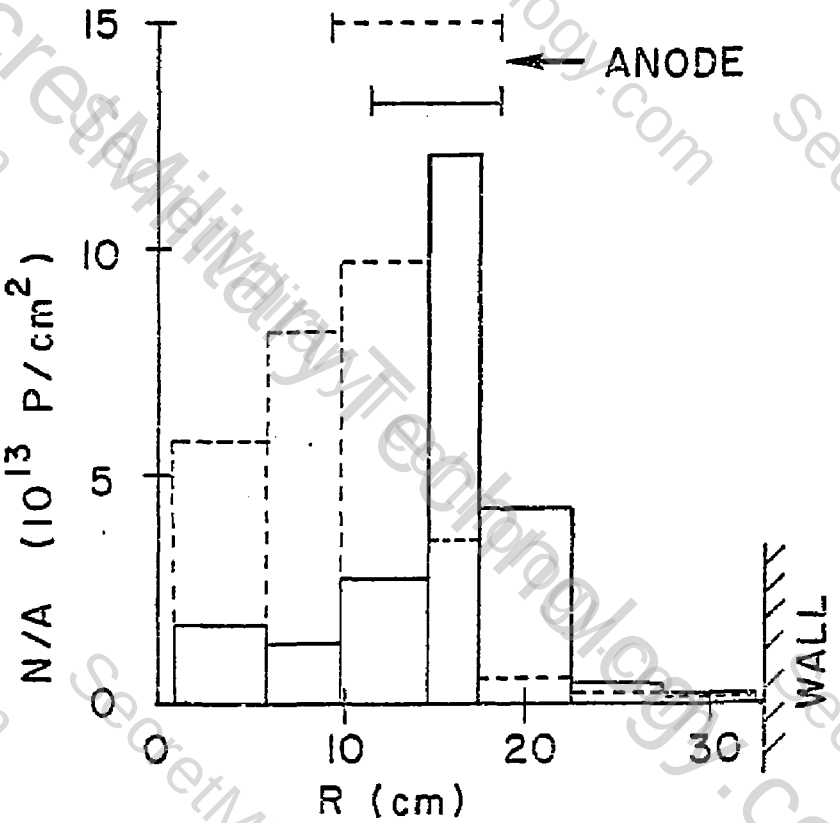

Fig. 2. Number of protons per unit area striking a carbon target 15 cm from the anode as a function of radius. The dashed line shows the radial distribution when the anode and cathode planes are perpendicular to the symmetry axis of the system. The solid line shows the radial distribution when the cathode and anode planes intersect the symmetry axis at an angle of 100°.

Thermal Background Effects On The Kink Instability of a Field-Reversing Ion Layer*

S. J. Yakura and T. Kammash
University of Michigan
Ann Arbor, Mich. 48109

Several papers have recently been written on the stability of electromagnetic modes in field-reversing ion layers immersed in cold background plasmas. Using a rigid rotor model Uhm and Davidson[1] (UD) examined the stability properties of a field-reversed ion layer by considering an infinitely long, thin layer situated in a cold magnetized background plasma which was treated by a fluid model. With a kinetic treatment of the layer ions these authors found that flute-like kink modes with frequencies near multiples of the mean ion-layer rotational frequency, ω_θ are unstable over certain ranges of positive and negative values of the compression ratio, and that the system with a dense background plasma can be stabilized by a sufficiently large transverse temperature of the layer ions.

In this paper we extend the work of (UD) by including the thermal effects of the background plasma and examining its impact on the stability of the kink modes. Because of the length and complexity of the analysis, the reader is advised to consult Reference 1 for the details and the notation; only the major modifications associated with the inclusion of the thermal effects will be presented here.

As in the above-mentioned reference we consider a space-charge neutralized ion layer with infinite axial extent and a mean radius and radial thickness of $\bar{R}_0 \left(= \frac{1}{2}(R_1 + R_2)\right)$ and $2a$ respectively. We assume that the equilibrium properties are azimuthally symmetric and that the layer thickness is much smaller than its radius. The layer is taken to be immersed in a warm background plasma and the whole system is placed in an equilibrium

*Work supported by DOE

magnetic field given by

$$B_z^0(r) = B_0 + \frac{2\pi e}{c}\,\omega_c\, n_b\,(R_2^2 - r^2) \qquad (1)$$

which can be utilized to define the compression ratio

$$\eta = B_z^0(r = R_1)\,/\,B_0 \qquad (2)$$

which in turn is related to Budker's parameter ν by $\nu = (1-\eta)/(1+\eta)$. A Vlasov treatment is used for the layer ions, while the remaining species including the background plasma are treated by a fluid model for which the momentum equation is given by

$$\left(\frac{\partial}{\partial t} + \vec{V}_j\cdot\nabla\right)\vec{V}_j = \frac{e_j}{m_j}\left(\vec{E} + \frac{\vec{V}_j\times\vec{B}}{c}\right) - \frac{\alpha_j^2}{n_j}\frac{\partial n_j}{\partial r} \qquad (3)$$

with α_j being the thermal velocity of the background plasma. If we take the equilibrium background plasma density to be uniform across the layer, and assume that the radial variations in its perturbed velocities to be small, we can linearize the fluid equations and calculate the perturbed radial current density which, along with the appropriate Maxwell equations and a Poisson equation that contains the layer's contribution to the perturbed surface charge density, give rise to an eigenvalue problem for the perturbed azimuthal electric field. The equation in question has the form

$$\left(\frac{1}{r}\frac{d}{dr}\,r\,\frac{d}{dr} - \frac{q^2}{r^2} + p^2 - A(r)\right)E_\theta(r) = 0 \qquad (4)$$

where

$$p = -\frac{\omega\,\omega_{p_i}}{c\,|\omega_{c_i}|}$$

$$q = \left\{1 + \ell^2\left(1 - \frac{2\omega}{\ell\,\omega_{c_i}}\right)\right\}^{1/2} \qquad (5)$$

and $A(r)$ is a lengthy term which contains the thermal effects to lowest order but which we will not list here due to space limitations. In the absence of $A(r)$ Eq. (4) reduces to that derived in (CD). When Eq. (4) is solved subject to the boundary conditions that the potential $= i r E_\theta/\ell$ is continuous across the layer ($r = R_0$) while its derivative is discontinuous, the wave

admittance[1] can be calculated from which a dispersion equation of the form

$$(\omega - \ell\omega_\theta)^2 = \ell^2 \frac{v_i^2}{R_0^2} - \frac{2\ell\nu c^2}{R_0^2} D(\ell\omega_\theta) \qquad (6)$$

is obtained with v_i being the layer ion thermal velocity. The thermal effects are hidden in the term $D(\ell\omega_\theta)$ and if we specialize to the case of a dense background plasma that results in a strong electromagnetic coupling[1] we find that the eigen functions of Eq. (4) are the ordinary Bessel functions $J_q(pr)$ with p and q given by Eq. (5).

The effects of the background plasma temperature on stability can be assessed by the sign of those terms in $D(\ell\omega_\theta)$ which are associated with the thermal effects. A positive contribution to the right hand side of Eq. (6) is stabilizing and such contributions are denoted by the shaded areas in Figs. 1 and 2. The first figure shows the thermally stabilizing regions for the $\ell = 2$ kink mode as a function of the compression ratio and the density parameter $(\omega_{pi} R_0/c)$ when compared to Fig. (8) of reference 1 it is seen that at $\eta = 0.82$ the stabilizing effects occur at those values of $(\omega_{pi} R_0/c)$ which correspond to the maximum growth rates. In Fig. 2 we observe the thermally stabilized regions for negative compression ratios. Although $\eta \geq -1$ i.e., complete field reversal is excluded from this analysis we note nonetheless the dramatic stabilizing effects of the background plasma temperature on layers with large field reversal. This figure should be viewed with Fig. 12 of reference 1 for comparison with the cold background case.

1. H. S. Uhm and R. C. Davidson, Phys. Fluids 22, 1329 (1979).

FIGURE 1

Shaded areas are thermally stabilized regions relative to the cold plasma case.

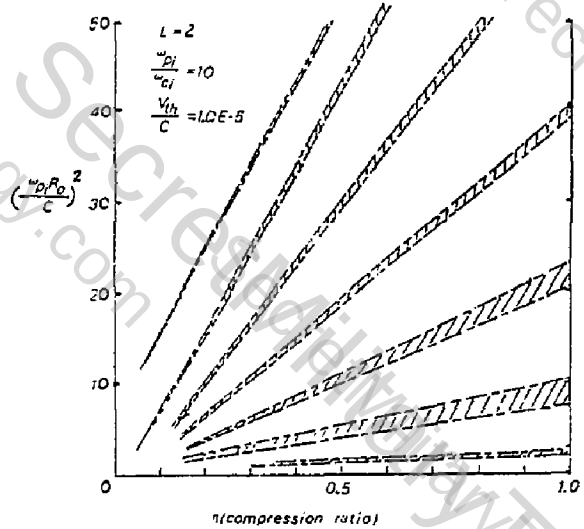

FIGURE 2

Shaded areas are thermally stabilized regions relative to the cold plasma case.

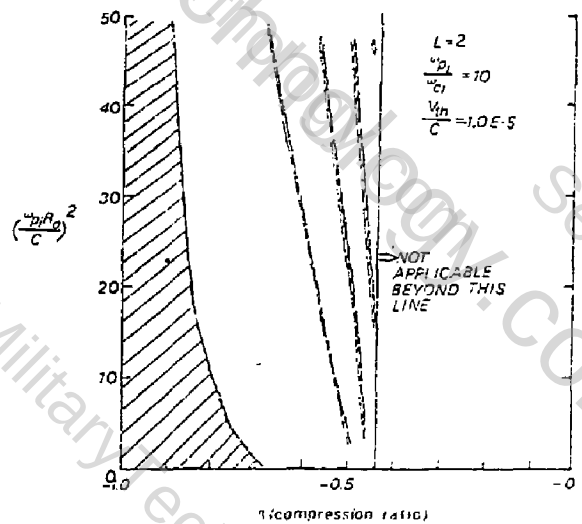

MAGNETIZED GUN EXPERIMENTS

T. R. Jarboe, I. Henins, H. W. Hoida, J. Marshall, A. R. Sherwood
Los Alamos Scientific Laboratory, Los Alamos, New Mexico 87545

In the Los Alamos Magnetized Gun Experiment we are attempting to produce a compact torus in a manner similar to an earlier experiment of Alfvén.[1] In our experiment a solenoidal coil is placed inside the inner electrode of a coaxial plasma gun. This coil produces an axial magnetic field inside the inner electrode which diverges and becomes a largely radial field in front of the gun muzzle. The idea is that when the gun is fired, the plasma escaping from the gun stretches these radial fields along the axial direction away from the gun, and these field lines can reconnect behind the plasma forming the poloidal field of the compact torus. The magnetic field generated by the gun current becomes the toroidal field and the major axis of the compact torus will be the same as the axis of the coaxial gun. Recent interest in this possible method of compact torus generation was stimulated by C. Hartman, and the approach is also being pursued in the field-reversed plasma gun experiment at LLL.

The objective of our initial experiments is to study the generation of compact tori hopefully formed in the above-described manner when the magnetized plasma gun is fired into a flux-conserving cylindrical shell. Preliminary results are reported for injection into a 0.46-m diameter, 1.2-m long, 1.6-mm thick stainless steel, flux-conserving shell placed 0.13 m from the gun muzzle. In these experiments we have demonstrated that the addition of a magnetic "bias" field between the gun electrodes parallel to the axis of the gun allows it to be operated at much lower fill pressure and makes the gun discharges much more repeatable. In the results discussed here, the total gas puffed into the gun is 0.75 atm cm^3 of D_2. The gun is energized with a 37-μF capacitor bank charged to 45 kV. The length of the gun is 0.70 m and the electrodes have 0.10-m and 0.15-m radii. The current peaks at a value of about 0.8 MA and reverses at about 4.5 μs. The gun current is about one-third of its peak value at 3.5 μs when the current sheath reaches the muzzle. The $\int VIdt$ shows that the gun absorbs almost all of the bank's energy during the first 2.5 μs of the discharge. So far, the only diagnostics used in the flux conserver are magnetic field probes. When the plasma emerges the gun muzzle, these probes see a disturbance which propagates at a velocity of about 10^8 cm/s into the resistive flux conserver. The strength of the initial radial magnetic field is found to strongly affect the downstream magnetic field pattern. For low radial fields the gun plasma pushes the magnetic field configuration completely through the shell, whereas for high fields the configuration barely penetrates. For intermediate values the configuration stops within the flux conserver. This effect is best shown by observing the axial component of the magnetic field on the axis of the flux conserver for various radial field values. (See Fig. 1.) For the rest of the data reported here the initial magnetic field inside the inner electrode of the gun was set at 8 kG. This is the average value over the 20-cm diameter inner electrode. With this field strength the field disturbance propagates into the flux conserver, stops with reconnection apparently occurring, and remains with little or no axial motion. This is possible, since the plasma can be almost stopped by the work required to stretch the

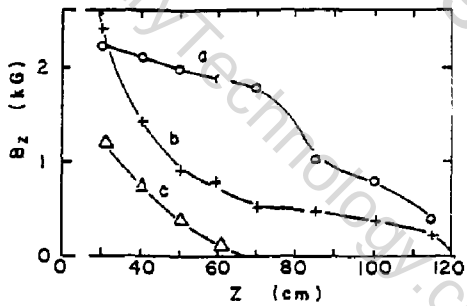

Fig. 1. B_z in the flux conserver at 10 μs after the voltage is applied to the gun for initial magnetic fields of a) 4.5 kG, b) 10 kG and c) 19 kG inside the inner electrode of the gun.

field lines and the remaining motion can be arrested like the current ring in Astron because the flux conserver is resistive.

We have a set of 20 probes in one jacket mounted perpendicular to the axis of the flux conserver. By rotating the probes we can measure either B_z or B_θ. These field directions are with respect to the natural cylindrical coordinate system for the magnetized Marshall gun and flux conserver. Figures 2 and 3 show B_z vs r and B_θ vs r at various times as measured by these probes. These measurements show an overall change in the magnetic field profile occurring over a period of roughly 10 μs. A possible interpretation of these data is shown in Fig. 4. In this interpretation the compact torus is generated with its major axis parallel to the axis of the gun. But then the axis of the torus rotates 90° to make a more "oblate" compact torus. This tipping of a prolate compact torus has been predicted.[2] The axis of apparent rotation is orthogonal to the probes' jacket in the data shown here and thus if the probes are measuring poloidal field before the rotation as in Fig. 2, they are measuring poloidal field after the rotation also. The same is true for toroidal field in Fig. 3.

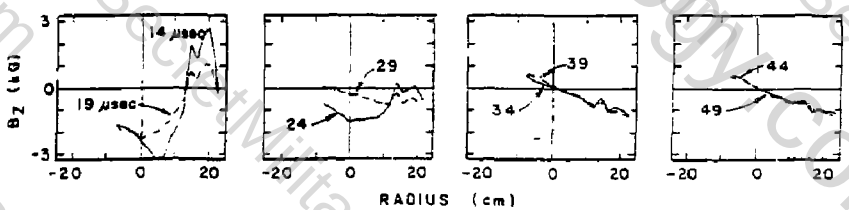

Fig. 2. B_z vs r at various times measured 0.49 m from the gun end of the flux conserver. The probes are measuring poloidal field.

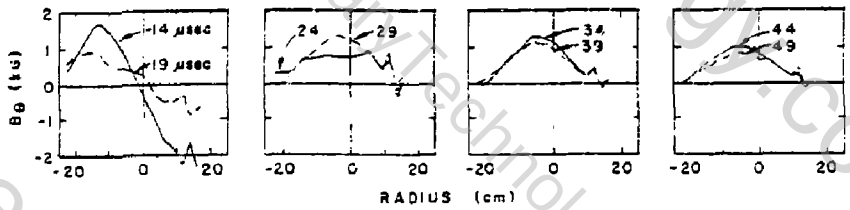

Fig. 3. B_θ vs r at various times measured 0.49 m from the gun end of the flux conserver. The probes are measuring toroidal field.

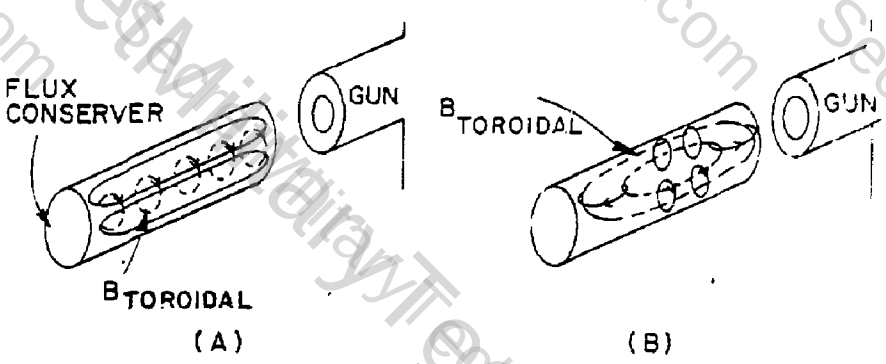

Fig. 4. One interpretation of the data shown in Figs. 2 and 3. a) Initially the compact torus axis is parallel to the axis of the flux conserver and the compact torus is prolate. b) Later the axis of the torus is perpendicular to the axis of the flux conserver and the compact torus is oblate.

Finally, we have another group of probes that have three coils at each position so that all components of $\vec{B}$ can be measured at each of seven locations. This group of probes is all in the axial plane which is orthogonal to the jacket of the 20-probe set. Figure 5 shows data from these seven positions for the same shot as shown in Fig. 2. These probes gave very similar data on the shot used for Fig. 3 except that the apparent rotation occurred earlier in this case. The shot from which data for Figs. 2 and 5 came was not typical in that the rotation occurred very late. On many shots the field profile has the signature of a rotated torus a few microseconds after the 20-position probe receives a signal and a prolate compact torus signature is never observed. Although the time history may vary from shot to shot, the apparent direction of the axis of the final configuration tends to be the same on most shots. However, on some shots the axis of rotation

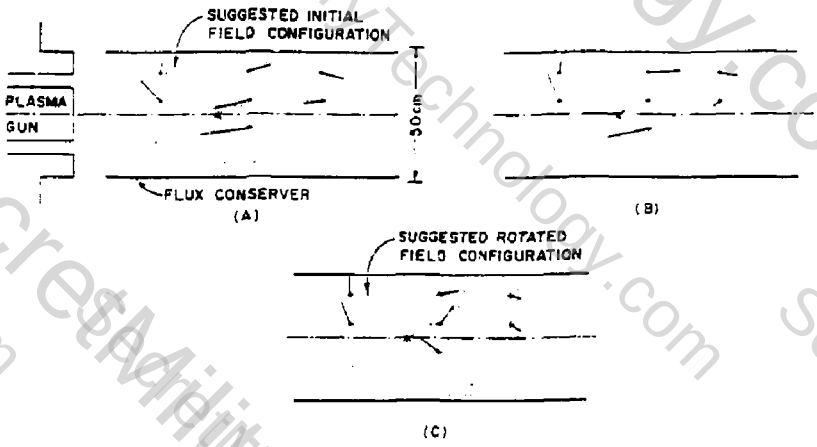

Fig. 5. Magnetic field data from seven multidirectional probes which are in the same plane. The + is the probe location and the line is the vector representation of $\vec{B}$ pointing away from the +. A) The initial poloidal fields are consistent with a prolate compact torus. B) This is during the transition period from prolate to "oblate." C) These final fields are the toroidal fields of the 90° rotated "oblate" compact torus. The * represents the position of the jacket of the set of 20 probes.

appears to be in a different direction but the data still seem to be consistent with a rotated compact torus. The data shown in Fig. 5 are consistent with the interpretation of the stopping of a prolate compact torus and its subsequent rotation of 90°. For these probes the axis of rotation is in the plane they define. Therefore, since this plane contains poloidal fields initially, it will contain toroidal fields finally. Once the final configuration is reached it appears to be MHD stable and the toroidal field decays away with a time constant of 40 μs. The L/R time of the flux conserver is about 300 μs.

Although these data are preliminary, it appears that there is considerable evidence for rotation of the configuration. Additional probes are being constructed so that a more detailed understanding of the history and spatial pattern of the magnetic field can be determined.

References

1. H. Alfven et al., J. Nucl. Energy, Part C: Pl. Phys. 1, 116 (1960).

2. M. N. Rosenbluth and M. N. Bussac, Nucl. Fusion 19, 489 (1979).

FORMATION OF A COMPACT TORUS USING A TOROIDAL PLASMA GUN

Morton A. Levine and Philip A. Pincosy

Lawrence Berkeley Laboratory
University of California
Berkeley, California 94720

Myers, Levine and Pincosy[1] report results using a toroidal plasma gun. The device differs from the usual coaxial plasma gun in the use of a strong toroidal bias current for enhanced efficiency, a pair of disk-like accelerating electrodes for reduced viscosity and a fast pulsed toroidal gas valve for more effective use of the injected gas sample. In addition, a technique is used for generating a toroidal current in the plasma ring. The combination offers an opportunity to deliver a plasma with a large amount of energy and to vary the density and relative toroidal and poloidal magnetic field intensities over a range of values. It is the purpose of this paper to report further experimental results, to project the gun's applications to the formation of a compact torus, and to propose a simple modification of the present apparatus as a test.

The gun consists of a pulsed toroidal gas valve (opening time ~ 50 microseconds) that injects a symmetric ring of gas between two annular plates. After a delay of about 100 microseconds, to allow time for the gas to distribute itself between the plates, a 4.4 microfarad capacitor charged to a maximum voltage of 50 kV is connected across the plates resulting in a half cycle time of 0.75 microseconds. Gas breakdown occurs in the breech of the gun in the region where the gas is injected and $\underline{J} \times \underline{B}$ forces accelerate a plasma ring outward. This acceleration is enhanced by the application of a bias toroidal magnetic field and its direction is determined by the relative direction of the current in the plasma and the bias current. Thus, normally during the first half cycle of the capacitor discharge the plasma is accelerated radially outward toward the muzzle of the gun, and during the second half cycle the gas in the gun is accelerated inward toward the breech which is left open in the gun.

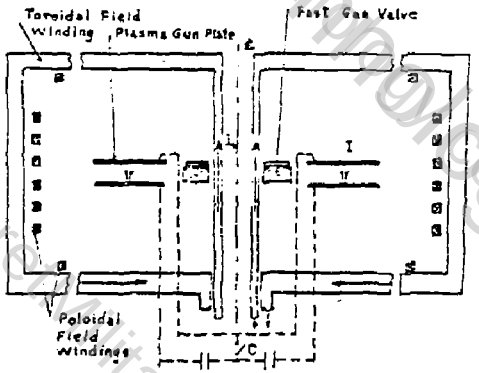

*This work was supported by the U. S. Department of Energy, Office of Fusion Energy, under contract No. W-7405-ENG-48.

The total number of particles in the plasma ring is regulated by the filling pressure of the plenum in the gas valve and in practice can be varied from 10^{18} to 10^{19} particles (hydrogen).

It has been shown in a computer program which solves a set of coupled equations for the driving circuit that the dynamics of the gun are such that the total plasma kinetic energy after leaving the gun is roughly constant (currently 50% capacitor stored energy) over a wide range of particle number.

$$(1) \qquad \frac{\partial v}{\partial t} = \frac{1}{M(R)} \left\{ \frac{\mu_o d}{4\pi R} [I^2 + 2I\ I_o] - \frac{\partial v_\rho}{\partial R} - v^2\ \frac{\partial M(R)}{\partial R} \right\}$$

$$(2) \qquad \frac{\partial M(R)}{\partial t} = m(R)v, \qquad (3) \qquad \frac{\partial R}{\partial t} = v, \qquad (4) \qquad \frac{\partial V_c}{\partial t} = \frac{I}{C}$$

$$(5) \qquad \frac{\partial I}{\partial t} = -\left(L_s + \frac{\mu_o d}{2\pi} \log\left(\frac{R}{R_o}\right)\right)^{-1} \left\{ \frac{\mu_o d}{2\pi} \left(\frac{I+I_o}{R}\right) v + I\ R_s + V_c \right\}$$

R(t) is the radius of the plasma sheet, V_ρ is the potential due to the poloidal magnetic field, R_o is the initial radius at t = o, v(t) is the velocity of the snowplow. M(R) is the total mass swept up by the snowplow when it reaches radius R, m(R) is the initial mass distribution per unit length between the plates, and I(t) and I_o are the plasma and bias current respectively. R_s and L_s are stray resistance and inductance and d is the separation of the plates. C is the capacitance of the driver with a voltage $V_c(t)$.

Early data was taken with accelerating plates 38 cm O.D., 19 cm I.D. and with a 3 cm separation. The capacitor driver had a SCYLLAC type spark gap with a 2.1 μF capacitor, 50 kV and 150 nH. The bias current was a 0.3 meg amperes.

In the earlier low energy test, plasma velocities of 15 cm/microsec to 20 cm/microsec were obtained. The accelerated plasma had 10^{18} to 6×10^{18} particles and had a Mach number of the order of 2. In this configuration the plasma could be stopped and trapped using a poloidal magnetic field in the form of a toroidal bicusp.

Measurements were made using magnetic probes, radiation detectors, Faraday cups and a moveable laser interferometer. Particle densities and velocities were inferred by assuming cylindrical symmetry from the interferometer data.

Velocities were measured from a series of shots in which the interferometer was moved. Particle count before the plasma was stopped was inferred from the measured line density of electrons and a velocity inferred from the shot series. These measurements indicated that over 60% of the particles came out of the gun during the first burst. The magnetic probe measurements showed the first burst to contain a paramagnetic plasma with 2 kiloamperes to 6 kiloamperes of toroidal current.

Stopping and trapping the plasma in a poloidal magnetic field depends on toroidal symmetry to close the currents generated in moving into such a field. In fact, when the plasma is known to be assymetric, trapping does not occur. Interferometer data measuring the trapped plasma indicates that essentially all the particles were trapped. This result coupled with the magnetic probe results seemed to justify the assumptions of toroidal symmetry.

More recently, in order to increase the plasma energy, a larger, low inductance driver was installed in the system. This system has a total inductance of 13.5 nanohenries for capacitors, switch, leads and gun; so that the new system shows efficiencies of greater than 50% of the energy in the capacitor delivered to the first burst of plasma. This system under limited tests has given a plasma velocity of 45 cm/microsecond for a burst of 8×10^{18} particles corresponding to a Mach 6 plasma.

The use of a bias magnetic field parallel to the driving magnetic field in a plasma gun has the advantage that it is inherently more efficient and less dirty. This can be seen from Equation (1) where the driver term is proprotional to $(I^2 + 2 I I_o)$. I_o is the bias current and I the plasma current. Since the plasma current is introduced through electrodes, this interaction is reduced when I is reduced. Also apparent from Equation (3), small values of I lead to higher electrical efficiency for the same drive.

The disadvantage to using a bias current is that the current is closed outside the plasma and the plasma is created within a coil structure. To form a compact torus it is necessary to remove the plasma from the coil by passing through spokes.

Removing the plasma from the coil may not be as difficult as it first seems. Predicting the behavior of the plasma is simplified if the plasma is moving at supersonic velocities. In the experiments so far performed with the toroidal plasma gun there has been a range of Mach numbers of from 2 to 6. Higher energy plasmas can be expected to give even higher Mach numbers.

Consider a toroidal plasma with a toroidal field moving with a Mach number, M. The toroidal field is produced by a current I_o flowing through the center of the system and returned through n bars each carrying I_o/n abamperes. We make the approximation that the magnetic field near the bars is given by $B = 2I_o/rn$ Gauss where r is the distance from the center of each bar. The toroidal magnetic field in the plasma is approximately $B_o = 2I_o/R_o$ Gauss. (The actual field is slightly higher due to a paramagnetic effect in the plasma as is characteristic of the Tokamak configuration.)

As plasma approaches the bars the plasma is compressed. However, the disturbance cannot be communicated to the rest of the plasma because of the supersonic flow. A characteristic bow shock then forms with a stand off distance such that the magnetic field pressure near the bar balances the directed momentum of the plasma, i.e., $1/2\ \rho v^2 = B^2/8\pi$ or $v = B/\sqrt{4\pi\rho}$ where v is the velocity of the plasma. Thus going through the bars disturbs a plasma of width 2r where $r = 2I_o/Bn$. In the limit of high Mach number and a thin plasma the fraction of plasma disturbed by the bars is $f = 2\pi r/2\pi R_o$. Using the fact that $B/B_o = M$ we find $f = 1/M\pi$. Thus for large Mach number, the bulk of the plasma passes through the bars unaffected. However, it is interesting

to speculate on the integrity of the magnetic configuration after passing through the bars.

Alfvén's theorem states that in a frame of reference, moving with and within a plasma, the magnetic field remains constant. Thus changes in magnetic field geometry are confined to the perturbances created at the bars where the plasma is cut. Since the cut is very thin, we can assume at some point down stream that the toroidal magnetic field will be symmetric and reconnection will have taken place. The question is thus one of asking in what distance or in what time this reconnection takes place. One notes that as the plasma flows by the bars, the field lines are bent, the volume available for the plasma to fill by flow along magnetic field lines becomes larger and larger. One also notes that there is a magnetic x-point or line in this region behind the bars. It has been shown[3] that in the region of an x-point reconnection can take place at the Alfvén velocity if it is accompanied by flow along magnetic field lines which drains plasma from the region of reconnection. Thus, in the region behind the bars reconnection can be expected to proceed at the Alfvén velocity. Since the plasma in this region can be expected to be subsonic and reconnection fast, this implies that the magnetic configuration will be effectively unchanged as the plasma passes through the bars.

As mentioned above, the current apparatus includes a large toroidal field coil surrounding a smaller poloidal field coil which is used in the plasma trapping experiments. The toroidal field coil has 16 turns. These turns can be shorted using thin rods near the muzzle of the gun. This would then leave the bias current and the poloidal field coil structure intact. Thus, a plasma produced by the gun would have to pass through the coil structure before interacting with the poloidal field. However, after passing through the coil, if the plasma maintains its configurational integrity it will not be able to penetrate the poloidal field and a sharp boundary of penetration of the plasma will be observed. However, unlike the current experiment where the plasma is trapped in place, in the proposed experiment the plasma can be expected to bounce back toward the gun. If this experiment is successful a very simple extension will lead to the formation of a compact torus.

1. Lawrence Berkeley Laboratory, Report LBL-9507

2. J. Marshall in "Plasma Acceleration (S. Kash, ed.) Stanford University Press, Stanford, California (1959).

3. V. Tunas, Review of Geophysics and Space Physics, 13, 303 (1975).

RECONNECTION CONDITIONS FOR FLOWING FIELD-REVERSED PLASMA FROM A PLASMA GUN

J. W. Shearer, J. L. Eddleman, and J. R. Ferguson, Lawrence Livermore Laboratory*

Although various theoretical models are known for magnetic reconnection, [1],[2] none of them are applicable to the BETA-II experiment because they do not model the plasma flow conditions. The coaxial gun produces a plasma stream with an axial velocity of $\sim 10^8$ cm/sec. In the plasma rest frame an aperture or snipper coil would appear to move in the opposite direction at this same velocity.

A more suitable model for the BETA-II reconnection problem was formulated based on the equations of fluid flow through a nozzle. Assuming a sharp-boundary model for the plasma (fig. 1), Bernouilli's law for an adiabatic fluid leads to an equation for the axial plasma velocity u:

$$u = u_m \left[1 - (P/P_s)^{(1 - 1/\gamma)} \right]^{1/2} \qquad (1)$$

where u_m is the maximum velocity (at $P = 0$), and P_s is the stagnation pressure. The plasma density ρ and stagnation density ρ_s are given by

$$\rho = \rho_s (P/P_s)^{1/2}. \quad \text{and} \quad \rho_s = \frac{2\gamma}{\gamma - 1} \frac{P_s}{u_m^2} \quad . \qquad (2)$$

Using the long thin approximation for the magnetic field, the plasma pressure P for the sharp boundary model equals the magnetic pressure

$$P = B^2/8\pi \qquad \text{and field B is } B = (\Phi_0 + 2\Phi_i)/\pi R^2 \qquad (3)$$

where R is the wall radius, Φ_0 is the open field line flux, and Φ_i is the field-reversed flux. The mean radius r of the plasma is:

$$r = (R/\sqrt{2}) (1 - \Phi_0/\pi R^2 B)^{1/2} \quad . \qquad (4)$$

The plasma thickness 2a is assumed to be small compared to the radius r, and is obtained from the equation of continuity:

$$a = F/(4\pi r u \rho) \qquad (5)$$

where F is the mass flow rate (gm/sec).

The diffusion of the magnetic field causes a loss of field-reversal flux Φ_i. From Faraday's law one obtains

$$\dot{\Phi}_i = -2\pi r B D/a \qquad (6)$$

*Work performed under the auspices of the U.S. Department of Energy by the Lawrence Livermore Laboratory under contract number W-7405-ENG-48."

where the diffusivity $D = \eta / 4\pi$, η being the electric resistivity. A simple approximation for η is

$$\eta \text{ (emu)} = \left[\frac{10^{8}}{(T_e)^{3/2}} \right] \exp \left(\frac{v_D}{v_i} \right)^2 \qquad (7)$$

where the term in brackets is the classical collisional resistivity,[4] T_e is the electron temperature in eV, v_D is the electron drift velocity, and v_i is the ion thermal velocity. The exponential term approximates the effect of unstable anomalous conductivity effects near their threshold. As these turbulent effects try to grow, the increased diffusivity D causes the current sheath to broaden, thus lowering the electron drift velocity v_D and stabilizing the current sheath.[5] The electron temperature T_e is fixed at 50eV, in agreement with plasma gun experiments. It is assumed to be constant throughout the flow due to its high parallel thermal conductivity. The ion temperature T_i is much higher ($T_i >> T_e$), so that the adiabatic equations (1) - (3) apply to the ions only.

These equations were combined into a differential equation for the rate of change of pressure with axial distance z.

$$\frac{dP}{dz} = \frac{1}{\pi R^2} \left(\frac{P}{2\pi} \right)^{1/2} \frac{d\Phi_0}{dz} - \frac{8 \pi D P}{u a R^2} \qquad (8)$$

where the first term approximates the clipper coil effect, and the second term is the diffusive effect.

Figure 2 presents results for one example, where $\gamma = 5/3$, $u_m = 100\text{cm}/\mu\text{sec}$, $z_m = 200\text{cm}$, $R = 20\text{cm}$, $F = 6\text{gm/sec}$, $P_s = 2$ atm, $P_0 = .25$ atm, and $T_e = 50\text{eV}$. In this example,

$$\Phi_0 \text{ (MG-cm}^2\text{)} = 4\pi \frac{z}{z_m} \left(1 - \frac{z}{z_m}\right) \qquad (9)$$

The largest flux losses are found to occur in the low field regions where the plasma density is lowest (Figure 2). Additional calculations showed that the flux losses increase strongly with decreasing mass flow rate F. These trends were traced to the sheath-broadening effect of the anomalous resistivity factor in eq. (7).

Figure 3 shows a two-dimensional MHD calculation[6] of a similar problem, but here the clipper coil flux Φ_0 is time-dependent. At t = 11.2 μ sec one of the plotted flux surfaces has reconnected near z = 152 cm due to magnetic diffusion downstream from the clipper coil. The velocity plot shows strong axial velocity divergence in that region because the upstream flow is being stagnated by the clipper coil. This lowers the mass flow rate F near z = 152, thus enhancing the anomalous diffusion effects, with consequent enhanced reconnection.

In summary, low density and low flow rate regions experience enhanced diffusion which broadens the current sheaths. When the width of these current sheaths approaches the scale size of the plasma, reconnection is rapid. A clipper coil compresses and stagnates the upstream flow, but the reconnection region is downstream where the flow rate is minimal.

References

1. Vytenis M. Vasyliunas, Reviews of Geophysics and Space Physics 13, No 1, pp 303-336 (1975).
2. V. D. Shafranov, Nuclear Fusion 19, No 2, pp 187-193 (1979).
3. E.R.C. Miles, pp 1-30 of "Supersonic Aerodynamics," Dover Publications New York (1961).
4. Lyman Spitzer, Jr., p 143 of "Physics of Fully Ionized Gases," 2nd ed. Interscience, New York (1962).
5. S. Hamasaki, R. C. Davidson, N. A. Krall, P. C. Liewer, Nuclear Fusion 14, No 1, pp 27-33 (1974).
6. J. L. Eddleman, C. W. Hartman, J. W. Shearer, Bulletin of the American Physical Society 23, No 7, p 343 (1978).

FIGURE 1
NOZZLE ANALOGY

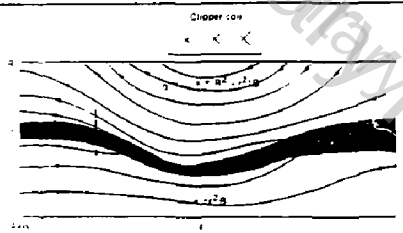

FIGURE 2
REFERENCE CASE RESULTS

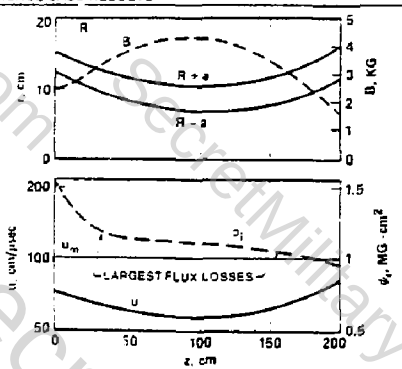

FIGURE 3

2D MHD CALCULATIONS OF REVERSED-FIELD PLASMA FLOW

$$\phi_i = 1.0 \quad MG\text{-}cm^2$$

$$\phi_0 = 14.1 \quad \sin \frac{\pi}{2}(t - 10.4)$$

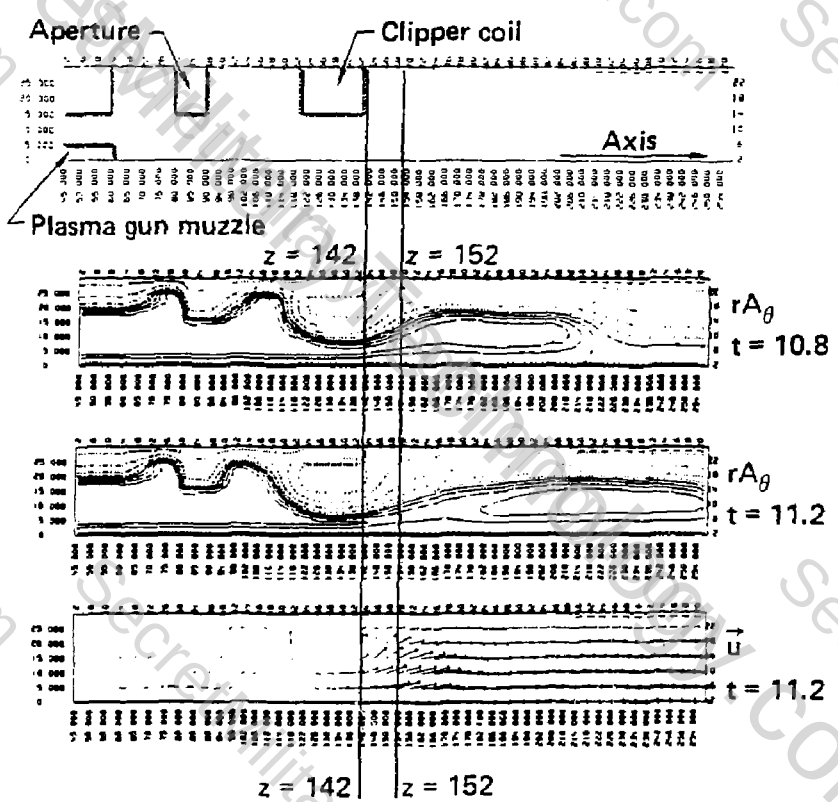

PHYSICS OF THE OHTE

T. Ohkawa and the OHTE Group
General Atomic Company, San Diego, California 92138

It is commonly known that stable toroidal magnetic plasma confinement requires both poloidal and toroidal magnetic fields. In axisymmetric confinement, the poloidal field is generated by toroidally directed plasma currents, while the toroidal field is supplied by external coils (tokamak), plasma paramagnetism (spheromak), or a combination of the two (reversed-field pinch). In tokamaks the dangerous m=1 current-driven kink is stabilized by periodicity ($q \geq 1$) while average magnetic well stabilizes the interchange modes. This q-limit drives tokamak designs toward low aspect ratios in order to obtain β values sufficient for fusion. In reversed-field pinches (RFPs) a conducting shell and magnetic shear ($q \ll 1$) provide stability. Since toroidal periodicity is irrelevant in RFPs, "cylindrical" tori of high aspect ratio are preferred. Relatively compact fusion reactors have thus been predicted, taking advantage of the high engineering β and the likelihood of ohmically heating the plasma to ignition.

The poloidal field may also be produced independently of plasma currents in helically symmetric toroidal systems by the combination of the magnetic field from a helical winding (helical field) with a strong externally generated toroidal field to provide rotational transform. This is the basis of stellarator and torsatron devices. Like tokamaks, they are limited to $q \gtrsim 1$ and to low β.

It is also possible to provide a net toroidal field by translational transform through the combination of a helical field with a predominantly poloidal field ($q \ll 1$), such as that of a paramagnetic pinch, and this is the basis of OHTE confinement. The similarities and differences among these toroidal systems are illustrated in Figure 1. Ideal MHD stability in low-q systems at high β requires high shear throughout the plasma. This is achieved only if q(r) decreases monotonically and reverses, and in fact, RFP experiments yield stable plasmas at higher β than stabilized pinches without reversal. The reversal of q in RFPs is achieved either by fast programming of the toroidal field during plasma setup or by self-reversal when the pinch ratio $\theta = B_p/\langle B_\zeta \rangle$ at the plasma boundary exceeds a profile-dependent value typically between 1 and 2.

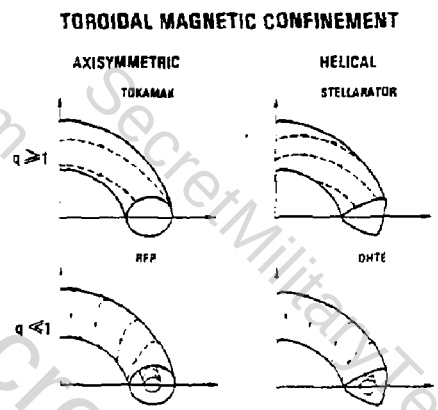

Fig. 1: A comparison of tokamak, stellarator, RFP, and OHTE configurations.

However, in RFP experiments self-reversal is driven either by turbulence (hence poor confinement) or by a reversed toroidal E-field (Poynting vector out of the plasma, hence a transient situation). In OHTE a steady-state q-reversal is independently imposed on the outer portion of the plasma by the evanescent helical field; q in the interior is determined by the plasma current profile and paramagnetism as in a conventional RFP. Since the OHTE aspect ratio may be large, it is technically feasible to drive large plasma currents inductively for long times. Calculations show that ohmic heating to ignition will be possible if energy loss is not much worse than Alcator na^2 empirical confinement. Because of the large shear, β is expected to be high. Therefore, an OHTE reactor should be smaller and simpler than a tokamak.

Ideal MHD numerical calculations in the straight helical plasma approximation with varying degrees of paramagnetism and a range of profile parameters have been performed for ℓ=2 and ℓ=3 configurations to map the parameter space of OHTE equilibria. Figures 2 and 3 illustrate typical ℓ=2 OHTE flux surfaces and pitch (P=qR) versus helical flux profile, respectively. Numerical equilibria are being tested for local, pressure-driven ideal interchange stability using the criteria given by Mercier (1) and Greene and Johnson (2). The minimum energy force-free helical pinch analytical equilibrium given by Taylor (3) is a special case of the ℓ=1 OHTE.

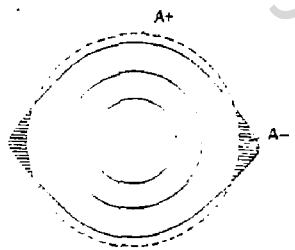

Fig. 2. Typical ℓ=2 calculated OHTE flux surfaces.

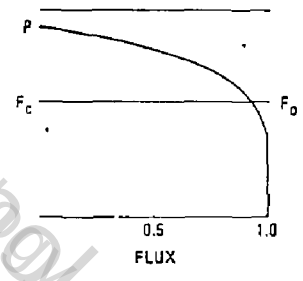

Fig. 3: Plot of a typical pitch versus flux profile. F_c and F_o are central and plasma boundary fluxes, respectively.

Field line tracing was used to study the loss of q-reversed volume owing to error fields. In this calculation, the transform reversal persisted for both a uniform vertical field and a local stray field up to 7% of the poloidal field at the separatrix.

Free boundary current-driven instabilities in helical plasmas have been investigated by two techniques. The first is to use averaged fields in the circular mode equation given by Robinson (4). It is found that helically enhanced pitch reversal tends to draw resonant surfaces inward, transforming some kinks into tearing modes. A stabilizing contribution for kink modes is also obtained for a given current profile. The second technique is to analyze

the helical free-boundary force-free equilibrium $\nabla\times\vec{B}=\mu\vec{B}$ in a circular conducting cylinder, adopting the approach of Rosenbluth and Bussac (5). The analysis can be formulated analytically when the perturbation has the same periodicity as the plasma. A shift of the mode resonant surfaces is again found, and the stability condition is the same as for a mode of the same helicity in a cylindrical equilibrium.

The OHTE experiment is under construction and is expected to begin operation late in 1980. It consists of a single, thin stainless steel bellows vacuum chamber bakeable to 125°C and pumped by turbomolecular pumps. The major radius is 1.24 m and the maximum internal minor radius is 0.19 m. The vacuum chamber is surrounded by an aluminum alloy conducting shell 15 mm thick, with internal minor radius 0.20 m, which provides stabilization against plasma kinking. The flux penetration time through the shell is approximately 40 ms. The shell also supports and aligns the helical winding, which is assembled by bolting together machined copper half-turn segments. An $\ell=3$, $m=16$ helical winding driven by a motor-generator-rectifier system was selected for the initial experiments. A toroidal field up to 0.4 tesla in either direction can be produced by supplying unequal currents to the positive and negative helical windings. A separate vertical field system is used to null the vertical field resulting from this mode of toroidal field generation, maintain plasma radial equilibrium for long discharges, and cancel the local stray fields at the conducting shell gap when radial equilibrium is maintained by image currents in the shell. Plasma current is driven inductively by an independent coil, which is rated for a 2.25 weber flux swing (unidirectional current) to allow for at least 200 ms discharges at 300 kA. The coil is designed for either inductive storage or externally driven modes of operation.

It is expected that the filling gas will break down inside a small diameter $\ell=3$ stellarator confinement volume produced by the strong helical field and a weak toroidal field. Current rise time will be 2 to 10 ms, and gas puffing will be used in attempting to program plasma density. If the electron energy loss obeys the empirical Alcator law, it is expected that central plasma temperatures will be ~1 keV.

References

1. C. Mercier, Nucl. Fusion 1, 47 (1960).

2. J. M. Greene and J. L. Johnson, Phys. Fluids 5, 510 (1962).

3. J. B. Taylor, Third Topical Conference on Pulsed High Beta Plasmas (Culham, 9-12 September 1975), Pergamon Press, 59.

4. D. C. Robinson, Nucl. Fusion 18, 939 (1978).

5. M. N. Rosenbluth and M. N. Bussac, Nucl. Fusion 19, 489 (1979).

FORMATION OF TOROIDAL PLASMA CONFINEMENT CONFIGURATIONS BY USING HOT ELECTRONS *

C. W. Hartman, Lawrence Livermore Laboratory, and M. A. Levine, Lawrence Berkeley Laboratory

I. INTRODUCTION

There exist a variety of reasons (and configurations) for employing hot electrons in toroidal or mirror-toroidal hybrid confinement. In addition to in situ heating of dense plasma,[1] the hot electron diamagnetic current can be employed to shape hydromagnetically unstable field configurations, as in EBT,[2] or to increase the allowable β of a closed system as in Tormac.[3] Alternatively, hot electron current along B, nearly dissipationless if classical, can be used to "construct" toroidal, pinch-like fields as in SPIRE.[4] In either case the tendency of hot electron plasma to be immune from usual MHD instability can play an important role.

This note discusses possible means of producing closed, toroidal pinch-like configurations with hot electrons starting from a collisionless, mirror-confined, hot electron plasma. The final configurations are directly related to Spheromak, Tormac, and the stabilized Z-pinch.

II. Initial Plasma and Field Shape

The "preheat" phase consists of establishing a mirror confined hot electron plasma either by well-known ECR heating or by injecting energetic electrons from a pulse source. Possible axisymmetric initial mirror configurations are shown in Fig. 1.

Typically, at the end of ECR heating or injection, a hot electron plasma could be produced with parameters, $n_{eh} = 10^{11} - 10^{12}$ cm^{-3}, $T_{eh} = 0.1$-0.5 MeV, and $\beta = 0.2$-0.7. If all of n_{eh} could be directed to carry current at $v_D = c$, current densities of 500-5000 A/cm^2 would be achieved.

III. Toroidal Pinch Formation

Starting with the toroidal hexapole mirror (Fig. 1a), the formation of a hot electron pinch has been discussed earlier neglecting all contributions to current other than by hot electrons.[4] A driving flux is introduced inside the x-point radius which induces toroidal pinch current to modify the poloidal field configuration of Fig. 1a to that shown in Fig. 2 which is qualitatively the same as that obtained in the Tokapole.[5] The subsequent buildup of current and collisionless reconnection of field lines in an anisotropic plasma can be seen from a single particle viewpoint. Guiding center trajectories shown in Fig. 2 drift perpendicular to B_p with velocity $v_D = \bar{E}_t \times \bar{B}_p/B_p^2$ as in Ware pinching in tokamaks

* Work performed under the auspices of the U.S. Department of Energy by the Lawrence Livermore Laboratory under contract number W-7405-ENG-48.

when the driving flux Ψ is changed. At the X-point the bannana undergoes a topological change (Fig. 2c). Further drift carries the bannana into tokamak-like orbits which drift towards the O-point to enter passing orbits as shown in Fig. 2b. Passing occurs when either the reflection points merge or when the bannana flattens to encompass the O-point, depending on the particle gyroradius and the field distribution. Electrons on passing orbits are then accelerated by E_t contributing current to pinch buildup. Outside the closed region almost all electrons oscillate in v and j is a purely diamagnetic current. It would appear therefore that field reconnection would be uninhibited by the hot electrons.

IV. Spheromak/Tormac Formation

The formation of a Spheromak/Tormac configuration begins with the Levitron-like, Min B mirror shown in Fig. 1b or the gun configuration of Fig. 1 c. To form an isolated, closed field region in Fig. 1b the current in the two small radius coils would be increased as shown in Fig. 3. In Fig. 1c the gun would be fired with the emerging plasma and embedded B_T stretching the field to cause reconnection and an isolated ring. Electron guiding center orbits (similar for both Fig. 1b and 1c) undergo topological transitions as illustrated in Fig. 3. Additional electrons trapped against the toroidal field gradient, have bannana orbits which do not intersect the midplane. These orbits undergo the transitions described earlier into trapped, tokamak-like bannanas and bannanas trapped on the small major radius side of the midplane ring.

The orbits shown in Fig. 3 all make a transition to passing electrons in the pinch region and are accelerated by the flux change of the small radius rings to increase the pinch current. If the small radius ring current if Fig. 1b is turned off, the pinch would be attracted to the outer ring and the outer x-point would flatten forming a Tormac biusp configuration imbedded in a hot electron, mirror confined plasma.

If the outer ring is levitated, plasma formation without a vacuum toroidal field becomes possible. For this case the electron guiding center orbits collapse to zero poloidal width and nearly coincide with poloidal flux surfaces. The transition in orbit topology at the x-point takes place by nonadiabatic scattering at the x-point ($B_p = 0$) and the field lines reconnect in the presence of both hot electrons and cold plasma. The resulting pinch (or field-reversed-mirror) current would be carried largely by diamagnetic current of the hot electrons. The ring without B_t, would be expected to be hydromagnetically unstable. However stability may be achieved by the tendency of hot electrons to be immune from MHD and other instabilities in the presence of dense cold plasma when the precessional drift frequency exceeds the ion gyrofrequency.

Alternatively, if a toroidal field is necessary for stability, the potential of very long lifetime of the hot electron rings (1-10 seconds) makes it possible to turn off the external toroidal field, remove the winding, and remove the ring on a technically nondemanding timescale.

References

1. O.A. Anderson et al., Fourth IAEA Conf. Plasma Phys. Contr. Nuc. Fus. Res., 1, p. 103 (1971).

2. R.A. Dandl et al., 7th IAEA Conf. on Plasma Phys. Contr. Nuc. Fus. Res. (1978).

3. M.A. Levine et al., Seventh IAEA Conf. on Plasma Phys. Contr. Nuc. Fus. Res., II, p. 81 (1978).

4. C.W. Hartman, Phys. Rev. Letts. 26, 826 (1971).

6. A. P. Biddle et al., UW report COO-2387-103, (1979).

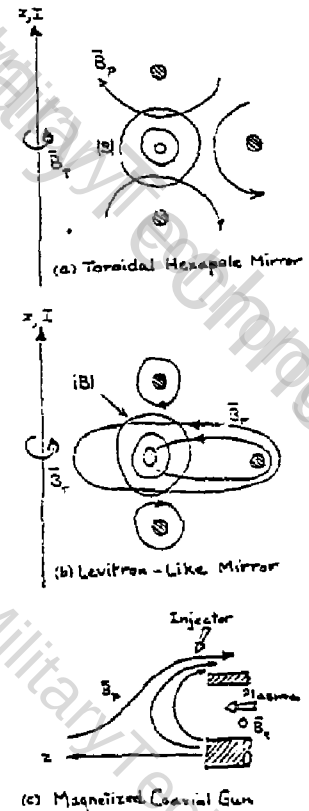

Fig. 1 (a) Min 'B' mirror formed by 3 supported current loops and B_z. (b) Min B mirror as in (a) and (c) mirror at the nozzle of a magnetized coaxial plasma gun.

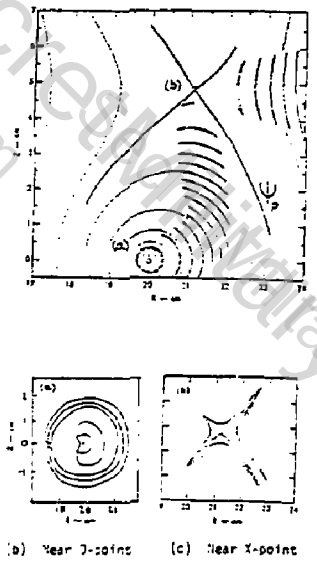

Fig. 2 Guiding Center drifts for Fig. 1a.

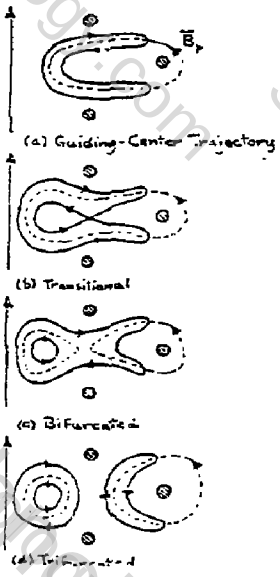

Fig. 3 Guiding-center orbits for Fig. 1b.

PARTICLE-FLUID HYBRID SIMULATION OF FIELD REVERSAL IN A MIRROR PLASMA

B. I. Cohen and T. A. Brengle, Lawrence Livermore Laboratory
Livermore, California 94550

A one-dimensional, cylindrically symmetric hybrid simulation code has been developed to investigate field reversal in a mirror plasma. The fluid momentum equation is used to determine the electron current density with $n_e m_e d\bar{v}_e/dt = 0$ and $n_e \approx n_i$. Large-orbit ions are followed by integrating particle equations of motion. Momentum-conserving electron-ion drag is included. Ion current is accumulated on a radial grid. $J_e^i + J_e^e$ is used in Ampere's law to determine the magnetic flux $\psi = rA_\theta$, and from Faraday's law $E_\theta = -\partial A_\theta/c\partial t$. On open field lines $|e\phi| \lesssim 4$ or 5 T_e, and electrostatic effects on ion orbits are negligible for $T_e \ll T_i$. However, electron temperature clamping and shorting of electrostatic fields need not occur on closed field lines. Good parallel electron conductivity forces $\phi \approx \phi(\psi)$; the code incorporates this by flux-tube averaging: $\oint d\ell B^{-1}(4\pi\bar{J} + \partial\bar{E}/\partial t) = 0 \rightarrow \phi = \phi(\psi)$. Of particular interest in the simulation are relaxation of electron return currents opposing ion-beam injection, the role of Ohkawa currents in sustaining field reversal, and large ion orbit effects on the diffusion and relaxation of an initially field reversed equilibrium.

Physics ingredients in code:

- Axisymmetry ($\partial/\partial\theta = 0$) and $B_\theta = 0$
- Particle ions obeying Newton-Lorentz equations → $\vec{J}^{ion}$
- "Massless" fluid electrons with drag on ions → $\vec{J}^{e}(A_\theta, \phi)$
- Limited use of quasi-neutrality in electron momentum eq.
- Open field lines -- line-tying

$$e\phi \sim T_e^{cold} << \frac{1}{2} m_{ion} \langle v_{ion}^2 \rangle$$

$$(\nabla_{rz}^2 - \frac{1}{r^2}) A_\theta = -4\frac{\pi}{c} J_\theta^{ion} \qquad E_\theta = -\frac{1}{c}\frac{\partial A_\theta}{\partial t}$$

ion velocity-space loss hole

- Closed field lines

Simultaneous solution of

$$(\nabla_{rz}^2 - \frac{1}{r^2}) A_\theta = -4\frac{\pi}{c} [J_\theta^{ion} + J_\theta^{e}(A_\theta, \phi)]$$

and

$$\int \frac{dl}{B} \nabla_{rz} [4\pi(\vec{J}^{ion} + \vec{J}^{e}(A_\theta, \phi)) - \frac{\partial}{\partial t} \nabla_{rz} \phi] = 0.$$

$A_\theta, \phi \rightarrow \vec{E}, \vec{B}$

Electron temperature evolution

- Injection of hot ions
- Boundary conditions: conducting radial limiter and continuity of A_θ and $\vec{B}$ at separatrix.

Code equations:

particle ions: $$m_s \frac{d\vec{v}_s}{dt} = z_s e(\vec{E} + \vec{v}_s \times \vec{B}/c) + m_s \nu_{se}(\vec{v}_e - \vec{v}_s)$$

Eulerian mesh
s = species index

$$\frac{d\vec{x}_s}{dt} = \vec{v}_s$$

$$(\vec{x}_s, \vec{v}_x) \rightarrow \vec{J}_s,\ n_s$$

"massless" fluid electrons:

$$0 = -en_e\vec{E} - en_e\vec{v}_e \times \vec{B}/c - \nabla \cdot \vec{p}_e$$

$$+ \nu_{ei}\left[\sum_s n_s z_s^2 (\langle \vec{v}_s \rangle - \vec{v}_e)\right]$$

where $\vec{P}_e = n_e T_{e\perp}\, \vec{\vec{I}} + n_e(T_{e\parallel} - T_{e\perp})\, \vec{b}\vec{b}$

$$\nu_{ei} = \frac{4\sqrt{2\pi}}{3\sqrt{m_e}} \frac{n_e e^4 \ln\Lambda}{T_e^{3/2}}$$ (classical) or anomalous

$\vec{b} = \vec{B}/B$

and $$n_e \approx \sum_s z_s n_s$$

$$-\vec{J}_e = n_e e \vec{V}_e = \text{nonlinear function of } \vec{E} \text{ and } \vec{B}$$

$$T_e = \begin{cases} T_e^{cold} & \text{open field lines (line-tying)} \\ T_e(\text{flux, time}) & \text{due to convection and Coulomb collisions with ions on closed lines} \end{cases}$$

or $P_e = P_e(\psi, t)$

Field equations:

For axisymmetry ($\partial/\partial\theta = 0$) and $B_\theta = 0$, $\vec{A} = \frac{\psi e_\theta}{r}$ and

$$\left(\nabla^2 - \frac{1}{r^2}\right) A_\theta = \frac{-4\pi}{c}\left[J^i_\theta + J^e_\theta(A_\theta, \phi)\right]$$

minuscule for $e\phi/T_e^{cold} = \delta(1)$

on open field lines

$$\vec{B} = \nabla \times \vec{A}_\theta \qquad \vec{E}_\theta = -\frac{1}{c}\frac{\partial}{\partial t}\vec{A}_\theta$$

$\phi =$ { Boltzmann-like on open field lines - negligible for $T_e^{cold} \ll \frac{1}{2} m v^2_{ion}$

determined on closed lines by

$$\int \frac{d\vec{\ell}\cdot\vec{B}}{B^2}\, \nabla\cdot\left[4\pi\vec{J}_i + \vec{J}_e - \frac{\partial}{\partial t}\nabla\phi\right] = 0$$

$$\langle \partial\phi/\partial\psi \rangle = \ldots$$

and $\frac{\vec{B}}{B}\cdot$ electron momentum equation →

$$e\frac{\partial\phi}{\partial s} = T_e(\psi)\frac{\partial}{\partial s}\ln n_e \text{ secondary dependence}$$

Solve equations iteratively. We guarantee continuity of A_θ and $\vec{B}$ at separatrix. There is a conducting wall at the radial limiter. An Eulerian mesh is used.

So far only a 1-D radial version of the code exists.

Work performed by Lawrence Livermore Laboratory for U.S. Department of Energy under contract W-7405-Eng-48

TWO DIMENSIONAL TIME-DEPENDENT TRANSPORT IN FIELD REVERSED EQUILIBRIA

S. P. Auerbach, H. L. Berk, J. K. Boyd, B. McNamara, D. Shumaker
Lawrence Livermore Laboratory, Livermore, CA 94550

Goal: Study buildup, steady state and decay of field-reversed mirrors, with emphasis on studying effects of neutral beams.

Method: Our method is very similar to H. Grad's "1½-D" method, with some techniques from N. Byrne and H. Klein's G2M code. Each time step is carried out in two stages, a transport stage and an equilibrium stage, as outlined next.

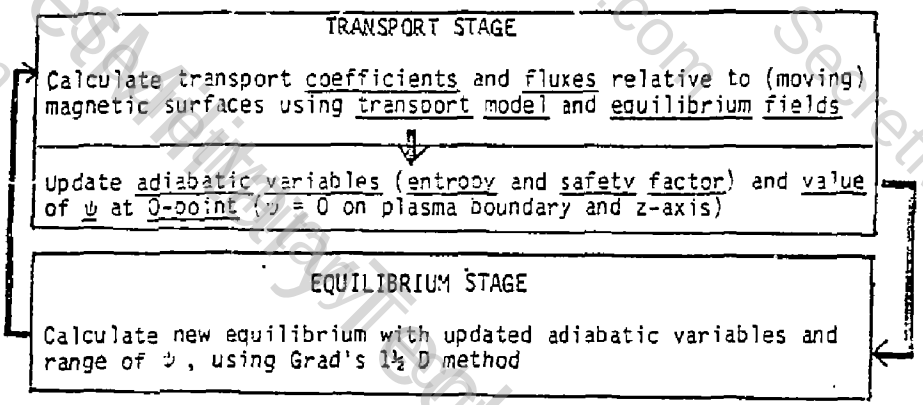

The computation domain is shown in Fig. 1.

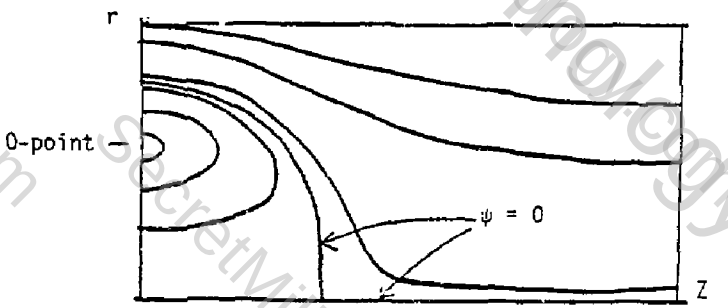

Fig. 1 Computational domain

The transport stage solves equations for the adiabatic variables particle number, entropy and safety factor. The adiabatic variables are conserved if there is no transport. In detail, we solve the following:

Particle Number:

$$\frac{D}{Dt}\left(n_r \frac{dV}{d\psi}\right) + \frac{d\Gamma_r}{d\psi} = \langle \sigma_n^r \rangle$$

Entropy:

$$\frac{DS_r}{Dt} + \left(\frac{dV}{d\psi}\right)^{2/3} \left\{ \frac{1}{n_r} \frac{dP_r}{d\psi} \Gamma_r + \frac{5}{3} \Gamma_r \frac{d\Gamma_r}{d\psi} + \frac{2}{3} \frac{d}{d\psi} \langle q_r \cdot \nabla V \rangle \right\}$$

$$= \frac{2}{3} \left(\frac{dV}{d\psi}\right)^{5/3} \langle Q_r - \underset{\sim}{U}^r \cdot \underset{\sim}{R}^r + \sigma_s^r \rangle$$

$$S_r = P_r \left(\frac{dV}{d\psi}\right)^{5/3}$$

Safety Factor:

$$\frac{Dq}{Dt} = \frac{1}{4\pi^2} \frac{dV}{d\psi} \langle \underset{\sim}{E} \cdot \underset{\sim}{B} \rangle$$

Flux at O-point

$$\left.\frac{\partial \psi}{\partial t}\right|_{\text{O-point}} = \frac{rc}{en_e} R_{e,\theta}$$

In these equations

D/Dt = $\partial/\partial t|_\psi$.

r = species label

ψ = poloidal flux, V = volume inside a constant-ψ surface.

$\langle \quad \rangle$ denotes averaging over a constant-ψ surface

$\langle \sigma_n^r \rangle$ = particle source due to beams

$\langle \sigma_s^r \rangle$ = entropy source due to beams

Γ_r = particle flux across (moving) constant-ψ surface.

$\langle q_r \cdot \nabla V \rangle$ = heat flux

$\langle Q_r \rangle$ = temperature equilibration term

$\langle \underset{\sim}{U}^r \cdot \underset{\sim}{R} \rangle$ = work against drag force $\underset{\sim}{R}$

The last 4 terms above are computed from whatever transport model is used. At present, we have in place the full surface averaged Braginskii equations

The equilibrium stage alternates between solving the 2-D equilibrium equation ($S_\psi = 0$ for simplicity):

$$\nabla\cdot\left(\frac{1}{r^2}\nabla\psi\right) = -\frac{dP}{d\psi}$$

with

$$\psi = \psi(r,z)$$

$$P = P(\psi)$$

elliptic boundary conditions

and the surface averaged equilibrium equation

$$\frac{d}{dV}\left(K(V)\frac{d\psi}{dV}\right) = -\frac{d}{d}\left(S(\psi)\left(\frac{d\psi}{dV}\right)^{5/3}\right)$$

with

$$\psi = \psi(V)$$

$$S = S(\psi)$$

Boundary conditions at plasma edge and at O-point

We iterate between these until consistency is achieved.

Some special features of the code:

a) 2-D equation solved with 5-point ICCG algorithm on non-uniform r-z grid.
b) We allow boundary conditions at infinity, or specified coil currents.
c) We can deal with moving plasma boundary, and separatrix touching the r-axis.
d) Surface averages near the O-point are computed by fitting a polynomial to ψ near the O-point, and using analytic formulae for averages.

Present status of the code:

A) Equilibrium: the equilibrium solver and the 1½ D algorithm have been extensively checked, using values of $S(\psi)$ computed analytically for Hill's vortex; i.e., we put in $S(\psi)$ and checked that the self-consistent solution reproduce Hill's vortex.

B) Transport: the transport stage is working, though more testing is required.

C) Interface: the interface between the transport and equilibrium stages is still being tested and debugged.

Acknowledgement: We would like to thank Dr. H. Grad for many useful conversations.

"Work performed under the auspices of the U.S. Department of Energy by the Lawrence Livermore Laboratory under contract number W-7405-ENG-48."

A STEADY STATE BEAM DRIVEN FIELD-REVERSED MIRROR

J. H. Hammer and H. L. Berk, Lawrence Livermore Laboratory, University of California, Livermore, California, USA

We present here a method for sustaining a current in a beam driven field reversed mirror. It has been shown[1] that attempts to drive steady state field reversed configurations (or Tokamaks, Spheromaks) with neutral beams may be foiled by electron currents. The plasma electrons are accelerated by collisional interaction with the beam-produced ion current, causing the net current to vanish asymptotically in time.

We show that the current cancellation can be avoided by weakly breaking the toroidal symmetry of the device, for instance by the addition of quadrupole magnetic fields. The symmetry breaking allows angular momentum transfer between the electrons and the external coil structures, without having plasma in contact with material surfaces. The momentum transfer is manifested as an additional drag force on the electrons, preventing them from accelerating to the ion velocity and cancelling the current.

The detailed mechanism for transferring momentum is magnetic pumping (synonymous with parallel viscosity, non-adiabatic pressure effects). The injected beam causes a toroidal flow which convects tubes of poloidal flux ($B_{toroidal} = 0$ for this analysis) in the ϕ direction. The flux tubes undergo a periodic compression-decompression as they move past the toroidally varying structure, causing electron pressure modulation. If the electron collision frequency, ν_e, were zero, the pressure would vary double-adiabatically, i.e., the magnetic moment and parallel velocity are conserved, at least in the long field line limit. If the electron collision frequency were large, $\nu_e/\Omega_{rotation} >> 1$, the pressure variation would again be adiabatic, $P_e \sim n_e^{5/3}$. In the intermediate regime, $0 < \nu_e/\Omega_{rotation} < \infty$, the pressure may vary non-adiabatically, causing a net transfer of energy from the flow to electron thermal energy. Corresponding to the energy transfer is a force which damps the flow. This force is the extra drag force on electrons that prevents current cancellation.

To see how the extra force arises, examine electron force balance:

$$\nabla \cdot \underline{P}_e + en_e(\underline{E} + \underline{u}_e \times \underline{B}) = m_e n_e \nu_{ei}(\underline{u}_i - \underline{u}_e)$$

If we take the toroidal average of $1/en_e$ x (toroidal component) of this equation we obtain:

$$\left\langle \frac{1}{en_e} \hat{\phi} \cdot \nabla P_{\perp e} \right\rangle + E_\phi + u_n B = \eta J_\phi$$

u_n = flow normal to flux surfaces

*This work was performed under the auspices of the U.S./ Department of Energy by the Lawrence Livermore Laboratory under contract number W-7405-ENG-48.

This is the usual Ohm's law except for the pressure term, which might be described as a thermo-electric effect. For symmetric systems, $\hat{\phi} \cdot \nabla P_{\perp e} = 0$, so this term vanishes. For adiabatic non-symmetric systems, $\hat{\phi} \cdot \nabla P_{\perp e}$ and n_e would be 90° out of phase giving zero average. When collisions are included, a phase shift arises that gives a non-zero average. We find:

$$\left\langle \frac{1}{en_e} \hat{\phi} \cdot \nabla P_{\perp e} \right\rangle = \frac{\nu_e r^2}{3e\, n_e\, u_e^3} P_{\perp e} \left\langle \left(\int^{\phi} d\phi' \, \nabla \cdot \underline{u} \right)^2 \right\rangle$$

$$\text{for } \nu_e r/u_e << 1$$

This is always of the correct sign to prevent current cancellation.

Using a fluid ion model and the long, thin approximation self-consistent steady state equilibria have been obtained by including the extra drag term in Ohm's law. The size of the symmetry breaking perturbation, ϵ, must typically be of order 10^{-1} to obtain an equilibrium. The directed velocity of the beam must be of the order of the ion thermal velocity and the required particle input rate of the beam corresponds to a particle loss rate close to the classical diffusion rate. Explicit substitution of experimental parameters into the theory for devices at LLL (Beta II, MFTF) indicates that steady state equilibria may be maintained using the present beam current and voltage capabilities. The necessary symmetry breaking can be provided by the existing yin-yang coils. A limitation on available facilities, however, is the need to run the experiment for times longer than the resistive decay time in order to test the existence of a steady state.

Two other considerations are necessary to complete the theory. First, in the region within an electron orbit size of the field null, the electron fluid equations break down. This is an important region since any equilibrium must have finite current at the null. Near the field null it can be shown that shear viscosity effects become important. Estimates indicate that the shear viscous force alone is sufficient to prevent current cancellation in this region. Second, the quadrupole (or other symmetry breaking) field must be matched to the solution. Implicit in the analysis has been the assumption that the quadrupole field in the bulk of the plasma is negligible. Penetration of the quadrupole field is deleterious to any field-reversed scheme since the field lines are opened up and the advantages of closed flux surfaces for confinement are lost. In this regard the equilibrium flow plays an important role. The toroidal flow "sweeps" the quadrupole field out of the main body of the plasma, confining it to a boundary layer of order $r_p/\sqrt{R_m}$ in thickness. r_p is the plasma radius and R_m is the magnetic Reynolds number $R_m \sim \mu_0 r_p/\eta$, typically $R_m >> 1$. A boundary layer analysis shows that the vacuum quadrupole fields can be smoothly matched to the interior solution where the quadrupole field vanishes.

References

1. D. E. Baldwin and T. K. Fowler, Lawrence Livermore Laboratory Report UCID 17691 (1977).

CALCULATION OF IDEAL MHD GROWTH RATES AND EIGENFUNCTIONS IN FIELD REVERSED MIRRORS IN THE LARGE TOROIDAL MODE NUMBER LIMIT

D. V. Anderson and W. A. Newcomb, Lawrence Livermore Laboratory, University of California, Livermore, California, USA; and D. C. Barnes, Los Alamos Scientific Laboratory, Los Alamos, New Mexico, USA

The observation of MHD stable configurations in field reversed theta pinches has led us to review the ideal MHD stability theory. We produce 2D r,z equilibria from assorted models, including Hill's vortex, which are intended to match various profiles measured in experiments such as the FRX series at Los Alamos. These equilibria are used as the starting point for several stability calculations:

1. MALICE Several 3D ideal MHD simulations of stationary and rotating plasmas have yielded good qualitative agreement with experiment.[1]
2. RIPPLE VI 3D linear ideal modes with m = 1 have been evolved showing an unstable tilting mode.[2,3]
3. ALIMO 2D m = 0 linear axisymmetric modes are seen to be stable or have very small growth rates.[3]
4. MHD-2D 2D non-linear modes seem stable.[3,4]
5. STA3GROW Growth rates are calculated from the generalized energy principle. This report is limited to the subject of STABGROW.

Equilibrium Model

Pressure balance and Ampere's Law are expressed by

$$J_z = cr\frac{\partial P}{\partial \psi} \qquad \psi = rA_\vartheta \tag{1}$$

and

$$\frac{\partial^2 \psi}{\partial z^2} + \frac{\partial^2 \psi}{\partial r^2} - \frac{1}{r}\frac{\partial \psi}{\partial r} = -\frac{4\pi r}{c} J_\vartheta \tag{2}$$

*This work was performed under the auspices of the U.S. Department of Energy by the Lawrence Livermore Laboratory under contract number W-7405-ENG-48.

Specification of the equilibrium is completed by giving the pressure function taken to be

$$P(\psi) = (1-H)P_1\left(\frac{\psi_s-\psi}{\psi_s-\psi_v}\right)^m + HP_1\left\{1 + \cos\left[\pi\left(\alpha + \gamma \tanh(a\psi + b)\right)\right]\right\} . \quad (3)$$

A special case of this $H = 0$, $\psi_s = 0$, $m = 1$ is Hill's vortex:

$$P(\psi) = P_1\psi . \quad (4)$$

Conventional Energy Principle

From Bernstein[5] a generalized Sturm-Liouville equation

$$\frac{\partial}{\partial s}\left(\frac{1}{r^2 B}\frac{\partial X}{\partial s}\right) + (\Lambda - P'D)\frac{X}{B} = \frac{D}{B(H + U/\gamma P)} \oint \frac{DX}{B}\, ds \quad (5)$$

is used to determine stability (instability) if the smallest eigenvalue Λ is positive (negative). This equation is obtained by taking the toroidal mode number $n \to \infty$ which is the least stable mode in ideal theory. However, since the above equation is obtained in the norm

$$1 = \frac{\pi}{2} \oint dS\, \frac{X^2}{B} \quad (6)$$

the value of Λ cannot be related to growth rates.

Energy Principle with Growth Rates

To get growth rates we need to use the kinetic energy norm

$$1 = K = \frac{\pi}{2} \int \frac{ds}{B}\, \sigma\left[\left(\frac{X}{rB}\right)^2 + (BZ)^2\right] . \quad (7)$$

Now the parallel displacement Z cannot be analytically eliminated from the energy principle. After minimizing with respect to X and Z we obtain

$$\frac{\partial}{\partial s}\left(\frac{1}{r^2 B}\frac{\partial X}{\partial s}\right) + \left(\frac{\Lambda}{r^2 B^2} - P'D - \frac{D^2}{1/B^2 + 1/\gamma P}\right)\frac{X}{B} = \frac{D}{1/B^2 + } \quad \frac{\partial Z}{\partial s} \quad (8)$$

$$\frac{\partial}{\partial s}\left(\frac{B}{1/B^2 + 1/\gamma P}\frac{\partial Z}{\partial s}\right) + \Lambda BZ = -\frac{\partial}{\partial s}\left(\frac{DX}{1/B^2 + 1/\gamma P}\right) .$$

Here the growth rates are obtained from $\omega^2 \sigma = \Lambda$. As before $\Lambda_{min} > 0$ gives stability.

Reduction to First Order Equations

The form of the above equations is

$$\frac{\partial}{\partial s}\left(f \frac{\partial X}{\partial s}\right) + hX = c \frac{Z}{s} \quad , \quad h = h(\Lambda) \quad , \tag{9}$$

$$\frac{\partial}{\partial s}\left(g \frac{\partial Z}{\partial s}\right) + kZ = - \frac{\partial}{\partial s}(cX) \quad , \quad k = k(\Lambda) \quad .$$

With the substitutions $U = f \frac{\partial X}{\partial s}$ and $W = g \frac{\partial Z}{\partial s} + cX$ we arrive at the first order system

$$\frac{\partial U}{\partial s} = c \frac{\partial Z}{\partial s} - hX \quad , \quad \frac{\partial X}{\partial s} = U/f \quad , \tag{10}$$

$$\frac{\partial W}{\partial s} = - kZ \quad , \quad \frac{\partial Z}{\partial s} = \frac{W - cX}{g} \quad .$$

These equations together with the equations defining a field line

$$\frac{\partial r}{\partial s} = \frac{B_r}{B} \quad , \quad \frac{\partial z}{\partial s} = \frac{B_z}{B} \tag{11}$$

are solved using a shooting method which adjusts Λ until all boundary conditions are satisfied.

Properties of the Numerical Solution Obtained in STABGROW

The equilibria are accurately known either from the equilibrium code CYLEQ (which employs a bi-cubic spline representation with the ICCG algorithm) or from the analytic Hill's vortex formula. A bi-cubic spline representation is also used in the stability code such that

$$\psi, \underline{B}, \nabla \underline{B}, \underline{k} = - \underline{b} \cdot \nabla \underline{b}, \nabla \cdot \underline{B} \equiv 0$$

are calculated analytically. From these the field lines and the coefficients in the above stability equations are known to arbitrary precision within the spline representation. These Sturm-Liouville like equations are solved by shooting first with a finite difference integrator and then when near convergence with the GEAR method. The GEAR method allows finite difference errors to be reduced arbitrarily to roundoff levels.

It follows from the foregoing that, within the spline representation, one can calculate the exact eigenfunctions and eigenvalues to roundoff precision.

References

1. D. V. Anderson, D. C. Barnes, W. A. Newcomb, and C. E. Seyler, Paper 2A4, Proc. of Annual Controlled Fusion Theory Conference, Mt. Pocono, PA., USA, April 18-20, 1979.

2. A. I. Shestakov, D. D. Schnack, and J. Killeen, Symposium on Compact Toruses and Energetic Particle Injection. December 12-14, 1979, Plasma Physics Laboratory, Princeton, New Jersey.

3. J. Killeen, D. D. Schnack, and A. I. Shestakov, Proc. of 4th IRIA Intl. Symp. on Computing Methods in Applied Sciences and Engineering, Versailles, France, Dec. 10-14, 1979. Also as Lawrence Livermore Laboratory report UCRL-83332.

4. D. D. Schnack and J. Killeen, J. Comp. Physics, accepted for publication.

5. I. B. Bernstein, E. A. Frieman, R. M. Kulsrud, and M. D. Kruskal, Proc. Royal Society A244, 17 (1958).

TOROIDAL REVERSED FIELD-PINCH EXPERIMENTS*

Compiled by D. A. BAKER
Los Alamos Scientific Laboratory, Los Alamos, New Mexico 87545

Small Experiments

The small Reversed Field Pinch (RFP) experiments are listed in Table I. These experiments demonstrated the favorable stability of the reversed-field profiles, which were predicted by MHD theory. Self reversal of the toroidal magnetic field has been demonstrated in many machines but the important feature of the reduced fluctuation period (quiescent period) following the turbulent start up was not observed. The best results on ZT-S were obtained by programming, i. e., by forcing the field reversal by reversing the current in the toroidal field windings. Well-behaved pinches were observed for ~ 40 μs. The pinch terminated in an instability when the fields profiles diffused and beta became too high.

Recently a pitch programming mode has been studied on ZT-S in which the toroidal and poloidal fields rise together. The method has been successful in that decreasing values of pitch ($P = rB_z/B_\theta$) programmed at the wall resulted in favorable monotonically decreasing values of pitch vs radius in the plasma. This method can give rise to reduced diffusion and a smaller energy loss during the set up of the RFP. When done slowly the method requires gross stability during the programming; methods for accomplishing this are being studied theoretically.

ETA BETA II

The ETA BETA II results are discussed in detail in the following paper and in Ref. [1]. It is worth emphasizing here that this experiment is significant in that it has shown that the transport and radiation losses can be overcome in an intermediate-sized experiment (bore = 25 cm) using a 0.1 ms rise time. The experiment has reproduced many of the results of the much larger Zeta experiment (1 m bore) and has reached electron temperatures above 100 eV by ohmic heating following a turbulent startup.

ZT-40

The ZT-40 experiment is one of a new generation of reversed-field pinches (RFP) that includes ETA BETA II and HBTX-1A. These experiments will extend the plasma temperatures and confinement times by an order of magnitude above previous RFP experiments, and will establish the physics base for the next generation devices RFX and LCX.

The ZT-40 device has a major diameter for the 2.28 m and a 0.4 m minor diameter for the vacuum wall (99.5% alumina). The experiment is designed to operate over a range of plasma current risetimes, 0.01 to 0.7 ms. During the initial operation the risetime of plasma current is ~ 0.1 ms, comparable to that of ETA BETA II [1] in which the limitation of oxygen impurity radiation was overcome.

The device has operated in the fill pressure range of 3-10 mtorr. After about 200 discharges with currents up to 400 kA, the initial ~ 0.15 ms current decay time was increased to ~ 0.25 ms showing an increase in the plasma conductivity and a reduction in the energy losses due to impurities as discharge cleaning of the vacuum chamber occurred. There have been a few test discharges with currents up to the full design value of 600 kA. A sample current waveform is shown in Fig. 1(a). A zero-dimensional plasma model consisting of a coupled set of equations governing the deuterium and impurity ionization states, the electron temperature, the ion temperature, and the

*Work performed under the auspices of the US Department of Energy.

circuit behavior is used to evaluate the ZT-40 performance. A primary impurity, as determined spectroscopically, is oxygen. Line radiation can explain the observed current decay times if oxygen is present in amounts of $\sim 7 \times 10^{12}$ cm^{-3} ($\sim 1\%$ at 10 mtorr deuterium fill pressure). The model also indicates that with the expected further reduction in the impurity level and/or a lower deuterium gas density a "burn through" of the oxygen line radiation will occur and the plasma temperature will rise above 100 eV with the present passive crowbars to extend the current.

The initial values of the pinch parameter ($\theta = B_{\theta_{wall}}/B_{z_0}$) have ranged from 1.5 to 3.5. The toroidal field winding is crowbarred at its maximum current. Because of the small amount of toroidal flux outside the discharge tube in this device, self-reversal is readily obtained without any programmed reversal of the current in the toroidal field windings [see Fig. 1(b)].

A multi-channel interferometer simultaneously measures the line-integrated electron density along seven parallel chords across the discharge tube. A sample display of the data is shown in Fig. 1(d). After a period of large density excursions, a reduction in the total density and in the fractional fluctuation level is often observed starting shortly after current peak [e.g. at ~ 0.14 ms in Fig. 1(d)]. This period is sustained during the current decay until the reversed field disappears [~ 0.21 ms in Fig. 1(b)]. The necessary conditions for this plasma behavior are toroidal currents above 500 kA and initial filling pressures below 6 mtorr. This interval of reduced activity is similar to that observed in ZETA and ETA BETA II.

Further discharge cleaning techniques will be used to reduce the impurity level and the expected burn through of OV and OVI ionization states will be observed spectroscopically and the increased electron temperature will be measured by Thomson scattering. In situ baking of the alumina torus can be used to further reduce the impurity level.

A power crowbar, to be installed in early 1980, will extend the current duration to times > 2 ms. The plasma behavior for longer current risetimes will be investigated when the impurity radiation barrier is overcome.

REFERENCES

[1] BUFFA, A., COSTA, S., DE ANGELIS, R., DI MARCO, J. N., GUIDICOTTI, L., MALESANI, G., NALESSO, G. F., ORTOLANI, S., SCARIN, P., "First Results from the ETA BETA II RFP Experiment," Ninth European Conference on Controlled Fusion and Plasma Physics, Oxford, England, September 1979.

Table I

SMALL RFP EXPERIMENTS

EXPERIMENT	COUNTRY	MAJOR RADIUS (cm)	MINOR RADIUS (cm)	I_p (kA)
ZT-1	US	33	5.15	60
ZT-S	US	40.4	7.7	65
ETA BETA	ITALY	40	5	55
HBTX-1	UK	100	5	50
STP-1	JAPAN	12	4.2	53
TPE-1	JAPAN	40		40-80
TPE-1R	JAPAN	90	20	

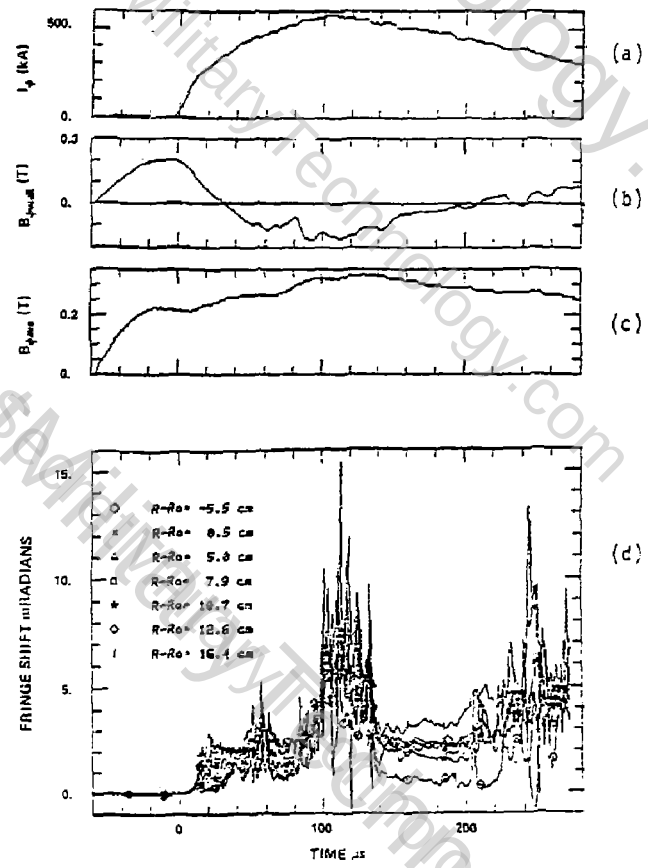

Fig. 1. Plots showing the time dependence of (a) toroidal current, (b) toroidal magnetic field at the wall, (c) average toroidal magnetic field, (d) integral of the electron density along seven chords normal to the torus midplane. The radial distance of each chord from the toroidal minor axis is shown in the insert.

SOME PROPERTIES OF THE HEATING AND CONFINEMENT IN THE RFP CONFIGURATION

S. Ortolani, Centro di Studio Sui Gas Ionizzati, CNR-Universita'di Padova, Association CNR-EURATOM, Padova, Italy

In this paper some properties of RFP plasmas as observed in the ETA-BETA II experiment[1] are discussed; and some comments on scaling laws appropriate to the RFP[2] are presented. In Fig. 1 the main experimental parameters of ETA-BETA II are summarized and the time evolution of the toroidal plasma current, I_ϕ, and of the toroidal field at the vacuum wall, B_ϕ, is sketched. The results obtained on ETA-BETA II can be summarized as follows. At high filling pressure ($\gtrsim$ 10 mtorr) radiation losses by light elements (oxygen in particular) dominate and prevent the plasma heating beyond a few tens of eV. The detailed study of the variation of the current decay time and of the electron temperature as a function of the filling pressure is discussed in Ref. 1 and here only a comparison between a RFP discharge and a nonreversed (NR) discharge in the nonradiation-dominated regime is discussed in some details. In Fig. 2 some results for the NR plasma (Fig. 2a) and for RFP plasma (Fig. 2b) are compared. In particular in the figure are shown as function of time, from top to bottom, the toroidal current, OIV and OIV visible line intensities, the dI_ϕ/dt signal, and, only for the RFP plasma, a streak picture and the local dB/dt signal as measured by a magnetic probe measuring the poloidal flux at ~ 3 cm inside the inner convolution of the stainless steel liner. The results shown in Fig. 2 can be discussed as follows. At low filling pressure ($\lesssim$ 6 mtorr) burning through of oxygen impurities is observed but in NR discharges complete overcome of the radiation barrier is not quite achieved because the temperature is probably held down by turbulent transport associated with the high level of fluctuations as measured on the toroidal current trace. When a RFP configuration is formed, higher temperatures are obtained with current e-folding times of up to 1.5 ms lasting for about 0.7 ms. This is associated with a distinct reduction in the fluctuations of the dI_ϕ/dt signal observed in the RFP as compared to the NR discharges. Internal magnetic probes (dB/dt) show a significant reduction in the fluctuation level during the slow current decay phase of a RFP discharge. Temperature measurements have also been made[1] and about 50 eV are measured on axis at the time of current peak. During the slow current decay the temperature increases up to ~ 100 eV before current termination. By using the filling density value a β_θ of ~ 0.1–0.2 is estimated at the time of the current peak. If the density remains about constant in time, β_θ will increase by more than a factor of 2 due to the increase in temperature and to the decay of the plasma current. An instability due to too high beta is then likely the cause of the current termination. The behaviour, in time, of the RFP plasmas on the F, θ diagram (where $F = B_{\phi w}/\langle B_\phi \rangle$ and $\theta = B_{\theta w}/\langle B_\phi \rangle$ are computed just inside the metal vacuum liner) is drawn in Fig. 3. Several discharges are superimposed in the figure and they all indicate that the RFP state is characterized by $|F| \lesssim 0.5$ and $1.5 \lesssim \theta \lesssim 2.5$. The importance of the external vacuum region separating the plasma from the flux conserving wall and the comparison with theoretical calculations is described by Turner in another paper at this meeting.[3]

The results, shortly discussed here, obtained on ETA-BETA II are rather encouraging and indicate good confinement properties of the RFP configuration, but the following questions are usually asked about the overall interest of the RFP as a magnetic confinement fusion experiment.

- why the temperature in the RFP is so low as compared to a tokamak of similar current?
- how can the too high beta (which eventually terminates the discharge) be avoided?

To possibly clarify these points a short discussion of some scaling laws appropriate to the RFP and a comparison with tokamaks is given below.

From tokamak research we know that there is an upper density limit associated with the problems of radiation losses and of plasma disruptions. This limit is usually written in terms of the average particle density as:

$$n \leq 5 \cdot 10^{19} \frac{B_\phi}{R} \quad , \tag{1}$$

where B_ϕ is the toroidal magnetic field and R is the major radius of the torus. By using the q parameter this limit can be written in terms of the average current density as

$$J/n = I/N \geq \frac{3.2}{q} \cdot 10^{-14} \ A \cdot m \quad , \tag{2}$$

which for high field tokamaks (q ~ 2-3) can simply be written as:

$$I/N \gtrsim 10^{-14} \ A \cdot m \quad . \tag{3}$$

Indeed, the high field tokamak experiments (as Alcator and FT), aiming at large ohmic heating and long energy confinement times, do operate in this range of parameters. Operation at lower densities is easily achieved in tokamak experiments but shorter energy confinement times are obtained in this case.

There is also evidence that, to obtain a good performance of an RFP plasma, experiments must operate above a minimum value of I/N.

In fact, in ETA-BETA II, to overcome the line radiation barrier due to light impurity elements, we had to operate at I ~ 200 kA and $p_o \leq 6$ mtorr. Only under these conditions was the good RFP performance (slow current decay and temperature increase vs time) observed in ETA-BETA II.[4] These parameters correspond to I/N as given in Eq. (3). Optimum conditions for quiescence in ZETA were obtained with $I \geq 0.42$ MA and $n = 5 \cdot 10^{19}$ m^{-3},[4] corresponding again to I/N as given in Eq. (3).

If ignition is eventually to be reached by ohmic heating alone, a minimum critical value for J/n will be required to overcome bremsstrahlung radiation; with classical resistivity this value is easily found to be described by Eq. (3).

The value of J/n can then define a class of experiments capable of scaling to ignition conditions by ohmic heating alone, provided the overall losses remain acceptable.[5]

As in the tokamak, there are arguments in the RFP posing limitations on the upper value for I/N at which an experiment can operate.

On ZETA, quiescence was not obtained at filling pressures lower than ~ 1.5 mtorr and streaming induced microinstability could have enhanced the transport and limited the achievable temperature. Values of $I/N \sim 2 \cdot 10^{-14}$ A·m were not reached with quiescent performance.[4]

Streaming induced microinstabilities should arise at high I/N values and a limit on I/N can be set as [5]

$$I/N \leq 3.5 \cdot 10^{-14} \sqrt{T} \text{ A·m} \quad , \tag{4}$$

with T in keV.

All these considerations suggest then that a value of I/N substantially larger than $2 \cdot 10^{-14}$ A·m can be incompatible with achieving good confinement of the plasma. The following optimum range of values:

$$10^{-14} \text{ A·m} \leq I/N \leq 2 \cdot 10^{-14} \text{ A·m} \quad , \tag{5}$$

is then indicated by the previous discussion.

Pressure balance simply requires for the average temperature:

$$T = 1.5 \cdot 10^{8} \beta_\theta N (I/N)^2 \text{ keV} \quad , \tag{6}$$

or

$$T = 1.5 \cdot 7^{8} \beta_\theta I (I/N) \text{ keV} \quad , \tag{7}$$

with T in keV; with the above discussed limitations on the values of I/N, this gives:

$$T = (1\text{-}2) \cdot 1.5 \cdot 10^{-6} \beta_\theta I \quad . \tag{8}$$

Compared to a tokamak with similar current, the temperature in the RFP will then be at least lower by $\beta_{\theta RFP}/\beta_{\theta TOK} = 0.1\text{-}0.2$. As an example, a temperature of ~ 1 keV with $I/N \sim 10^{-14}$ A·m requires:

$$I\beta_\theta \sim 0.64 \cdot 10^{6} \text{ A}$$

which, with $\beta_\theta \sim 0.1$, prescribes:

$$I \sim 6.5 \text{ MA} \quad , \tag{9}$$

and

$$N \sim 6.5 \cdot 10^{20} \text{ m}^{-1} \quad . \tag{10}$$

These figures are of course inversely proportional to β_θ, but once the radiation losses are overcome and transport losses dominate, the eventual β_θ will be limited, and one way to be conservative about the transport losses is to conceive operation at $\beta_\theta = 10\%$.

There are reasons to believe that an RFP will have a larger and more persistent level of fluctuations than a tokamak, because of the large number of resonant surfaces which characterizes the RFP as compared to the few

resonant surfaces that characterize the tokamak configuration. Moreover, the ion heat conduction should be more relevant in the pinch than in the tokamak because of the lower magnetic field.

All these considerations support the idea that a very high β_θ will not be reached in large-current experiments.

The study at high temperatures of the resistive stability properties of the RFP will be a major objective of the future experiments, but the temperature regime in which these studies can be done must first be achieved. If we base our estimates on $\beta_\theta \sim 30\%$, we assume to already know that high temperature stabilizing effect will lead to low fluctuations and to transport properties at least as good as in tokamaks. Compared to tokamaks, RFP's do not require high toroidal fields, but it can be expected that large toroidal currents (even taking into account the poloidal currents) will be necessary to overcome the losses.

The discussed scaling is plotted in Fig. 4 where graphs of I vs N and of T vs N as given by Eqs. (5) and (6), are drawn for $\beta_\theta = 0.1$–0.2.

There is clear evidence that high current (> 2 MA) experiments are required for a significant step toward high temperature (0.5–1 keV) RFP plasmas.

References

1. Buffa, A., et al., 9th Europ. Conf., Oxford, Sept. 1979.

2. Ortolani, S., Rostagni G., internal note G.I.P. 79-20.

3. Turner, L., contribution to this meeting.

4. Newton, A. A., Proc. RFP Workshop, UPee 78-08, Padova, Sept. 1978, Section II.

5. Ortolani, S., internal note G.I.P. 78-20.

ETA BETA II
EXPERIMENTAL PARAMETERS

MAJOR RADIUS	0.65	m
INSIDE RADIUS OF LINER	0.175	m
PEAK PLASMA CURRENT AT 25 kV	220	kA
RISE TIME TO PEAK CURRENT	~100	μs
DECAY TIME OF THE PRIMARY CURRENT	3	ms
PEAK TOROIDAL FIELD AT 25 kV	0.3	T
QUARTER PERIOD OF B_ϕ FIELD	150	μs
FILLING PRESSURE D_2	4–15	mtorr
BASE PRESSURE	4×10^{-6}	torr

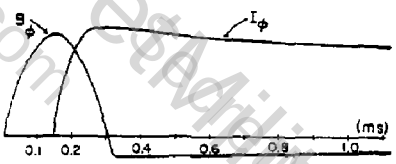

Fig. 1

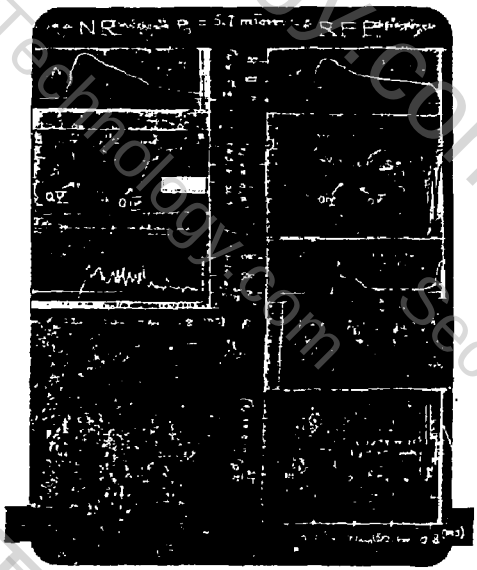

a) Fig. 2 b)

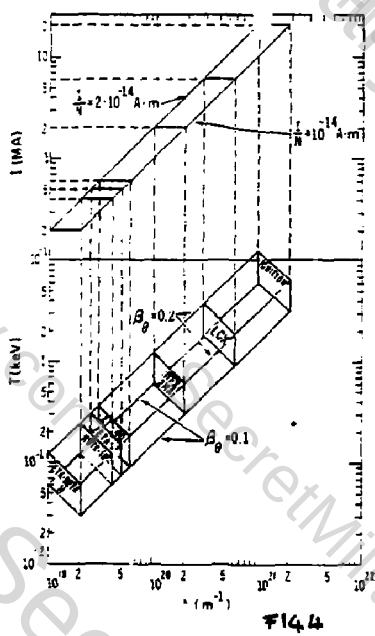

Fig. 4

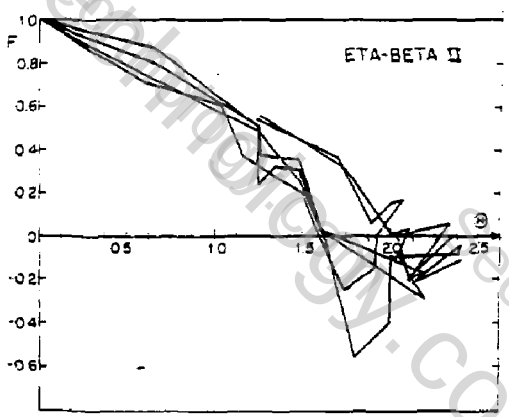

Fig. 3

RELAXATION OF TOROIDAL DISCHARGES*

Leaf Turner, Los Alamos Scientific Laboratory, Los Alamos, New Mexico 87545

The variational principle of Taylor[1] provides the guiding spirit for calculations concerning the relaxation of turbulent plasma discharges. The principle states that a turbulent, high-magnetic-Reynolds-number plasma confined by a perfectly conducting shell will achieve the state of minimum magnetic energy consistent with specified magnetic helicity and magnetic flux. It yields the Euler equation $\vec{\nabla} \times \vec{B} = \lambda \vec{B}$ where, for reversed-field pinch geometries, the eigenvalue λ is a continuous variable that specifies the ratio of net toroidal current to net toroidal magnetic flux. Although this principle has not as yet received rigorous justification, it has been able to reproduce much of the gross experimental features of the British reversed-field pinch experiment ZETA. The quiescent ZETA plasma was observed to follow closely the theoretical F-θ trajectory predicted by use of the Taylor principle.[2] {See Fig. 1. $\left[F(r) = B_z(r)/B_z^{avg}(r' < R),\quad \theta(r) = B_\theta(r)/B_z^{avg}(r' < R)\right]$} For a quiescent ZETA plasma with field reversal, $1.2 \lesssim \theta \lesssim 1.6$. On the basis of the Taylor principle, the upper limit is explained as that point beyond which the symmetric ($m = 0$, $k_z = 0$) state is no longer the minimum energy state; the lower limit is that point at which field reversal first occurs.

The Taylor principle received some theoretical support in the work of Montgomery, Turner, and Vahala.[3] By representing the velocity and magnetic fields in terms of a truncated expansion of Chandrasekhar-Kendall vector eigenfunctions[4] whose time-dependent coefficients obey a Liouville theorem for the case of three-dimensional ideal magnetohydrodynamics, an absolute equilibrium ensemble was established that specified the probability distribution of the coefficients. It was observed that the state corresponding precisely to the minimum energy state of Taylor was the only state that was quiescent in the sense: $\langle v^2 \rangle = 0$. The study suggested a physical mechanism causing evolution toward the minimum energy state; namely, resistive dissipation, which, acting predominantly at high wave numbers, more readily dissipates magnetic energy than magnetic helicity because (1) the magnetic energy spectrum peaks at higher wave numbers than the corresponding magnetic helicity spectrum, and (2) the natural

direction of magnetic energy flow is toward higher wave numbers whereas that of magnetic helicity flow is toward lower wavenumbers.

Recently there have been concerns[5,6] regarding the possibility that the continuous nature of the eigenvalue spectrum of the minimum energy state is a pathological result of the assumption of a circular plasma cross section. To allay these fears, Rasband and Turner[7] demonstrated that the continuous spectrum for λ is neither an artifact of the straight cylindrical geometry nor of the circular nature of the cross section. They proved that for any value of λ, the solution of the above Euler equation in either a straight cylindrical or a toroidal geometry with arbitrary cross section can be reduced to the the solution of either an inhomogeneous Helmholtz equation or an inhomogeneous Grad-Shafranov equation with simple boundary conditions. Using standard Green's function theory they obtained analytical solutions for the case of rectangular cross sections, with relevance to force-free regions within cusped geometries. Further support for the presence of the continuous spectrum comes from the current numerical work of Baker and Mann who are solving the inhomogeneous Grad-Shafranov equation for a constant pressure plasma utilizing the LASL axisymmetric toroidal magnetohydrodynamic equilibrium code.[8] It is crucial to remark here that there is only a discrete eigenvalue spectrum for plasmas contained in simply-connected regions; e.g., spheromak plasmas.

The most recent reversed-field pinch experiment to achieve the quiescent-like results of ZETA is the Padua experiment ETA-BETA II.[9] This experiment has a plasma column confined to a radius of 12.5 cm by a stainless steel liner. A vacuum occupies the region between the liner and the flux-conserving shell at radius 17.8 cm. In an attempt to explain the experimental data, we have made a generalization[10] of the variational principle of Taylor to the case where an insulating or resistive liner at radius r_o maintains a vacuum region between the plasma column and the perfectly conducting shell at radius R.

We demand that

$$\delta\{\varepsilon - \lambda K - \gamma\Phi - \eta[B_r(r_o^+) - B_r(r_o^-)]\} = 0 \qquad (1)$$

for arbitrary variations $\delta B_\theta(\vec{r})$, $\delta B_z(\vec{r})$ in the plasma and for arbitrary

variations of the independent components of the vacuum magnetic field. The parameters λ, γ, and η are undetermined Lagrange multipliers. Since the total magnetic flux Φ within the flux-conserving shell is time-independent and prescribed, we define K to be the total magnetic helicity inside the flux-conserving shell in order that the field equations remain gauge-invariant. This invariance is physically required by the dynamical isolation of the plasma from magnetic fields external to the flux-conserving shell. The jump in the normal component of $\vec{B}$ at the liner $\left[B_r(r_o^+) - B_r(r_o^-)\right]$ is constrained to be zero. We then solve Eq. (1) for the state of minimum magnetic energy within the flux-conserving shell, ε, with prescribed values of K and Φ.

We find that in the minimum energy state the confined plasma is force-free and enveloped by a skin current. (See Fig. 2, for example.) The $F - \theta$ trajectory evaluated at the flux-conserving shell with ETA-BETA II parameters is depicted in Fig. (1). The θ interval discussed above has become in this case $1.4 < \theta < 2.2$.

Note that skin currents must also occur at the surfaces of relaxed (force-free) spheromak plasmas where a liner maintains a vacuum region between the plasma and the conducting shell.

1. J. B. Taylor, Phys. Rev. Lett. 33 1139 (1974).

2. E. P. Butt, A. A. Newton, and A. J. L. Verhage, Pulsed High Beta Plasmas (Proceedings of the Third Topical Conference, Culham, 1975) ed. by D. E. Evans (Pergamon Press, Oxford, 1976) paper C2.1, 419 (1975).

3. D. Montgomery, L. Turner, G. Vahala, Phys. Fluids 21, 757 (1978).

4. S. Chandrasekhar and P. C. Kendall, Astrophys. J. 126, 457 (1957).

5. G. Vahala, "Stability and Force-Free Fields in an Elliptical Cylinder," (Sherwood Meeting on Theoretical Aspects of Controlled Thermonuclear Research, Mount Pocono, Pennsylvania) paper 2B44 (1979).

6. C. Chu and M. Chu, "Force-Free Magnetic Fields in Noncircular Cylinders," (Annual Meeting of Division of Plasma Physics, Boston) paper 6F6 (1979).

7. S. Neil Rasband and Leaf Turner, "Solutions of the Helmholtz Equation with Boundary Conditions for Force-Free Magnetic Fields," LA-UR-79-2316, to be published.

8. D. A. Baker and L. W. Mann, Pulsed High Beta Plasmas (Proceedings of the Second Topical Conference, Garching) paper B7 (1972).

9. A. Buffa et al. "First Results from the ETA-BETA II RFP Experiment," (Ninth European Conference on Controlled Fusion and Plasma Physics, Oxford, U.K.) post-deadline paper (1979).

10. Leaf Turner, in preparation.

*Work performed under the auspices of the USDOE.

Figure 1

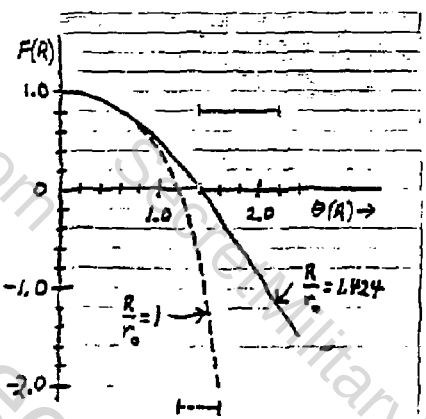

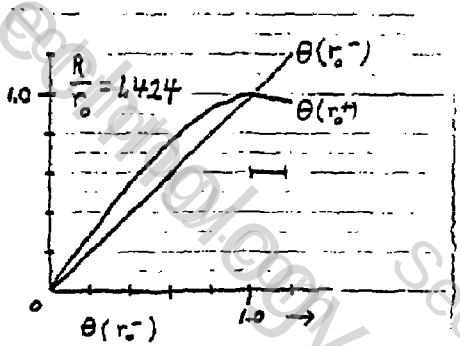

Figure 2

EFFECTS OF IMPURITY RADIATION ON REVERSED-FIELD PINCH EVOLUTION

E. J. Caramana* and F. W. Perkins

Plasma Physics Laboratory,
P. O. Box 451, Princeton, N. J. 08544

Spheromak and reversed-field pinch plasmas share the property that Ohmic heating must overcome strong radiative cooling by oxygen impurity atoms which peaks at a temperature $T_o \simeq 25$eV. We present results of transport code studies of this phenomenon, for several reversed-field pinch devices, and summarize these results in terms of two nondimensional parameters which parametrize the impurity content and the device size.

Both spheromak and reversed field pinch plasmas depend on Ohmic heating to raise the plasma temperature past the peak of the radiative cooling caused by the presence of oxygen impurity atoms. The peak of this cooling curve lies near $T_o \simeq 25$eV. Two conditions must be satisfied for this to occur: First the Ohmic heating power $\eta(T_o)j^2$ must exceed the maximum cooling rate $C(T_o)n_o n_e$ [$C(T_o) \simeq 9 \times 10^{-19}$ erg cm^3/sec]. In other words the inequality

$$\Gamma = \frac{C(T_o)n_o n_e}{\eta(T_o)j^2} < 1 \qquad (1)$$

must be satisfied over a good portion of the plasma. Secondly, the energy expended in heating the plasma to a temperature $T_1 \simeq 40$eV, must be a small fraction of the magnetic energy stored in the poloidal magnetic field or else a serious erosion of the poloidal field will result. The first criterion is evidently a criterion involving impurity concentration, plasma density, and current density. The second criterion, which can be written as

$$T_1 << \frac{B_\theta^2}{8\pi n_e} = (\text{const.}) \frac{j^2 a^2}{n_e} \qquad (2)$$

involves device size and plasma density.

---

*Present Address: Los Alamos Scientific Laboratory

A transport code for reversed-field pinches, which embodies classical transport and impurity radiation loses, has been developed[2] and applied to the three devices listed in Table 1. The results are summarized in Figure 1. The evolutionary parameter τ is given in terms of the loss of poloidal field energy Wp

$$\tau = \frac{1}{2} \ln \frac{Wp(t=0)}{Wp} \quad . \tag{3}$$

The definition of β_T is $\beta_T \equiv \frac{2U}{3Wp(t=0)}$ (4)

where U is the internal kinetic energy content of the plasma. The parameter Σ_o is defined by $\Sigma_o = \frac{C\,(T_o) < n_O > < n_e >}{n\,(T_o) \quad < j >^2}$ (5)

where the $< >$ brackets indicate a mass-weighted average. In practical units, the formula for Σ_o is

$$\Sigma_o = (0.005) \left(\frac{1 kA/cm^2}{< j >} \right)^2 \left(\frac{< n_O >}{10^{12} cm^{-3}} \right) \left(\frac{< n_e >}{10^{14} cm^{-3}} \right) \quad . \tag{6}$$

In terms of these nondimensional evolutionary parameters, each of the three devices is quite similar. Figure 1d provides an empirical fit to many transport code runs, giving the β_T which will be achieved for a given expenditure of magnetic field energy (parameterized by τ) as a function of impurity concentration (parameterized by Σ_o). The location of various devices (with β_D being the β_T value at 40eV) is also shown.

	ZT-5	ZT-40	ZPX
Vacuum Wall Radius	7.7 cm	20 cm	60 cm
Conducting Wall Radius	7.9 cm	22 cm	63 cm
I_z Current	70 kA	500 kA	750 kA
Toroidal Field On Axis	4000 G.	13,500 G.	5100 G.
Density On Axis	$1 \times 10^{13} cm^{-3}$	$5 \times 10^{14} cm^{-3}$	$5 \times 10^{13} cm^{-3}$
Initial Temperature	10 ev	10 ev	10 ev
Initial Beta	5.1 %	.38 %	.16 %

Table 1

Figure 1d is intended to provide a design guide for reversed-field pinch and spheromak devices. For a given design, one computes Σ_o from Eq. (5) or (6) and the β_D value corresponding to T = 40eV from Eq. (4) and plots the resulting point on Figure 1d. A design falling in region I ($\Sigma_o > 0.45$)

will not break through the radiation barrier. Designs in region II ($0.25 < \bar{\zeta}_c < 0.45$) will experience substantial difficulty in breaking through the radiation barrier and should be regarded as risky. Region III [$\bar{\zeta}_c < 0.25$, $\beta_D > \beta_T$ ($\tau = 0.05$)] corresponds to devices that have too small a size for their density. In the shaded region IV, the plasma should safely break through the radiation barrier. Within region IV, the value τ corresponding to a design point gives, via Eq. (3), fraction of the initial poloidal field energy which must be expended to achieve temperature of 40eV.

According to Figure 1d, ZT-S was much too high a density (or too small a device) to break through the radiation barrier. The ZT-40 device is predicted to work well for oxygen concentrations below 0.4%, but to experience grave difficulties at 1.6% (given the density of Table 1). The RFX parameters produce a successful device at 2% oxygen impurity concentration due to its low density.

Clearly, oxygen impurity radiation cooling remains a key issue for reversed field pinch and spheromak devices.

This work was supported by the Air Force Office of Scientific Research, Contract F49620-76-C-0005 with University of Colorado and by The Department of Energy, U. S. DoE Contract EY-76-C-02-3073 with Princeton University.

REFERENCES

1. D. E. Post, R. V. Jensen, C. B. Tarter, W. H. Grasburger, and W. A. Lokke, "Steady State Cooling Rates for Low Density, High Temperature Plasmas" PPPL - 1352 (July 1977).

2. E. J. Caramana and F. W. Perkins, "Effects of Impurity Radiation on Reversed-Field Pinch Evolution", PPPL - 1626 (Feb. 1979).

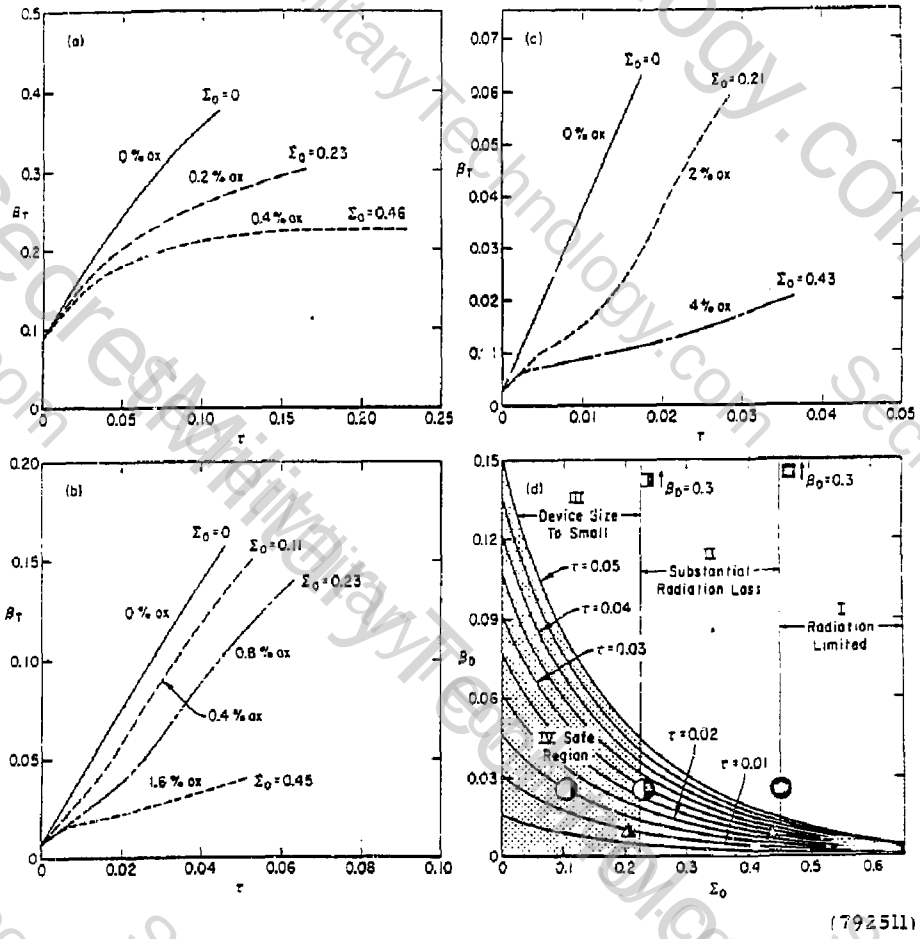

Fig. 1. (a-c) Nondimensional Evolution of the reversed-field pinch plasmas listed in Table 1, for indicated concentrations of oxygen impurities; (a) ZT-S, (b) ZT-40, (c) RFX.

Fig. 1d. Design guide for reversed-field pinch plasmas. Full, half, and quarter-shaded symbols correspond to the maximum, half-maximum, and quarter-maximum oxygen concentrations of Figs. 1(a), 1(b), and 1(c). The △ represent RFX, ○ represent ZT-40, and □ represent ZT-S. (Note that ZT-S is off-scale.)

Field Reversal Experiments, FRX-A and FRX-B Results*

W. T. Armstrong, R. K. Linford, J. Lipson, D. A. Platts, and E. G. Sherwood

I. Introduction

The equilibrium, stability, and confinement properties of the Field Reversed Configuration (FRC) are being studied in two theta pinch facilities referred to as FRX-A, and FRX-B. The configuration is a toroidal plasma confined in a purely poloidal field configuration containing both closed and open field lines (see Fig. 1). The FRX system produces highly elongated tori with major radius R=3-5 cm, minor radius a ~ 2 cm, and a full length ℓ ~ 35-50 cm. Plasma conditions have ranged from T_e ~ 150 eV, T_i ~ 800 eV, and n_{max} ~ $10^{15}/cm^3$ to T_e ~ 100 eV, T_i ~ 150 eV, and n_{max} ~ 4 x $10^{15}/cm^3$. The plasma remains in a stable equilibrium for up to 50 μs followed by an n=2 rotational instability which results in termination of the FRC. The plasma behavior with respect to equilibrium, stability, and rotation is consistent with recent theoretical work in these areas.

II. FRX-A Recent Results

Independently driven, crowbarred mirror coils were recently included on FRX-A. With optimum mirror timing, it was found that the particle inventory increased as compared with plasmas created with passive mirrors or without any mirrors, the increase being largely due to greater plasma length. It is thought that the mirrors produce a more localized tearing and reconnection of field lines during the formation phase by providing more favorable field curvature at the ends. This should contribute to increased inventory. After the first few microseconds, the mirrors act more like an extension of the implosion coil which would also increase plasma length and inventory. An increase in plasma lifetime from 20 to about 35 μs is also observed.

An experiment in plasma translation was performed by disconnecting one of the driven mirrors. Where the remaining mirror was activated 0-5 μs before the implosion, the plasma was observed to translate towards the opposite end with an initial drift velocity of 3-3 cm/μs, exiting the coil in 15 μs. This time is intermediate between the plasma stable time (t_s) and an Alfvén transit time (t_A) so that the plasma can undergo a collective translation prior to instability. A 6328 Å fractional fringe interferometer, external field probes, and a side on streak camera all indicated a well defined plasma column forming in the center of the implosion coil and then drifting uniformly out of the system. End-on framing photography indicated retention of an annular equilibrium as the plasma moves axially.

*Work performed under the auspices of the U. S. Department of Energy.

III. FRX-B Spatial Scans

Radial scans with Thomson scattering have recently been made on FRX-B. The scattering system has all its components rigidly mounted to a single table surface such that all relative alignments remain fixed. To shift the instrument for either radial or axial scans of the plasma, the table is translated by means of air bearings. This versatility is permitted because a three grating polychromator[1] has been employed. This instrument has sufficient rejection at 6943 Å to obviate the necessity of a beam or viewing dump. Observations were made on the axial midplane at a constant filling pressure of 17 mtorr. Over the stable lifetime of the plasma, the electron temperature was essentially constant in both time and space at about 100 eV for radii interior to the seperatrix. Relative density was also fairly constant as a function of time at these radii.

Line-integrated density across a diameter and excluded flux radius have been determined as a function of axial coordinate (z). Measurements were taken along a half-length of the coil at 17 mtorr fill pressure. Interferometry measurements indicate a plasma half-length of about 22 cm. The excluded flux radius near the midplane is found to be close to the separatrix radius, as inferred from Thomson scattering and image converter measurements. This correlation is expected from several equilibria models. Plasma shape modeling is required to unfold the data in the region z > 20 cm due to field curvature effects in this region.

IV. FRX-B Scaling Studies

Scaling of plasma parameters with fill pressure have been made for P_o = 9, 13, 17, 21 mtorr. Density measurements were made using Thomson scattering and two fractional fringe interferometers operated at different wavelengths. The Thomson scattering measurement was made near the midplane with r = 4 cm, the approximate value of the major radius. The peak density (corresponding to r = 4 cm) was unfolded from the interferometers integral measurement through profile information from excluded flux and luminosity measurements. The peak density (determined at 10 us) varies from 1.8×10^{15} cm $^{-3}$ with Po = 9 mtorr, to 4.2×10^{15} cm^{-3} with Po = 21 mtorr.

Electron temperature measurements were made at the axial midplane and r = 4 cm with Thomson scattering. Ion temperatures were deduced from CV(2271Å) Doppler broadening measurements. The carbon impurity radiation was collected along a diameter in the midplane of the plasma configuration. At all fill pressures, the electron temperature appears rather constant in the range of 100-150 eV. Whereas, the ion temperature approaches the electrons on an approximately classical time scale. T_i (measured at 10 us) varies from ~500 eV with Po 9 mtorr, to ~180 eV with Po = 21 mtorr.

Interferometer, Thomson Scattering and Doppler broadening measurements were used to examine pressure balance with the measured external field as a function of time and fill pressure. The errors associated with the determination of the temperatures and peak density

result in a cumulative uncertainty in the plasma pressure of 40%. Pressure balance is satisfied within these uncertainties.

V. Rotation

The plasma lifetime is limited by the onset of an n=2 rotational instability which has been treated theoretically by Seyler[2] using a Vlasov fluid code, and by Freidberg and Pearlstein[3] using an FLR expansion. In Seyler's model $-\omega_r/\Omega^* = 1.64$ where ω_r is the real part of the perturbation frequency, and Ω^* is the diamagnetic drift frequency. For FRX, this ratio is about 2.0 where ω_r is determined by end on framing photography. The Vlasov fluid model also indicates a critical value of $\alpha \equiv -\Omega/\Omega^* = 1.40$ for stability where Ω is the ion rotational frequency. Attempts have been made to establish the value of α experimentally using the Doppler shifted profile of the 2271 Å line of CV. The measured value of 0.4 is highly suspect for the following reason. The ion fluid equilibrium equation requires that when CV and D^+ ions are both rotationally and thermally equilibrated the CV density profile must be highly peaked at the major radius. The experimentally determined CV radial distribution is in total disagreement with this requirement. The failure of the data to satisfy the theoretical criterion $\omega_r < n\Omega$ is further evidence that the assumption of rotational equilibration is faulty. The critical Ω however has been observed to scale with Ω^* as predicted.

The most plausible explanation for the spin-up of the plasma has also been advanced by Seyler[4] where the preferential loss of particles with negative angular momentum is considered. These particles are found to be located either outside the seperatrix or encircling the axis, precisely the locations of anticipated large losses. This mechanism requires ~50% plasma loss for $\alpha = 1.5$. Inventory estimates of particles were made from combined measurements of plasma parameters at 17 mtorr. Particle loss at the time of the rotational instability was ~40%. The inherent uncertainties in the determination of the particle inventory prevent a definitive correlation with Seyler's hypothesis, however, the results are not inconsistent with this model.

VI. Transport/Scaling

The energy confinement time during the stable period is of the order of tens of microseconds which is significantly shorter than a classical diffusion time. One candidate for enhanced transport is anomalous diffusion due to the lower hybrid drift (LHD) instability which is driven by strong pressure gradients. A 1D hybrid code developed by Hamasaki[5] to consider both classical and anomalous transport has yielded preliminary results indicating significant LHD transport exists near the separatrix. From this code, times for 50% particle loss are calculated. The scaling of this loss time with $1/\rho_i$ and R^2/ρ_i compares favorably with stable time scaling from FRX-A and FRX-B (see Fig. 2).

Experimentally, the study of transport and scaling is limited by the relatively restricted parameter range of existing machines. A larger experiment called FRX-C has been proposed to alleviate the difficulty.

VII. Conclusions

Considerable progress has been made in defining the equilibrium, stability, and rotational properties of the FRC. These efforts have been aided by the addition of Thomson scattering and excluded flux measurements to FRX-B, and by substantial new results from the theoretical community. Many key issues however remain unresolved both experimentally and theoretically. The range of equilibria for which the FRC will remain MHD stable is still poorly defined. The stability of the plasma to resistive modes has not yet been characterized either by experiment or theory. Finally, transport and scaling are inadequately understood particularly with regard to anomalous processes. The next generation of experiments combined with more sophisticated 2D computer codes will hopefully elucidate these key points.

References

1. R. Siemon, Appl. Optics 13, 697 (1974)
2. C. E. Seyler, LASL Rpt. LA-UR-79-185 (1979)
3. J. P. Freidberg, L. D. Pearlstein, Phys. Fluids 21, 1207 (1978)
4. C. E. Seyler to R. K. Linford, private communication
5. S. Hamasaki, Conf. Record of 1979 IEEE, Intl. Conf. on Plasma Science, p. 143

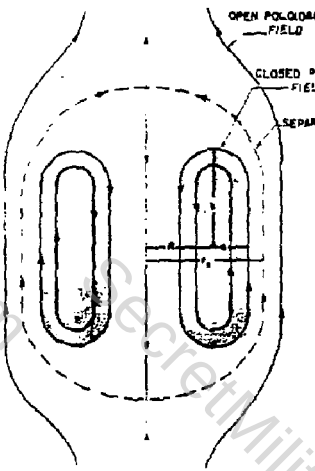

Figure 1

Field Reversed Configuration

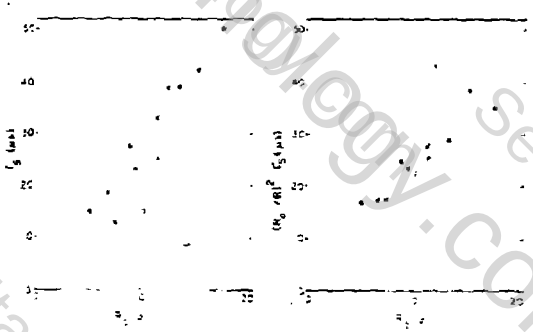

Figure 2

Scaling of the Stable Period - Open circle is FRX-A data, dots and crosses are old, and recent FRX-B data respectively. R_o = 4 cm.

FRX-C AND MULTIPLE-CELL EXPERIMENTS

R.E. Siemon, and LASL Compact Torus Staff
Los Alamos Scientific Laboratory, Los Alamos, New Mexico 87545

Background

Two new compact torus experiments have recently been proposed[1] and one (FRX-C) is now under construction. The proposed experiments are based on recent theoretical advances[2] and experimental results obtained with the LASL FRX-A and FRX-B field-reversed theta-pinch devices.[3] These recent experiments demonstrate a formation method and establish some of the confinement properties for one type of plasma compact torus--an elongated prolate plasma torus confined by purely poloidal magnetic field. The plasma displays a quiescent phase, free of any gross MHD instabilities, that persists much longer than either characteristic MHD times or open-field line loss times. The quiescent phase is terminated by an n=2 mode that is correlated experimentally with a steadily increasing plasma rotation that eventually exceeds the theoretically predicted threshold for instability (approximately 1.5 Ω^* where Ω^* is the angular diamagnetic drift frequency). The rotation is interpreted as resulting from a preferential loss of ions that carry angular momentum in a particular direction leaving the plasma to spin in the opposite direction. According to this point of view a significant fraction (about one-half) of the plasma must be lost to the closed-field configuration before the plasma reaches the threshold for instability, and therefore the n=2 disruption can be viewed as a secondary consequence of the more important cross-field transport processes. Both the FRX-C and Multiple-Cell experiments are intended to investigate ways of reducing cross-field transport.

FRX-C

The FRX-C experiment is a scaling study which will extrapolate the FRX-B results toward the higher temperature and longer lifetime needed for fusion. As shown in Fig. 1, the FRX-C coil dimensions are approximately twice those of FRX-B. Two high-voltage banks in a dual-feed arrangement are used to produce strong implosion heating. Larger variation of plasma density and temperature should be possible as a result of the higher voltage, because the higher voltage allows a larger variation in initial filling pressure as shown in Table I. For the same temperature in FRX-C as in FRX-B, the larger diameter coil results in an increase of a/ρ_i, where a is the plasma minor radius and ρ_i is the ion gyro radius. Thus, the important scaling of confinement with plasma size will be tested.

Another important design objective of FRX-C is to use a small amount of adiabatic compression, and thereby to produce a "fat" plasma characterized by a large ratio of the separatrix radius to the metal wall radius, r_s/r_w. As a general rule, better confinement in this type of field-reversed configuration has been observed experimentally when r_s/r_w is made larger (see discussion of literature in Ref. 1). The reason for improved confinement with large values of r_s/r_w (typically > 0.4) is, theoretically, a result of reduced pressure on

the separatrix and a corresponding reduction of cross-field transport at the boundary of the plasma. It is a necessary consequence of pressure balance that the plasma pressure at the separatrix is reduced as r_s/r_w increases.[4]

The minimum amount of adiabatic compression (maximum r_s/r_w) results when the maximum reversed flux is trapped in the plasma. Trapping the maximum flux in the ordinary theta pinch requires reversing the magnetic field quickly, because during the reversal phase the preionized plasma tends to expand, interact with the wall, and allow flux to be lost. The high voltage of FRX-C produces a rapid magnetic field reversal, and the resulting ratio r_s/r_w should be larger than in FRX-A or FRX-B.

The FRX-C experiment is located adjacent to, and on a centerline with, the CTX vacuum tank and d.c. magnetic mirror coils. Thus, the device is planned to serve as a plasma source for confinement studies of CT's containing no toroidal field. As much flexibility as possible is being designed in the FRX-C system to allow variation of the basic configuration. Important options are the addition of electrodes for I_z to include toroidal field,[4] and the introduction of barrier fields and trigger coils for study of the Kurtmullaev mode of operation.[5]

Multiple-Cell Experiment

In addition to possible reactor implications, a linear array of compact torus plasma cells makes possible interesting studies of the confinement system. In a single-cell experiment such as FRX-B, the plasma on open field lines is unconfined, and ions leave in approximately one thermal transit time. The radial pressure profile presumably drops abruptly at the separatrix producing enhanced cross-field transport. In the proposed Multiple-Cell Experiment, the confinement of plasma on open field lines is expected to be markedly improved by the influence of multiple magnetic mirrors created by the linear array of plasma cells as shown in Fig. 2. The resulting pressure profile should be smoother and the plasma confinement in the closed-field configuration should improve.

The improved confinement on the open magnetic field lines is a consequence of multiple magnetic mirror effects that become important when the classical ion mean free path becomes comparable to the cell length. For the plasma parameters expected in the experiment, the mean free path is approximately 30 cm, and the required condition is satisfied. Consequently, the plasma decay time on the open fields is increased from approximately 3 μs in FRX-B ($\tau \sim L/v_{th}$ where L is the half-length and v_{th} is the ion thermal speed) to approximately 60 μs in the proposed Multiple-Cell Experiment ($\tau \sim M^2L^2/\lambda v_{th}$ where M is the magnetic mirror ratio, and λ is the mean free path).

An experiment to test the effects of multiple plasma cells can be done by a straightforward modification of the existing 5-m Scylla IV-P theta pinch. The coil, discharge tube, and capacitor bank would be modified to match the FRX-B experiment in all respects except length. Providing field line tearing and reconnection can be controlled to generate a linear array of cells in the

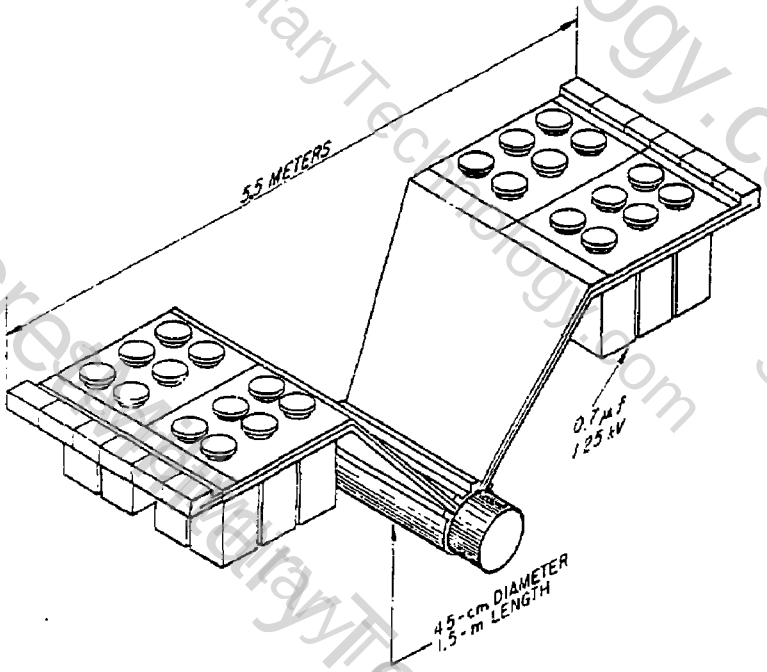

Fig. 1. FRX-C experiment showing high-voltage capacitor banks, dual-feed collector plates, theta-pinch coil, and discharge tube. "Gull wing" arrangement makes optimum use of the available space adjacent to the CTX, a vacuum tank and mirror coil for compact torus translation, trapping, and confinement studies.

TABLE I.
FRX-C Experimental Parameters

Theta-Pinch Parameters		
Coil diameter (cm)		45
Coil length (cm)		150
Source voltage (kV)		250
Magnetic field (kG)		9
Field quarter period (μs)		1.6
Anticipated Plasma Parameters		
Initial filling pressure (mtorr)	2.4	24
Plasma density (cm^{-3})	1.2×10^{15}	6.8×10^{15}
Electron temperature (eV)	500	90
Ion temperature (eV)	1100	200

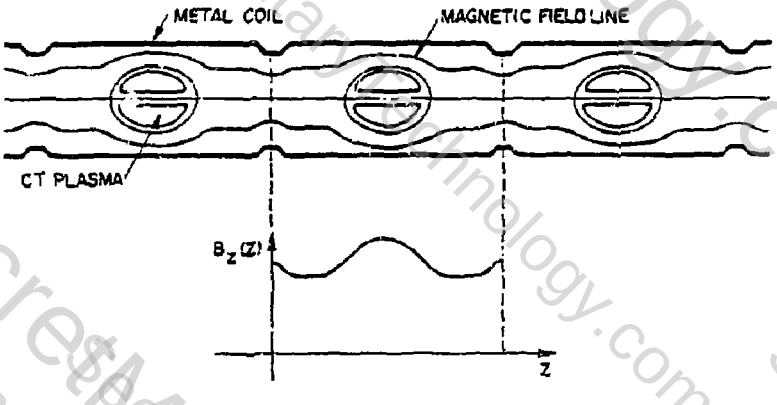

Fig. 2. Schematic drawing of magnetic fields surrounding linear array of compact torus plasma cells.

5-m coil, the influence of multiple cells can be studied for a plasma with the known single-cell characteristics of FRX-B. It has been pointed out that weak magnetic mirrors in the external coil structure may not produce tearing;[6] preliminary tests of methods for controlling tearing are being planned for FRX-A or FRX-B.

References

1. H. Dreicer et al., Proposal for FRX-C and Multiple-Cell Compact Torus Experiments, Los Alamos Scientific Laboratory Report LA-8045-P (1979).

2. D.C. Barnes, these Proceedings.

3. W. T. Armstrong, et al., Proceedings this conference.

4. G. C. Goldenbaum, Bull. Am. Phys. Soc. 24, 1072 (1979).

5. A. G. Es'kov et al., Proc. of the Seventh IAEA Conference on Plasma Physics and Controlled Thermonuclear Research, 3E 15 (Innsbruck, 1978).

6. A. E. Robson, private communication.

COMPACT TORUS THEORY--MHD EQUILIBRIUM AND STABILITY

D. C. Barnes and C. E. Seyler, Los Alamos Scientific Laboratory, Los Alamos, N. M. 87545 and D. V. Anderson, Lawrence Livermore Laboratory, Livermore, CA 94550

Introduction

Field reversed theta pinches at Los Alamos and elsewhere [1,2] have demonstrated the production and confinement of compact toroidal configurations with surprisingly good MHD stability. In these observations, the plasma is either lost by diffusion or by the loss of the applied field or is disrupted by an $n = 2$ (where n is the toroidal mode number) rotating instability only after 30-100 MHD times, when the configuration begins to rotate rigidly above a critical speed.

These experiments have led us to investigate the equilibrium, stability, and rotation of a very elongated, toroidally axisymmetric configuration with no toroidal field. Many of the above observations are explained by recent results of these investigations which are summarized here.

Equilibrium

The MHD equilibrium of a very elongated, field reversed configuration has been considered by a number of authors.[3-5] Suppose an elongated plasma is reflection symmetric about a midplane and is terminated by a separatrix which is of radius r_s at the midplane and which extends to the axis at the plasma end. Assume further that this equilibrium is contained in a uniform cylindrical conductor of radius r_w which extends axially well beyond the plasma end.

Integrating the equilibrium equations over the volume bounded by the midplane, the cylindrical wall, and an endplane leads to

$$\int_0^{r_w} r\,dr\,\left(P - \frac{1}{2}B^2\right)_{\text{midplane}} = \int_0^{r_w} r\,dr\,\left(P - \frac{1}{2}B^2\right)_{\text{endplane}} \qquad (1)$$

where B is the (predominantly axial) magnetic field and P is the plasma pressure. At the endplane, $P_1 = 0$, $B = B_e$ which is approximately constant in r. At the midplane, $P + \frac{1}{2}B^2 = \frac{1}{2}B_0^2$, where B_0 is the external magnetic field. Finally, since the same vacuum flux passes through the midplane and the endplane, $B_0(r_w^2 - r_s^2) = B_e r_w^2$. Using these, Eq. (1) becomes

$$\langle\beta\rangle = 1 - \frac{\kappa^2}{2} \qquad (2)$$

where $\langle\beta\rangle = 2/r_s^2 \int_0^{r_s} r\,dr\,(P / \frac{1}{2}B_0^2)$, is the average β and where $\kappa = r_s/r_w$.

For specific pressure profiles, the relative pressure at the separatrix, $\Delta = P(r_s)/P_{max} = \beta(r_s)$, may be expressed as a function of the radial compression, κ. Two examples are shown in Fig. 1. As $\kappa \to 0$ (very compressed plasma), Eq. (2) indicates that $\langle\beta\rangle \to 1$, the central β. Thus, in this limit, the profile becomes very flat, Δ approaches 1, and the details of the profile are less important. This is indicated by the convergence of the two curves as $\kappa \to 0$. Experimentally, $\kappa = .5$, $\Delta = .7$, which is consistent with either profile considered.

The above analysis gives no details of the axial structure of the equilibrium. Elongated solutions have been found numerically using a two-dimensional, r-z, equilibrium code, CYLEQ. These solutions have gradual z variation and associated elliptical flux surfaces. Experimentally, the z variation occurs over only a fraction of the plasma length and the overall picture is of a more racetrack like equilibrium. This feature is not well understood, but might be explained by considering configurations with internal islands.

Stability

The simplest modes to consider are gross displacements of the plasma. For very elongated configurations, the applied field has a maximum in the midplane. Thus, sideways displacements of the equilibrium (normal to the axis) are stable. Axial displacements are unstable without a conducting wall but are neutral for a smooth cylindrical boundary and become stable if the wall is moved closer.

To examine stability in more detail, consider δW[6]. For incompressible modes δW may be written as

$$\delta W_n = \frac{\pi}{2} \int d\psi\, J\, d\chi \left\{ \frac{1}{r^4 B^4 J^2} \left(\frac{\partial X}{\partial \chi}\right)^2 + B^2 \left(\frac{\partial X}{\partial \psi}\right)^2 - P'' X^2 + fY \right\} \qquad (3)$$

where Y and f are functionals of X defined by

$$L_n Y = \frac{1}{n^2} \frac{1}{J} \frac{\partial}{\partial \chi} \frac{r^2}{J} \frac{\partial Y}{\partial \chi} - B^2 Y = f = B^2 \frac{\partial X}{\partial \psi} + P' X \qquad (4)$$

and where the notation of Ref. 6 has been used.

Since all eigenvalues of L_n are negative, the last term in Eq. (3) is negative definite. An examination of the remaining terms indicates that, for elongated configurations, δW is large and positive, unless $X = xrB_r$ or $X = xrB_z$, where x is a slowly varying function, i.e., does not have rapid variation near the turning points of the field lines. The choices B_r and

B_z in the above lead to axial or radial displacements respectively. For the axial mode

$$\delta W_n = \frac{\pi}{2} \int d\psi\, J\, d\chi \left\{ r^2 B_\zeta^2 \left[\frac{1}{r^2 B^2 J^2 \iota^2} \left(\frac{\partial x}{\partial \chi}\right)^2 + B^2 \left(\frac{\partial x}{\partial \psi}\right)^2 \right] + fY \right\} \quad (5)$$

The second term on the right above is small for elliptical, elongated equilibria. The first term vanishes for $x = x(\psi)$. Thus, we find that axial, internal displacements are unstable for all n for sufficiently elongated configurations with elliptical flux surfaces. For racetrack equilibria, this scaling does not apply, and the possibility of stabilizing small n modes exists. Similarly, for radial modes, the stability of small n modes is determined by the external boundary conditions.

These conclusions are reproduced by numerical simulations. Using equilibria generated by CYLEQ as initial conditions, the MALICE[7] code has been used to study stability of large scale modes. Equilibria completely stable to $n \leq 3$ have been constructed. When κ is made too small, however, the $n = 2$ radial mode is found to be unstable. These results are shown in Fig. 2. In independent work, Shestakov *et al.*[8] have observed an $n = 1$ internal, axial instability. This is related to the spheromak tilting mode but becomes nearly an azimuthally varying axial translation of the plasma for the very elongated case considered.

Local modes with $n \to \infty$ are of two types. For the interchange mode, the normal displacement is approximately constant along a field line and the plasma compressibility must be taken into account. Interchange stable solutions have been constructed by analytic[9] and numerical means. For the remaining co-interchange modes, compressibility is less important. In an independent paper, we report recent work on these local modes.[10]

Rotation

The rotational stability of infinitely long field reversed theta pinches has been studied by Pearlstein[11], Freidberg[12], and Seyler[13]. Freidberg used the finite Larmor radius equations in which he treated the field null in an ad hoc manner. The predicted value of the critical rotation velocity was about $\Omega = 1.6\ \omega_*$, where ω_* is the ion diamagnetic drift frequency. Using the exact Vlasov-Fluid equations in which no field null singularities occur, Seyler found the critical rotation velocity to be somewhat lower, $\Omega = 1.3\text{-}1.5\ \omega_*$, depending upon the profiles. Both results, however, are in qualitative agreement, the threshold for $n = 2$ rotational instability is $\Omega > \omega_*$. Direct experimental measurement of the critical rotation velocity is extremely difficult, however, the real part of the eigenfrequency has been measured and is in agreement with the theoretical prediction, thus lending indirect experimental support for the theory.

The mechanism which causes the plasma to spin up to this instability threshold has not been positively identified. However, three types of explanations have been proposed. First, the plasma may initially rotate and because of profile changes related to transport later reach the critical rotation. The magnitude of initial rotation for this explanation to hold requires the ions to carry a large fraction of the current initially. Since this is inconsistent with observations in other theta pinches, this explanation seems unlikely.

A second possible explanation of plasma rotation might be end shorting on the open field lines and viscous transfer of rotation to the remainder of the plasma. This is unlikely to be the full explanation because the energy available in the open field region is much less than the final rotational energy of the plasma.

Finally, particle loss from the closed field region might result in the loss of angular momentum from the system and corresponding plasma rotation. This appears to be the most likely cause of rotation. There are five types of particle orbits in a field reversed configuration and those encircling the axis or outside the separatrix have negative mechanical angular momentum. These particles are lost in a thermal transit time, resulting in a net gain of angular momentum by the confined plasma. In fact, for a neutral plasma, the total mechanical angular momentum of all particles is a constant of the motion. Thus, if a fraction F of particles are lost from a plasma with no initial rotation, this conservation law is approximately

$$(1-F)m_i NR^2 + Fm_i N\langle r^2\omega_d\rangle = 0 \qquad (6)$$

where m_i is the ion mass, N is the total number of particles, R is the plasma major radius, ω_d is the drift frequency of an ion at radius r where it is lost, and $\langle\ \rangle$ indicates an average over the particle distribution. For a rigid rotor distribution with cold electrons, the rotational velocity reaching the instability threshold requires the loss of about one half of the plasma. Experimental measurement of the particle confinement time gives a value of about 35% ±15% for the fraction of particles lost at the time the rotational instability is observed. This result is somewhat inconclusive in determining the rotation mechanism, however, other factors could account for rotation in addition to the particle transport mechanism.

1. R. K. Linford et al., Proc. Seventh IAEA Conf. on Plasma Physics and Controlled Nuclear Fusion Research, Innsbruck, Austria (1978).

2. A. G. Es'kov et al., ibid.

3. J. K. Wright, R. D. Medford, and B. Chambers, Plasma Physics 12, 242 (1961).

4. A. Kadish, Phys. Fluids 22, 2248 (1979).

5. R. Linford, private communication.

6. I. B. Bernstein, et al., Proc. Roy. Soc. A 244, 17 (1958).

7. J. U. Brackbill, Meth. in comp. Phys. 16, 1 (1976).

8. A. I. Shestakov, D. D. Schnack, J. Killeen, these proceedings.

9. D. C. Barnes and C. E. Seyler, LASL Report, LA-UR-79-13, January 1979.

10. D. V. Anderson, D. C. Barnes, W. A. Newcomb, these proceedings.

11. L. D. Pearlstein et al., Paper No. CN-37-5-1-2, Proc. Seventh IAEA Conf. on Plasma Physics and Controlled Nuclear Fusion Research, Innsbruck, Austria (1978).

12. J. P. Freidberg, private communication.

13. C. E. Seyler, submitted to Phys. Fluids.

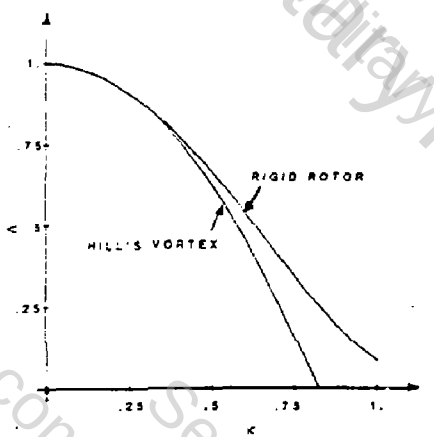

Figure 1 - Normalized separatrix pressure, P, as a function of normalized plasma radius K for two profiles. Hill's vortex curve for $P'(\psi) = -\lambda$ (constant). Rigid rotor profiles for $P'(\psi) = \alpha \exp(-\psi/\psi_0)$.

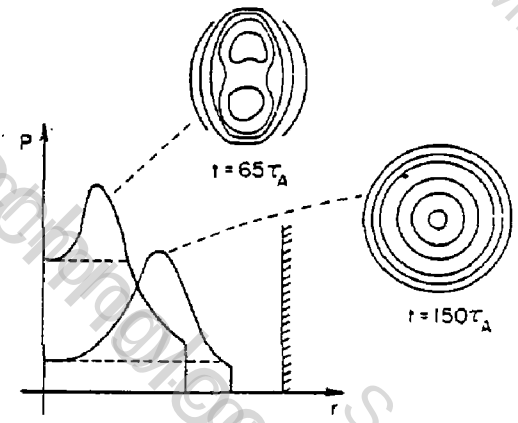

Figure 2 - Results of three-dimensional simulations for two different elongated plasmas. Curves indicate P in midplane as a function of r for two cases. Conducting wall position is indicated by shaded line. Density contours at late times indicate n = 2 instability for compressed case, stability for less compressed case.

TWO-DIMENSIONAL SIMULATION OF COMPACT TORUS FORMATION

D. W. Hewett, Los Alamos Scientific Laboratory, Los Alamos, New Mexico 87545

A recently-developed two-dimensional algorithm[1] is now being used in formation studies of the FRX configuration at LASL. The new procedure is part of a quasi-neutral R-Z hybrid code which, by representing the ion component by the particle-in-cell technique, correctly represents the complicated orbits exhibited by the ions in such field-reversed configurations. The electron and Maxwell's equations are combined in the new part of the algorithm in the zero-electron-inertia limit to eliminate electron time scales. The resulting combination is solved so that electron source terms and the electric and magnetic fields are provided self-consistently even in strongly inhomogeneous plasmas with arbitrary plasma-vacuum intermixing. As will be seen, this last feature makes simulation of such highly dynamic configurations as the FRX much more tractable.

The FRX formation studies are accomplished by simulating the time evolution of a homogeneous plasma with a negative bias B_z-field (-500 gauss) which is subjected at $t = 0$ to an external implosion B_z-field (5 KG). The implosion field drives the plasma toward the axis where it exhibits rapid radial oscillations for a period of about 1.5 μs. After this initial chaotic behavior, the plasma settles into a configuration which, while not yet in thermal equilibrium, attains the macroscopic appearance of an infinitely long field reversed θ-pinch configuration. Figure 1 shows the ion particle positions in R-Z space at this time. The surrounding magnetic flux contour is also shown.

After the gross radial motion has subsided, the plasma develops inhomogeneities along the outer surface of the configuration in the Z-direction. Given the restrictions of R-Z geometry, these perturbations are necessarily $m = 0$ modes. As is apparent in Fig. 2, these perturbations continue to grow, and after approximately 3 μs from the $t = 0$ implosion break the axially homogeneous configuration into elongated current rings or compact toroids with dimensions of roughly 2.5 cm in minor radius in the R direction and 10 cm in minor radius in the Z-direction. The initial configuration had a 10 cm radius and has a periodicity length in Z of 50 cm. Also shown in Fig. 2 are the contours of constant toroidal flux, which now indicate reconnection.

The $t = 0$ temperature of both electrons and ions was 1 eV and at $t = 3$ μs the ions were roughly 4 keV. A self-consistent electron temperature has not yet been included in the model. For this run T_e was artifically raised from 1 eV to 50 eV linearly during the first 500 ns of the simulation and then held constant. The electrical resistivity is the Spitzer value consistent with this electron temperature.

1. D. W. Hewett, "A Global Method of Solving the Electron-Field Equations in a Zero-Inertia-Electron-Hybrid Plasma Simulation Code", accepted for publication in J. Comp. Physics, (1979).

FIGURE 1

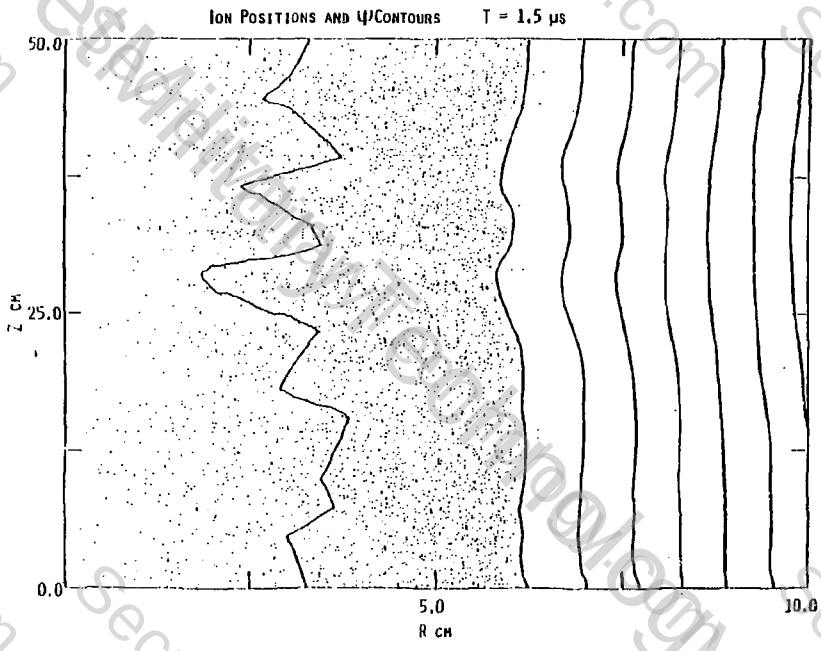

FIGURE 2

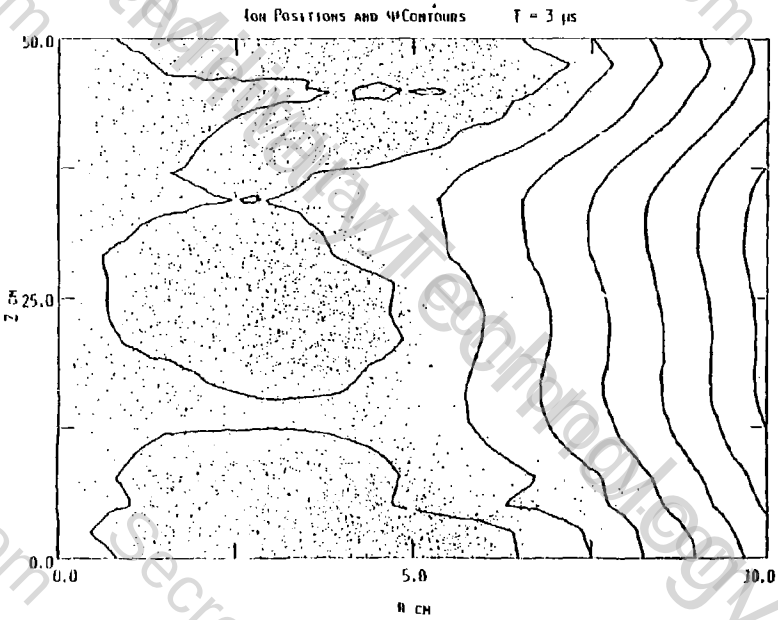

Two-Dimensional Compression in General Compact Tori

E. Hameiri and W. Grossmann

Courant Institute, New York University, New York, N. Y. 10012

Introduction

Field-reversed θ-pinches are observed to rotate, presumably as a result of of the loss of particles. If the rotating plasma is compressed, conservation of angular momentum dictates that the rotation frequency will increase by approximately the square of the radial compression ratio. Thus, even a small initial rotation may affect the equilibrium state and stability properties of the compressed plasma.

In this work we generalize the adiabatic compression code of H. Grad [1] to include the effects of rotation. The situation envisioned is a compression process much slower than acoustical transit times across the major dimensions of the plasma. The plasma waves then cause fast equilibration and on the compression time scale the plasma is seen as creeping from one equilibrium state to the next. The different states are related to each other by maintaining constants of the motion of the exact dynamical system, namely: the magnetic flux and the mass and angular momentum within each flux tube. The compression itself is created either by increasing the magnetic flux in the vacuum region, or by moving the external wall to a new radial position (to simulate the liner experiment).

For the work described here, transport processes have been neglected and the plasma is assumed to obey the ideal MHD equations. We also assume that the plasma is contained completely within the closed separatrix. This represents a slight departure from reality since experimental measurements have shown a small but finite pressure on the separatrix. It offers, however, a substantial numerical advantage in eliminating surface currents which may appear in a compressed plasma which spills outside the separatrix. In addition, the assumption makes it possible to guarantee that the computed equilibria will be interchange stable. (The interchange stability criterion was generalized to cover rotating systems.)

The Equilibrium State

In a rotating axisymmetric equilibrium state, if the magnetic field has a toroidal component B_θ, compression of the plasma will generate both toroidal and poloidal flows. To avoid this complication and consider purely toroidal flows we assume $B_\theta = 0$ if the plasma rotates. In the static case we allow $B_\theta \neq 0$.

The rotating equilibrium state can be described by a poloidal flux function ψ such that $\underline{B} = \hat{\theta} \times \nabla\psi/r$, and three functions of ψ: the entropy $s(\psi)$, the toroidal rotation frequency $\Omega(\psi)$, and the Bernoulli function $H(\psi)$. (Notice that each field line must rotate like a rigid body.) The equilibrium equations are then

$$-\operatorname{div}(\nabla\psi/r^2) = r^2\rho\Omega\dot{\Omega} + \rho\dot{H} - \rho^\gamma\dot{s}/(\gamma-1) \tag{1}$$

$$\gamma s\rho^{\gamma-1}/(\gamma-1) = H + r^2\Omega^2/2 \tag{2}$$

with the dot derivative denoting $d/d\psi$. Given the value of ψ on the plasma boundary, and using equation (2) to solve for the density $\rho = \rho(r,\psi)$, Eq. (1) becomes a standard elliptic problem. Notice that (2) can be easily solved for $\gamma = n/(n-1)$, with n some integer, since then $\gamma-1 = 1/(n-1)$. The correct γ value (5/3) between $n = 2$ ($\gamma = 2$) and $n = 3$ ($\gamma = 3/2$). Here, for simplicity, we use $\gamma = 2$.

During compression, $s(\psi)$ is unchanged but H and Ω vary. To find them it is convenient to present a variational formulation for the rotating equilibrium (along the lines of a known static formulation [2]).

$$\begin{aligned} &\text{Minimize} \quad E = \int \underset{\sim}{B}^2/2 + \rho\, r^2\Omega^2/2 + s\rho^\gamma/(\gamma-1) \\ &\text{subject to} \quad \int_{V(\psi)} \rho\, dv = M(\psi)\ , \quad \int_{V(\psi)} r^2\rho\,\Omega\, dv = L(\psi) \end{aligned} \tag{3}$$

and the range of ψ in the plasma is also given. $V(\psi)$ is the domain within a particular ψ surface. The two constraints represent conservation of mass and angular momentum, and the functions $s(\psi), M(\psi), L(\psi)$ are unchanged during compression.

Following Grad [1], we introduce a surface average, $\langle f\rangle \equiv \int f\, dS/|\nabla\psi|$, with the function $V(\underset{\sim}{x})$ describing the volume within any ψ-curve. We also define the inductance function $K(V) = \langle|\nabla\psi|^2/r^2\rangle$. After differentiating the constraints with respect to V and defining $\mu(\psi) = S\dot{M}^\gamma$, $\lambda(\psi) = L/\dot{M}$ and $\rho \equiv M\psi' u$ ($\psi' \equiv d\psi/dV$), the variational problem takes the form

$$\begin{aligned} &\text{Minimize} \quad E = \int \frac{1}{2}K(V)\psi'^2 + \frac{1}{2}\lambda^2\psi'/\langle r^2u\rangle + \mu\psi'^\gamma\langle u^\gamma\rangle/(\gamma-1) \\ &\text{subject to} \quad \langle u\rangle = 1\ . \end{aligned} \tag{4}$$

Assuming for the time being that the geometry is known, i.e., $V(\underset{\sim}{x})$ is given but not $\psi(\underset{\sim}{x})$, K(V) is then known and averages can be taken. The Euler equation for u yields (for $\gamma = 2$)

$$u = a(V) + r^2 b(V)\ . \tag{5}$$

$\langle u\rangle = 1$ implies $u = 1 + (r^2 - \langle r^2\rangle)b$. This expression is inserted into (4), yielding an unknown function b(v) instead of $u(\underset{\sim}{x})$. E now is minimized with respect to ψ and b by solving the corresponding Euler equations (an ODE for ψ, an algebraic cubic equation for b).

Numerical Algorithm

(i) Initial level curves in the plasma region are assumed.
(ii) $\psi(V)$ is obtained by solving a mixed ODE-algebraic system as described before. The shooting method is used to satisfy the boundary conditions of given ψ values at $V = 0$ and at the total plasma volume.

(iii) A comparison of (2) and (5) enables us to determine H, Ω at each point in space.

(iv) The right-hand side of (1) is evaluated as a function of ψ. In particular it is set to zero in the assumed vacuum region. Eq. (1) is solved as a linear Poisson problem. The boundary conditions used are a constant value of ψ at the outer wall and $\psi = \text{const.} \cdot r^2$ at the two ends of the device. This last condition equals the behavior of ψ in the absence of any plasma.

(v) The geometry of the new solution is determined. Steps (ii)-(v) are repeated until convergence is achieved.

Interchange Stability

When $B_\theta = 0$, all field lines within the plasma region are closed, regardless of rotation. Thus, the relative positions of fluid elements carrying specific mass μ and angular momentum λ, cannot be predetermined but have to be found as part of the solution. Specifically, it means that instead of specifying the functions $\mu(\psi),\lambda(\psi)$ one gives the set of values of these functions but allows "permutations". Presumably, the plasma will pick a permutation corresponding to the lowest energy state. From a numerical point of view, however, this state is rather difficult to find. We treat the problem as a stability problem (the usual misconception) where we specify $\mu(\psi),\lambda(\psi)$ and then check if the energy decreases after local permutations. After some experimentation it is possible to find states which remain stable throughout the compression.

The criterion for stability can be obtained in the following way: specify functions $\mu_0(\psi),\lambda_0(\psi)$, and let $\mu(\psi) = \mu_0(f(\psi))$, $\lambda(\psi) = \lambda_0(f(\psi))$. $f(\psi)$ expresses the original flux coordinate of the particle now residing in ψ. Because of the flux conservation, f is required to be measure preserving, with the measure expressing total flux. Thus $\text{meas}\{f^{-1}(E)\} = \text{meas}\{E\}$ for every set E in the ψ interval. For a given magnetic field and density, the energy has the form $E = \int F(f(\psi),\psi)\, d\psi$ and has to be minimized with respect to all measure preserving f. It can be shown that a necessary condition for the function $f(\psi) \equiv \psi$ to be a local minimum (local in the maximum norm sense), is to have $\partial^2 F/\partial f \partial \psi \leq 0$ at $f = \psi$, for all ψ in the plasma. In terms of the variables in Eq. (4), stability requires

$$\psi'\{\dot{\mu}(\langle u^\gamma\rangle\psi'^{\gamma-1})'/(\gamma-1) + \lambda\dot{\lambda}(1/\langle r^2 u\rangle)'\} \leq 0 . \qquad (6)$$

It is difficult to decide analytically when the criterion will be satisfied except for the static case $\lambda \equiv 0$. Then $u \equiv 1$ and we have the condition $\dot{\mu}\psi'' \leq 0$. This is recognized as the well known interchange stability criterion, where it is pointed out that $2\pi\psi' = (\oint d\ell/B)^{-1}$ and $\mu\psi'^\gamma$ is the pressure. In the inside region of a reverse field configuration it appears that always $\psi'' > 0$, hence we need μ to be *nondecreasing* towards the boundary. Notice that the pressure can still vanish at the plasma boundary if $\psi' \to 0$ there. Fortunately, this is the case since $K \to \infty$ at the boundary due to the singularity associated with the separatrix while $K\psi'$, which is the total toroidal current, remains finite. The current density however depends on the derivative of singular quantities and will tend to infinity towards the separatrix. This "skin current" appears regardless of the rotation only if we insist on interchange stable equilibria. The computation also suggests that

it is favorable for stability to have λ^2 decrease towards the separatrix.

Results

1. Typical compressions by increase of the magnetic flux in the vacuum region, tend to make flux surfaces circular while preserving the aspect ratio (defined as the ratio of the plasma radius to the radius of the magnetic axis).
2. Typical liner compressions tend to elongate the flux surfaces.
3. In all cases β increases by a few percent during compression. (β is defined in terms of volume integrals over the plasma region.)
4. The Mach number of the rotation (with respect to the relevant fast magnetoacoustic wave) increases by only a few percent during compression, thus removing the possibility of shocked solutions as the result of the increase in rotation frequency.
5. The evolution of the ratio $\alpha = \Omega/\Omega_*$, with Ω_* the diamagnetic frequency ($\Omega_* = \nabla p \times B/(2rneB^2)$), was monitored during compression. $\alpha < 1$ is known [4] to be a sufficient condition for stability within the FLR model. We find in the few cases computed, that α decreases during compression thus suggesting that the compression itself will not give rise to rotational instabilities.

Acknowledgment

The authors wish to thank J. Saltzman and D. Stevens for assistance in the computations. Work performed under Contract No. EY-76-C-3077 with the Department of Energy.

References

1. H. Grad, P. N. Hu and D. Stevens, Proc. Nat. Acad. Sci. USA, Vol. 72, 10, 3789 (1975).

2. M. D. Kruskal and R. M. Kulsrud, Phys. Fluids 1, 265 (1958).

3. H. Grad, Phys. Fluids 7, 1283 (1964).

4. J. Freidberg and D. Pearlstein, Phys. Fluids 21, 1207 (1978).

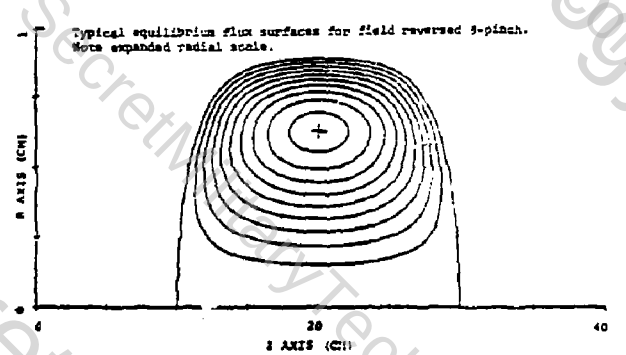

TEARING-MODE STABILITY ANALYSIS OF A CYLINDRICAL PLASMA

H. L. Berk, J. Sayer, D. D. Schnack, University of California, Lawrence Livermore Laboratory, Livermore, CA, USA

Reversed field θ-pinch experiments exhibit long lifetimes,[1-3] and the question of stability to the tearing mode frequently arises. In this note, we use neighboring equilibrium arguments originally developed by Pfirsch[4] to show that tearing-mode stability is strongly enhanced if two conditions are fulfilled: the first that the flux tend to be excluded in the bulk of the plasma, and the second that the plasma edge lie close to the axis. Such conditions tend to be fulfilled in reversed-field θ-pinch experiments and may be responsible for lack of observations of tearing instability. This beneficial effect can also arise in steady-state plasmas with a significant bootstrap effect, where the flux is low throughout the body of the plasma.

First, let us consider a class of MHD cylindrical equilibria for the flux ψ that satisfy the Grad-Shafranov equation,

$$r \frac{\partial}{\partial r} \frac{1}{r} \frac{\partial \psi}{\partial r} + r^2 \frac{\partial p}{\partial \psi} = 0 \quad , \tag{1}$$

where p is the pressure, and the magnetic field $B_z = \frac{1}{r} \frac{\partial \psi}{\partial r}$. We choose

$$\frac{\partial p}{\partial \psi} = - \alpha^2 \psi \, \theta(\psi_e - \psi) \quad , \tag{2}$$

where ψ_e is the flux at the plasma edge.

The solution to Eq. (2) in the region containing plasma is

*Work performed under the auspices of the U.S. Department of Energy by the Lawrence Livermore Laboratory under contract number W-7405-ENG-48.

$$\psi = \frac{B_e \cosh\,[\alpha(r^2 - r_0^2)/2]}{\alpha \sinh\,[\alpha(r_0^2 - r_e^2)/2]}$$

$$r_e^2 < r^2 < 2r_0^2 - r_e^2 \qquad (3)$$

$$B = \frac{B_e \sinh\,[\alpha(r^2 - r_0^2)/2]}{\sinh\,[\alpha(r_0^2 - r_e^2)/2]}$$

Here r_0 is the position of the field null, and the inner and outer boundaries of the plasma are $r^2 = r_e^2$, $2r_0^2 - r_e^2$, respectively. We assume the presence of a wall ($r^2 = r_w^2$) that traps the flux of the plasma.

To apply the neighboring equilibrium method, we need to consider perturbations of the form $\delta\psi = \delta\psi_k(r) \exp(ikz)$ that satisfy the equation

$$r \frac{\partial}{\partial r} \frac{1}{r} \frac{\partial}{\partial r} \delta\psi - k^2 \delta\psi = -r^2 \frac{\partial^2 p}{\partial \psi^2} \delta\psi \quad , \qquad (4)$$

with the boundary condition $\delta\psi(r^2 = 0) = 0$. If we can show that $\delta\psi(r^2)$ has no nulls between $0 \le r^2 \le r_w^2$, then the system is stable to tearing. (This is the same technique used by Marx.[5])

We now have, from Eq. (2),

$$\frac{\partial^2 p}{\partial \psi^2} = -\alpha^2\, \theta(\psi_e - \psi_1) + \alpha^2 \delta(\psi - \psi_e)\, \psi_e$$

$$= -\alpha^2\, \theta(r^2 - r_e^2)\, \theta(2r_0^2 - r_e^2 - r^2)$$

$$+ \frac{\alpha^2 \psi_e}{\pi B_e} \left\{ \delta(r - r_e) + \delta[r - (2r_0^2 - r_e^2)^{1/2}] \right\} \qquad (5)$$

Hence the equation for $\delta\psi$ becomes,

$$\frac{1}{r}\frac{d}{dr}\left(\frac{1}{r}\frac{d\delta\psi}{dr}\right) - \alpha^2\delta\psi\,\theta(r^2 - r_0^2)\,\theta(2r_0^2 - r_e^2 - r^2) - k^2\delta\psi/r^2$$

$$= -\frac{\alpha^2\delta\psi}{rB_e}\psi_e\left\{\delta(r - r_e) + \delta[r - (2r_0^2 - r_e^2)^{1/2}]\right\} . \qquad (6)$$

The easiest case to analyze (and the most difficult to stabilize) is $k = 0$, and we now limit ourselves to this case.

After solving for Eq. (6), the marginal stability condition found is,

$$\alpha r_w^2 \leq 2\alpha r_0^2 + 2\sinh\left[\alpha(r_0^2 - r_e^2)\right]\left\{1 - \frac{\alpha r_e^2}{2}\coth\left[\frac{\alpha(r_0^2 - r_e^2)}{2}\right]\right\} . \qquad (7)$$

The most dramatic aspect of this result is the improvement of the stability criteria for large α if $\alpha r_e^2 < 2$. If we first consider $r_e = 0$, we have

$$\frac{r_w^2}{2r_0^2} \longrightarrow \begin{cases} 2 \;, & \alpha r_0^2 \to 0 \\ \dfrac{1}{\alpha r_0^2}\exp(\alpha r_0^2) \;, & \alpha r_0^2 \gg 1 \;, \end{cases} \qquad (8)$$

which shows that the wall can be exponentially far as α becomes large. Physically, α increasing corresponds to increasing the flux exclusion in the plasma. The flux contained in the plasma is $\psi(r_e) - \psi(r_0)$, which from Eq. (3b) gives,

$$\psi(r_e) - \psi(r_0) \xrightarrow[\alpha r_0^2 \to 0]{} \frac{B_e}{4}(r_0^2 - r_e^2) \qquad \xrightarrow[\alpha r_0^2 \gg 1]{} \frac{B_e}{\alpha}$$

The stabilizing property of flux exclusion disappears if the plasma edge is away from the axis, i.e., $\alpha r_e^2/2 \geq 1$. Assuming $\alpha r_0^2 \gg 1$, αr_e^2, Eq. (7) is approximately

$$r_w^2 \leq r_{ed}^2 + r_e^2 - \frac{2}{\alpha}\left(\frac{\alpha r_e^2}{2} - 1\right) \sinh(\alpha r_0^2) \quad . \tag{9}$$

Then a wall outside the plasma can stabilize only when $\frac{\alpha r_e^2}{2} < 1$.

REFERENCES

1. A. Eberhagen, W. Grossman, Z. Phys. 248, 30 (1971).
2. A. G. Eskov et al., Proceedings of the 7th IAEA Conference on Plasma Physics and Controlled Thermonuclear Research (1978).
3. R. K. Linford et al., Proceedings of the 7th IAEA Conference on Plasma Physics and Controlled Thermonuclear Research (1978).
4. D. Pfirsch, Z. Naturforshg. 17a, 861 (1962).
5. K. Marx, Phys. Fluids 11, 357 (1968).

THE TILTING MODE IN THE REVERSED-FIELD THETA PINCH*

A.I. Shestakov, D. D. Schnack, and J. Killeen, National Magnetic Fusion Energy Computer Center, Lawrence Livermore Laboratory, Livermore, CA 94550

1. Introduction

There is currently active interest in plasma confinement schemes in which the separatrix extends to the major axis. Fusion experiments based on such configurations (e.g. the field-reversed theta pinch, the field-reversed mirror, Spheromak, etc.) are expected to avoid certain engineering difficulties associated with conventional toroidal devices. Higher values of β may also be attainable.

The MHD stability of such equilibria has been investigated analytically by Rosenbluth and Bussac [1] who used a modified energy principle to determine marginal stability to all ideal modes and most tearing modes. They found stability against magnetically driven modes for all toroidal mode numbers $n>1$, but found an unstable $n=1$ mode for prolate spheroidal plasmas (prolomaks). This mode, which is characterized by a rotation of the major axis inside the separatrix, is termed the tilting mode.

In this paper we describe preliminary results of a numerical investigation of the resistive stability of such devices. We employ an initial value approach in which the linearized resistive MHD equations are used to follow the time evolution of an arbitrary perturbation in a known equilibrium configuration until an exponentially growing eigenmode appears. The fastest growing mode is thus determined. This differs from previous work [2] in that Fourier decomposition is performed only in the toroidal direction so that two-dimensional equilibria can be treated. The specific model is described briefly in section 2, and in more detail elsewhere [3].

We have applied our model to a numerically determined equilibrium [4] which contains no toroidal field and closely resembles the FRX-B experiment at Los Alamos. We find this prolate configuration to be unstable to an $n=1$ tilting mode, in qualitative agreement with ref. [1]. These results, and their relevance to experimental observations, are described in section 3.

2. Computational Model

We assume that the hydromagnetic approximation is valid, that the resistivity is isotropic; neglect pressure and inertia terms in Ohm's law, and take the fluid to be incompressible. When a static equilibrium ($\vec{v}_0=0$) and constant density are assumed, and the effects of perturbed resistivity are neglected, the resulting linearized resistive MHD equations are:

$$\frac{\partial \vec{B}_1}{\partial t} = \text{curl}\left(\vec{v}_1 \times \vec{B}_0 - \frac{c^2}{4\pi}\eta_0 \text{ curl } B_1\right), \tag{1}$$

$$\text{div } \vec{B}_1 = 0, \quad \text{div } \vec{v}_1 = 0, \tag{2}$$

$$-\rho_0 \nabla^2\left(\frac{\partial \vec{v}_1}{\partial t}\right) = \frac{1}{4\pi} \text{ curl curl } \left[(\vec{B}_0\cdot\nabla)\vec{B}_1 + (\vec{B}_1\cdot\nabla)\vec{B}_0\right]. \tag{3}$$

*Work performed under the auspices of the U.S. Department of Energy by the Lawrence Livermore Laboratory under Contract Number W-7405-ENG-48.

We obtain Eq. (3) by taking the double curl of the equation of motion.

The component equations are written in cylindrical coordinates and the equilibrium is specified by: $\bar{B}_o = \hat{r}\, B_{ro}(r,z) + \hat{\phi}\, B_{\phi o}(r,z) + \hat{z}\, B_{zo}(r,z)$. The perturbations are of the form $f_1(r,z,t)\exp(in\phi)$. In the following we consider non-axisymmetric instabilities ($n \neq 0$). The conditions (2) allow us to express $v_{\phi 1}$ and $B_{\phi 1}$ in terms of their corresponding r and z components. The Reversed Field Theta Pinch (RFTP) experiment contains no toroidal field ($B_{\phi o} = 0$). This allows us to consider only the four variables v_{r1}, v_{z1}, B_{r1}, and B_{z1}. In the general case with non-zero $B_{\phi o}$, we need to compute both the real and imaginary parts of the complex perturbations giving a total of eight unknown quantities.

It is convenient to put the equations in dimensionless form. There are two characteristic time scales in the problem, the resistive diffusion time, $\tau_R = 4\pi a^2/c^2\langle\eta\rangle$, and the hydromagnetic transit time, $\tau_H = a(4\pi\langle\rho_o\rangle)^{1/2}/\langle B\rangle$. The symbol $\langle\ \rangle$ denotes a characteristic value for the enclosed variable; "a" denotes a characteristic distance. We non-dimensionalize time by τ_H, spatial coordinates by "a", magnetic fields by $\langle B\rangle$ and velocities by $v_A = a/\tau_H$. The magnetic Reynolds number is $S = \tau_R/\tau_H$.

In the RFTP case, the above substitutions in Eqs. (1) and (3) yield four equations of which we present only the B_{z1} equation in detail:

$$\frac{\partial B_{z1}}{\partial t} = \frac{n}{S} L(B_{z1}) - S^{-1}\frac{\partial \eta}{\partial r}\left(\frac{\partial B_{r1}}{\partial z} - \frac{\partial B_{z1}}{\partial r}\right) + \left(B_{ro}\frac{\partial v_{z1}}{\partial r} + B_{zo}\frac{\partial v_{z1}}{\partial z} - \frac{\partial B_{zo}}{\partial r}v_{r1} - \frac{\partial B_{zo}}{\partial z}v_{z1}\right) \qquad (4)$$

where $L(u) = \frac{1}{r}\frac{\partial}{\partial r}\left(r\frac{\partial u}{\partial r}\right) + \frac{\partial u}{\partial z^2} - \frac{n^2}{r^2}u$.

Implicit Difference methods are used to solve the system of four equations. The same equations are assumed to hold inside the plasma and in the vacuum. We presently assume constant resistivity ($=1$) in the plasma but set η to an arbitrarily high value ($=10^{20}$) in the vacuum.

These assumptions allow the use of a modified leap-frog, predictor-corrector algorithm to advance the system one equation at a time. In the η=constant case under consideration, Eq. (4) does not contain B_{r1}. Given B_{z1} at time $n\Delta t$ and $(n-1)\Delta t$ and v_1 at $t = n\Delta t$, B_{z1} is advanced by its implicit discretization at $(n+1)\Delta t$, and a leap-frog discretization of v_1 at $n\Delta t$. Once B_{z1}^{n+1} is computed, a similar approach is used in the analogue of Eq. (4) to compute B_{r1}^{n+1}. Using B_1 at $t=n\Delta t$ and the newly computed B_{r1}^{n+1}, B_{z1}^{n+1}, the v_{r1}, v_{z1} equations are solved by implicit methods to compute the poloidal velocity. This describes the predictor phase of the time advancement. The fields can be corrected in a similar manner, however in practice the correction cycle is rarely used.

We are also able to compute axisymmetric ($n=0$) instabilities by similar initial value methods. The equations in this case are modified and are

described elsewhere [3]. Results for the RFTP indicate that those instabilities are less dangerous than the n=1 case to be described below.

3. Preliminary Results

We apply the methods described above to a numerically obtained equilibrium with zero toroidal field [4]. The particular case has a half-length of 45 cm., and a conducting wall of r_w= 12.5 cm. The resulting plasma properties are $n= 2\times10^{16}$ cm^{-3}, $B_{z\text{wall}}$= 8.84 KG, and T= 100 eV. The midplane plasma radius is 6 cm, the vortex radius is 3.4 cm, and the separatrix radius is 4.7 cm. The separatrix intersects the major axis at z_{sep}= 20.9 cm, so that the plasma resembles a prolomak with elongation z_{sep}/r_{sep}= 4.45. This configuration closely models the FRX-B experiment, and the poloidal flux surfaces are shown in figure 1. As stated above, we model the vacuum as a highly resistive region, and choose the scale length to be a= r_{wall} = 12.5 cm. This results in a magnetic Reynolds number S ≈ 10^3.

As described above, we excite an n=1 perturbation and follow the solution forward in time until an exponentially growing eigenmode appears. In figure 2a we display the resulting poloidal velocity field $\vec{v}_p = v_r \hat{r} + v_z \hat{z}$, and figure 2b shows contours of constant toroidal velocity v_ϕ. We remark that the results portrayed in figures 2a,b lie on distinct ϕ= const. planes that differ by an angle of $\pi/2$. This is due to the description of the perturbations as $\mathrm{Re}[u(r,z,t)\exp(in\phi)]$ and the use of Eq. (2) to express $v_{\phi 1}$ in terms of v_{r1} and v_{z1}. While the largest displacements are clearly concentrated near the vortex, a more detailed analysis reveals that there is net flow across the major axis corresponding to a tilting of the plasma inside the separatrix. Figure 3a shows the magnetic field vectors for the equilibrium configuration $\vec{B}_o = B_{ro}\hat{r} + B_{zo}\hat{z}$. This is to be contrasted with figure 3b in which we plot $\vec{B} = \vec{B}_o + .1\vec{B}_1$, thus displaying the distortion due to the presence of the eigenmode. The tilting of the major axis is evident.

We have found the growth rate for this mode to be $\omega\tau_H$= 0.47, approximately independent of resistivity. This corresponds to an e-folding time of ~ 2μsec. However, experimental results indicate that such configurations can persist in a quiescent state for times approaching 30 μsec, the discharge being lost due to a rotationally driven n=2 interchange instability. There are several possible reasons for the lack of observation of the tilting mode [5]. Firstly, it is thought that the experimental flux surfaces may be more "racetrack" than elliptical, as they are in our model. In that case the concentration of magnetic field in the regions of high curvature may be stabilizing. Secondly, even if the experimental flux surfaces were elliptical, nonlinear effects may cause the field in the high curvature regions to increase, leading to a reduced growth rate or complete saturation. Thirdly, the effect of finite particle orbits on this mode is unknown, but is probably stabilizing.

References

1. M.N. Rosenbluth and M.N. Bussac, Nucl. Fusion 19, 489 (1979).
2. J.A. DiBiase and J. Killeen, J. Comp. Phys. 24, 158 (1977).
3. J. Killeen, D.D. Schnack, and A.I. Shestakov, Lawrence Livermore Laboratory Report UCRL-83332 (1979).
4. D.V. Anderson, W.A. Newcomb, and D.C. Barnes, these proceedings.
5. D.C. Barnes, C.E. Seyler, and D.V. Anderson, these proceedings.

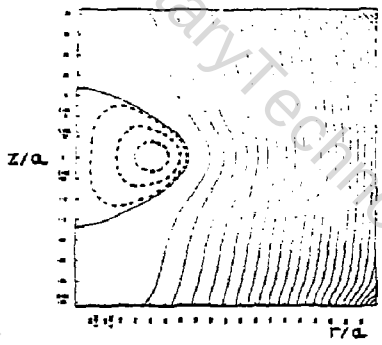

Fig. 1. Equilibrium ψ_0

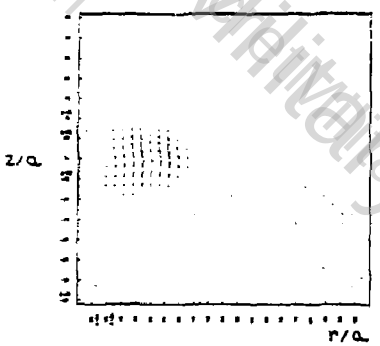

Fig. 2a. Perturbed poloidal velocity

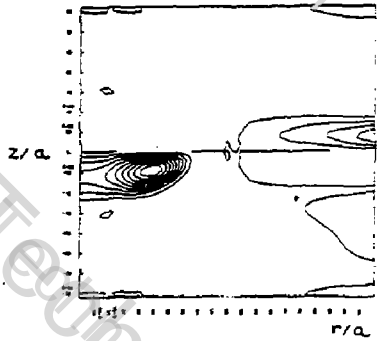

Fig. 2b. Perturbed toroidal velocity

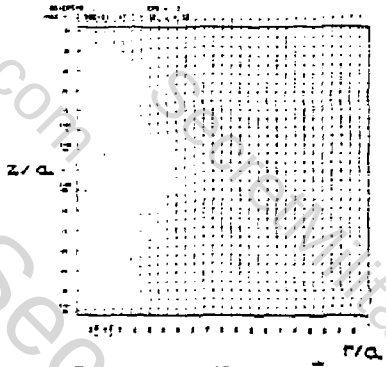

Fig. 3a. Equilibrium $\vec{B}_0$

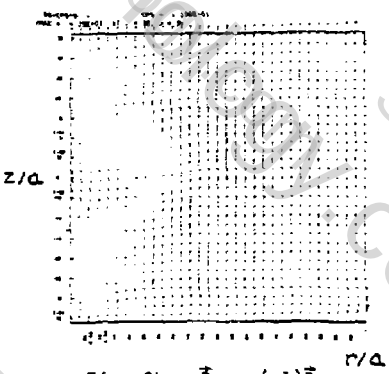

Fig. 3b. $\vec{B}_0 + (.1)\vec{B}_1$

PERIODIC FIELD-REVERSED EQUILIBRIA FOR A MULTIPLE-CELL LINEAR THETA PINCH*

H. Meuth and F.L. Ribe
University of Washington
Seattle, Washington 98195

I. Introduction

Analytical solutions for azimuthally symmetric reversed-field MHD equilibria were the object of several early investigations.[1] Recently, there has been renewed interest in these solutions, particularly in the investigation of the MHD stability of a Field-Reversed Theta Pinch.[2,3] In this paper we report the possibility of producing periodic field-reversed equilibria in the High-Beta Q Machine.[4] We give analytical solutions within the framework of a linear flux approach:[5]

$$p' = dp/d\Psi = \bar{p}\cdot(a + b\Psi)$$
$$I^{2\prime} = dI^2/d\Psi = \bar{I}^2\,(r_a^2 a + r_b^2 b\Psi)\ , \qquad (1)$$

where Ψ is the longitudinal flux, p the plasma pressure and I the longitudinal current. All other quantities are independent of r,z. The disposable parameters a and b are constrained by certain stability criteria[2] for the case where I=0 and Ψ is periodic in z.

II. The Problem

A. Inside the plasma: We assume $p \neq 0$ and take the Fourier expansion of the real quantity $\tilde{\Psi} = \Psi + a/b$. After a change of variable to $x = \alpha r^2$, the differential equation for the flux[1] takes the following form:

$$\frac{d^2}{dx^2}\tilde{\Psi}_k(x) + \left(\frac{b}{4\alpha^2} + \frac{1}{x}\,\frac{br_b^2 - k^2}{4\alpha}\right)\tilde{\Psi}_k(x) = \frac{1}{x}\,\frac{a(r_b^2 - r_a^2)}{4\alpha}\,\delta_{k,0}\ . \qquad (2)$$

Depending on the sign of b, we can choose the scaling parameter α conveniently to transform (2) into the form of the Coulomb-Wave equation (b>0) or into Whittaker's standard form (b<0).[5]

For $\Psi(r=0,z) \equiv 0$, and with $X_{(b)} = \tfrac{1}{2}\sqrt{|b|}\,r^2_{(b)}$, the general solution of the homogeneous part of (2) (i.e., $r_a = r_b$) reads[5] as follows:

(1) for b < 0:

$$\Psi(r,z) = \frac{a}{|b|}\,(1 - \Gamma(\tfrac{1}{2}\chi_b)\,W_{\kappa(0),\frac{1}{4}}(2X)) + \sum_{k\geq 0} M_{\kappa(k),\frac{1}{4}}(2X)(A_k e^{ikz} + A_{-k}e^{-ikz}) \qquad (3a)$$

where $\kappa(k) = -k^2/4\sqrt{|b|} - \tfrac{1}{2}\chi_b$. The M's and W's are the regular and irregular Whittaker functions respectively.

(2) For b > 0:

$$\Psi(r,z) = \frac{a}{b}\,(G_0(-\tfrac{1}{2}\lambda_b;X) - 1) + \sum_{k\geq 0} F_0(\kappa(k),X)(A_k e^{ikz} + A_{-k}e^{-ikz})\ , \qquad (3b)$$

*Work supported by the U.S. Department of Energy.

where $\eta(k) = k^2/4\sqrt{b} - \frac{1}{2}x_b$. Here F_L and G_L are the regular and irregular Coulomb-wave function.[6]

For reference we give only the resulting fields on axis ($r \to 0$) for $I = 0$;

$$B_r = 0;\ B_z = \frac{\sqrt{|b|}}{2\pi}\left(2A_0 + \sum_{k\neq 0}\left(A_k e^{ikz} + A_{-k}e^{-ikz}\right)\right) . \qquad (4)$$

If there is only one non-zero Fourier component, (4) implies for a multiple cell solution: $2A_0 < A_k + A_{-k}$.

B. Vacuum solution: For $p = 0$ (and also for $p' = \text{const}$) the k-dependent solutions are modified Bessels functions for $m = 1$:

$$\Psi_{vac}(r,z) = A_0^v + B_0^v r + r\sum_k e^{ikz}\left(A_k^v I_1(kr) + B_k^v K_1(kr)\right) + c.c. \qquad (5)$$

Regarding boundary conditions, three cases are of importance:

C. Boundary conditions across a current sheath (coil): For a current $j_\phi(r,z) = \delta(r-b)\cdot\exp ikz\cdot j_{\phi,k}$ on a cylindrical surface one has, in addition to the continuity of Ψ_k:

$$\lim_{\varepsilon\to 0}\left(\frac{d}{dr^2}\Psi_k\Big|_{b_c+\varepsilon} - \frac{d}{dr^2}\Psi_k\Big|_{b_c-\varepsilon}\right) = \frac{4\pi^2}{c}\, j_{\phi,k} . \qquad (6)$$

D. Boundary condition on a metallic wall (perfect skin effect):

$$\Psi_k(r>b_w) = \lim_{\varepsilon\to 0}\Psi_k(b_w-\varepsilon) = \text{const} . \qquad (7)$$

E. Plasma-vacuum interface: This interface is determined by the condition $p \to 0$ in the plasma and $p \equiv 0$ in vacuum. This boundary condition is non-linear. Generally, it has to be evaluated numerically, for on the surface both flux and its derivatives have to be continuous, and $\Psi(r_s,z_s) = \bar{\Psi}$, where $\bar{\Psi}$ is the first zero (w.r.t. increasing r) of $p(\Psi)$. In our case (c.f. (1)), depending on the choice of a, b, and $p_0 = p(\Psi=0)/\bar{p}$:

$$\bar{\Psi} = -\frac{a}{b} \pm \sqrt{\frac{a^2}{b^2} - \frac{2p_0}{b}} . \qquad (8)$$

Of course, we require $p_0 \leq a^2/2b$ in the case $b > 0$ to ensure real $\bar{\Psi}$. For preliminary demonstration, we have assumed appropriate surface values.

III. Results

The following stability criteria may be applied:[2]

A. Interchange stability: Finite pressure on the separatrix, i.e., $\bar{\Psi}<0$.* With (8), this always holds true for $b>0$, but for $b<0$ it implies that Ψ within the plasma never exceed $a/|b|+(a^2/b + 2p_0/|b|)^{\frac{1}{2}}$. This is the case for multiple cell parameters.

*We choose $\Psi>0$ inside the separatrix.

B. Surface stabilization: Zero pressure gradient on plasma surface: $\nabla p|_{s=p'\nabla\Psi}|_s = 0$, i.e., $\overline{\Psi} = -a/b$ and therefore $b>0$ and $p_o=a^2/2b$, where we used (8) and (a).

C. Roman candle stability: A sufficient condition is $p''<0$; i.e., $b<0$.

In conclusion, we see that not all conditions can be satisfied simultaneously. For characteristic values of the parameters (cgs-units), field-lines (Ψ=const), B_{local}, and pressure are depicted in Figures 1, 2 and 3.

IV. Application to the High-Beta Q Machine

This is a 3-meter, low density theta pinch whose plasma radius is about 5 cm. Its compression coil is segmented axially into 30 rings which can be excited with currents of alternating sign, before or after they are all excited in parallel to form the theta pinch. Figure 4b shows schematically the periodic vacuum bias field which might be used to form the field reversed cells of Figure 4a.

Acknowledgment

The authors wish to thank R. Sanchez for numerous discussions and assistance with the computational evaluation.

References

1. V.D. Shafranov, in: "Reviews of Plasma Physics," Vol. 2, M.A. Leontovich (ed.), Consultants Bureau, New York (1966), p. 103, and refs. 10, 18, 27, 28 and 30 therein; H. Grad, in: Proc. of Symposia in Applied Mathematics, Vol. XVIII, H. Grad (ed.), American Mathematical Society, Providence, RI (1967), p. 162; D. Dobrott and G.K. Morikawa, Phys. Fluids 16, 140 (1973).

2. D.C. Barnes and C.E. Seyler, "Ideal MHD Stability of a Field Reversed Theta Pinch," LLL Theory Seminar (1978), LASL Preprint LA-UR-79-13.

3. A.E. Robson, "Equilibrium of a Reversed Theta Pinch," informal note (1978); L. Steinhauer, "Field-Reversed Plasma Rotation and Transport," Sherwood Meeting (1979); H. Weitzner, H.L. Berk and J. Hammer, "Analytic Field-Reversed Equilibria," in: Mirror Theory Monthly, LLL Magnetic Fusion Energy Program, Sept. 1979.

4. F.L. Ribe and L. Turner, Bull. Am. Phys. Soc. 23, 836 (1978); H. Meuth and E. Sevillano, "The Radio-Frequency Heating System for the High-Beta Q Machine," University of Washington Report UWFPP-4, March 1979.

5. The essential change for p containing third and higher order terms is that there then emerge more than one solution. w.r.t. the non-uniqueness, see also J.P. Freidberg and R.L. Morse, Phys. Fluids 12, 887 (1966) and S. Fisher, Phys. Fluids 14, 962 (1971).

6. W. Magnus, F. Oberhettinger, and R.P. Soni, "Formulas and Theorems for the Special Functions of Mathematical Physics," Springer, New York (1966); M. Abramowitz, in: "Handbook of Mathematical Functions," M. Abramowitz and I.A. Stegun (eds.), National Bureau of Standards, Washington, D.C. (1964). We use the following normalization, compared with Abramowitz' notation (A): $F_L(\eta,\rho) = F_L^A(\eta,\rho)/C_L^A(\eta)$, $G_L = C_0^A(\eta)\cdot G_L^A(\eta,\rho)/C_L^A(\eta)$; A.R. Curtis, "Coulomb Wave Functions," Royal Society Mathematical Tables, Vol. 11, University Press, Cambridge (1964).

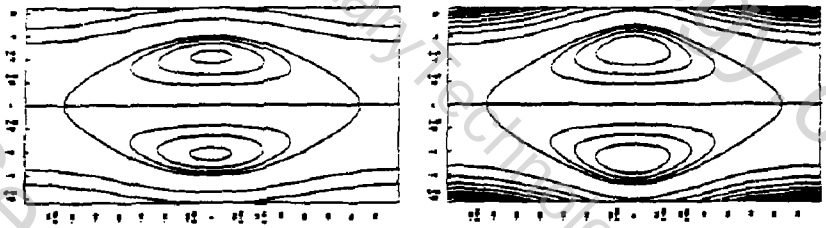

Fig. 1. Fieldlines for a=4, A_0=0.5, A_k=A_{-k}=0.5125, k=π/4, and b=+1 (left), b=-1 (right). Flux scale: inside separatrix $\Delta\Psi$=0.2, outside $\Delta\Psi$=2.

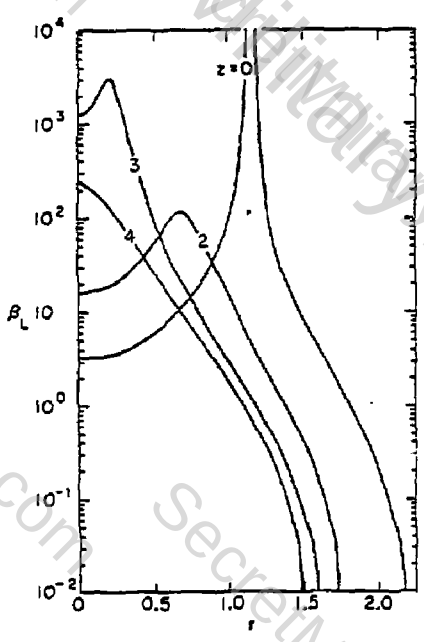

Fig. 2. β_{local} as a function of r and z for same parameters as in Fig. 1, with b=+1 and p_0=8. β_{local} is not very sensitive to changes of b for $-1 \le b \le +2$.

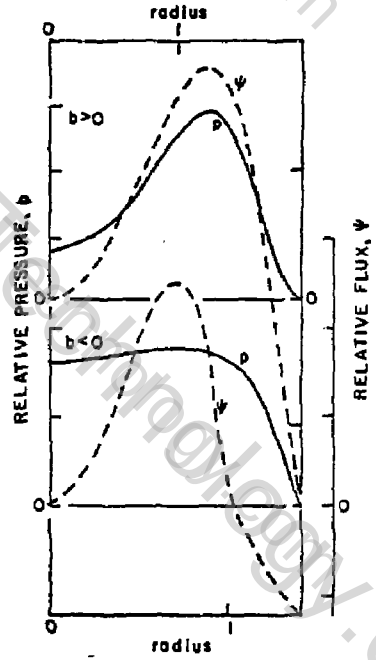

Fig. 3. Variation of magnetic flux and pressure with radius for negative and positive values of the parameter b of Eq. (1) at z=0.

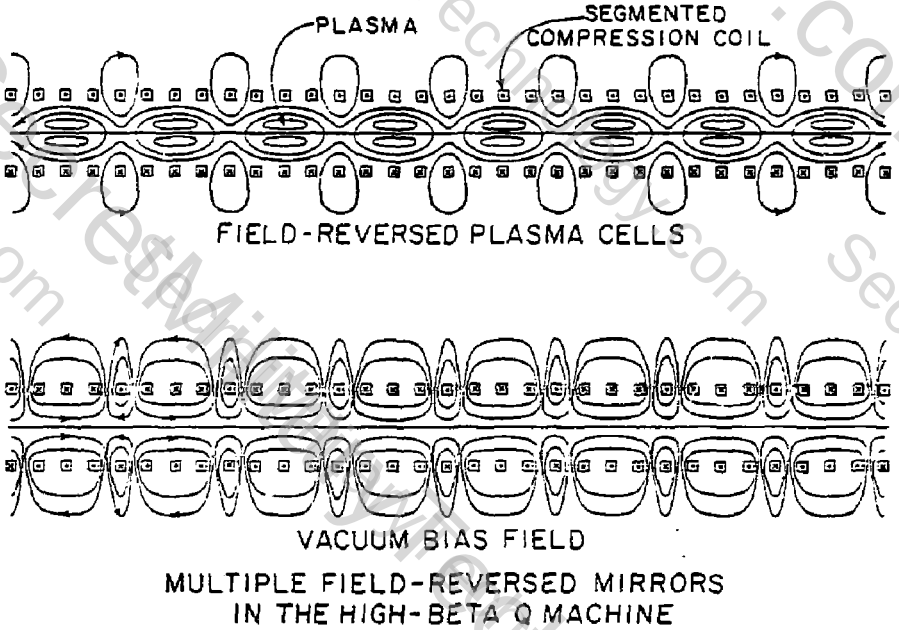

Fig. 4. Qualitative plots of periodic magnetic fields in the High Beta Q machine in vacuum (lower) and after plasma compression (upper).

ZERO DIMENSIONAL MODELING OF FIELD-REVERSE THETA PINCH MACHINES

Edward H. Klevans, The Pennsylvania State University

A zero-dimensional (0-D) time dependent computer model is developed to describe post-implosion behavior of field-reverse theta pinch machines.[1-3] The model consists of six equations, representing the rate of change of plasma particle number, electron internal energy, and ion internal energy; radial pressure balance; axial tension balance; and the change of the flux inside the major radius R, where B(R) = 0. It is assumed that the length ℓ is much larger than either R or the minor radius a, so that particle and heat losses are taken to be predominately radial. However, axial losses (through the X point, for example) can be included by use of phenomenalogical coefficients in the particle and heat loss confinement times.

A rigid rotor model[2] is chosen to describe the radial behavior of the density and B field:

$$n = n_m \operatorname{sech}^2 K[(r^2/R^2) - 1] \qquad (1)$$

$$B = B_\infty \tanh K[(r^2/R^2) - 1] \qquad (2)$$

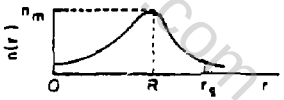

Fig. 1. n(r) vs. r.

where n_m and R, shown in Fig. 1, and K are time dependent parameters, and B_∞ is a specified function of time. The electron and ion temperatures are assumed to be uniform inside the separatrix. By setting $B(r_s) = -B(0)$, where r_s is the separatrix radius, one finds that $r_s = \sqrt{2}R$. The minor radius is defined by Linford[2] through the relation

$$n_m 2\pi R(2a) = \int_0^\infty n 2\pi r dr \text{ which yields } R/a = 4K/(1 + \tanh K) \qquad (3)$$

Assuming axial uniformity of n and B within the separatrix, the equations for

$$N = \ell 2\pi \int_0^{r_s} drrn(r) \equiv \ell \bar{n}(\pi r_s^2) = \ell \pi r_s^2 n_m (\tanh K)/K \qquad (4)$$

$$W_e = \ell 2\pi (3/2) T_e \int_0^{r_s} drrn(r) = \ell \pi r_s^2 1.5 T_e n_m (\tanh K)/K \qquad (5)$$

$$W_i = \ell 2\pi (3/2) T_i \int_0^{r_s} drrn(r) = \ell \pi r_s^2 1.5 T_i n_m (\tanh K)/K \qquad (6)$$

can be reduced to

$$\frac{1}{n_m}\frac{dn_m}{dt} = -\frac{1}{\tau_-} - \frac{2}{R}\frac{dR}{dt} - \frac{1}{\ell}\frac{d\ell}{dt} - \left(\frac{2K}{\sinh 2K} - 1\right)\frac{1}{K}\frac{dK}{dt} \qquad (7)$$

$$\frac{1}{T_e}\frac{dT_e}{dt} = \left(\frac{T_i - T_e}{T_e}\right)\left(\overline{\frac{1}{\tau_{eq}}}\right) - \frac{1}{\tau_{th}^e} - \frac{4}{3}\frac{1}{R}\frac{dR}{dt} - \frac{2}{3}\frac{1}{\ell}\frac{d\ell}{dt} + \frac{\dot{H}_\Omega}{W_e} \qquad (8)$$

$$\frac{1}{T_i}\frac{dT_i}{dt} = -\left(\frac{T_i - T_e}{T_i}\right)\left(\overline{\frac{1}{\tau_{eq}}}\right) - \frac{1}{\tau_{th}^i} - \frac{4}{3}\frac{1}{R}\frac{dR}{dt} - \frac{2}{3}\frac{1}{\ell}\frac{d\ell}{dt} \qquad (9)$$

where τ_- is the particle confinement time; τ_{th}^e and τ_{th}^i are the electron and ion thermal conduction times; $(1/\tau_{eq})$ is the average of the inverse of the electron-ion equilibration time, defined by

$$\overline{(1/\tau_{eq})} = \frac{\ell}{N} 2\pi \int_0^{r_s} drrn(r)/\tau_{eq}(r) = \left[\frac{8\sqrt{2\pi}\, m_e^{1/2}\, e^4\, Z^2 \ell n\Lambda}{3m_i}\right]\frac{n_m}{T_e^{3/2}}\left(1 - \frac{\tanh^2 K}{3}\right) \qquad (10)$$

where the Spitzer expression for $\tau_{eq}(r)$ was used; and $\dot{H}_{\Omega}$ is the Ohmic heating rate given by

$$\dot{H}_{\Omega} = 2\int_0^{r_s} dr 2\pi r \eta_{\perp}^{\phi} j_{\theta}^2 \tag{11}$$

with $\eta_{\perp}^{\phi}$, the classical cross field electrical resistivity (associated with flux annihilation), and j_{θ}, the diamagnetic current density, given by

$$j_{\theta} = -\frac{c}{4\pi}(\partial B_z/\partial r) = -(rcKB_{\omega}/2\pi R^2)\mathrm{sech}^2\, K[(r^2/R^2) - 1] \tag{12}$$

Particle confinement is governed by $\tau_{\perp} = N/[2\pi r_s \ell (nu_r)_{r_s}]$. Assuming diffusive loss at the separatrix,

$$(nu_r)_{r_s} = -(D\frac{\partial n}{\partial r})_{r_s} = -\{[(c^2 \eta_{\perp}^{p} n(r_s)(T_e + T_i)]/B^2(r_s)\}(\partial n/\partial r)_{r_s} \tag{13}$$

where $\eta_{\perp}^{p}$ is the resistivity governing particle loss. Several expressions for $\eta_{\perp}^{p}$ have been tested, including classical resistivity and the lower hybrid drift resistivity.[5] The former expression resulted in particle losses which were too small and did not agree with experiment. Consequently, we have chosen[4]

$$\eta_{\perp}^{p} = \frac{2\sqrt{2\pi}}{5\Omega_i}^{3/2} \left(\frac{m_e}{m_i}\right)^{1/2} \frac{(T_i/T_e)^{5/4}}{1 + (T_i/T_e)} \frac{\Omega_i^2}{\omega_i^2} (\varepsilon_n a_i)^2 [1 - \frac{1}{\sqrt{10}}(\frac{T_i}{T_e})^{1/4}] \tag{14}$$

where Ω_i is the ion cyclotron frequency and ω_i is the ion plasma frequency. The quantity ε_n is the inverse gradient length, and a_i is the ion gyro-radius. When ε_n is evaluated at the separatrix using a rigid rotor profile, the value ε_n is sufficiently small that particle loss times are larger than those observed experimentally. Hamasaki[5] has found from 1-D modeling that the density drops very rapidly outside the separatrix, so ε_n should be larger than the value obtained from the rigid rotor profile. These uncertainties have led us to take the quantity $\varepsilon_n a_i$ as a parameter which can be varied. Typically we have found that $\varepsilon_n a_i = 2$ yields good agreement with experimental data.

The treatment of thermal conduction is uncertain because the temperature is constant inside the separatrix and is unknown outside the separatrix. If it is assumed that hot ions which cross the separatrix flow out the ends without collision then there is no ion thermal conduction loss across the separatrix. *Classical cross field ion thermal conduction with an ion gyro-radius temperature gradient length has also been studied.* Although the differences in results are not great, dropping ion thermal conduction gives better agreement with experiment.

For electron thermal conduction we use

$$\tau_{th}^{e} = W_e/(q_r^e)_{r_s} \text{ where } (q_r^e)_{r_s} = -K_{\perp}^{e}(\partial T_e/\partial r)\big|_{r_s} = -K_{\perp}^{e}(T_e/\delta) \tag{15}$$

where δ is the thermal sheath length and K^e is the classical value for electron thermal conductivity. The value of δ is not known, but two choices were examined: $\delta = a_i$ and $\delta = \sqrt{a_i a_e}$. When $\delta = a_i$ is used, electron thermal conduction times are so long that electron thermal conduction is unimportant. When the hybrid gyro-radius is used, electron thermal conduction is no longer negligible, and may be responsible for the observed "clamping" of the electron temperature, in spite of a continual energy input from the hotter ions. Consequently the hybrid radius was chosen for the present studies. [Radiation

from oxygen impurities was also considered as a possible mechanism for electron temperature clamping, but it was found to be small.]

The unknowns in this theory are n_m, K, R, ℓ, T_e and T_i. Consequently three more equations are needed. The first is obtained from pressure balance:

$$(1/n_m)(dn_m/dt) = -[1/(T_e + T_i)](dT_e/dt + dT_i/dt) + (2/B_\infty)(dB_\infty/dt) \quad (16)$$

The next equation represents magnetic flux change inside R:

$$d\phi/dt = (d/dt)\int_0^R drrB = \int_0^R drr(\partial B/\partial t) \quad (17)$$

Using Ampere's Law and Ohm's Law to compute $\partial B/\partial t$, the integral on the right can be evaluated. The integral in the middle is evaluated using Eq. (2). After differentiation, Eq. (17) can be reduced to the expression

$$\frac{2}{R}\frac{dR}{dt} = -\frac{1}{\tau_\phi} - \left(\frac{K \tanh K}{\log \cosh K} - 1\right)\frac{1}{K}\frac{dK}{dt} - \frac{1}{B_\infty}\frac{dB_\infty}{dt} \quad (18)$$

where $\tau_\phi = (\pi R^2 \log \cosh K)/(\eta_\perp \phi c^2 K^2)$ is the decay time for the flux.

The final expression is obtained from axial tension balance (see Fig. 2).

$$\int_0^{r_w} drr[B^2(r,z_o)/8\pi - p(r,z_o)] = \int_0^{r_w} drr(B^2(r,o)/8\pi - p(r,o)] \quad (19)$$

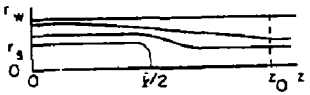

Fig. 2. B line behavior.

where r_w is a conducting wall, and $\ell/2 << z_o <$ chamber half length. We neglect particle pressure at z_o, and take $B(r,z_o) = B(z_o)$. Also we neglect particle pressure beyond the separatrix at $z = 0$, and set $B(r,o) = B_\infty$ for $r_s < r < r_w$. Using flux conservation, $B(z_o)\pi r_w^2 = B_\infty \pi(r_w^2 - r_s^2)$. Then Eq. (19) can be evaluated, resulting in the expression $(R^2/r_w^2) = 1 - (\tanh K)/K$. Note that setting $r_s^2 = 2R^2 = r_w^2$ results in a maximum value for K of 1.91. Converting the last expression into a differential equation we obtain

$$(2/R)(dR/dt) = [K \tanh^2 K/(K - \tanh K) - 1](1/K)(dK/dt) \quad . \quad (20)$$

The set of six equations can be reduced to obtain an equation for ℓ:

$$\frac{1}{\ell}\frac{d\ell}{dt} = -\frac{3}{5}\left[\frac{1}{\tau_\perp} + \left(\frac{T_e}{T_e + T_i}\right)\frac{1}{\tau_{th}^e} + \left(\frac{T_i}{T_e + T_i}\right)\frac{1}{\tau_{th}^i}\right] + \frac{3}{5}\frac{\dot{H}_\Omega}{W_e} + \frac{\alpha}{\tau_\phi} - \left(\frac{6}{5} - \alpha\right)\frac{1}{B_\infty}\frac{dB_\infty}{dt} \quad (21)$$

where α is a function of K and is approximately 0.5 for the LASL experiments.

It is seen that ℓ can expand or contract depending on the relative size of the heating and loss terms, and the behavior of the $\dot{B}$ field.

The set of Eqs. (7), (8), (9), (16), (18) and (20) has been solved simultaneously on the computer. Comparison with a recent FRX-B set of experiments[3] conducted at 17 mTorr fill pressure of D_2 are shown in Figs. 3 and 4. Initial values correspond to t = 10 μs in the experiment. Initial conditions are the following: B_o = 6.8 kG, T_i = 200 eV; T_e = 120 eV; $n_m = 3.6 \times 10^{15}$ cm^{-3}; K = 1.1; R = 4 cm; ℓ = 50 cm and $N = 1.3 \times 10^{19}$. The magnetic field behavior is given approximately by $B = B_o[1 - (t/96\ \mu s)]$. Fig. 3 shows temperature behavior. Ion temperature behavior, which is dominated by ion-electron equilibration, is in good agreement with experiment. Electrons gain heat from ions and and lose it slowly through electron thermal conduction. The experimental re-

sults suggest a greater electron energy loss, either from anamolous electron thermal conduction or from radiation. Fig. 4 shows the decay of N and n_m, both with an exponential decay time of $\tau = 50$ μs. These results are within the large error bars of the experimental values. Quantities not shown include length ℓ, which decreased from 50 cm to 46 cm in 20 μs; R, which increased from 4.0 to 4.2 cm; and K, which increased from 1.1 to 1.2. These results are consistent with experimental observation.

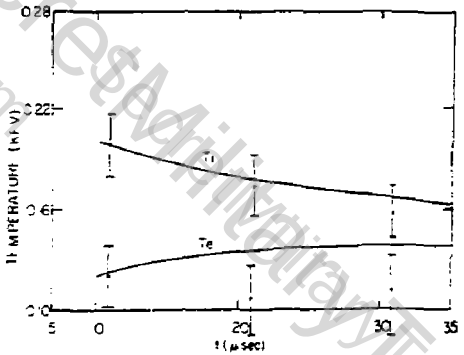

Fig. 3. T_e and T_i vs. t. $(\varepsilon a_i) = 2$; $\delta = \sqrt{a_e a_i}$

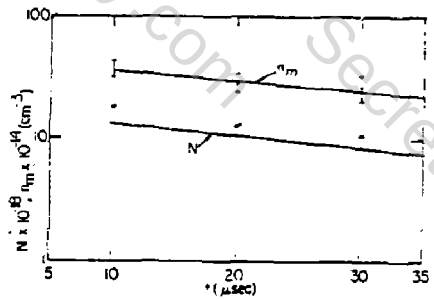

Fig. 4. N and n_m vs. t. $(\varepsilon a_i) = 2$; $\delta = \sqrt{a_e a_i}$

In conclusion, a 0-D model has been constructed which predicts behavior consistent with behavior observed in FRX-B. Additional work on electron temperature modeling may be needed. The model will next be used for scaling studies and comparison with the 1-D model of Hamasaki.[5]

Acknowledgement. I want to thank Rulon Linford and Peter Gary for helpful discussions in the development of the model, W. Tom Armstrong for supplying FRX-B data, and John McCowan for assistance with the computational work. Part of the work was performed while the author was a visitor at Los Alamos Scientific Laboratory. This work was supported by the U.S. Department of Energy.

References.

1. R. K. Linford, W. T. Armstrong, D. A. Platts and E. G. Sherwood, 7th IAEA Conference on Plasma Phys. and Controlled Fusion Research, Innsbruck, 1978.
2. R. K. Linford, D. A. Platts and E. G. Sherwood, LASL Controlled Thermonuclear Research Annual Report, Jan.-Dec. 1977.
3. W. T. Armstrong, et al., Bull. APS, 24, 1979 (1082).
4. S. P. Gary, "Wave-Particle Transport From Electrostatic Instabilities," 1979, submitted to Phys. Fluids.
5. S. Hamasaki and R. K. Linford, Bull. APS, 24, 1979 (1081).

SPHEROMAK FORMATION BY THETA PINCH

Y.Nogi, H.Ogura, Y.Osanai, K.Saito, S.Shiina and H.Yoshimura
College of Science and Technology, NIHON University
Kanda-Surugadai, Chiyoda-ku, TOKYO 101, JAPAN

Abstract

Spheromak configuration is formed by using a theta pinch combined with a z-discharge. Toroidal field is generated by the z-current flowing in the plasma and the reverse current on its surface. The reverse mechanism is investigated here by the analysis of z-discharge circuit including the plasma. It is easy to reverse 70% of z-current on the plasma surface by using a very low external inductance circuit.

1. Introduction

Compact torus has a number of advantages in order to simplify the machine design.[1] However, it is not easy to generate the toroidal field because of the spherical design. The toroidal field can be produced by z-discharge current operated with a linear theta pinch. It is necessary for the formation of magnetic surface that most of z-current flowing in the plasma returns on its surface as soon as the reverse field configuration is formed. Two methods are considered to produce this closed current loop. One is the return of z-current due to an inverse voltage applied from an external circuit between the electrodes.[2] The other is that due to an inverse voltage associated with the compression of plasma column. The latter case is investigated here from analysis of the electric circuit including the compressed plasma. The analysis shows that the large reverse ratio of z-current is obtained by the small external inductance of z-discharge circuit and the large compression ratio of plasma. Experimental results agree well with that of the analysis.

2. Generation of Reverse Current

It was already shown that the reverse toroidal current emerged on the plasma column when the tokamak plasma was compressed by the fast rising toroidal field.[3] It is expected that the reverse current can be also generated in the linear machine. The z-current is initially flowed in the plasma along the bias field through the electrodes without the self pinch. When the current is compressed by the theta pinch field, the reverse current emerges on the plasma surface. The reverse current will link with the initial current at the ends where the conductivity of plasma is very low.

Two conditions must be imposed on the generation of reverse current. One is that the field diffusion time is longer than the compression time due to the theta pinch field. The other is a condition to the z-discharge circuit. The present experimental circuit is shown in Fig.1-(a). Since the theta pinch field is applied to the current after the short of the 1st crowbar circuit, it is important to take out only the right side net-

work. Its equivalent circuit is shown simply in Fig.1-(b), where L_e and R_e are the inductance and the resistance of external circuit, respectively, and L_p and R_p are the inductance and the resistance of plasma. The L_p is sum of the external inductance, L_{pe}, and the internal inductance, L_i, of plasma. Then the circuit equation is written as follows

$$\frac{d}{dt}\left[(L_e + L_p) I \right] + (R_e + R_p) I = 0 \qquad (1)$$

By using the conservation of poloidal flux in plasma, reverse ratio of z-current, α, is calculated from Eq.(1) as follows [4]

$$\alpha = \frac{I_o - I}{I_o} = \frac{(\mu_o l/2\pi)\ln(a/r_p)}{L_e + (\mu_o l/2\pi)\ln(b/r_p)} \qquad (2)$$

where I_o is trapped current in plasma, l is length of plasma column, a is initial plasma radius, r_p is compressed plasma radius and b is inner radius of conducting shell. From this equation the next conditions are needed for the effective generation of the reverse current;

(1) much smaller external inductance of the circuit than that of the compressed plasma,
(2) large compression ratio,
(3) small distance between the conducting shell and the tube wall as possible.

We show the reverse ratio as functions of the compression ratio, r_p/a, and L_e in Fig.4, where l, a and b are values in the present experiment.

3. Apparatus

The experimental machine consists of a theta pinch system and a z-discharge one, as shown in Fig.2. The machine is so designed as to generate largely the reverse current. The theta pinch coil produces 800 G negative bias field and 10 kG compression field having 2 us rise time. The discharge tube has two cylindrical electrodes at both ends, which are 230 cm apart each other. The z-current flowing in the plasma returns to the electric circuit through the conducting shell. The z-current can be obtained till 50 kA by varying the inductance L_o shown in Fig.1. The 1st crowbar circuit is connected in order to reduce the external inductance, L_e. This switch is clamped at a quarter period of the current ringing. The decay behavior of the current in plasma is mainly determined by the inductance, L_p, and the resistance, R_p. The 2nd crowbar switch is set for decoupling the current flowing in condenser with the current in plasma. This switch is usually clamped at a half period of the current ringing. The theta pinch field is applied to compress the plasma near the time when the 2nd crowbar switch is clamped. A typical wave form of plasma current is shown in Fig.3.

4. Experimental Results

At first the plasma is produced by the z-discharge. The magnitude of z-current must be selected to get a initial plasma without self pinch. It is also necessary that most of the

current flows in the plasma, but does not on its surface. The reason is that the reverse current emerges on the plasma when the plasma is compressed. The slow rise time and the crowbar of the plasma current are favorable to this condition. At the present experiment, the current is adjusted to 10 kA with the rise time of 10 μs. The plasma current shows the rapid decrease with the increase of the compression field and the slow decrease after the crowbar of compression field, as shown in Fig.3. At the present experiment three values of 60, 150 and 270 nH are prepared for L_e. The observed values of α = 70, 62 and 49 % coresponding to each inductance are plotted with small circles in Fig.4. The radius predicted from the analysis is about 2.5cm which is independent of experimental values, and L_e. The similar size radius is an anticipated result because the compression ratio will not depend on almost the external inductance, L_e. The internal profiles of magnetic field are measured by a magnetic probe inserted into the plasma in case of L_e=60 nH. The B_z and B_θ profiles at 1 μs after the plasma compression are shown in Fig.5 and Fig.6,respectively. The data of three shots are plotted in these figures at every radial position. The dotted line in Fig.6 is the current density profile calculated from the observed radial profile of the average value of B_θ on the assumption that the z-current flows cylindrically along the axis. Because of bad reproducibility of B_θ near the axis, the current density is not calculated there. The current density profile shows the clear generation of the reverse current. The plasma radius estimated from this profile is about 3cm. The radial position of the null current surface in the plasma agrees well with that of B_z=0. The total B_z flux trapped in the plasma equals nearly the flux produced by the compression field within 2.5cm. This radius is almost the same within experimental errors as the current flowing region calculated from B_θ profile and the radius predicted from the reverse ratio of the current.

5. Conclusion and Discussion

Productions of the toroidal field for spheromak configuration are studied from the analysis of electric circuit of z-discharge. The analysis shows the generation of reverse current on the plasma column with the plasma compression due to the theta pinch. Magnetic probe measurements show clearly not only the generation of reverse current, but also the establishment of spheromak configuration.

Merits of the present method are that the reverse of z-current can be done by using a simple technique like a theta pinch and its magnitude can be controlled by such parameters as the external inductance of z-discharge circuit, the compression ratio and the length of plasma. The effect of the externally supplying voltage is excluded here, it will be needed in such case that the studies of spheromak configuration are made at the unfavorable condition to the generation of the reverse current.

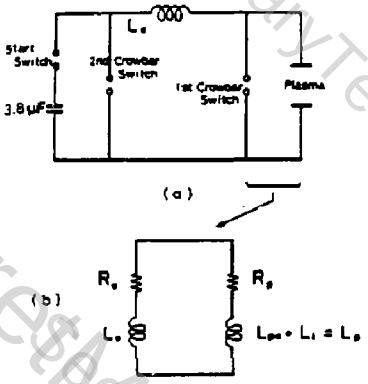

Fig.1 L-discharge Circuit

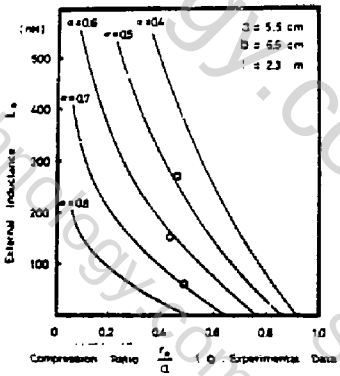

Fig.4 Current Reverse Ratio

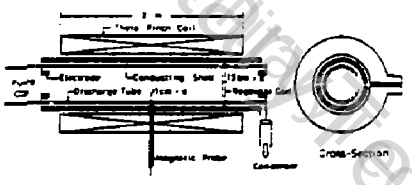

Fig.2 Experimental Apparatus

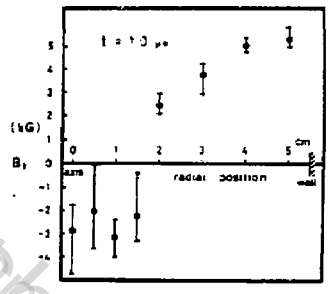

Fig.5 Radial Profile of B_z

Upper Beam : Compression Field
10kG/div, 5μs/div
Lower Beam : Plasma Current
4 kA/div, 5μs/div

Fig.3 Oscilloscope Trace

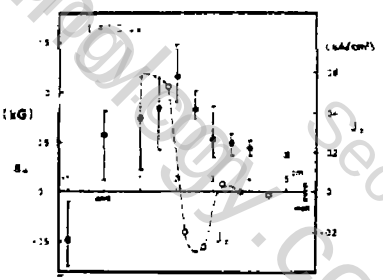

Fig.6 Radial Profiles of B_θ and J_z

References

(1) M.N.Bussac et al. 7th Inter. Conf. on Plasma Physics and Controlled Fusion Research,Innsbruck,(1978) CN-37/K-1
(2) G.C.Goldenbaum et al. 9th European Conf. on Controlled Fusion and Plasma Physics, Oxford, (1979) 129
(3) K.Yokoyama et al. Plasma Physics 19 (1977) 671
(4) Y.Nogi et al. Nihon University report(1979) NUP-A-79-16

FIELD-REVERSED PLASMA GUN BASED ON THE INVERSE-PINCH DISCHARGE

W. D. Getty, Electron Physics Laboratory, Department of Electrical and Computer Engineering, University of Michigan, Ann Arbor, Michigan 48109

The inverse pinch (i.e., hard-core pinch or unpinch) discharge possesses several properties that make it potentially useful as the basis of a plasma gun for injecting a field-reversed plasma into a confinement device. The useful characteristics are: (1) the possibility of initial resistive heating by axial current flow followed by compression heating; (2) the controlled generation of toroidal and poloidal plasma currents and the associated magnetic field components; and (3) the relatively slow plasma formation time which permits the use of pulse technology on the time scale of several microseconds. These characteristics are shared with the imploding-pinch concept upon which the Paramagnetic Spheromak (PS-1)[1] is based, but in addition the inverse pinch is theoretically stable to ideal MHD instabilities as predicted by the Suydam criterion[2]. It may therefore offer some advantages in high-power regimes of operation or for certain geometrical shapes.

To produce a useful hot plasma the pinch discharge must be separated from the electrodes and translated axially to clear them before further heating by compression or other means takes place. Several recent experiments have shown that this separation can be done.

The experimental properties of the inverse pinch discharge were reported by Colgate and Furth[3] in 1960 and by Aitken, et. al.[4], in 1964. Improved MHD behavior relative to the imploding pinch was found, but non-MHD instabilities identified as the tearing mode were observed. This mode was apparently more prominent in the Aitken experiment, a result attributable to the longer length of the discharge tube. More recently, the inverse pinch discharge was successfully used as a preionizer in a Marshall coaxial gun[5] and as a plasma injector for TORMAC[6]. The TORMAC plasma injector has recently been reported to have produced a detached plasma ring with many of the properties expected from the analysis presented in this paper[6].

The basic operation of the proposed inverse-pinch plasma gun is illustrated in Fig. 1. A discharge with an initial positive (or negative) B_z bias field is accelerated radially by the inverse-pinch $\bar{J} \times \bar{B}$ radial force. A toroidal field (B_θ) is produced in the plasma by the z-directed current flow. As the plasma ring crosses the axial magnetic field it will develop a toroidal current J_θ to preserve constant flux linkage by the plasma ring. Thus a toroidal and poloidal magnetic field component will be generated in the plasma. The plasma ring must be separated from the inverse-pinch electrodes while maintaining

this magnetic structure. From the results of the TORMAC and PS-1 experiments[1,6] it appears that this separation can occur. Following separation the ring must be transported axially to clear the gun electrodes. Axial transport velocities observed in field-reversed ring experiments range from 1 to 20cm/μsec, limited by eddy-current drag in the adjacent metal walls.[7,8] Therefore the time scale for axial transport should be a few microseconds, sufficiently fast in comparison to the pinch time and the plasma energy confinement time (expected to be 20-40 μsec). Radial compression could then follow to reheat the plasma as shown in Fig. 1(c,d).

Inverse pinch experiments[3,4] indicate that one can use axial currents up to 300kA and produce plasmas with B_z and B_θ values in the 1-10kG range, and toroidal currents of several kA. Electron temperatures are estimated to be 5 to 10 eV and densities are 10^{14} to $10^{16}/cm^3$. The β for the plasmas produced in References 3 and 4 is of the order of unity. The aspect ratio R/a (see dimensions in Fig. 1) varies from ≈0.1 in the Aitken apparatus to ≈10 in the TORMAC gun. The range of B_θ and B_z, and the geometry make these plasmas similar to belt-pinch of tokamak plasmas.

As shown in Figure 1, the ejected plasma may have an aspect ratio of the order of 3 to 10, and the geometry is similar to that of a tokamak. Since stability requires the safety factor

$$q = \frac{a}{R}\frac{B_\theta}{B_z} \simeq 1 \qquad (1)$$

this configuration will have B_θ much larger than B_z and $\beta_\theta \simeq R/a$ as in tokamaks; thus $\beta \simeq a/Rq^2$ may have to be small to maintain stability. In this geometry several azimuthal coils would be pulsed to supply dB_z/dz to translate the plasma ring in a manner similar to the use of radial B-field control to position a tokamak plasma vertically.

By using a smaller aspect ratio one approaches belt-pinch geometry and

$$q = \frac{2a}{\pi R}\frac{B_\theta}{B_z} \qquad (2)$$

with $2a \geq R$. Thus one can obtain $q \simeq 1$ with $B_\theta \simeq B_z$ and high β. The axial inverse-pinch plasma current would control B_θ and the azimuthal coil currents control B_z. The magnetic field and plasma parameters of the early experiments give $q \simeq 1$ from Eq. (2) and $\beta \simeq 1$.

A plasma in the belt-pinch geometry could be generated directly by using a B_z reverse-bias field in the inverse pinch. Discharges with a reverse field of 4kG inside the plasma and a positive B_z field of 3.5kG outside the plasma have been produced by an inverse-pinch with $2a/R \simeq 4$ at a time of 15 μs after

initiation of the discharge[3]. By forcing reconnection of the field lines at each end, one may be able to form a reversed-field plasma in this geometry and translate it axially. Es'kov, et. al.[9], have reported doing this in a hard core device with q=1 and β=.6-.9. In their device the hard core current did not return through the plasma as in the inverse pinch.

An inverse-pinch plasma gun utilizing belt-pinch geometry and the field reconnection and axial transport scheme of Es'kov, et. al.,[8,9], is illustrated in Figure 2. A plasma cylinder with entrapped B_θ and reverse-bias B_z is injected from the inverse-pinch electrodes and a positive B_z field is applied by an external coil. A pulsed coil at one end forces reconnection at that end and accelerates the plasma cylinder axially. A similar pulsed coil causes reconnection at the other end before the pinch electrodes are cleared, and axially compresses the plasma. A transverse octupole "barrier" field similar to that of Es'kov, et. al.[9], could be used to prevent the plasma from striking the wall. The new feature in the scheme of Figure 2 is the entrapped B_θ field, which with the induced poloidal field should allow a stable high-β equilibrium to exist from the onset of the discharge.

CONCLUSION

The inverse-pinch discharge has a proven magnetic-field configuration with stability and geometric properties that make it attractive for generating a reversed-field plasma. A high-β plasma cylinder or ring can be generated with frozen-in poloidal and toroidal magnetic field components. The inverse-pinch discharge is theoretically MHD stable and has shown superior stability properties in experiments. By choice of the aspect ratio, one can produce tokamak- or belt-pinch-like geometries. In the latter case one could use azimuthal coils to force reconnection of field lines and axially compress the plasma.

REFERENCES

1. G. C. Goldenbaum, Invited Paper, Bull Amer. Phys. Soc., 24: 1072 (October, 1979) (Abstract).
2. W. B. Thompson, An Introduction to Plasma Physics, Pergamon Press (1962) pp. 117-120.
3. S. A. Colgate and H. P. Furth, Phys. Fluids, 3:982-1000 (1960).
4. K. L. Aitken, et. al., Plasma Phys. (J. Nucl. Energy Part C) 6:39-69 (1964).
5. P. Deschamps, et. al., Proc. IAEA Conf. on Plasma Phys. and Controlled Nuclear Fusion, Culham, vol. II, pp. 449-461 (1965).
6. B. R. Myers, M. A. Levine, and P. A. Pincosy, Bull. Amer. Phys. Soc., 24:1087 (October, 1979). (Abstract).
7. D. J. Rej, et. al., Appl. Phys. Lett. 33:910-912 (1 Dec. 1978).
8. A. G. Es'kov, et. al., Proc. IAEA Conf. on Plasma Phys. and Controlled Nuclear Fusion Research, Innsbruck, vol. II, pp. 185-204 (1979).
9. A. G. Es'kov, et. al., Nucl. Fusion Supp. 1975, pp. 155-161 (IAEA Conf. on Plasma Physics and Controlled Nucl. Fusion Research, Tokyo).

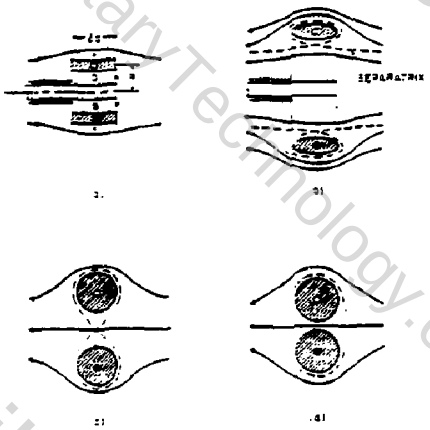

Fig. 1 (a) Inverse pinch stage with B_z bias field. (b) After separation from inverse pinch electrode and formation of separatrix by induced azimuthal current. (c) After axial translation and radial compression. (d) After additional compression.

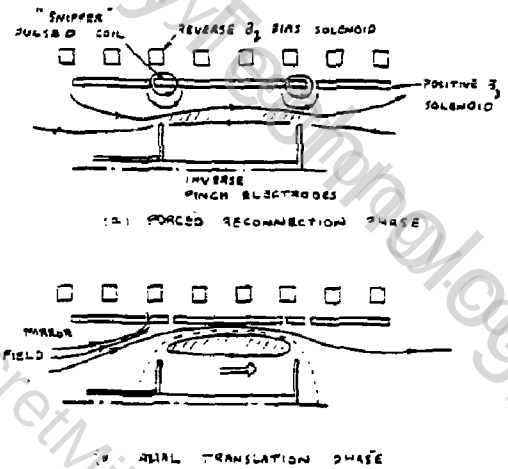

Fig. 2 General scheme for separation from electrodes, forced reconnection, and axial translation of an elongated plasma ring.

A TRIGGERED-RECONNECTION COMPACT TOROID EXPERIMENT

A.L. Hoffman and G.C. Vlases
Mathematical Sciences Northwest, Inc.

Field reversed theta pinches have been the subject of renewed interest both in the Soviet Union and the United States. The primary reason for this interest is the attainment of plasma configurations which are stable for many Alfven times. One particularly interesting and very promising compact torus experiment is the 8H-I device of Kurtmullaev and co-workers at the Kurchatov Institute.[1] This group has observed plasma lifetimes of up to 100 μsec in a 1 m long device. The lifetime was limited by electrical circuit parameters alone, with no tendency toward rotational instability, which has been the lifetime terminating process in all other long lived field reversed theta pinch experiments.

The principal feature of the 8H-I experiment is careful control of the field line reconnection process so as to maximize the trapped poloidal flux. A byproduct of this technique is an increase in the non-adiabatic plasma heating through rapid axial compression, which has important implications for both current experiments and eventual reactor designs. Mathematical Sciences Northwest, Inc. (MSNW) has initiated a reversed field theta pinch experiment which is designed to incorporate and improve on the features of the Kurchatov experiment, to thoroughly explore the controlled reconnection process, and to investigate the full parameter space between conventional "radial" compression processes and the axial compression brought about by triggered reconnection. An additional principal objective of this experiment is to explore the causes and cures for plasma rotation.

A schematic of the MSNW experimental apparatus, which is closely patterned after the Soviet experiment,[1] is shown in Figure 1. A bias field is created by an "external" quasi-steady solenoid. An additional quasi-steady coil at each end is used to apply a mirror or cusp field configuration. Eight pairs of oppositely directed longitudinal conductors are located as shown to form a pulsed octopole field near the tube wall. In addition, at each end there is a very fast pulsed mirror "trigger coil" used to force reconnection at the desired time.

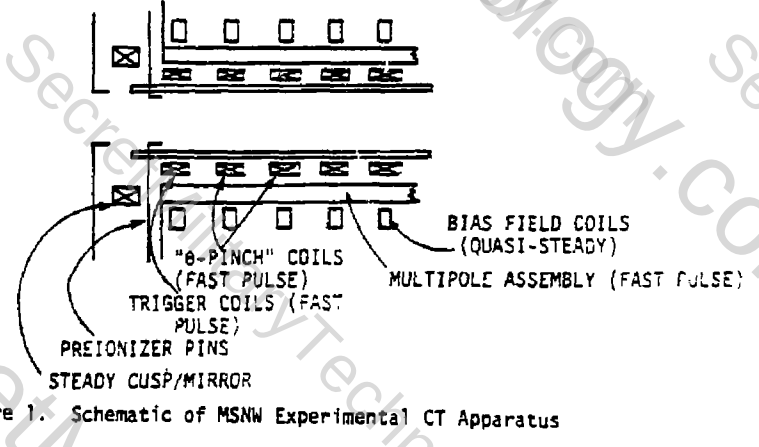

79 03455

Figure 1. Schematic of MSNW Experimental CT Apparatus

Figure 2 shows sketches of the field line topology at various phases of a second half cycle "Russian operating mode". A bias field with a weak mirror is established, and the plasma is preionized (Stage 1). The main field is then applied, first in the direction of the bias. It rings through the first half cycle and reaches a maximum in the opposite direction, creating a cusp in the outer field lines (Stage 2). During the period when the main field passes through zero, the octopole field is pulsed on in order to minimize plasma-wall contact and to thus prevent rapid cooling and loss of trapped bias field. This technique maximizes the compact toroid poloidal flux, and

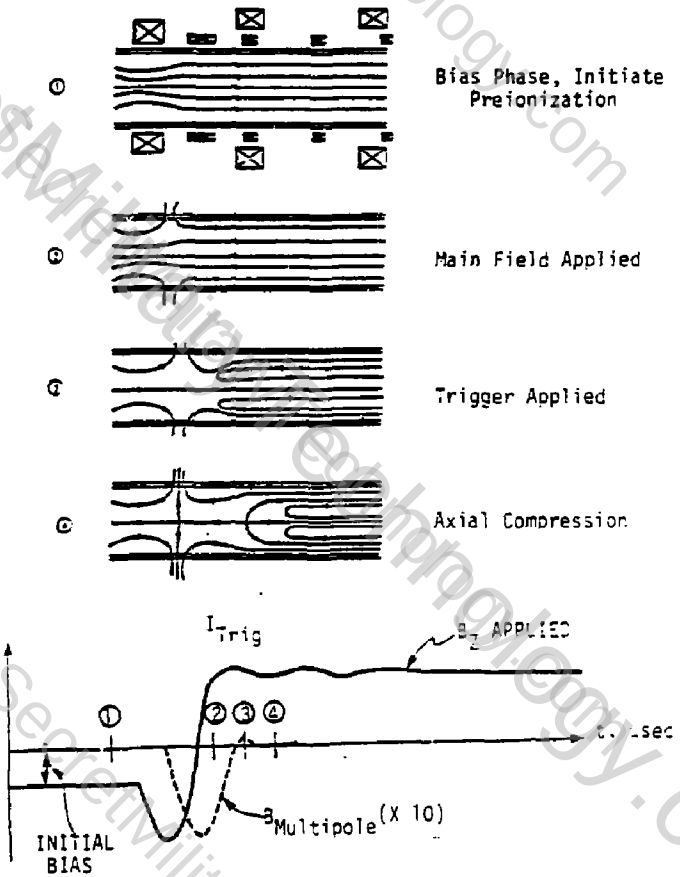

Figure 2. Stages of Toroid Formation Using Cusp Holdoff and Triggered Reconnection (second half-cycle operating mode)

may also inhibit development of rotation. When the main field is near its peak value, the fast trigger coil is energized, causing rapid reconnection (Stage 3). The resulting toroid is not in equilibrium and strong axial compression o urs (Stage 4). In the Russian experiments, it was shown that this axial contraction increased the line energy density and the separatrix radius, resulting in long plasma lifetimes.

The MSNW experiment, while incorporating all of the features of the Kurchatov experiment, has the capability of providing a higher rate of field rise so that it can explore the trade offs between radial and axial "shock" heating. It employs an axial Z discharge, so that high levels of preionization are possible and it can operate on either first or second half cycles. First and second half cycle operation is indicated by the B_z plots on Figure 3a labelled "conventional operation". Also shown is a mode labelled "compound magnet operation" which uses a quasi-steady outer solenoid and a fast pulsed concentric inner "theta pinch" coil set. In this second mode, the initial quasi-steady field is nulled out by the inner theta pinch coils, and operation from that point proceeds as it does in the "standard" mode. The principal experimental advantage is the ability to achieve a fast rise (10 μsec) followed by a very long (~ 100 msec) flat-top, rather than the 100 - 200 μsec decay of conventional crowbarred θ-pinches. The principal uncertainty with the compound magnet technique lies in the limited time to preionize, and in the relatively lower rate of field rise at the zero field cross-over point. Both difficulties can be overcome, if need be, by a pulse shaping network driving the inner magnets.

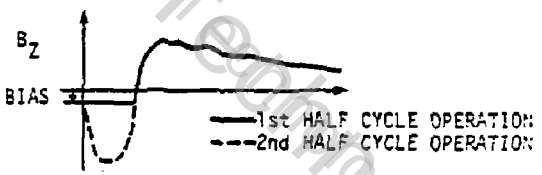

(a) Conventional Operation

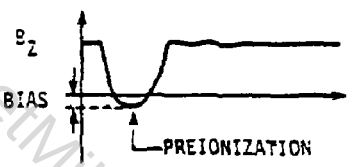

(b) Compound Magnet Operation

Figure 3. Schematic of Operating Modes

A drawing of the magnet system is shown on Figure 4. The basic plasma tube is 1 m long and has a 20 cm bore. Fast theta pinch and trigger coils are fed through gaps between the quasi-steady bias and cusp coils. The octopole rods can produce 0.20 tesla fields at the inner edge of the plasma tube. Initial operation will be in the standard mode with 1 tesla theta pinch fields produced with 3 μsec quarter cycle times. The compound magnet will be operable up to 2.0 tesla fields. Depending on the efficiency of the axial heating process, scaling analyses predicts that toroids with 10^{15} cm^{-3} peak densities and up to 500 eV temperatures could be produced. Containment times based on classical perpendicular thermal diffusion are 10 msec, and the quasi-steady field decay time is designed to exceed this value by a factor of 10.

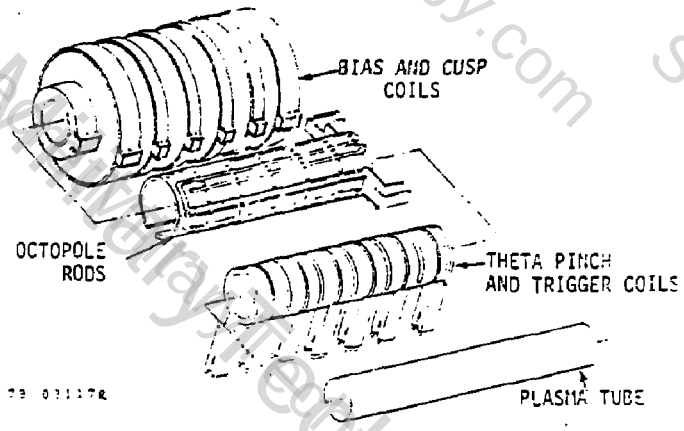

Figure 4. Assembly of Compound Magnet

The experiment is supported by an analytical-computational program which incorporates a 2-D hydrodynamics code and examination of the effects of anomalous transport and impurity radiation.

REFERENCE

1. A.G. Es'kov, et al., in Plasma Physics and Controlled Nuclear Fusion Research (IAEA, Vienna 1978).

PLASMA ROTATION IN FIELD-REVERSED THETA PINCHES

L.C. Steinhauer
Mathematical Sciences Northwest, Inc., Bellevue, Washington 98009

Field-reversed plasmas (FRP) have for many years been observed to spin up and develop a destructive m=2 instability. While the instability threshold for rotating modes has been reasonably well characterized, the cause of rotation remains obscure. Several mechanisms have been proposed to explain the rotation. The most promising seems to be the following: end shorting on open field lines causes that portion of the plasma to spin up; viscous friction then transfers the rotating motion to plasma on closed field lines. We develop theoretical models to describe this mechanism.

Structure and Rotational Stability of Field-Reversed Theta Pinches. The separatrix in a field-reversed pinch divides the plasma into two distinct regions, the central closed magnetic field line region and the surrounding open line region. In a straight coil theta pinch, the magnetic fields are purely poloidal (field vectors in r-z plane) and have negligible toroidal field.

Rotating FRP stability was treated recently by Barnes, et al.[1] They calculate that the stability threshold for the commonly observed rotating m=2 mode is $\Omega \cong 1.35$ to $1.55 \times \Omega_*$ where $\Omega_* = -(1/ren_i B)\partial p_i/\partial r$ is the ion diamagnetic drift frequency; i.e., the threshold is similar to that predicted for non-reversed field pinches.[2]

MHD Picture of Plasma Rotation. Treating the plasma as a magnetohydrodynamic fluid, the principal equations governing the rotation are the ion angular momentum law,

$$\frac{1}{r^2}\frac{D(r^2\Omega)}{Dt} - \frac{1}{nr^2}\nabla\cdot(r^2 n\nu_\perp \nabla\Omega) = \frac{\bar{B}}{\mu r}\cdot\nabla(rB_\theta) \qquad (1)$$

and a reduced form of Ohm's law, which in simplified form is

$$\frac{\partial}{\partial t}\left(\frac{B_\theta}{r}\right) - \nabla\cdot\left[\frac{\eta}{\mu r}\nabla(rB_\theta)\right] - B_z\frac{\partial}{\partial z}(\Omega + \Omega_*) = S \qquad (2)$$

where D/Dt is the convective derivative, $\nu_\perp$ is the ion kinematic shear viscosity, and S is a source term containing principally gradient terms in the poloidal field, temperature and other plasma properties.

Evidently from (1), changes in angular momentum arise from either viscous forces or jxB forces. The latter are manifested heuristically as magnetic field line tension exerting an azimuthal torque on the plasma. The rotational kinetic energy is not carried by transport processes or torsional Alfven waves[3] (else the waves would decay) but instead springs out of polarization energy latent in the non rotating plasma. This is principally in two forms; static energy due to ion displacement in the presence of the electric field (proportional to E_r^2); and convective energy due to displacement when there is a radial ion pressure gradient (proportional to $E_r dp_i/dr$). The $B_\theta^2/2\mu$ and rotational kinetic energies appearing in a spinning plasma are, in the course of establishing a new plasma equilibrium, drawn naturally from the transverse kinetic energy, p, and axial field energy $B_z^2/2\mu$.

Rotation on Open Field Lines. Open line plasma contact with end walls shorts the transverse electric field. This initiates a torsional Alfven wave which imparts an angular velocity of $\Omega = -\Omega_*$ to the plasma (if shorting produces $E_r = 0$). In the dissipationless problem, the interaction of waves from opposite ends alternately sets Ω to $-\Omega_*$, to $-2\Omega_*$, then to zero, and so on. The dissipation (diffusivities $\eta_\parallel/\mu$, $\eta_\perp/\mu$, $\nu_\parallel$ appearing in (1), (2), which are comparable at $\beta \approx 1$) leads to spatial spreading of approximately

$$\delta_{diff} \equiv \rho_i (L/\lambda_e)^{1/2} \tag{3}$$

where ρ_i is the ion larmor radius in vacuum and L/λ_e is the axial collisionality. Evidently the spreading, $\propto \rho_i$, is small compared to the axial dimension L and would be negligible if the torsional waves had uniform velocity over the plasma cross section. In fact, they do not since their speed $V_A \propto B_z/\sqrt{n}$ is very high at low density and vice versa. Consequently, the rotation, Ω, quickly develops an evolving closely-spaced spatially-oscillating radial structure with length scales less than ρ_i. In short, dissipation produces a roughly uniform rotation $\Omega = -\Omega_*$ in at most a few Alfven transit times (based on the Alfven speed at the separatrix).

Even after end shorting, a net outward-pointing electric field can arise on a transient basis as observed by Ekdahl.[4] There is another effect which even in quasistatic conditions can cause a reversed (outward) electric field. If the electrical potential is uniform across the plasma at the end wall, then the thermoelectric potential in the plasma interior is proportional to kT_e/e. If in addition, the plasma has a negative radial temperature gradient, there will be an outward electric field. Such gradients are expected because the internal closed line plasma remains hotter, not being in contact with the end walls. The resulting rotation is found by applying the appropriate electric field to Ohm's law

$$\Omega = -\Omega_* \left[1 + \frac{0.93}{\delta_{T_e}} \left(\frac{T_e}{T_i} \right) \left(\frac{1}{\delta_n} + \frac{1}{\delta_{T_i}} \right)^{-1} \right] \tag{4}$$

where $\delta_{T_e} \equiv -T_e/(\partial T_e/\partial r)$ is the local electron temperature gradient length, and δ_{T_i}, δ_n correspond likewise to T_i and n. Clearly $-\Omega/\Omega_*$ can exceed unity as a consequence of the expected ∇T_e. The thermoelectric potential then provides a physical basis for the outwardly oriented electric fields needed to explain observed rotational instabilities in non reversed field theta pinches.[2]

Rotation on Closed Field Lines. In contrast to the open-line plasma, the closed-line plasma is spun principally by viscous forces rather than jxB forces. Shorting can take place within a closed field line, but the result only produces uniform rotation along the flux line, $\Omega = \Omega(\psi)$. This result holds so long as n, T_e and T_i are uniform along the flux line. Angular momentum imparted by viscous drag to plasma near the separatrix is therefore transmitted at the Alfven speed to plasma on the same flux line near the axis; this in

effect increases the moment of inertia of the outer layers.

The transient spinup of the closed line plasma accounting for the inertia enhancement and ignoring cross-field particle diffusion is governed by

$$\frac{\partial \Omega}{\partial t} = \frac{1}{nr}\frac{\partial}{\partial r}\left[\frac{nr\nu_\perp}{2}\left(\frac{r}{R}\right)^2\frac{\partial \Omega}{\partial r}\right] \qquad (5)$$

where R is the radius of the magnetic axis (where B = 0). This is a simple diffusion equation with spatially dependent diffusivity; since it is in fact linear, it can be solved by a normal mode analysis. The transient behavior is dominated by the lowest order (fundamental) mode, the decay time of which is

$$\tau_{spin} = \alpha\frac{a^2}{\nu_1} \; ; \; \frac{a^2}{\nu_1}(\mu sec) = \frac{a^2(cm)T^{3/2}(eV)}{39} \qquad (6)$$

for a deuterium plasma with $T_e = T_i = T$ and $\ell n\Lambda = 15$; ν_1 is $\nu_\perp$ at $\beta_\ell = 1$ (β_ℓ is based on the local magnetic field). The proportionality factor α depends on the aspect ratio of the toroidal plasma; calculated values for a rigid rotor density profile are shown in Table I.

Table I

Transient Spinup Factor

Aspect Ratio, R/a	α
2	0.16
3	2.3
4	22
5	165

Several trends emerge from this result.

(1) The transient spinup time scales with plasma size (minor radius) and temperature in the same way as the classical cross field particle transport time $\tau_\perp = \mu a^2/2\eta_\perp$; since $\nu_\perp \cong 3.2\eta_\perp/\mu$ (deuterium, $T_e = T_i$) then $\tau_{spin}/\tau_\perp \cong \alpha/1.6$.

(2) The proportionality factor α from Table I is extremely sensitive to aspect ratio. The physical basis for this is clear considering that the kinematic viscosity varies as $\nu_\perp \propto n/B^2T^{1/2}$; low aspect ratio plasmas have high average density and low average field inside the separatrix, therefore they tend to be highly viscous; high aspect ratio plasmas have low average density and average fields almost as high as the vacuum field, B_o. Of course a highly viscous plasma will rapidly spin up in response to a rotation applied at the surface, and a low viscosity plasma will spin up slowly.

(3) Evidently for $R/a \leq 3$, the transient spinup time is shorter than the plasma decay time; for $R/a \geq 3$ the plasma tends to decay faster than the spin transient.

The above analysis only treats the transient aspect of the spinup. The other side of the question is the quasisteady rotation rate that is approached. The asymptotic state has uniform Ω (rigid body) inside the separatrix with $\Omega = \Omega_s$, the rotation rate at the separatrix. (Note, Ω_s is equal to or slightly greater than $(\Omega_*)_s$ according to (4)). If, e.g., the asymptotic rotation rate, Ω_s, were relatively fast, than the rotational stability limit ($-\Omega/\Omega_* \equiv O(1)$) could be reached in a time less than τ_{spin}. In this case the stable time to reach $-\Omega/\Omega_* = 1$ is

$$\tau_{\alpha=1} = \tau_{spin} <\Omega_*>/\Omega_s \qquad (8)$$

where $<\Omega_*>$ denotes the average value inside the separatrix. If, on the other hand, $\Omega_s < <\Omega_*>$ then the asymptotic state should itself be stable. What distinguishes these two cases is the plasma profile, in particular the radial profile of Ω_*. If the radial pressure profile becomes very steep near the separatrix, such as may arise as a result of endloss in the open field line plasma, then $\Omega_s > <\Omega_*>$ and $\tau_{\alpha=1}$ may be short indeed. If, on the other hand, the gradients near the separatrix become more gentle, which is the case for an anomalous radial transport sheath, then $\Omega_s > <\Omega_*>$ and the asymptotic state may be rotationally stable.

Summary. The open field line region is spun up principally by jxB forces, and the closed line plasma by viscous forces (although jxB forces insure uniform Ω along a closed flux line). The non uniform speed of torsional Alfven waves caused by end shorting creates a highly transient, highly structured radial Ω-profile; dissipative processes smooth the profile in at most a few Alfven transient times, producing $\Omega \cong -\Omega_*$. The transient spinup time in the closed line plasma scales in the same way as the transverse particle diffusion time, but has extreme sensitivity to aspect ratio; it is short for "viscous" low aspect ratio plasmas, and vice versa. Ultimately, the rotational stability depends on the ion pressure profile; endloss (which steepens the profile near the separatrix) is destabilizing, and anomalous radial transport (which flattens the profile) is stabilizing.

REFERENCES

1. D.C. Barnes, C.E. Seyler and D.V. Anderson, Bull. Am. Phys. Soc. 24, 988 (1979).

2. J.P. Freidberg and L.D. Pearlstein, Phys. Fluids 21, 1201 (1978).

3. A. Kadish, Phys. Fluids 19, 141 (1976).

4. C.A. Ekdahl, R.R. Barch, R.J. Commisso, R.F. Gribble, K.F. McKenna, G. Miller and R.E. Siemon, submitted to Phys. Fluids.

ACKNOWLEDGEMENT

This work was supported by USDOE contract DE-AC06-76ET53027 (formerly EY-76-C-06-2319).

STELLARMAK A HYBRID STELLARATOR - SPHEROMAK

Charles W. Hartman, Lawrence Livermore Laboratory, University of California, Livermore, California 94550

I. Introduction

It has been known for some time that nonaxisymmetric, vacuum-field, toroidal confinement systems can be formed by combination of axisymmetric multipole fields and modified Stellarator-like fields.[1] This "hybridization" can result in improved negative V'' properties and shear. In addition, simpler coil topology, as compared with a conventional Stellarator, is possible since the Stellarator-like windings need not link the torus. Initial calculations were concerned largely with vacuum fields however, it is apparent that plasma current can also serve to provide a poloidal field which can then be transformed in the toroidal direction by helical stellarator windings as has been recently suggested[2].

This paper discusses hybridization of modified Stellarator-like transform windings (T-windings) with a Spheromak[3] or Field-Reversed-Mirror configuration.[4] This configuration-Stellarmak-retains the important topological advantage of the Spheromak or FRM of having no plasma linking conductors or blankets. The T-windings provide rotational transformation in toroidal angle of the outer poloidal field lines, in effect creating a reversed $B_{Toroidal}$ Spheromak or adding average B_T to the FRM producing higher shear, increased limiting β, and possibly greater stability to kinks and tilt. The presence of field ripple in the toroidal direction may be sufficient to inhibit cancellation of directed ion current by electron drag to allow steady state operation with the toroidal as well as poloidal current maintained by neutral beams.

II. Stellarmak Configuration

The basic hybrid approach is shown in Fig. 1. Axisymmetric fields are provided by I_z, the two rings, and a uniform B_z to give the poloidal-field pattern shown. Helical windings, centered on the z-axis, provide Stellarator-like rotational transform. The combined fields give numerically computed toroidal magnetic surfaces as shown with the rotational transform on the small-major-radius side of the surfaces provided by the axisymmetric poloidal field and the transform on the large-major-radius side provided by the helical windings. Continuation of the rotational transform by the axisymmetric B_p eliminates the need for helical windings which link the toroidal surfaces.

Application of T-windings to produce toroidal rotational transform t_T of the basic poloidal field of a Spheromak is shown in Fig. 2. The modular T-windings shown in Fig. 2(a) lie on a sphere and follow loxodromic spiral trajectories with latitudinal cross-links. A vacuum poloidal field line near $\psi = 0$ passes near the axis of the Spheromak,

emerges at the poles, and returns near the spherical surface where the T-windings induce toroidal transform modifying the basic Spheromak configuration to that shown in Fig. 2(b). Numerical calculations in progress (assuming vacuum B_p) have given $t_T/t_p = .04$ for 8 T-winding modules with flux surfaces as shown in Fig. 2(c). Alternatively T-windings for a highly prolate reversed-field- configuration would more nearly resemble the helices of Fig. 1 and arbitrarily large t_T/t_p could be obtained depending on the elongation.

III. MHD Stability Aspects

The most striking aspect of introducing transform windings to a Spheromak/FRM is that shear and reversed toroidal transform can be introduced externally without hole-linking conductors. For a large aspect ratio stabilized Z-pinch the maximum stable β is increased from 15% to 40% in going from a field profile having $B_T = 0$ on the last ψ_p surface to the usual reversed B_T configuration. A similar factor of 3 in β can possibly be obtained for the Stellarmak providing ballooning limits are not encountered. Similarly, T-windings added to the FRM can lend shear stabilization to an otherwise MHD unstable configuration.

Since a conventional stellarator is stable to tilt and slip solid body motions, the transform windings would presumably give improved stability in the Stellarmak.

IV. Equilibrium Aspects

Probably the most significant advantage to be gained by introducing symmetry perturbing transform windings is the potential of sustaining the plasma currents by injection of directed neutral beams. Electron trapping and viscous effects caused by the field ripple can prevent electron cancellation of the ion directed current opening the way to a truly steady state system. For a large spheromak reactor with resistively decaying currents the Q based on resistive losses is,[3]

$$Q_M = \int P_F \, dt/W_M \simeq 100 \sim \beta^2 B^2$$

so that a relatively small current-sustaining beam power is necessary if the process is fairly efficient. This is especially true if βB is increased by a factor of 3 by enhanced stability.

References

1. H.P. Furth and C.W. Hartman, "Strong Negative-T" Torus " Physics of Fluids, vol. 11, No. 2 (Feb. 1968) p. 408.
2. T. Ohkawa, "Physics of the OHTE (Ohmically Heated Toroidal Experiment)," in these Proceedings.
3. M.N. Bussac et al., in Plasma Phys. & Cont. Nuc. Fusion, Proceedings 7th Inter. Conf. (IAEA, Vienna, 1979).
4. G. Carlson, "Neutral-Beam-Sustained, Field-Reversed-Mirror Reactor," in these Proceedings.

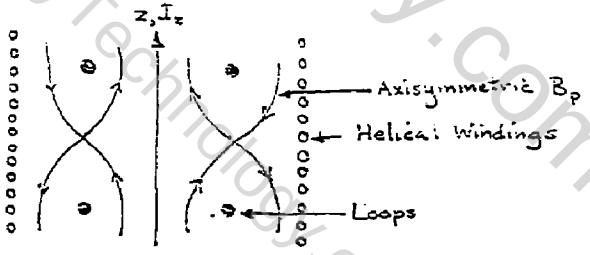

(a) Coil Configuration

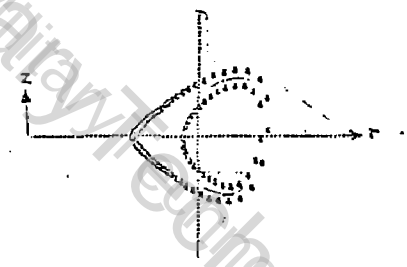

(b) Magnetic Surfaces

Fig. 1. Hybritron Configuration. Intersections of magnetic surfaces with the r-z plane [Fig. 2(b)] were computed for the coil configuration [Fig. 2(a)] with $B_I = 1/r$, $B_{zo} = 0.12$, $L_{Loops} = -0.12$ (at $r = 1$, $z = \pm 1$) and with a helical magnetic potential $\chi = C_\lambda I(kr) \cos(\lambda\phi + kz)$ where $\lambda = 6 = k$ and $C_\lambda = 1$.

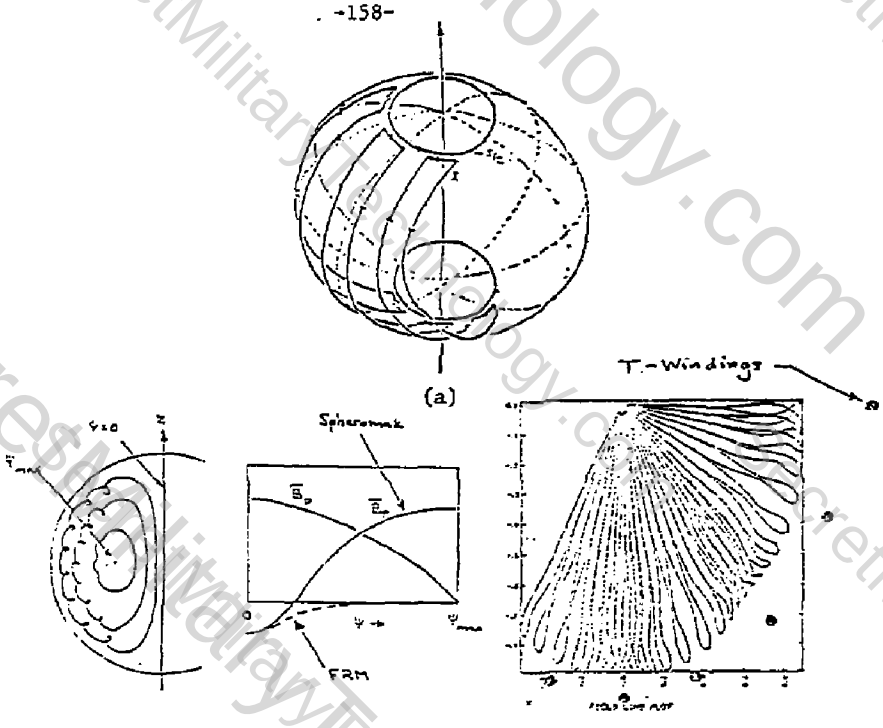

Fig. 2. Stellarmak Properties. Fig. 2(a) shows three modular T-windings based on loxodromic spirals and latitudinal cross links. Also shown are compensating loops. Fig. 2(b) shows heuristic field-line-trajectory projections in a meridinal plane. Also shown are average $\overline{B}_p$ and $\overline{B}_\perp$ vs ψ for Spheromak and FRM configurations. Fig. 2(c) shows computed field-line projections in the equatorial plane for 8 modular windings.

UTILIZATION OF ELECTRON COILS FOR AN ADVANCED TOKAMAK AND CONJECTURE ABOUT THE CAUSE FOR CURRENT STEP (DOWN).

Shoichi Yoshikawa, Plasma Physics Laboratory, Princeton University, Princeton, New Jersey 08544

1. Utilization of electron coils for an advanced tokamak

The use of relativistic electron beam current (REB) in the plane of plasma current in tokamaks offers several possible advantages such as:

(i) reduction in q;

(ii) lowering A(≡ R/a);

(iii) avoidance of current driven microinstabilities.[1]

We repeat, though, the above advantages may well be illusionary.

The fourth advantage is the possibility of a current-sustained tokamak. In this scenario, the REB electron current or electron coil will be set up either by runaway discharges à la UCLA or by REB injection à la IPP, Nagoya University. The resultant configuration will be kept for a while until the cold plasma trapped in this magnetic trap is heated to high temperatures leading to ignition or high Q (Fusion Power/N.B. Power) modes. Then the REB current will be maintained by the rf wave acceleration of electrons. This should be compared with the rf maintenance of plasma current.[2] The rf power needed, P_{rfw}, for maintaining the REB current is given by

$$P_{rfw} \propto n_b v_{ph} E_{OH} \propto n_b v_{ph} \eta J \tag{1}$$

but

$$\eta \sim \frac{1}{W^{3/2}} \frac{n_p}{n_b} \tag{2}$$

where n_b is the beam density, W is the energy of relativistic electrons, n_p is the plasma electron density. Therefore ($v_{ph} \approx c$)

$$P_{rfw} \propto n_p \frac{1}{W_e^{3/2}} J \ . \tag{3}$$

This should be compared with the rf power needed to couple to superthermal electrons, P_{rfT}, which is

$$P_{rfT} \propto n_p \frac{v_e}{T_e^{3/2}} \int f\left(\frac{v_{ph}}{v_e}\right) \tag{4}$$

where f may be between 1/3 to 1/10 and v_e is the electron thermal velocity. The rf power needed for REB is then lower than P_{rfT} by the ratio

$$\frac{P_{rfw}}{P_{efT}} \simeq \frac{1}{f\left(\frac{v_{ph}}{v_e}\right)} \cdot \frac{T_e}{W} \tag{5}$$

which could be easily 1/10 to 1/30.

2. Conjecture about the Cause for Current Step

As Mohri has shown, the current in the SPAC experiment[3] decays in step. One possible explanation of this phenomenon is the inability of the REB beam to maintain toroidal equilibrium.

REB is moving in toroidal directions, hence there is a centrifugal force, $\vec{F} = (F_\theta, 0, 0)$. This force is not derivable from the surface function $\phi(\psi)$. The situation is analogous to toroidal equilibrium of rotating plasma under gravity.[4] Thus the plasma pressure must be finite, so that

$$\vec{\nabla} p + \vec{F} = \vec{\nabla} \phi. \tag{6}$$

It is conjectured that the plasma pressure decays with its own energy confinement time until when Eq. (6) could not be maintained. Then the equilibrium is lost. The resultant partial loss of REB may contribute to the production of background plasma either by instability (yet unidentified) or by beam-wall interaction. The increased plasma pressure, restores the equilibrium by satisfying Eq. (6). The process repeats itself, hence current steps. Normal resistive interaction between REB and background plasma is not expected to keep the plasma temperature high.

The experimental verifications of this conjecture may be done by measuring plasma pressure. Also, if the plasma can be heated by rf or other means without upsetting the electron coil, the current step may be avoided. Finally Thompson scattering may enable the measurement of pressure gradient within the magnetic surface.

References

[1] S. Yoshikawa, PPPL Tech. Memo, 260.

[2] S. Yoshikawa and H. Yamato, Phys. Fluids, 9, 1814 (1966).

[3] A. Mohri, this proceeding.

[4] S. Yoshikawa (to be published).

DYNAMICALLY FORMED SPHEROMAK PLASMA (PS-1)

G. C. Goldenbaum, Y. P. Chong, G. Hart, J. H. Irby
Department of Physics and Astronomy, University of Maryland
College Park, Maryland 20742

Formation Phase

In this paper we discuss our recently reported observations of the formation of a highly elongated spheromak configuration.(1) In the present context, we define a spheromak as a toroidal configuration with both toroidal and poloidal field components, but with no toroidal field coils and no transformer. The toroidal field vanishes on the symmetry axis and has a maximum near the magnetic axis. Both the toroidal and poloidal fields have approximately equal maximum values. Our experiment is called Paramagnetic Spheromak (PS-1). The present vacuum chamber is a circular cross section cylinder (R = 11 cm) filled with deuterium gas at a pressure of 5 to 30 mTorr. A capacitor bank is discharged into a single turn solenoid surrounding the cylinder creating an axial B_z field. The field rises to 4 kG in 9 μsec and is clamped to give a 100 μsec L/R decay time. At about peak B_z field a second capacitor bank is discharged between annular electrodes to produce an annular shell of I_z current. This current puts the B_ϕ toroidal flux into the plasma. The current rises to 150 kA in 4 μsec. Finally a fast rising current is produced in the external solenoid creating a 9 kG B_z field opposite in direction to the initial B_z field. This field rises in 1.5 μsec. Presently, this circuit is clamped so that it decays to 1/e of its maximum in 58 μsec. Most of the results reported in reference 1 were obtained without the clamp switch however, i.e. the circuit oscillated. The plasma radially implodes at approximately the snowplow speed to give an ion energy of $B_z^2/4\pi n_e$, where B_z is fast rising piston field and n_e is the density. For the conditions of this experiment, the radially directed ion energy is about 1.0 keV. Typically, in theta pinches, some of this directed energy is randomized resulting in larger ion temperature than electron temperature. The ion and electron temperatures may then equilibrate if there is no other heating or loss mechanism dominating one of the species.

Three important physics questions arise in the formation phase: 1) Will closed poloidal magnetic surfaces form? 2) Will the toroidal field be peaked approximately in the center of the closed flux surfaces (paramagnetic toroidal field)? 3) Will heating occur as a result of the implosion? In the previously referred to paper (1) all these questions are answered in the affirmative. An experimentally determined poloidal flux surface contour map is shown in figure 2, demonstrating closed surfaces. Flux surface closure occurs within 0.5 μsec of the start of the reversed B_z field. Initially, two magnetic islands form which coalesce to form the structure shown in figure 2. In reference (1), it was shown that for the conditions chosen, the maximum of toroidal field is about 6 kG and occurs near the center of the magnetic island shown in figure 2. The poloidal field on the outer edge rises to about 9 kG. Finally, Doppler broadening spectroscopy has indicated a temperature of 190 eV for carbon impurity ions while the same type of measurements on the D_α line indicates 290 eV at 2 μsec. Thomson scattering

measurements give an electron temperature of 30–50 eV at the same time. He-Ne laser interferometry indicate a density of $3\times10^{15}cm^{-3}$ in the center of the island at 2 usec.

Equilibrium Phase

In any dynamically formed plasma, an important consideration is the relaxation of the imploded state to the desired equilibrium configuration. An appealing feature of the spheromak is the possibility of a near force-free configuration corresponding to a minimum magnetic energy. Rosenbluth and Bussac(2) have considered a classical force-free spheroid as well as slightly prolate and oblate spheroids. They find a tilting instability for a prolate spheroid. We have no internal magnetic field data for times later than 2 usec and consequently, cannot, with certainty, say whether the magnetic surfaces exhibit any tilting after 2 usec. We do have interferometer measurements of the integral of the density along lines parallel to the z axis so that the integrated density as a function of radius can be determined. We find that at 30 usec, the plasma still exhibits an annular shape with no indication of grossly unstable behavior. During this time there are about 40 Alfvén transit times from the end to the center.

Since it is desirable to know what the largest β value is for which the plasma remains grossly stable, it is of interest to know what the value of beta is here. We will assume an operational value of beta defined as

$$\beta_e = \frac{8\pi p(r = 5\ cm)}{B_z^2(r = 11\ cm)} .$$

Because the ion lines used for the ion temperature measurement burn out, we do not know the ion temperature after about 5 μsec. Thomson scattering measurements indicate an electron temperature of about 30 eV as late as 40 μsec. Since the electron and ion equilibration time is of the order of a few microseconds, we have to presume the ion temperature has dropped to the electron temperature. From the interferometer measurements we get the line integral of the density at r=5 cm as a function of time. Assuming a length of 30 cm, we calculate the density and hence the pressure. In figure 3, we ploc β_e as a function of time. We see that as the field, density and temperature drop, the value of beta stays almost constant, in the vicinity of 0.3 to 0.4. From this we conclude that it is possible to confine $\beta = 0.4$ plasmas. The question of whether the internal magnetic field structure remains the same during this time is difficult to answer at this time. We note, however, that at t=2 usec, the radial profiles of the toroidal and poloidal fields are to a good approximation, given by Bessel functions, $[B_\phi \propto J_1(k_r r)$ and $B_z \propto J_0(k_r r)]$. The Bessel function model has the property of retaining its configuration as it diffuses. Since the configuration decay time ($\tau = 4\pi\sigma/k_r^2c^2$) for these parameters is about 66 μsec, the configuration should not drastically change in 30 usec if only classical resistive diffusion is present.

This work is supported by the U.S. Department of Energy under contract DE-AC05-77ET 53044.

References

1. G. C. Goldenbaum, J. H. Irby, Y. P. Chong and G. Hart, University of Maryland, Department of Physics and Astronomy, Report PU 80-057, revised December 1979.

2. M. N. Rosenbluth and M. N. Bussac, Nuclear Fusion 19, 489 (1979).

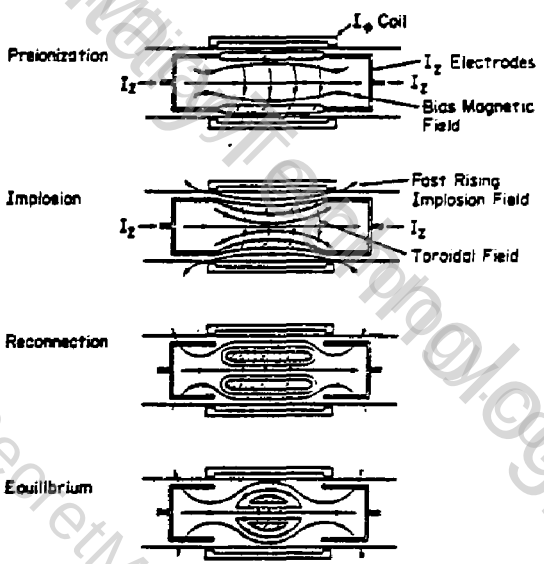

Figure 1 Schematic diagram of the formation and equilibrium phases of the spheromak configureation in PS-1.

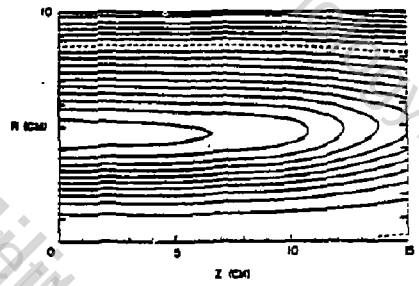

Figure 2 Contours of constant poloidal flux at 2 μsec after the start of the fast B_z field. The contours are calculated from magnetic field measurements made in the plasma and are plotted in intervals of 20πkG-cm^2.

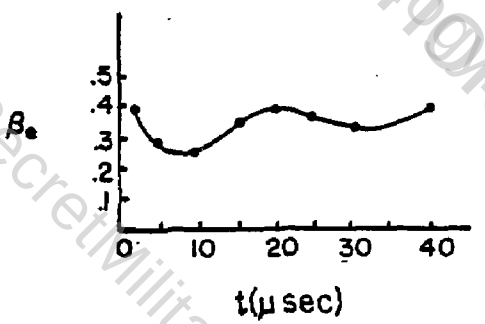

Figure 3 Time dependence of β_e. At 40 μsec the externally applied field has dropped to half its maximum.

SPHEROMAK EQUILIBRIUM AND STABILITY AND NUMERICAL STUDIES OF A SPHEROMAK FORMATION SCHEME

M. Okabayashi, S. Jardin, H. Okuda, T. Sato*, G. Sheffield, Plasma Physics Laboratory, Princeton University, Princeton, New Jersey 08544, and A. Todd Grumman Aerospace Corporation, Princeton, New Jersey 08540

Recently, intensive theoretical studies of the spheromak configuration have been carried out to reveal possible advantages towards a commercial reactor [1-3]. These MHD analyses have shown that stable configurations exist at medium beta with respect to the externally applied equilibrium field. The focus of recent theoretical work has therefore shifted toward the study of plasma formation processes without a toroidal or inductive coil on the axisymmetric axis.

The formation scheme proposed by Princeton is quasi-static where the configuration formation takes place over many Alfvén transit times (≥1000), through a sequence of quasi-MHD equilibrium states. The process is controlled by three groups of coils: (1) external equilibrium field coils; (2) a "flux core" consisting of toroidal coils producing poloidal flux, and a toroidal solenoid producing toroidal flux; and (3) a pair of "pinching coils."

Initially, the equilibrium field coils are turned on and the resultant field, which supports the final plasma equilibrium, penetrates the vacuum vessel. All subsequent field programming proceeds on a faster time scale, whereby the vacuum vessel acts as a perfect conductor. The toroidal coils in the core and the pinching coils are now turned on, to generate the vacuum field pattern of Fig. 1a. Breakdown is initiated around the core and the solenoid is energized. Field pressure balance causes the plasma to expand preferentially towards the low field region on the symmetric axis side of the core. As the toroidal flux penetrates the plasma, a reduction of the toroidal current in the core and an increase of the negative pinching coil currents induces a positive toroidal current in the plasma, leading to the equilibrium configuration of Fig. 1b. The core currents are now crowbarred while the pinching coil currents are further increased until a section of the plasma is severed from the core, as shown in Fig. 1c. The core and pinching coil currents are now turned off leaving a 0.25-m minor radius spheromak plasma with an aspect ratio of two, supported by the initial external field.

The formation configurations shown here were calculated as force-free MHD equilibrium solutions satisfying $\Delta^*\Psi = -2\pi^2[dg(\Psi)^2/d\Psi]$, where Ψ is the poloidal magnetic flux and $g(\Psi) = RB_T$. Such sequences are currently being advanced in time using the circuit equations to produce a more self-consistent picture of the evolution. However, it is clear that the importance of resistivity with regard to flux loss and field-line reconnection requires a two-dimensional time-dependent solution.

---

*Permanent address: Geophysics Research Laboratory, University of Tokyo, Japan.

The incompressible MHD equations are solved on a nonorthogonal grid. Grid lines are lines of constant i or constant j. Derivatives with respect to either i or j have the other held fixed. If (x,ϕ,z) are cylindrical coordinates, then the Jacobian $\delta = (\Delta i \times \Delta\phi \cdot \Delta j)^{-1}$ $= x[(\partial x/\partial i)(\partial z/\partial j) - (\partial x/\partial j)(\partial z/\partial i)]$. The velocity and magnetic field are represented in the form

$$\vec{B} = \nabla\phi \times \nabla\psi + \frac{x^2}{\delta} g\nabla\phi ,$$

$$\vec{v} = \nabla\phi \times \nabla A + \frac{\omega}{\delta} \nabla\phi .$$

Here, ψ, g, A, and ω obey the time advancement equations:

$$\frac{\partial\psi}{\partial t} = \frac{1}{\delta}\left(\frac{\partial\psi}{\partial j}\frac{\partial A}{\partial i} - \frac{\partial\psi}{\partial i}\frac{\partial A}{\partial j}\right) + \eta\Delta^*\psi ,$$

$$\frac{\partial g}{\partial t} = \frac{\partial}{\partial i}\left(\frac{\omega}{x^2}\frac{\partial\psi}{\partial j} - \frac{g}{\delta}\frac{\partial A}{\partial j}\right) + \frac{\partial}{\partial j}\left(-\frac{\omega}{x^2}\frac{\partial\psi}{\partial i} + \frac{g}{\delta}\frac{\partial A}{\partial i}\right) + \delta\nabla\cdot\frac{1}{x^2}\eta\nabla\left(\frac{x^2 g}{\delta}\right) ,$$

$$\frac{\partial}{\partial t}\left(\frac{\delta}{x^2}\Delta^* A\right) = \frac{\partial}{\partial i}\left[\frac{1}{x^2}\Delta^*\psi\frac{\partial\psi}{\partial j} + \frac{g}{\delta}\frac{\partial}{\partial j}\left(\frac{x^2 g}{\delta}\right) - \frac{\Delta^* A}{x^2}\frac{\partial A}{\partial j} - \frac{\omega}{x^2\delta}\frac{\partial}{\partial j}\left(\frac{\omega}{\delta}\right)\right]$$

$$+ \frac{\partial}{\partial j}\left[-\frac{1}{x^2}\Delta^*\psi\frac{\partial\psi}{\partial i} - \frac{g}{\delta}\frac{\partial}{\partial i}\left(\frac{x^2 g}{\delta}\right) + \frac{\Delta^* A}{x^2}\frac{\partial A}{\partial i} + \frac{\omega}{x^2\delta}\frac{\partial}{\partial i}\left(\frac{\omega}{\delta}\right)\right] ,$$

$$\frac{\partial\omega}{\partial t} = \frac{\partial}{\partial i}\left(\frac{x^2 g}{\delta}\frac{\partial\psi}{\partial j} - \frac{\omega}{\delta}\frac{\partial A}{\partial j}\right) + \frac{\partial}{\partial j}\left(-\frac{x^2 g}{\delta}\frac{\partial\psi}{\partial i} + \frac{\omega}{\delta}\frac{\partial A}{\partial i}\right) .$$

The core boundary conditions are that $\vec{v}\cdot\hat{n} = 0$, and that the voltages, $\oint E\cdot dl$ in the poloidal and toroidal directions, are prescribed functions of time. The equations are advanced using a leap-frog scheme with Dufort-Frankiel differencing of the diffusive terms.

We illustrate the results of one calculation using these equations in Figs. 2-6. Figure 2a shows the poloidal flux surfaces (ψ = constant contours) at time $t = 0$, while Fig. 2b shows the computational mesh (lines of constant i and constant j). Initially, a current of 600 k amps is flowing in the shell (core) in the toroidal direction. At time $t = 0$ voltages are applied to the shell to reduce the toroidal current and to induce a current in the poloidal direction.

Figure 3 shows contours of constant ψ (3a) and constant toroidal field ($x^2 g/\delta$) at time $t = 3.0$ usec, when the toroidal core current is almost half its original value and current has been induced in the plasma. Note that a magnetic axis has formed near the inside of the shell and that some closed magnetic field lines now exist.

Figure 4 shows the flux surfaces at time t = 6.7 μsec after two-thirds of the current has been induced into the plasma. More closed flux surfaces have now been formed around the plasma magnetic axis. Figure 5 shows the flux surfaces at t = 36 μsec, after all of the toroidal current has been transferred to the plasma by induction. This method of spheromak formation is very efficient in transferring current from the flux shell to the plasma. Figure 6 shows the time histories of the currents in the shell and the plasma, and the total kinetic energy in the plasma.

In addition to this incompressible code, we have developed a two-dimensional simulation code which solves the compressible one-fluid resistive MHD equations [4] using a two-step Lax-Wendroff algorithm. Initially a low-beta plasma is assumed to exist everywhere between the vacuum vessel and the circular core. The toroidal and poloidal magnetic fields at the surface of the core are given as functions of time, and their penetration into the plasma is being studied. Preliminary results indicate that the toroidal field can penetrate into a plasma, preferentially toward the axi-symmetric axis, in a stable manner; hence suggesting the successful formation of a spheromak plasma under actual conditions.

ACKNOWLEDGMENT

This work supported by US Department of Energy Contract No. EY-76-C-02-3073.

REFERENCES

[1] BUSSAC, M. N., FURTH, H. P., OKABAYASHI, M., ROSENBLUTH, M. N., TODD, A. M. M., in Plasma Physics and Controlled Nuclear Fusion Research (Proc. 7th Int. Conf., Innsbruck, 1978) III (IAEA, Vienna, 1979) 249.
[2] ROSENBLUTH, M. N., BUSSAC, M. N., Nuclear Fusion 19 (1979) 489.
[3] OKABAYASHI, M., TODD, A. M., PPPL-1540 (August 1979); submitted to Nuclear Fusion.
[4] SATO, T., HAYOSH, T., Physics of Fluids 22 (1979) 1139.

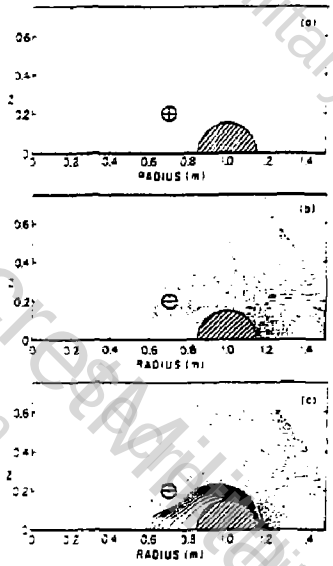

Fig. 1(a-c).
(PPL 792439)

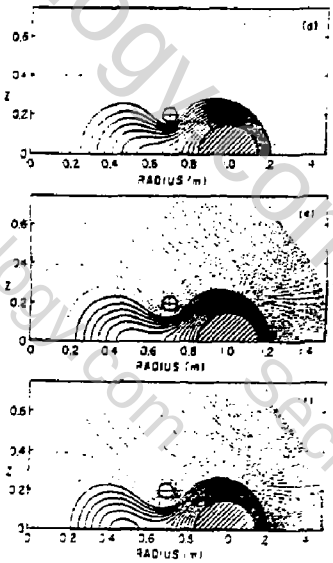

Fig. 1(d-f).
(PPL 792440)

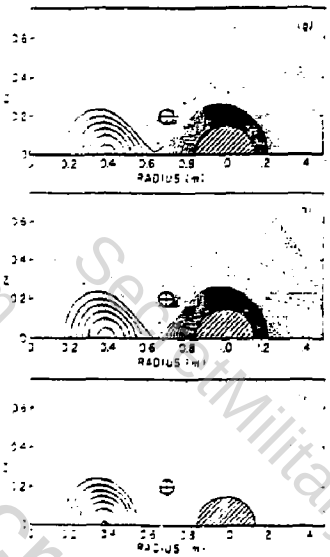

Fig. 1(g-i).
(PPL 792441)

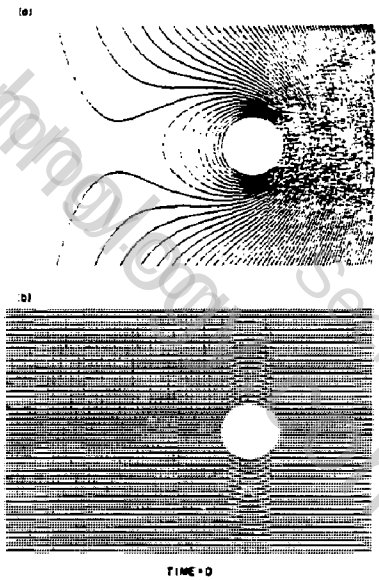

Fig. 2.
(PPL 792640)

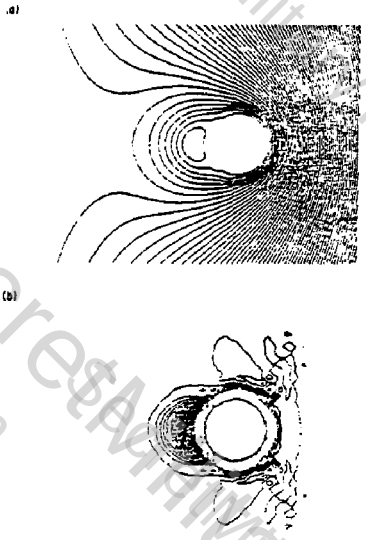

Fig. 3.
(PPL 792639)

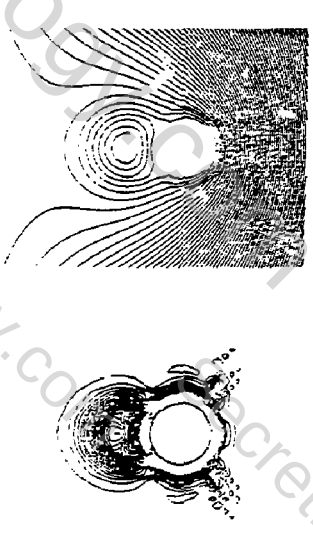

Fig. 4.
(PPL 792638)

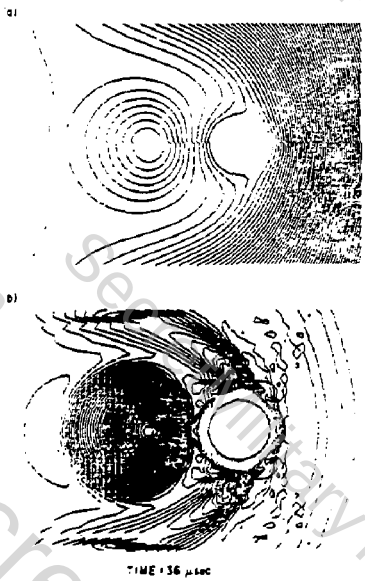

Fig. 5.
(PPL 792641)

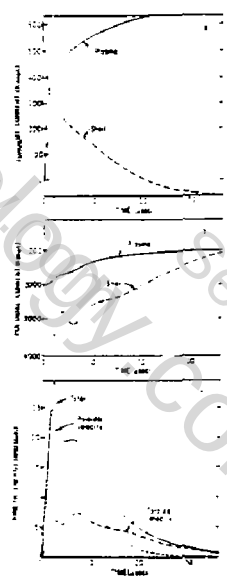

Fig. 6.
(PPL 792648)

Design and Fabrication of the S-1 Spheromak Device

M. Yamada, J. Sinnis, H. P. Furth, M. Okabayashi, G. Sheffield,
T. H. Stix and A. M. M. Todd*
Plasma Physics Laboratory, Princeton University
Princeton, New Jersey 08544

ABSTRACT

The S-1 experiment will develop an electrodless "slow" spheromak formation technique to produce a 500 kA toroid of a = 25 cm, R = 40 cm. The formation scheme is based on a transformation of poloidal and toroidal magnetic flux into a plasma from a flux core and two-dimentional MHD calculations of the formation process are described in an accompanying paper. Physics background and engineering aspects of the S-1 apparatus are presented. The objectives of the S-1 experiment are:

(1) development of a slow "quasi-static" formation scheme, suitable for future scale-up to large magnetic energy contents at moderate forming powers.

(2) investigation of spheromak stability and energy confinement properties on a slow time scale of magnetic diffusion time.

I. Introduction

1.1 The Spheromak Configuration and stability

The spheromak concept is characterized by magnetic field lines that are closed — as in a tokamak — and by a coil-blanket topology that does not link the plasma — as in a mirror machine.[1,2,3] The magnetic field configuration of the spheromak (Fig. 1) includes both toroidal and poloidal components, but the toroidal component is maintained entirely by plasma currents, and therefore vanishes outside the plasma. Correspondingly, there are no toroidal-field-coils — only poloidal-field coils, as in a mirror machine. The outward pressure of the toroidal field and of the plasma is balanced by the inward pressure of the poloidal field.

The equilibrium and stability of the spheromak configuration has been investigated and it was concluded that an oblate spheromak configuration (Oblimak) of aspect ratio 2.0, ellipticity 0.5, having a peaked current profile will be stable to ideal MHD modes up to $\beta_{edge} = 15\%$. Global modes can be stabilized by a loose-fitting shell. Another theoretical approach to the problem is Taylor's ($a_w/a_p \geq 1.5$) treatment of RFP, which finds that the idealized large-hole spheromak is stable for low beta condition. However, it should be noted that a resistive MHD theory demands a close-fitting shell for stability against high number modes. It also predicts interchange modes growing at all β values although various stability effects due to finite-gyroradius effects, non-linear self-stabilization and line-trying of the diverted edge plasma have to be assessed in the future. An encouraging feature of the experiments[5,6] to date is that there is no sign of gross instability even though the walls are not near. But the long-time confinement characteristic of the spheromak configuration is yet to be proved.

---

*Grumman Aerospace Corporation, Princeton, New Jersey 08540

1.2 Spheromak Forming Scheme

In the S-1 experiment, we will employ a "slow" (quasistatic) spheromak formation scheme, suitable for future scale-up to large reactor-level experiments. The formation time scale (~100 μsec) is intermediate between the dynamic time scale ($\tau_A = \frac{a}{V_A} \approx 0.1$ μsec) and the resistive time scale ($\tau_R \approx \frac{\mu a^2}{2\eta}$ ~1 msec). We expect that the present slow formation scheme will exploit a certain advantage of slow RFP (ZETA, Eta-beta) experiments.

The proposed scheme (Fig. 2) will create a spheromak plasma configuration without using coils which link the compact toroidally shaped plasma. In this scheme an initial poloidal field is generated by a winding inside a toroidal ring-shaped flux core. The initial poloidal field is weakened on the small-major-radius side of the ring by superposition of an external vertical field. The ring also contains a toroidal solenoid, which is able to generate an interior toroidal flux, and is therefore able to emit an equal and opposite toroidal flux on its exterior. When the toroidal solenoid is energized, it induces a poloidal current in a sleeve-shaped plasma surrounding the ring. The associated toroidal field distends the poloidal-field sleeve, stretching it in the direction towards the magnetic axis, where the poloidal field is weakest. When the pinch coils are energized, the plasma will be pinched off from the topology linked to the flux core, producing a separated spheromak plasma configuration. The electric currents inside the ring can then be allowed to decay, while the spheromak configuration remains.

II. Parameter Survey for the Spheromak Experiment.

In order to select parameters for an experimental spheromak device, we begin by considering the simultaneous requirements of MHD stability and microstability, which impose a limitation on the line density. We then determine values of plasma current, field strength and size that should allow adequate plasma temperature.

Theoretical studies indicate that optimal finite-β stability will be achieved in a spheromak that is somewhat oblate and has an appreciable "flux hole" around the axis of symmetry. Conducting-wall stabilization also takes place more easily with large-hole devices. Beta-values close to maximum are achieved for a toroidally shaped plasma of aspect ratio $R/a \approx 2$, as in Fig. 1. The significance of a central "flux hole" in practical experimental terms is that an outer flux region is maintained free of plasma current, so that the shear at the edge of the current-carrying region becomes large. Various options for realizing this situation are available, including appropriate initial field-programming, edge-cooling, and shaping of the "divertor flux."

The range of appropriate plasma size density is determined basically by the MHD β-limit and by the limit on the electron streaming velocity V_{stream}. The typical β-requirement is

$$\beta_o^* = \frac{2\mu \langle p^2 \rangle^{1/2}}{B_0^2} \lesssim 0.02 \,. \qquad (1)$$

Assuming that MHD stability can be achieved at this β-level, it will be important, next, to avoid microinstabilities. For this purpose, the electron drift velocity associated with the strong internal currents of the magnetic field configuration has to be well below the electron thermal velocity. We require

$$\frac{v_{stream}}{v_{thermal}} < 0.03 \ . \qquad (2)$$

The conservative limit .03 was chosen by examining data from various toroidal pinch experiments and noting that the onset of plasma anomalies very generally tends to occur at this level. Combining the conditions on β and v_{stream} with the large-flux-hole condition (R/a = 2), we obtain

$$\frac{v_{stream}}{v_{thermal}} = \left(\frac{3 \cdot 10^{11} \ cm^{-1}}{\beta_o^* n_e a^2} \right)^{1/2} < 0.03 \ . \qquad (3)$$

The parameter region that is stable from the point of view of Eq. 3 is shown in Fig. 3 for the case $\beta_o^* = 2\%$. This figure shows that in a spheromak plasma with R = 40 cm, a = 20 cm and a density $n_e > 5 \cdot 10^{13} cm^{-3}$, one can hope to operate without generating gross MHD or current-driven microinstabilities, provided the beta limit is reached. Once the line-density is determined, the maximum electron temperature to satisfy Eq. 1 and Eq. 2 must scale as $T_e \alpha I_t^2$, where I_t is the toroidal current. In the desirable temperature range $T_e > 100$ eV, a 500 kA toroidal current provides an appreciable operating margin. (Fig. 4) The nature of the ohmic-heating power balance in S-1 is illustrated graphically in Fig. 5. Above the 100 eV level in which classical magnetic-field decay time τ_R exceeds 10 milliseconds, the ohmic heating power falls below 10 MW. For $n_e = 10^{14} cm^{-3}$, this heating power would be sufficient to balance the radiation cooling due to one percent of metalic impurities, plus transport losses comparable to Bohm diffusion. The most critical temperature limitation in the initial discharge cycle is expected to arise from heat losses along field lines to the ring supports. As a result, T_e will probably be "clamped" in the 50 eV range. As soon as some reconnection of field lines has taken place, so as to create a "private flux" within the spheromak section of the plasma, the local electron temperature will begin to grow again; finally the temperature of the whole detached spheromak plasma will begin to rise to a new limit. In Fig. 6 a typical evolution of flux-core currents, plasma current and plasma parameters are shown together with a sequence of field configurations during formation.

III. The S-1 Facility.

The machine configuration and its main components are shown in Figures 7. The flux ring contains the Poloidal Flux Core (PC) and the Toroidal Flux Core (TC). These two coil systems induce the toroidal and poloidal currents of the initial plasma. The pinching coils (PN) are to separate a fraction of the initial plasma and to move it towards the center of the vessel where it takes on the spheromak configuration. The Equilibrium Field Coils (EF) hold the final spheromak plasma in a position near the center of the vessel. The vacuum vessel is made of 1/2" stainless steel with no insulating breaks, since it constitutes a passive element in the overall spheromak magnetic circuit.

The EF coils are driven by a generator and have a relatively long pulse length; the EF is basically constant during the time of the experiment. The PC, TC, and PN coils are all driven by fast capacitor banks. Principal parameters of the S-1 facilities are as follows.

R_{RING} = 100 CM
a_{RING} = 15 CM
TOROIDAL RING CURRENT ≤600 kA T
POLOIDAL RING CURRENT ≤15 MA T
TOTAL MAGNETIC ENERGY ≤1 MJ

FORMATION TIME ~100 usec
MAXIMUM V_{TOR} ~10 kV
MAXIMUM V_{POL} ~1.6 kV
EQUILIBRIUM FIELD = 2.2 kG

The flux core contains toroidal and poloidal copper windings housed in a insulating ceramic material. It can emit 0.1 volt-sec of toroidal flux and can induce a 0.5 volt-sec of poloidal flux change requiring about a $\frac{1}{4}$MJ of capacitor energy for each circuit. The core will be covered by 10 mil thick metalic liner (stainless-steel or inconel) that will not only protect the core-surface from sputtering and erosion but also will smooth an induced field at the initial breakdown stage. The core is self supported against induced forces and is powered by six sets of electrical leads.

References

1. M. N Bussacr, et al., in Plasma Phys. Cont. Nuc. Fusion (Proc. 7th Int. Conf. Innsbruck, '78) Vol. 3. and references there in (IAEA- N-37-X-1)
2. M. N. Rosenbluth, M. N. Bussac. Nucl. Fusion 19 (1979) 489.
3. M. Okabayashi and A. M. Todd, PPPL-1580 to be published.
4. J. B. Taylor, Phys. Rev. Lett. 33 (1974) 1139.
5. G. C. Goldenbaum et. al Univ. Maryland Rep. PP80-011.
6. R. K. Linford et al., Plasma Phys. Conf. Nuc. Fusion (Proc. 7th Int. Conf. Innsbruck '78) 2 IAEA (1979) 447.

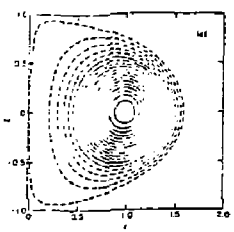

Fig. 1

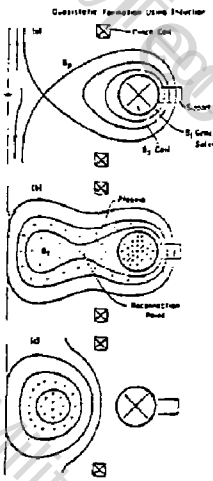

Fig. 2

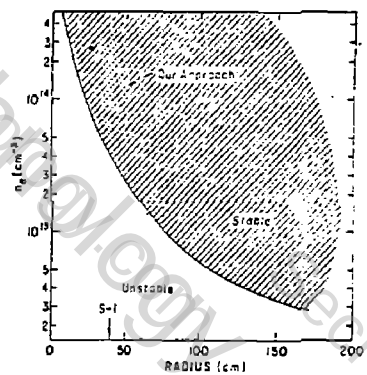

Fig. 3

Fig. 4

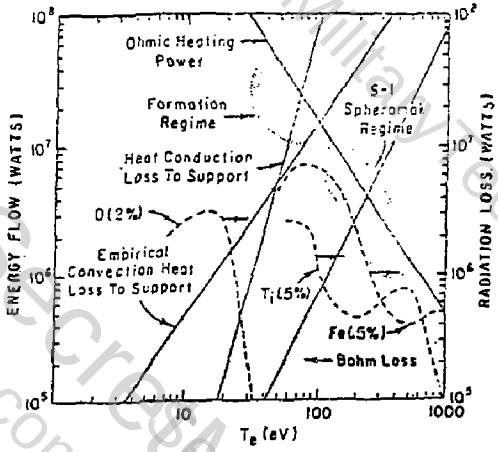

Fig. 5

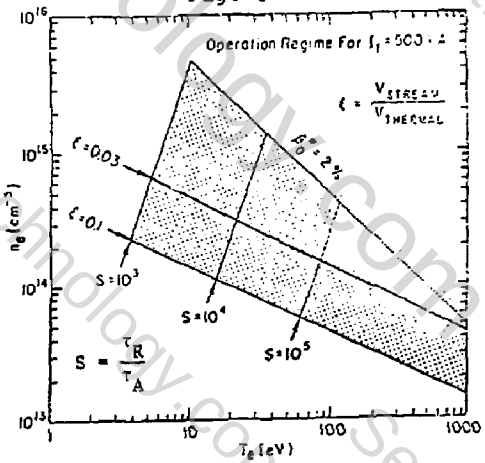

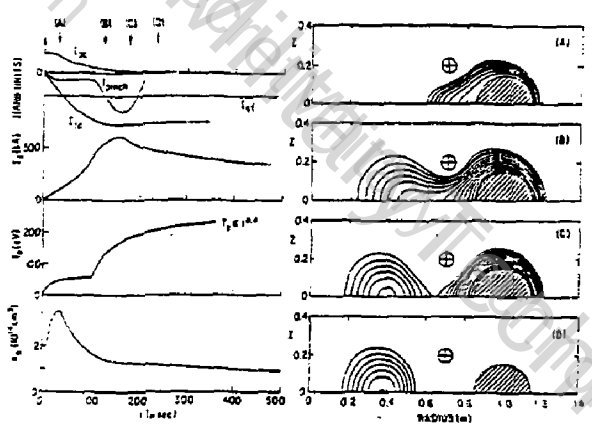

Fig. 6

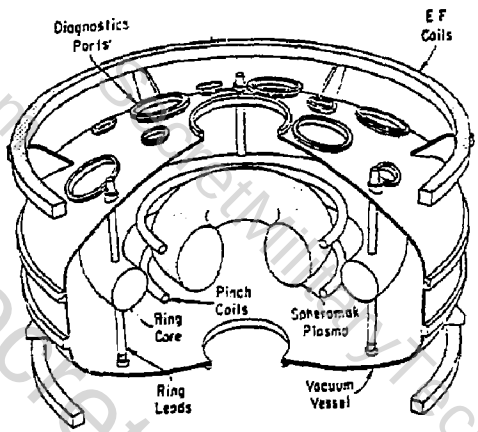

Fig. 7

The S-1 Spheromak device

TWO-DIMENSIONAL SIMULATION OF THE FORMATION OF THE PPPL SPHEROMAK

A. Aydemir, C. K. Chu, H. C. Lui Plasma Physics Laboratory, Columbia University, New York, NY 10027

This paper is a progress report on the simulation of the formation of the PPPL spheromak with a dissipative MHD calculation. We present the precise formulation of the problem, emphasizing particularly the time-dependent boundary conditions. We also present some very preliminary results, which are by no means complete or conclusive, but which do indicate that the general trend is correct and that this model has the basic capability to make a realistic simulation.

Assuming axisymmetry, we describe the plasma in the poloidal plane by the usual single-fluid MHD equations with dissipation, see e.g. Ref. 1. The ohmic dissipation used is either classical Spitzer or anomalous, the thermal conductivity is usually (but not necessarily) taken to be constant, and viscosity is neglected, except for a small numerical viscosity to remove numerical oscillations in regions of sharp gradients or low densities. Vacuum regions are not handled explicitly: a low density cut-off (or "density pedestal"), typically 0.1 of the initial filling density, is used. Equivalently, one can allow a small flow velocity from the walls into the plasma. Simulations of this type have been carried out successfully on screw and belt pinches[1], reversed-field pinches, and Tormac[2]. Agreement with experiment has been invariably good.

Initial conditions for the plasma are a low-temperature (say 1 ev) conducting fluid at rest. A vacuum equilibrium "vertical" field is already present in this plasma.

The set of equations uses the variables ρ (density), $\underline{v}$ (velocity), T (temperature), ψ (the poloidal flux function), and $\chi = rB_\phi$ (toroidal field function). Boundary conditions on ρ and $\underline{v}$ are standard for inviscid fluids, while T, ψ and χ are given on all boundaries (or their normal derivatives). Relating the boundary values of ψ and χ to the externally controlled fields and currents is not immediately obvious, and we shall describe it in some detail.

Fig. 1(a) shows the geometry of the spheromak in the poloidal plane; detailed descriptions are given elsewhere in this conference[4]. The equilibrium vertical field current I_e is

assumed to be d.c. and already fully established at $t = 0$. The toroidal current I_t is also already on, and then drops as shown in fig. 1(b), while the solenoidal current I_s rises as shown in fig. 1(b). We have not yet simulated the pinching current I_p, shown in the same figure.

On the outer boundaries, we stipulate $\psi = \psi_{initial}$ and $\chi = 0$, since the conducting shell has essentially a frozen-in field. On the inner tube, which is also conducting, we write $\psi = \psi_{initial} + \psi_B(t)$, and $\chi = \chi_B(t)$. Here both ψ_B and χ_B are constant on the tube but change with time, while $\psi_{initial}$ is fixed in time but nonuniform on both the tube and the outer walls.

To relate ψ_B to the current I_t, we must solve the problem in the plasma, then calculate $\partial\psi/\partial n$ on the tube boundary, which is equal to the tangential B field. I_t is then given by

$$I_t = \oint \underline{B}\cdot\underline{dl} \quad \text{on the tube surface}$$

To relate χ_B to the solenoid current I_s, we note that χ is also constant everywhere inside the tube, and in fact, it is equal to $\chi_B = NI_s$, where N is the number of turns per unit radian. Thus, the total toroidal flux Φ inside the tube can be expressed in terms of the boundary value χ_B and the current I_s. Now from the solution of the MHD problem, we have $\underline{E} = -\underline{v} \times \underline{B} + \underline{j}/\sigma$, and thus,

$$\oint (-\underline{v} \times \underline{B} + \underline{j}/\sigma)\cdot\underline{dl} = -d\Phi/dt \quad \text{on tube surface}$$

which is the condition that links I_s to χ_B.

Using the differential equations and boundary conditions shown in fig. 1(c), we obtained the results shown in fig. 2. Fig. 2(a) shows the poloidal flux, 2(b) the density, and 2(c) the toroidal field, at the peak of the toroidal field rise on the tube boundary. These results are preliminary, in that we have not yet shifted to the correct time scale (our basic code, written for pinches, deals with $\sim$5 μs while the present problem has a time scale of $\sim$100 μs), we have not understood all the seemingly anomalous results, we have not varied the input parameters or optimized them, and we are still dealing with a coarse grid and crude geometry (e.g., the circular tube is replaced by an octagon, etc.). Nevertheless, we see that (1) the poloidal flux lines do close at the right locations, (2) the density increases in about the same area, and (3) considerable toroidal field is trapped in the closed poloidal flux region. These features indicate that the model as well as the proposed formation scheme are operating in the right direction. More conclusive results will be provided at a later occasion.

References

1. H. C. Lui, C. K. Chu, Phys. Fluids 18, 1277 (1975); 19 1947 (1976).

2. W. Park. C. K. Chu Nuc. Fus. 17, 1100 (1977); Columbia Plasma Lab. Report, No. 75 (1978).

3. A. Aydemir, Columbia plasma Lab. Report, No. 80 (1979).

4. M. Okabayashi et al, paper presented this conference.

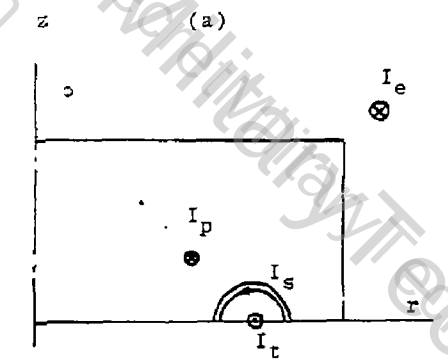

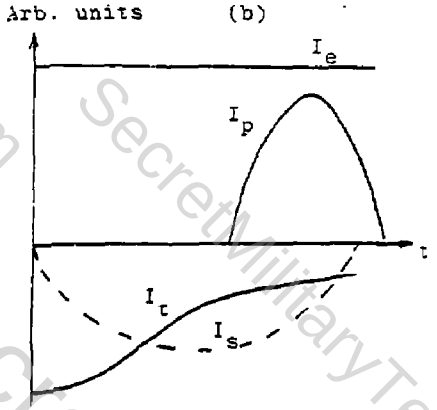

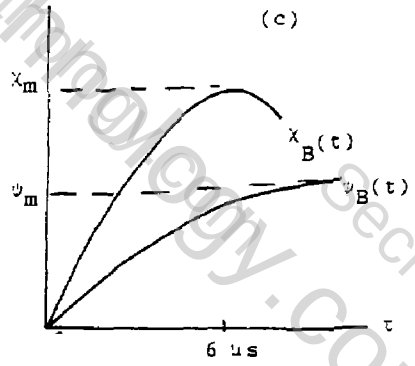

Fig. 1. (a) Schematic diagram of spheromak.

(b) Proposed time-programmed currents.

(c) Boundary values used in this simulation.

$\chi_m = 6 \times 10^5$ G-cm

$\psi_m = 9 \times 10^6$ G-cm^2

Fig. 2. (a) Contours of ψ at 6 μs.

(b) Contours of ρ .

(c) Contours of χ .

(All units suitably normalized)

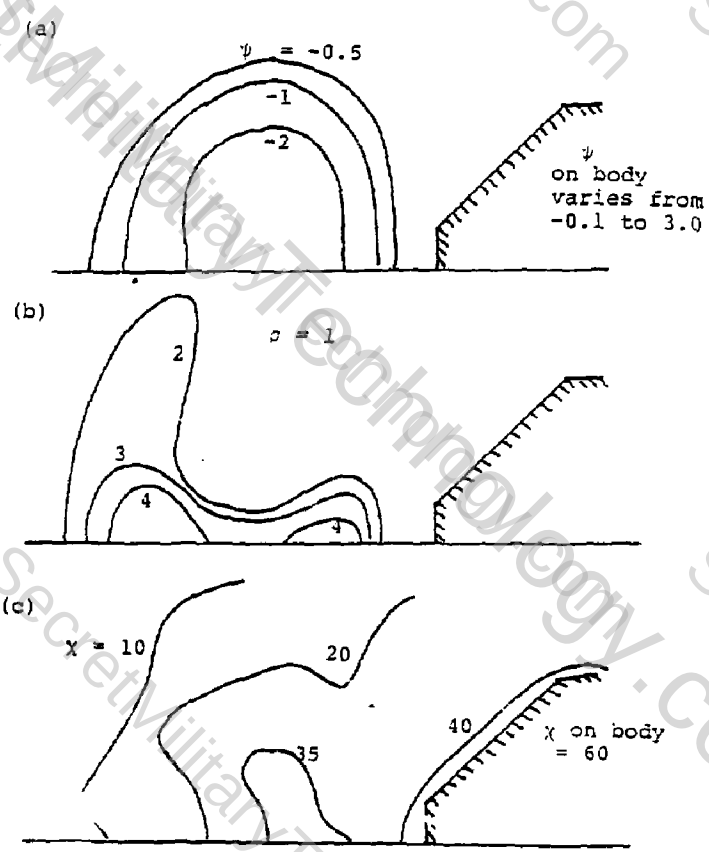

BIFURCATION OF TOROIDAL PLASMA IN A POLOIDAL QUADRUPOLE FIELD

H. Ikezi and K. F. Schwarzenegger
Bell Laboratories, Murray Hill, New Jersey 07974

We have studied the effect of a poloidal quadrupole field on the elongation and bifurcation of a current-carrying toroidal plasma. The experiment was carried out by using an argon discharge in a small tokamak with the toroidal field B_t=2-5KG the major radius R_0=11cm, the plasma current I_p= 2-5KA, T_i=T_e=10eV, and n=(5-10)×10^{13}/cc.

The quadrupole field B_{qp}, which increases as a function of time, is applied after the tokamak discharge has settled. As B_{qp} increases, the plasma crossection elongates until B_{qp} reaches a critical value. The photographs in Fig. 1 were taken from the tangential direction and show the plasma crossection. The crossection is circular when B_{qp}=0 [Fig. 1(a)]. Near the critical value of B_{qp}, the plasma is elongated vertically as shown in Fig. 1(b). The elongation ratio, b/a, reaches about 3, where b and a are the larger and the smaller radii. The horizontal dark stripe at the middle of the cross-section is a shadow caused by the quadrupole field winding. When B_{qp} exceeds the critical value, the plasma divides in two within a few microseconds and each section migrates toward the wall [Fig. 1(c)]. This splitting time is shorter than the resistive field penetration time which is about 20 μs, but much longer than the Alfvén time (0.05 μs).

We have measured the horizontal component of the poloidal field B_R on the vertical axis, y, which is crossing the minor axis. Fig. 2 shows the profiles of B_R, the current density J_z and the safety factor q. The quadrupole field is turned on at a time t=0. As B_{qp} increases and the plasma elongates, B_R decreases, which is consistent with the theory for elongated equilibria. B_{qp} reaches the critical value at t=17 μs. An oscillatory profile of B_R, indicating the existence of a magnetic island, is seen at t=20 μs. The magnetic field reconnection occurs at this stage.

We write the flux function of the quadrupole field as

$$\psi = \frac{1}{2} A r^2 \cos 2\theta, \qquad (1)$$

where r and θ are the minor radius and the angle around the minor axis, respectively. Strauss[1] has shown that the elongated equilibria are found when $A/J_z = A_{cr}/J_z \simeq 0.0^-3$. He also found that b/a=2.9 when $A=A_{cr}$. The experimentally observed value of A_{cr} is about 50% larger than the theoretical value.

The addition of the quadrupole field to the vertical field yields a large field index (the sign of index is negative in our case), which constitutes an unstable field

configuration with respect to the translative movement along the vertical direction. No stable discharge has been obtained, if a DC quadrupole field is applied. We have also tried to produce elongation in the horizontal direction. The experiment has not been successful, however, because of the positional instability.

The present experiment suggests some ideas for the design of a proposed spheromak plasma source[2] which requires plasma splitting.

1. H. R. Strauss, Phys. Fluids 17, 1040 (1974).

2. M. Yamada et al., Bull. Am. Phys. Soc. 24, 1022 (1979).

Fig. 1(a) Fig. 1(b) Fig. 1(c)

Fig. 1 Photographs showing plasma crossection.
(a) No quadrupole field. (b) Most elongated.
(c) After plasma bifurcates

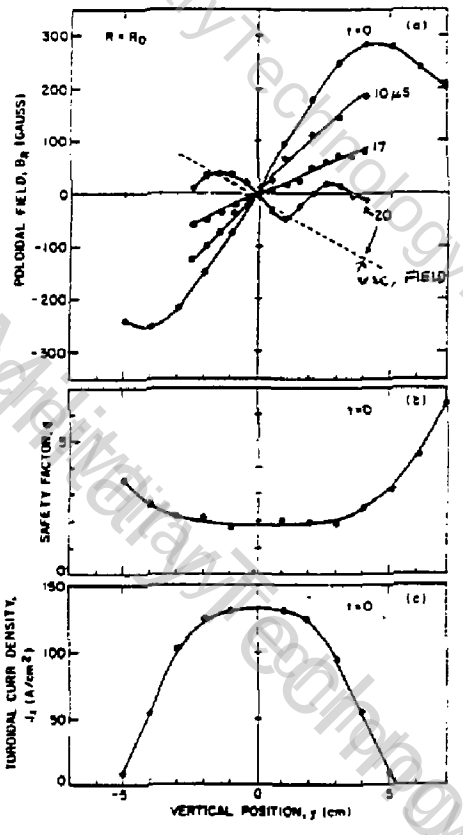

Fig. 2 (a) Profiles of the poloidal field. The quadrupole field starts rising at t=0 and reaches the critical value at t=17 μs. (b), (c) The safety factor and the toroidal current density at t=0.

Start-up Scenario of Compact Tori Based on REB-injection Developed in SPAC-group

Kazunari Ikuta

Institute of Plasma Physics, Nagoya

Quasi-static start-up of compact tori without toroidal field coil is reviewed thoroughly in a proposal of the S-1 spheromak. During the formation phase we should note that the rapid heat loss from the plasma will give a bad effect for the generation of the confinement configuration. In the case of fast start-up of the configuration plasma can safely pass over the dangerous state of the instability toward the desirable stable state with a bonus of producing hot plasma.[1] By this reason it is intended to discuss a fast start-up scenario of the compact tori based on REB injection developed in SPAC group.[1]

Well-known coaxial plasma gun is assumed, throughout in this story, to act as a injection chamber of REB when the gun is working. Consider a coaxial plasma gun with a third electrode which is a REB ejector. One of the arrangement is shown in Fig.1-a. A low temperature plasma disc is made to drift toward the end of the inner electrode. As soon as the disc reaches the end, the strong pulse voltage is applied to the third electrode in order to eject the REB which propagates along spiral lines of force to the disc. As soon as the REB is trapped in the disc plasma (Fig. 1-b), it heats the plasma rapidly. As the REB together with the hot plasma emerges downstream from the end of the inner

electrode the REB ring is formed and settled in as shown in Fig.1-c. After adjusting and improving properly the parameters of the plasma thus formed the configuration could work as a reactor.[2] The impurity problem must be solved in this device.

1) A. Mohri et al: in Plasma Physics and Controlled Nuclear Fusion Research (Proc.7th Int. Conf. Inusburg)

2) K. Ikuta: Jpn J. Appl. Physics 19(1980) in press.

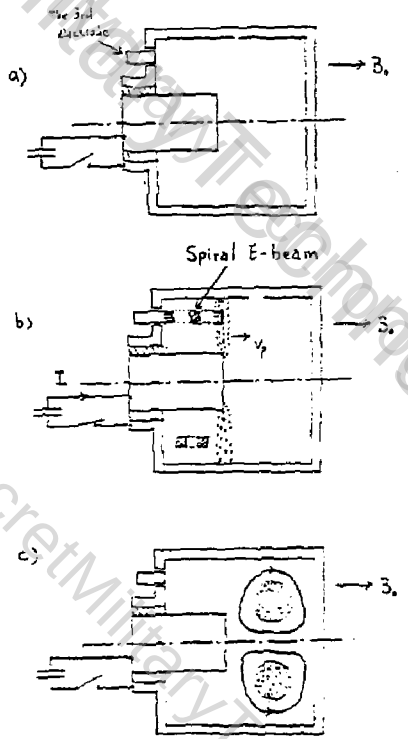

Fig. 1

THE SPS COMPACT TORUS EXPERIMENT

A. DeSilva
Department of Physics and Astronomy, University of Maryland, College Park, Maryland 20742

I. Introduction

Balancing the apparent advantages of the spheromak configuration as a potential reactor are the difficulties in creating such a configuration in the first place. In particular, creating a toroidal field without material conductors threading the torus is a nontrivial exercise. We propose here a scheme that utilizes an intermediate energy storage within the plasma in the form of ordered kinetic energy, that may be released to drive poloidal currents and thereby create a toroidal magnetic field. The scheme is seen as a means of obtaining, in a short time, a spheromak configuration isolated from external current sources, for study of basic stability properties.

The proposed scheme rests on some unpublished observations in rotating-plasma machines made in Berkeley in the early 1960's, and on subsequent work on normal ionizing shock waves performed at Columbia University[1,2,3] and the University of Sydney.[4,5] In order to describe the proposal, it is necessary to first describe briefly the properties of the normal ionizing shock wave in a cylindrical geometry.

II. The Normal Ionizing Shock

Figure 1 shows the shock and driver schematically. A steady axial bias magnetic field is initially applied. Application of a high voltage pulse to the coaxial electrode structure causes the gas to break down, and a radial current flows near the end insulator. This current ionizes the gas, and through the $j_r \times B_z$ body force, sets the plasma into rotation about the tube axis. The current front advances at constant speed parallel to the tube axis, leaving behind a rotating, nearly fully ionized plasma. Typically the rotational kinetic energy per ion is about equal to the ionization energy. Such shocks have been studied extensively.[2,4,5]

III. Compact Torus Initiation

The compact torus is to be created by utilizing a reverse-bias theta pinch to make the poloidal fields and to perform plasma heating, with the normal ionizing shock used to initially ionize the gas and to make the toroidal B_θ field. Figure 2 shows schematically the sequence of events. Ionizing shocks having opposite polarities, and therefore the same sense of axial current flow, are driven from both ends. The unpublished work referred to in the introduction concerns this phase. It was observed in Berkeley that simultaneous application of opposite polarity potentials to the end electrodes in such a geometry did indeed lead to the creation of oppositely-directed shocks. Unfortunately this observation was not pursued.

As the shocks approach one another, plasma energy is stored as rotational kinetic energy. At the time the shocks meet in the center, fuses open the driving circuits, leaving the plasma without external current linkages (Fig. 2b). At the midplane, the opposite potentials associated with the rotation short-circuit in an internal crowbar. Since E_r goes to zero, v_θ must also go to zero. The information that E_r and v_θ are zero at the midplane is carried axially outward by MHD shock waves with a poloidal current structure as in Fig. 2b. The radial current flow in the shock front provides the impulse that halts rotation, and the kinetic energy of rotation is converted to B_θ magnetic field energy. The process is analogous to the short-circuiting to each other of two freely spinning generators, with the result that a large pulse of current is driven and the generator's kinetic energy converts to field energy associated with the short-circuit current.

As the MHD shocks propagate outward, the reversed theta pinch is rapidly applied, compressing and trapping the plasma through field line reconnection at the ends (Fig. 2c).

IV. The SPS Experiment

A schematic of the experimental apparatus is shown in Fig. 3. Initial experiments are directed at determining whether the sequence of events postulated in Section II will work out in practice. If so, a theta pinch coil and capacitor bank will be added to the circuit to complete the necessary set of drivers.

V. References

1. W. B. Kunkel and R. A. Gross, in Plasma Hydromagnetics, ed by D. Bershader (Stanford U. Press, 1962).

2. B. Miller, Phys. Fluids 10, 9 (1967).

3. R. T. Taussig, Phys. Fluids 8, 1616 (1965); 9, 421 (1966).

4. M. H. Brennan, J. A. Lehane, D. D. Millar, C. N. Watson-Munro, Aus. J. Physics 16, 340 (1963).

5. R. C. Cross, R. A. Gross, R. W. James and C. N. Watson-Munro, Phys. Fluids 11, 444 (1968).

VI. Figure Captions

1 Schematic of coaxial driver for normal ionizing shock wave.

2. Sequence of events to form toroidal magnetic field. (a) Normal ionizing shocks are driven from each end. (b) Shocks meet at midplane and internal short-circuit occurs. Simultaneously, fuses open up external circuit. MHD shocks propagate axially out from midplane, with radial current at shock fronts returning via axial paths along the tube axis and near wall. (c) Application of reversed B_z field by theta pinch coil sets up poloidal field by reconnection at ends and some compressional heating follows.

3. Schematic of experiment.

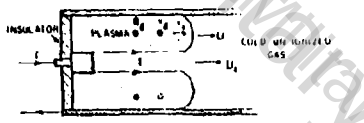

Figure 1

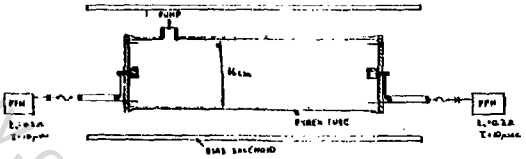

Figure 3

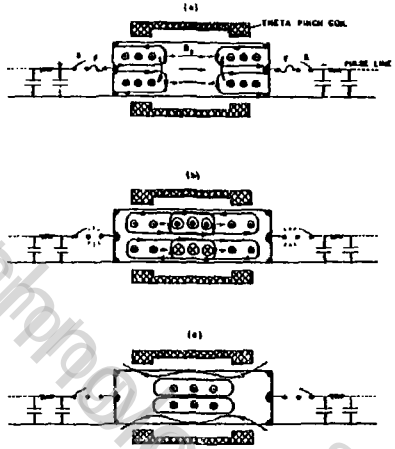

Figure 2

MINIMUM ENERGY EQUILIBRIA

A. Reiman and R. N. Sudan

Laboratory of Plasma Studies, Cornell University, Ithaca, New York

Taylor's theory of the relaxation of toroidal plasma discharges has accounted remarkably well for the experimentally observed behavior of toroidal z-pinches [1]. His analysis also leads to particularly stable magnetic configurations which have served as the starting point for work on the speromak [2]. We present here a corrected version of Taylor's analysis, including a term improperly left out of his expression for the energy of a force-free state. We also present force-free equilibrium solutions in cusp and higher order multipole external fields. These are to serve as the starting point for a study of modified spheromak configurations having improved magnetic field line curvature.

Taylor's prescription is to minimize the magnetic energy,

$$W = \frac{1}{2}\int_V B^2 d^3x, \tag{1}$$

subject to the constraints of global flux conservation and conservation of

$$K = \int_V \underset{\sim}{A}\cdot\underset{\sim}{B}\, d^3x. \tag{2}$$

In Eqs. (1) and (2) the integration is over the plasma volume, with plasma boundaries assumed rigid. From the method of Lagrange multipliers it follows that the state of minimum energy must satisfy

$$\nabla \times \underset{\sim}{B} = \mu\underset{\sim}{B}, \tag{3}$$

where μ is a constant independent of position. This is of course a necessary but not a sufficient condition for minimum energy.

Equation (3) has an infinite set of solutions. Taylor gives an expression for the most general solution in a large aspect ratio torus of circular cross section [1]. We want to know which solution has the lowest energy, consistent with a given initial value of K and of toroidal flux. Integrate by parts, using Eq. (3), to express the energy in terms of K plus a boundary term,

$$(1/2)\int_V B^2\, d^3x = \mu K/2 + (1/2)\int_S (\underset{\sim}{A}\times\underset{\sim}{B})\cdot\hat{n}\, d^2x. \tag{4}$$

Here V denotes the plasma volume, S is the surface of the plasma, and $\hat{n}$ is a unit vector normal to the plasma surface.

Taylor expresses the energy difference between two solutions corresponding to the same K as $W_a - W_b = (1/2)(\mu_a - \mu_b)K$. He then minimizes the energy by finding the state of lowest μ. His expression for the energy difference is incorrect. The surface integral in Eq. (4) is in general a nonvanishing function of μ.

We evaluate the surface integral in Eq. (4) explicitly, using the general solution to Eq. (3) given in Ref. 1 for a torus of large aspect ratio and circular cross section. The torus is represented by a cylinder of radius a and length $2\pi R$, with its ends identified. The result is

$$W = (1/2)(R/a)\,\Psi^2\mu[(a/R)(K/\Psi^2) + J_0(\mu a)/J_1(\mu a)]. \tag{5}$$

Because our expression for W is not a monotonic function of μ, as was Taylor's, the determination of the minimum energy state is now more complicated. Although the analysis using the correct expression for the energy is considerably different in some respects from that of Taylor, it yields the same minimum energy state for a large aspect ratio torus of circular cross section. Because of the dependence of the boundary term on μ, this term cannot be removed by a gauge transformation. Whether the boundary term can alter the minimum energy state for some other geometry is at present an open question.

Now we show how to find the state which minimizes Eq. (5), subject to fixed K and Ψ [3]. In addition to satisfying Eq. (3), $\underline{B}$ must also satisfy the boundary condition, $B_r = 0$ at $r = a$. The $m = 0$, $k = 0$ solution has $B_r = 0$ everywhere, and thus always satisfies the boundary condition. (Here m is the azimuthal mode number and k the axial wave number.) If $m \neq 0$ or $k \neq 0$ the boundary condition gives an eigenvalue equation.

Only the $m = 0$, $k = 0$ mode contributes to Ψ. The amplitude of this mode is therefore determined by Ψ,

$$b_0 = a\Psi/[2\pi a\, J_1(\mu a)]. \tag{6}$$

Once we fix b_0 in this way, we automatically satisfy the constraint on Ψ. We need only minimize

$$V(\mu a) \equiv \mu a[(a/R)(K/\Psi^2) + J_0(\mu a)/J_1(\mu a)], \tag{7}$$

subject to a given value of

$$\alpha \equiv (a/R)(K/\Psi^2). \tag{8}$$

Only the $m = 0$, $k = 0$ mode contributes to the boundary term of Eq. (4). We therefore consider first the pure $m = 0$, $k = 0$ mode. In Fig. 1 the solid line is a plot of $V(\mu a)$ vs. $\alpha(\mu a)$ for the $m = 0$, $k = 0$ solutions. For each value of α there is a discrete set of μa consistent with the $m = 0$, $k = 0$ mode. The lowest such value of μa corresponds to the $m = 0$, $k = 0$ mode with lowest energy.

Now suppose we superpose a discrete eigenmode on the $m = 0$, $k = 0$ solution. Let the coefficient of this mode be b_m. Evaluating α for such a mode, we find that it is of the form $\alpha(\mu a) = \alpha_0(\mu a) + (b_m/b_0)^2\alpha_{m,k}(\mu a)$, with $\alpha_{m,k} > 0$. As b_m goes from 0 to ∞, with μ fixed, α goes from α_0 to ∞. V increases linearly with increasing α. In Fig. 1, each such mixed state would correspond to a straight line originating on the $m = 0$, $k = 0$ curve. The four dashed lines in Fig. 1 correspond to four such solutions.

The lowest dashed line in Fig. 1 corresponds to $\mu a = 3.11$, which is the lowest discrete eigenvalue. This line clearly lies below the solid line, so the pure $m = 0$, $k = 0$ mode is unstable to the $\mu a = 3.11$ mode when it can exist (that is, for $\lambda > 8.21$). The lines corresponding to all other discrete eigenvalues lie above this one. We thus arrive at the same conclusion reached by Taylor.

Our derivation of the minimum energy state has been specific to a large aspect ratio torus of circular cross section. Are there geometries for which the minimum energy state is not the one with lowest eigenvalue? We don't know at present. A rough estimate indicates that the ratio of the boundary term to μK is of the order $S/(\mu V)$, where S is the surface area of the boundary and V is the plasma volume. This suggests that the boundary term will be most important for a geometry with large surface to volume ratio. We are led to a study of tori with noncircular cross section.

The eigenfunctions of Eq. (3) subject to the condition $\underset{\sim}{B}\cdot\hat{n} = 0$ at the boundary have recently been determined for a large aspect ratio torus of elliptical cross section [4]. We can use these solutions in determining the state of minimum energy. The eigenfunctions corresponding to the continuous part of the spectrum are now sums of products of Mathieu functions. We have verified that again the discrete eigenfunctions do not contribute to W or to the boundary term. This allows us to carry through our analysis exactly as for a circular cross section. We have expressed $W(\mu a)$ and $V(\mu a)$ for the continuous eigenfunction as a sum of integrals over radial Mathieu functions. These expressions are being evaluated numerically to produce a graph corresponding to that of Fig. 1. The mixed states with fixed eigenvalue will again produce straight lines on this graph.

Finally, we turn to the problem of improving the field line curvature of the spheromak. Our motivation in doing this is to improve the stability of surface modes and to increase the β allowed by the Mercier criterion. Previous work on improving the spheromak stability has focused on the introduction of a hole to improve shear [5]. Our approach is an outgrowth of recent work on systems with mass flow.

It was shown by Woltjer that the force-free solutions with

$$\underset{\sim}{\nabla} \times \underset{\sim}{B} = \underset{\sim}{B}/\sqrt{1-I}$$

represent a minimum energy state for a plasma bounded by an infinitely conducting wall, subject to the constancy of K and of $\int_V \underset{\sim}{A}\cdot\underset{\sim}{B}\, d^3x$ [6]. Stability to surface perturbations, if the boundary is no longer assumed rigid, has recently been established for such a system in an external cusp field [7]. This suggests that in the absence of mass flow, too, we study force free equilibria in cusp-type external fields. We have constructed analytic equilibrium solutions of this type, for use in studies with and without mass flow.

We work in spherical coordinates, treating the plasma boundary as a perturbation about a spherical surface. The boundary is thus given by

$$r = r_0 + \Delta r(\theta),$$

where $\Delta r << r_0$ is assumed. The general solution for the poloidal flux function is

$$\psi_{p\ in} = \frac{r}{\mu} \sin^2\theta \sum_m c_m P'_m(\cos\theta) j_m(\mu r)$$

inside the plasma, and

$$\psi_{p\ vac} = \sin^2\theta \sum_m \left[\frac{a_m}{m+1} r^{m+1} - \frac{b_m}{m} r^{-m}\right] P'_m(\cos\theta)$$

in the vacuum. Here P_m is a Legendre polynomial, j_m is a spherical Bessel function, and we have assumed axial symmetry.

A vacuum cusp solution with the field coils far away corresponds to having only $a_2 \neq 0$. Requiring $\psi_{p\ in} = 0$ for $\theta = \pi/2$, we find that the interior solution can have only even modes. Beginning with only $m = 2$, we progressively add modes until we get the kind of solution we are seeking. For only $c_2 \neq 0$, the boundary is spherical. The matching external solution has only $a_2, b_2 \neq 0$, and is a cusp at large r. Adding $c_4 \neq 0$, $c_4 << c_2$, makes the surface oblate or prolate. With $c_6 \neq 0$, $c_4, c_6 << c_2$, we can choose the coefficients so that $\Delta r = \varepsilon \cos^2\theta \sin^2\theta$. This gives us the qualitative behavior we seek. It matches to external modes having $m = 2, 4, 6$. If we wish to sharpen up the corners further, we can do so by adding more modes.

References

1. J. B. Taylor in Plasma Physics and Controlled Fusion, Tokyo 1974 (IAEA, Vienna, 1975).
2. M. N. Rosenbluth and M. N. Bussac, Nucl. Fusion 19, 489 (1979).
3. A. Reiman, Phys. Fluids 23, (Jan. 1980).
4. R. Moses and L. Turner, private communication.
5. M. N. Bussac, H. P. Furth, M. Okabayashi, M. N. Rosenbluth, and A. M. Todd in Plasma Physics and Controlled Nuclear Fusion, Innsbruck, 1978 IAEA, Vienna, 1979).
6. L. Woltjer, Proc. Nat. Acad. Sci. 44, 833 (1958) and 45, 769 (1959).
7. R. N. Sudan, Phys. Rev. Lett. 42, 1277 (1979).

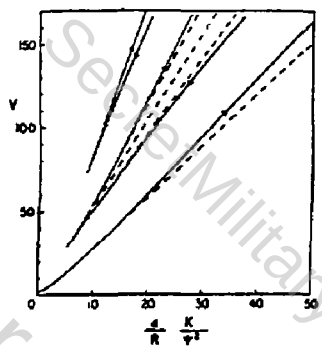

Figure 1. Energy of the force free solutions. The arrows indicate the direction of increasing Δa.

COMPACT TOROIDAL PLASMA EQUILIBRIUM AND IMPLICATIONS ON STABILITY

George K. Morikawa
Courant Institute of Mathematical Sciences, New York University,
New York, New York 10012

The very enthusiastic interest and activity during the past year or so in compact toroidal plasma containment is gratifying to those of us who have been studying various low-aspect-ratio configurations and devices for a number of years. From an experimental viewpoint a desirable feature of compact-torus studies is that relatively small-scale working devices are apparently possible [1] and this fortunate state-of-affairs may hold up to break-even fusion states. This happy possibility is in striking contrast to the present development of the next generation of tokamak-type machines with large external poloidal current-carrying coils surrounding a toroidal plasma container.

However, my earlier [2] and present studies indicate that some caution is necessary in the on-going process of reducing the external toroidal magnetic field B_ϕ to a small value in compact tight toruses; in fact both present theoretical and experimental spheromak studies apparently hope to eliminate this field completely. Such configurations may be feasible for relatively fast pinch-type low β experiments and plasmoid guns; but for future longer-lasting higher β devices, albeit in the moderate β paramagnetic regime, provision for some external B_ϕ is necessary particularly as the diamagnetic regime is approached. To satisfy this modest B_ϕ requirement we only need to provide an electric current I_0 along the major axis with the initial flexibility of using either a straight material conductor or straight charged beams.

The present discussion is limited primarily to the close relationship between the plasma-current-density distribution (mostly poloidal J_ϕ) and the need for an external axial current I_0 to prevent unreal singular behavior in the plasma or plasma-vacuum interface. Consider the configuration (shown in Fig. 1) which is related to spheromaks; the toroidal plasma ($p \geq 0$) is nominally in the double-cross-hatched region, and the single-cross-hatched region represents a toroidal vacuum (or force-free pressureless plasma $p = 0$) region between the spherical separatrix (plus the major axis) and the plasma. For axially symmetric magnetohydrodynamic (MHD) equilibrium ($\partial(\ )/\partial\theta = 0$) in spherical polar coordinates, the magnetic field in terms of the poloidal flux function $\Psi(\rho,\vartheta)$ is

$$\vec{B} = (B^{(\rho)}, B^{(\vartheta)}, B^{(\theta)}) = \frac{1}{\rho \sin\vartheta}\left[\frac{1}{\rho}\Psi_\vartheta,\ -\Psi_\rho,\ I(\Psi)\right] \qquad (1)$$

Specifically we choose $\psi = \psi(\vartheta)\cdot\sin^2\rho$ (separable); and also $I^2 = I_0^2 + \lambda(\psi^2 - \psi_0^2)$, $I\cdot I'(\psi) = \lambda\psi$, where λ is the poloidal current parameter and $\psi_0 = \beta^2 << 1$ is the flux function value at the plasma-

vacuum interface. We choose $\Psi = 0$ on the spherical separatrix and along the major axis and $\Psi \geq \delta^2$ in the interior of the plasma with Ψ attaining its maximum value on the magnetic axis. In addition if we choose the plasma pressure $p = \kappa(\Psi-\delta^2)$ the electric current density is

$$\vec{J} = \left(J^{(\rho)}, J^{(\phi)}, J^{(\theta)}\right)$$

$$= \left\{I'(\Psi)\cdot B^{(\rho)}, I'(\Psi)\cdot B^{(\phi)}, \frac{1}{\rho \sin\phi}\left[\kappa\cdot\rho^2\sin^2\phi + I\cdot I'(\Psi)\right]\right\} \qquad (2)$$

where κ is the pressure parameter; and

$$I'(\Psi) = \frac{\lambda\Psi}{I} = \frac{\lambda\Psi}{\left[I_0^2 + \lambda(\Psi^2 - \delta^4)\right]^{1/2}} . \qquad (3)$$

In particular for $\kappa = 0$ (or $p = 0$) the current density is

$$\vec{J} = I'(\Psi)\cdot\vec{B} \qquad (4)$$

where $\lambda = \Lambda = 20.2$, the lowest eigenvalue; the pressureless plasma is moderately paramagnetic. Initially this force-free-field configuration was studied with D. S. Gardner as a possible model for a megagauss magnet. Now in any viable plasma equilibrium configuration we require that the magnetic field be bounded (nonsingular). Then for any $\beta \geq 0$ (or $\kappa \geq 0$) the nature of the current-density distribution $\vec{J}$ given by (2) depends primarily on the structure of $I'(\Psi)$ shown in (3); this is particularly so for the pressureless plasma. For $\kappa > 0$ this factor mainly affects the poloidal component $J_p = (J^{(\rho)}, J^{(\phi)})$. In the entire paramagnetic regime $\Lambda \geq \lambda > 0$, J_p has a singularly high value for $I_0 = 0$ and $\Psi = \delta^2$. When β is increased into the diamagnetic regime $\lambda < 0$, $I(\Psi)$ becomes unreal unless $I_0 > 0$; and the required I_0 rapidly becomes excessive as β is increased (cf. Ref. 2 and earlier work sited therein). In addition the toroidal current density $J^{(\theta)}$ changes sign (plasma current reversal) in the diamagnetic regime as β increases. Apparently there will be a severe restriction on β for compact toroidal equilibrium in the diamagnetic regime; fortunately the useable range of β is about $0 \leq \beta \leq 1/2$. In the transition region between the paramagnetic and diamagnetic regimes $|\lambda| < \pi^2/4$ an analytic study of equilibrium configurations with slightly anisotropic pressure ($p_\perp \gtrless p_\parallel = p$) has been made using the guiding-center-fluid (GCF) formulation. For $\lambda = 0$ the lowest order plasma boundary (for $\delta = 0$) can be a prolate or oblate spheroid depending on whether $p_\perp > p_\parallel$ or $p_\perp < p_\parallel$ (initially studied with D. Dobrott). However for $\lambda \lesssim 1$ (paramagnetic) a spherical plasma boundary can be maintained for $p_\perp \gtrsim p_\parallel$; and the preceding MHD arguments for $0 < \delta << 1$ appears to be valid in the full paramagnetic regime ($\Lambda \leq \lambda < 0$). The implication of these GCF calculations is that a small (but nonlinear) prolate-oblate oscillating MHD mode is stable in this paramagnetic transition region; and an estimate on the required size of I_0 obtains.

We conclude this brief discussion with a short description of a more elaborate compact plasma confinement configuration (initiated with E. Rebhan and Tyan Yeh) for future consideration (Fig. 2). From the viewpoint of a possible "steady-state" (or slowly oscillating α) reactor, the introduction of a center ring-coil to produce a spherical (or spheroid) vacuum hole of radius $\rho = a$ may have benefits which override the increased design complexity. Aside from the advantages stated in Ref. 2 other benefits of an a-vacuum hole are: (1) The configuration will be steadied from global disturbances such as vertical, sideways and tilting motions; for example these movements can arise when ring plasmoids are fed axially into the main body of plasma periodically and ring impurities are rejected; and (2) the plasma remains paramagnetic for larger β with increasing α, decreasing the I_0 requirement.

Finally the implication of our work is that a study of nonlinear stability of compact toroidal configurations with plasma-vacuum interfaces is needed. Numerical computations may involve a combined Eulerian-Lagrangian formulation to handle the free boundary and to choose the proper vacuum flux surface to locate the shaped external current-carry toroidal coils.

REFERENCES

1. G.C. Goldenbaum, J. H. Irby, Y. P. Chong and G. W. Hart, University of Maryland Preprint No. PL80-010 (Sept. 1979), to be published.

2. G. K. Morikawa, Phys. Fluids 22, 1994 (Oct. 1979).

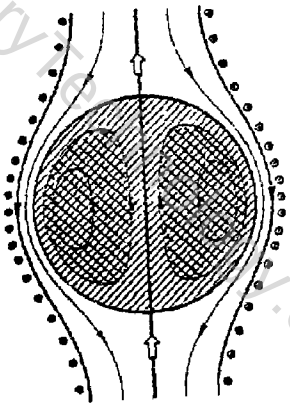

FIG. 1. The axially symmetric geometry of an equilibrium configuration when there is no dipole at the origin.

FIG. 2.

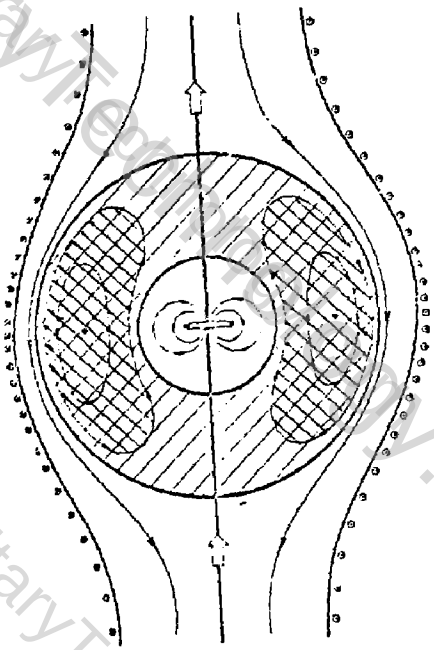

RADIO FREQUENCY FLUX CONTROL OF TOROIDAL PLASMAS

Sanae Inoue and Kimitaka Itoh[+]
Institute for Fusion Theory, Hiroshima University, Hiroshima 730, Japan
[+]Japan Atomic Energy Research Institute, Tokai, Ibaraki 319-11, Japan

One of the most important problems in the research of thermonuclear fusion is how we confine inhomogeneous plasmas in the stable state. The series of experiments in the world has been showing that the plasma suffers from its anomalous cross-field transport, particularly in particle and electron heat losses. There has been much work done to try to understand the anomalous losses. A spontaneous excitation of the waves, which is the consequence of instabilities, is believed to be a cause of anomalous loss mechanisms. This anomalous transport mechanism, however, implies a possibility to control actively plasma confinement by RF waves. We have proposed a concept of Radio Frequency Flux Control (RFFC), a new scheme to control plasma losses [1].

The basic concept of RFFC is to drive inward plasma fluxes by supplying the momentum via waves so as to compensate the outward fluxes induced by instabilities. The particle fluxes and electron heat flux due to arbitrary low frequency electromagnetic (EM) waves are given as [1,2]

$$\Gamma_x = \Sigma \frac{ecn}{BkT_e} \frac{\omega_* + k_\parallel u - \omega}{\sqrt{2}|k_\parallel| v_e} \mathrm{Im}\, Z\left(\frac{\omega - k_\parallel u}{\sqrt{2}|k_\parallel| v_e}\right) \left| \tilde{E}_y + \frac{\omega}{k_\parallel c} \tilde{B}_x - \frac{i v_e k\rho_e}{c} \tilde{B}_z \right|^2 \qquad (1)$$

$$Q_x = \Sigma \frac{ecn}{3kT_e} \frac{\omega_* + k_\parallel u - \omega}{\sqrt{2}|k_\parallel| v_e} \mathrm{Im}\, Z\left(\frac{\omega - k_\parallel u}{\sqrt{2}|k_\parallel| v_e}\right) \left\{ 2T_e + m\left(\frac{\omega}{k_\parallel} - u\right)^2 \right\} \left| \tilde{E}_y + \frac{\omega}{k_\parallel c} \tilde{B}_x - \frac{i v_e k\rho_e}{c} \tilde{B}_z \right|^2 \qquad (2)$$

where x-axis is taken in the direction of gradients, and other notations are standard. The general expression of the particle flux, i.e., $\Gamma_x = (c/B)\mathrm{Re}(\langle \tilde{n} \tilde{E}_y \rangle + 1/c \langle \tilde{p} \times \tilde{B} \rangle] + (c/B) n \tilde{E}_y$, electron heat flux, energy and momentum balance equations including the magnetic fluctuations E_x terms are obtained in Ref. 3. Concerning the ion particle flux we have also demonstrated that the ion particles follow to electrons so as to maintain the ambipolarity of the particle flux in the presence of any low frequency electromagnetic waves [2]. Due to a strong dependence of the ion heat flux on the nonlinear effect, fortunately, ion heat loss flux remains small [4]. Therefore, we should consider the particle fluxes and electron heat flux. The equations (1) and (2) are saying that, by the proper choice of the RF waves which satisfy the condition $(\omega_* + k_\parallel u - \omega)k < 0$, i.e., the wave momentum is absorbed by electrons via Landau

resonance near the resonant surface in the plasma column, the inward fluxes are to be obtained. The plasma fluxes, as far as a quasilinear approximation is used, are proportional to the fluctuating amplitude of the parallel electric field which particles feel, $|\tilde{E}_{\parallel}|^2 = |\tilde{E}_z + (x/Ls)\tilde{E}_y|^2 \equiv |(k_{\parallel}/k)|^2|\tilde{E}_y + (\omega/k_{\parallel}c)\tilde{B}_x - (iv_e k\rho_e/c)\tilde{B}_z|^2$, and the wave particle resonance rate, namely, the momentum and the energy exchange rate between particles and the waves.

The total plasma fluxes, firstly neglecting the nonlinear interactions, are given by

$$\Gamma_x = \Gamma_x \text{ (anomalous)} + \Gamma_x(\text{RF}) \tag{3}$$

$$Q_x = Q_x \text{ (anomalous)} + Q_x(\text{RF}). \tag{4}$$

In RFFC scheme, we induce the negative diffusions of particle and heat fluxes.

In order to untilize RFFC, we have to examine various kinetic RF waves one by one to search out the optimum condition in parameters such that input power, frequency ranges and wave numbers, taking the plasma energy and momentum balances correctly into considerations. We examine the EM low frequency RF waves to study the efficiency and the optimum condition for RFFC scheme, solving the radial propagation equations and show its accessibility and dependences of induced fluxes, $\Gamma_x(\text{RF})$ and $Q_x(\text{RF})$, on the wave structures.

We have basic equations for RF waves in current-carrying finite-β cylindrical plasma in sheared magnetic field, which are the same as for drift-tearing and EM-drift waves [5]. The resonant surface must be inside the plasma column.

We launch a MHD shear Alfvén wave at the plasma edge r = a, demanding E_r = 0, which propagates into the plasma. The kinetic interactions become ignorable in the region $|k_{\parallel}v_i/\omega| \leq 1$. In the region $|k_{\parallel}v_A/\omega| \leq 1$, the wave turns out to be kinetic drift-Alfvén mode exciting outgoing drift modes. Due to strong ion Landau damping, in-coming drift waves are suppressed. With these boundary conditions we solve the propagation equations, dividing the plasma column into MHD and kinetic regions [5]. The radial wave structure and the excited fluxes for the parameters $\omega = 3\omega_{*i}$, m = - and n = 1 are shown in Fig. 1. One sees the wave accessibility and that the controllable fluxes can be induced at arbitrary magnetic surfaces by RF waves with sharp spectrum. A broad spectrum one, on the other hand, gives rise to fluxes in the whole plasma column [6]. The required power of RF wave for particle confinement time being twice larger than the one without RFFC can be estimated. The rate of RF heating which is simultaneously caused by the RF wave can also be calculated.

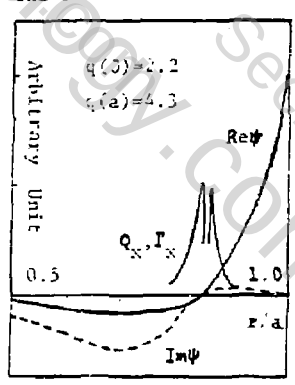

Fig. 1

In conclusion, the plasma parameters are improved through the reduction of the losses and the increment of the input. We thus have additional freedom by RFFC scheme to optimize plasma confinement; one finds the possibilities to control temperature, density and current profiles, impurities, scrape-off and boundary plasmas and the global stability by employing RFFC.

The authors thank Drs. S. Yoshikawa, T. Takizuka and K. Nishikawa for discussions. Work partially supported by Grant in Aids for Scientific Research of MOE Japan.

References

(1) K. Itoh and S. Inoue, Comments Plas. Phys. Con. Fus. 4 (1979) No. 6 in press.
(2) S. Inoue, T. Tange, K. Itoh and T. Tuda, Nucl. Fusion 19 (1979) 1252.
(3) T. Tange, S. Inoue, K. Itoh and K. Nishikawa, J. Phys. Soc. Japan 46 (1979) 266.
(4) M. Shigheta, T. Tange and K. Nishikawa, Phys. Rev. Letts. 42, 762 (1979).
(5) S. Inoue, K. Itoh and S. Yoshikawa, Institute for Fusion Theory Report HIFT-11 (1979. (to be published in J. Phys. Soc. Japan)
(6) S. Inoue, K. Itoh and Y. Terashima, J. Phys. Soc. Japan 48 (1980) No. 1 in press.

Field-Reversed Configurations: Theoretical Considerations and Reactor Applications*

George H. Miley
Fusion Studies Laboratory, Nuclear Engineering Program
University of Illinois, Urbana, Illinois 61801

Introduction -- The Motivation

A major motivation for studying *compact toroid* (*CT*) is the desire for a small low-capital cost fusion plant with easy access for maintenance. Access is achieved by having plasma currents produce most of the confining field, reducing external coils. Small size is achieved by the combination of high-β and closed-field confinement embedded within an open-field to form a natural divertor.

The potential advantages of a *small* power plant require comment. For a capital intensive plant, "economy of scale" dictates that the electrical output cost in $/kW-hr decreases with size. (Size limit: ~ 10-20% of network capacity). Consequently, some *CT* concepts run the risk of being too small to be economical! Still a low capital cost pilot (demonstration) unit could significantly speed up fusion development. This suggests an important, if not essential, feature -- that increased power is possible by addition of modules [1]. This has the dual advantage that the pilot unit would provide a test of the basic module while the desired sizing and improved economics would be achieved by mass production of modules [2].

Another desirable feature of the *CT* concepts is that their high-β makes them candidates for burning advanced fuels. Smaller plants are most logically located near the user, reducing transmission costs. Such siting would require relatively clean units, suggesting the concept of a satellite plant burning fuels such as D-^{3}He [3,4].

In summary, *CT* concepts should be judged on their ability to achieve: • Small size with possible modular addition; • Easy maintenance (minimum obstructing coils); • High-β (favorable power density and extension to advanced fuels).

Reactor Concepts -- General Considerations

A *CT* reactor contains three basic components (Fig. 1): formation, heating and burning zones. Reactor designs either incorporate these functions into a single chamber or use a linear configuration based on the moving ring or plasmoid concept. Examples of static burn-chamber designs are the FRM concepts [4,5] and reversed field pinch (RFP) reactors [10, 11], while linear configurations include the moving ring FRM [6], the moving plasmoid heater (MPH) [7-9] and the ion ring compressor (IRC) [12]. The MPH differs from the other concepts in several respects, including the use of injection heating rather than compression.

Typical reactor designs are summarized in Fig. 2. FRM and RFP concepts are quite small (< 10 MW_e per module) due to finite Lamor radius (FLR) stabilization theory which is thought to require the S-factor (plasma radius/ion gyro radius) to be < 10 [13,14] (a fundamental issue requiring much more study). In contrast, the Spheromak and RFP, being described by MHD theory, cover a range of larger sizes. Except for the FRM, all *CT* concepts to date have involved pulsed operation.

*Work Performed for EPRI (Contract 645-1) and DOE (EY-76-S-02-2213).

Figure 1: BASIC CT COMPONENTS

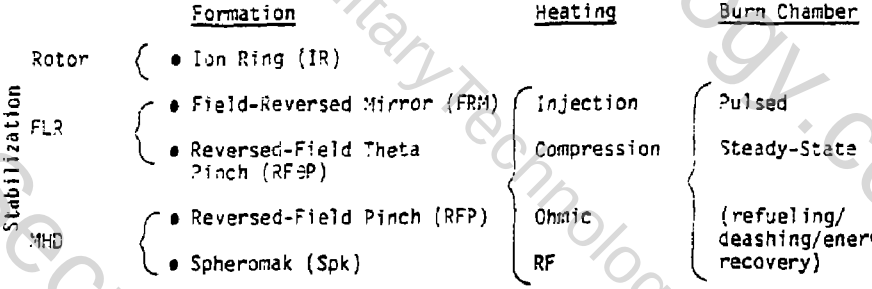

Figure 2: REACTOR CHARACTERISTICS

Power (MW_e)	< 10	100 - 300	500-1000
Maj. Rad. (m)	< 0.3	1 - 5	6-12
Plasma β	1	0.3 - 1	0.3-0.5

FRM [4,5] - - - - - - -Spk [8,9] - - - -
MRFRM [6] - - - - - - -RFP [10,11] - - - - -
MPH (RFΘP) [7] - IRC [12] - - - -

Reactor Concepts -- Examples

We briefly review four illustrative examples of CT reactor concepts.

1. SAFFIRE: a quasi-steady state FRM

SAFFIRE is a D-^{3}He fueled FRM designed as a pilot unit for satellite operation [3,4]. It is quite small (see comparison with 2X-II in Table 1). Reversed-field targets generated by a conical pinch coil are first built-up in density and heated by neutral-beam injection. Then, a quasi-steady state burn is achieved using the three features of Fig. 3. Because of SAFFIRE's small size (radius ~ 20 cm), detailed Monte Carlo studies [15,16] of fusion product (fps) heating were done. Despite the small fraction of fps confined in the closed field (~ 10%), significant heating is obtained from fps that circulate through both open and closed regions. Thus, ~ 50% of the alpha energy (protons ~ 20%) in SAFFIRE goes into the closed-field plasma, approaching ignition. Indeed the S-factor is the key parameter: for S = 5, an energy multiplication (Q) of ~ 5 would result while at S = 15 ignition is predicted.

Table 1: PILOT UNIT PARAMETERS

	SAFFIRE	2X-II
Avg. ion, elect. energy (keV)	80, 68	20,4
Max. Magnetic Field (Tesla)	5	1
Plasma Volume (Liters)	30	25
Fusion, Net Elect. Power (MW)	1.2, .32	-

Figure 3: SELF-SUSTAINED *SAFFIRE* CONCEPT

- Cold fueling maintains pressure profile/diamagnetic current
- Fusion product heating supplemented by auxiliary heating
- Cold plasma blanket provides divertor/energy recovery

2. Spheromak Moving Plasmoid Reactor (SMPR)

Preliminary studies of the SMPR were carried out in support of the PPPL Spheromak project to establish a possible operating "window" using moderate technology assumptions [8]. Physics assumptions are listed in Fig. 4.

Figure 4: *SMPR* ASSUMPTIONS

- Creation of MHD-Stable, Reactor-Scale Plasma
- Stabilization of Tilting Mode by Conducting Shell
- Ohmic Heating to Ignition
- Marginal Internal-Mode Stability During the Burn
- High-Efficiency Recovery of Magnetic Energy in Plasma

A modified PEST code computed equilibrium at each time step during the burn, plasma loses being assumed at a rate to satisfy stability requirements. The β was optimized using an ellipticity of ~ 0.5, a flattened current profile, and a center hole of ~ 10%. The "window" found is listed in Table 2.

Table 2: *SMPR* "WINDOW"

- $3 < B_e < 6$ Tesla
- $0.5 < a < 1.0$ meters
- $10 < \tau_{CR} < 50$ sec
- $1.5 < r_{wall}/r_{pl} < 2$
- $100 < P_{net} < 1000$ MW

3. A "Compact" Reversed-Field Pinch (CRFP)

While prior reversed-field pinch (RFP) reactor studies [10] concentrated on larger reactors (2-3000 MW_{th}), the RFP could potentially make an attractive small reactor. It operates at high β (> Kruskal-Shafranov), with arbitrary aspect ratio being stabilized by shear and a conducting wall. Ignition is by ohmic heating; operation is in a long pulse mode (10-100 s) with either a batch or refueled burn.

A 3-fluid, 1-D code (RFPBRN) [11,12] used in prior designs [13] was used here to seek a small RFP (~ 100 MW_e) design termed CRFP. Preliminary results (Table 3) indicate that, even with Bohm-like thermal conduction, a reasonable energy gain factor can be maintained. Larger conduction losses necessitate higher densities and larger B-fields for ignition, resulting in shorter burns. Still, the CRFP concept appears to warrant further study.

Table 3: COMPARISON OF CRFP AND PRIOR DESIGNS

	"Large" RFPR [10]	CRFP
First-Wall and Major Radius: r_w(m), R(m)	1.5, 12.7	0.75, 6.35
Burn and Cycle Times; τ_B(s), τ_c(s)	21, 26	10, 15
Total Th. and Elect. Power, P_{TH} (MW_{th}), P(MW_e)	3000, 750	628, 150
Q_p = (fusion energy)/(ohmic & field energy)	14	10

4. Reversed-Field Theta Pinch (RFΘP) Moving Plasmoid Heater (MPH) Concept

Preliminary studies suggest use of the MPH concept for RFΘP operation is potentially attractive with ~ 10 MW_e output using a 0.5-m drift tube with R = 0.15m, and B = 3 T [7]. A key component is neutral-beam-assisted heating which also builds up reversal currents and, most importantly, controls rotational instabilities [20].

References

[1] J. G. Gilligan, et al., "Modularization of Plasmoid Reactors, Proc. IEEE Fusion Tech. Conf., S. F., CA (1979).
[2] J. G. Gilligan, Fusion Economics, Report EPRI-AFR-93, U. IL (1979).
[3] G. H. Miley and J. G. Gilligan, Energy, Vol. 4, No. 2, 163-170 (1979).
[4] G. H. Miley, et al., SAPPIRE, EPRI 645-1 Report (1979).
[5] G. A. Carlson, et al., "Conceptual Design FRM Reactor," UCRL-52467 (1978).
[6] A. C. Smith, Jr., et al., Prel. Concept Design MRFRM Reactor, Pacific Gas & Elec. Rpt. 78FUS-1, (1978).
[7] J. D. Galambos, et al., Trans. Am. Nucl. Soc., 32, 28 (1979).
[8] R. E. Olson, et al., Bull. Am. Phys. Soc., 24, 1022 (1979).
[9] Y. K. Peng, ORNL, private communication, (1979).
[10] R. L. Hagenson and R. A. Krakowski, "Reactor Design for the RFPR," LA-UR-78-2268 (1978).
[11] R. A. Nebel, "CRFP Design Parameters," U. IL report in preparation.
[12] H. H. Fleischmann and T. Kammish, Nuclear Fusion, 15, 1143 (1975).
[13] G. H. Miley, et al., FLR Effects in a FRM, 9th European Conf. Fusion, Oxford, UK (1979).
[14] Ed Morse, "Stability of the FRM," Ph.D. Thesis, U. IL (1979).
[15] D. Driemeyer, et al., "M. C. Method for Fusion Product Behavior in FRMs," ANS Mtg. Comp. Methods, Williamsburg, VA, 2, 7-37 (1979).
[16] D. Driemeyer, "A Study of Fusion Product Effects in Field-Reversed Mirrors," Ph.D. Thesis, U. IL (1980).
[17] R. A. Nebel, et al., IEEE Int. Conf. Plasma Sci., 5C1, 146 (1979).
[18] G. H. Miley, et al., "Reversed Field Pinch Plasma Model," 9th European Conference on Controlled Fusion, Oxford, UK (1979).
[19] R. A. Nebel, et al., "Comparison of 0- and 1-D Burn Computations for the RFP Reactor," LASL Report, in press.
[20] Q. T. Fang and G. Miley, Trans. Am. Nucl. Soc., 33, 36 (1979).

THE HOLOMAK — A TOROIDAL SPHEROMAK

Thomas H. Stix and Alan M. M. Todd, Plasma Physics Laboratory
Princeton University, Princeton, New Jersey 08544

ABSTRACT. Recent spheromak stability analysis favors a profile of plasma current concentrated in the toroidal core of the spheromak, with very low current density (and correspondingly low temperatures) in the region immediately about the major axis. Considering a *toroidal* (rather than spheroidal) spheromak therefore produces little change in the physics, but the existence of a permanently accessible central hole introduces major options in the reactor engineering. The "holomak" geometry (from holos, Greek: whole, safe) is a low-$|q|$ toroidal pinch which exploits these options:

*A close-fitting toroidal stabilizing shell.
*Divertor capability.
*Tokamak-type Ohmic heating transformer.
*Tokamak-type start-up with finite toroidal field, a quadrupole or hexapole null in the poloidal field, and protection from impurities by a large scrape-off region.
*Programmed toroidal field. The stabilizing shell also serves as a transformer-coupled one-turn toroidal field coil. In a reactor, a non-superconducting shell could provide a medium-strength temporary field for start-up, followed by a weak forward or reversed field, all with low energy dissipation.
*Magnetic shear profile adjustable over a broad range.
*Spheroidal blanket.
*Axial disassembly.

Engineering features which would be eminently desirable in the apparatus for a CTR reactor include axial and/or radial disassembly and a spheroidal blanket. With toroidal magnetic confinement, one also looks for high beta, closed magnetic surfaces, high shear and, possibly, divertor compatibility. Satisfying these criteria are spheromaks and low-$|q|$ toroidal pinches. The latter correspond exactly to the toroidal "core" portion of the spheromak, but the existence of an actual accessible central hole permits a close-fitting toroidal shell, a weak external toroidal B field, and a normal-conductor Ohmic-heating transformer. Motivating research on such "holomak" devices is the following: confirmation of adequate confinement for a low-$|q|$ pinch would provide the scientific basis for a CTR reactor engineered with *existing* technology.

The holomak design introduces a toroidal stabilizing shell which also serves as a one-turn toroidal-field coil. (Incorporation of such a toroidal one-turn non-superconducting shell in a reactor is still consistent with axial disassembly and a spheroidal blanket!) Current to produce the external toroidal B field is induced by transformer coupling to the shell; after start-up, this field can be driven to a low value, to zero, or can be reversed. (In a reactor after start-up, a weak toroidal field may be maintained with modest power dissipation in the non-superconducting shell.) Quasi-steady-state current in two large outer Helmholtz coils provides the vertical field (in a reactor, the vertical field would be produced by constant-current superconducting coils located *outside* the spheroidal reactor blanket), while inner coils form, for start-up, a temporary hexapole or

quadrupole null in this poloidal field. After start-up, these nulling currents may also be driven to zero, to form a conventional toroidal z-pinch, or to reduced values, leaving the plasma with one or two poloidal divertor lobes. In a reactor, these (normal-conductor) coils may also be driven in a pulsed mode, to remove helium ash from time to time. See Figs. 3 and 4.

An ideal holomak would have, after start-up, zero net external toroidal field on the plasma surface, obviating the need for steady-state current in the toroidal-field coil. But without compromising the CTR engineering technology — i.e., the axial-disassembly and spheroidal-blanket concepts — one may allow a relatively weak external toroidal field driven with modest power dissipation by current flowing poloidally in the non-superconducting toroidal shell. (A conducting shell fitting close to the plasma appears necessary for spheromaks and holomaks to suppress plasma instabilities.) The S-1 spheromak apparatus can, without major changes, be operated in the "holomak" mode and Fig. 3 indicates the placement of an inner shell into the S-1 vacuum chamber to achieve this end. The low impedance of the shell — considered as a single-turn inductor — suggests transformer coupling to the (higher impedance) supply. The S-1 spheromak core with its programmed toroidal flux provides exactly such a transformer and operation of the S-1 apparatus in the holomak mode makes use of this compatibility. Pulsing the core will induce poloidal currents in the shell with toroidal magnetic field values up to several kilogauss. The exact value of this B field will depend on the shape of the shell and particularly on the closeness of fit of the shell to the plasma and to the core. After start-up, the core can be programmed to bring the toroidal B field down to a low value, to zero, or to a reversed field value.

Ohmic-heating current is induced by the Ohmic-heating transformer, an array of coils which produces a changing magnetic flux through the hole of the plasma-stabilizing shell and linking the plasma. The shell shields the plasma itself from the OH B-field, which is channeled around the plasma by eddy currents induced in the shell and in the vacuum-chamber wall.

In equilibrium, the radial hoop force of the plasma, due to magnetic and particle pressure, is balanced by the interaction of the toroidal plasma current and the so-called vertical field. In S-1, the equilibrium vertical field is induced by quasi-steady-state current in two Helmholtz coils located outside the vacuum vessel and the field is thus "frozen" into both the vacuum vessel and shell. For start-up, the vertical field is annihilated locally by pulsing the "pinch" coils, now lowered to 12.5 cm above and below the central plane, and producing a hexapole null on the midplane approximately at R=57.5 cm. (Fig. 1) As plasma current start to flow, the cross-section of the closed magnetic surfaces is small and a large scrape-off region protects the interior plasma from wall impurities released at this early stage of the discharge. (Fig. 2) As the plasma current then builds up further, radial force balance requires a stronger net vertical field and it is necessary to reduce the current in the nulling coils. At this point, several scenarios can be followed: reducing the current to zero in both nulling coils leads to the standard toroidal z-pinch with plasma current I_o force-balanced by the full vertical field. Reducing the nulling-coil current to half its original value allows force balance with the toroidal current at about 60% of I_o and leaves the cross-section still with two divertor lobes (Fig. 3). Or, in a reactor, occasional pulsing of the nulling coils could be used to reduce I^2R loss while still removing the helium

ash as needed (Fig. 4).

The early work on low-|q| and reversed-field pinches, particularly that on the British Zeta device, showed a promise that has been neither adequately explored nor exploited in the laboratory. On the other hand, the theoretical calculations which argue stability for the spheromak may be applied to reach the same optimistic conclusions for the low-|q| pinch. Holomak mode-operation of S-1 shares with Zeta the concept of the low-|q| toroidal pinch, and addresses approximately the same parameter regimes of gas density, magnetic field strength, and time scale. But the differences between the devices are significant and include (a) an externally produced vertical field "frozen" into the shell, (b) a programmed toroidal field which, after start-up, may be driven to low positive or negative values, (c) a hexapole or quadrupole null for start-up, with a large scrape-off region which protects the interior plasma from wall impurities released at this early stage of the discharge, (d) divertor or pulsed divertor operation, (e) an adjustable shear profile, via programming of the OH, divertor and toroidal fields, and (f) axial disassembly.

In common with other compact-torus reactor concepts, there are major questions which are still unresolved — stability, maintenance of the q-profile, and overall reactor economics. Nevertheless, a low-|q| pinch with adequate confinement would form the scientific basis for a holomak CTR reactor engineered with existing technology. It will, therefore, be the experimental objective of holomak-mode research on S-1 to apply the laboratory knowledge and experience of successful tokamak research to seek experimental confirmation of the stability indicated by recent theory, and to chart the path toward a CTR reactor which could be built with engineering based on present technology.

This work has been supported in part by the U. S. Department of Energy Contract No. EY-76-C-02-3073.

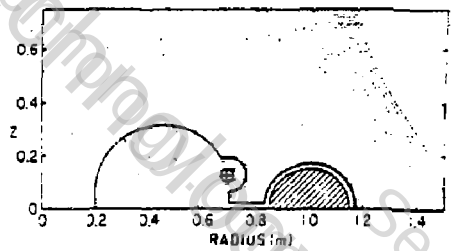

Figure 1. Vacuum field for S-1 in holomak-mode operation. Hexapole null, for start-up, is placed at R=0.575, Z=0. Equilibrium coils: I_E=393,000 amperes @ R=1.5, Z=±0.825; Nulling coils: I_N=85,370 amperes @ R=0.7, Z=±0.125. (PPPL-79243)

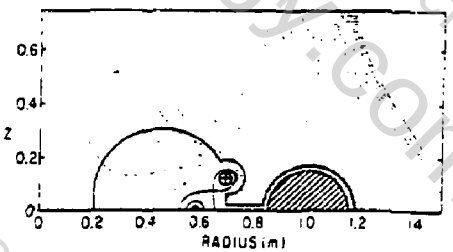

Figure 2. Start-up of S-1 in holomak mode. Flux plot with plasma current modeled by I=50,000 amperes at R=0.575, Z=0. Coil currents as in Fig. 1. (PPPL-792454)

HOLOMAK - MODE OPERATION FOR S-1

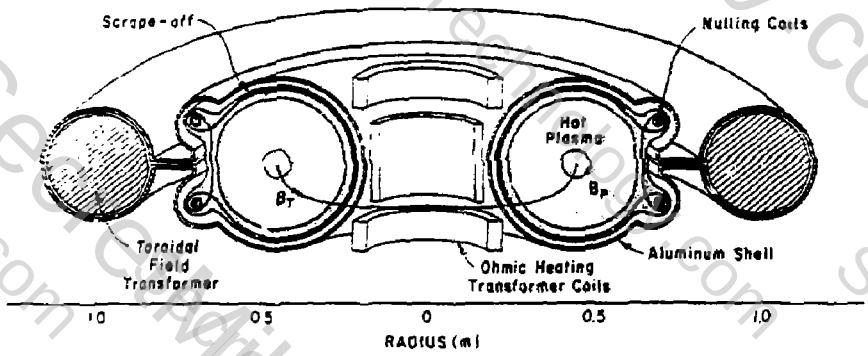

Figure 3. Sketch of S-1 interior configured for holomak operation, showing addition of aluminum shell and of OH transformer. S-1 vacuum chamber and vertical field coils not shown (see Fig. 7, M. Yamada et al., these proceedings). PPPL-793947

HOLOMAK REACTOR - SCHEMATIC REPRESENTATION

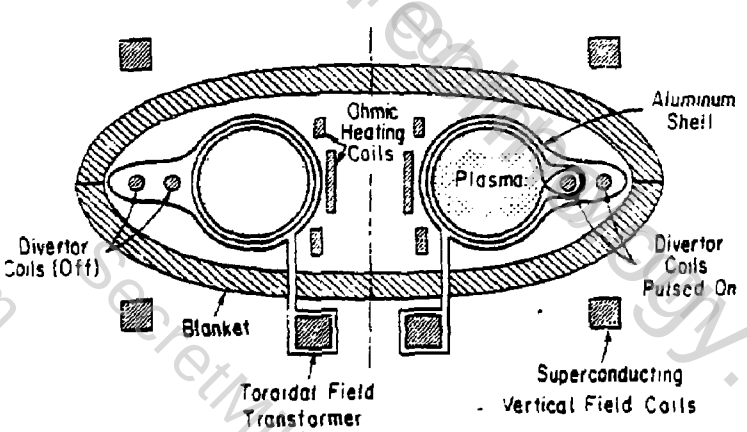

Figure 4. Schematic representation of a holomak reactor. Spheroidal blanket encloses aluminum stabilizing shell which also serves as a one-turn toroidal-field coil. Divertor shown pulsed on (right-side) and off (left-side). Design is compatible with axial disassembly. (PPPL-796525)

THE LINUS REACTOR: COMPRESSION OF A COMPACT TORUS BY A LIQUID METAL LINER

A. E. Robson, Naval Research Laboratory, Washington, D.C. 20375

The Linus reactor concept[1,2,3], is based upon a nondestructive, reversible, compression-expansion cycle in which a rotating liquid lithium liner is imploded mechanically, using high pressure helium as the energy source, and acts as a cylindrical piston to compress a magnetically-confined plasma adiabatically from a few hundred eV to about 15keV. The magnetic field at peak compression is ~0.4-0.5MG, corresponding to a peak density of $\sim 10^{17}$ ions. cm^{-3}. In the subsequent expansion the plasma energy and the fusion energy carried by trapped α-particles is directly recovered; the α-particle energy compensates for the electrical and mechanical losses in the system, making the mechanical cycle self-sustaining (Fig. 1). The Linus reactor can thus be regarded as a fusion engine, except that there is no shaft output: all the nuclear energy appears in the liner as heat. At peak compression the liner is thick enough (~1m) to absorb the fusion neutrons, and so serves as both tritium-breeding blanket and the heat-transfer medium, as well as providing a continuously-regenerated 'first wall' whose mean power loading can be 3-5 times greater than in a reactor with a permanent wall. The combination in one element, the liner, of functions which in other fusion concepts require separate systems, leads to a rather simple reactor design.

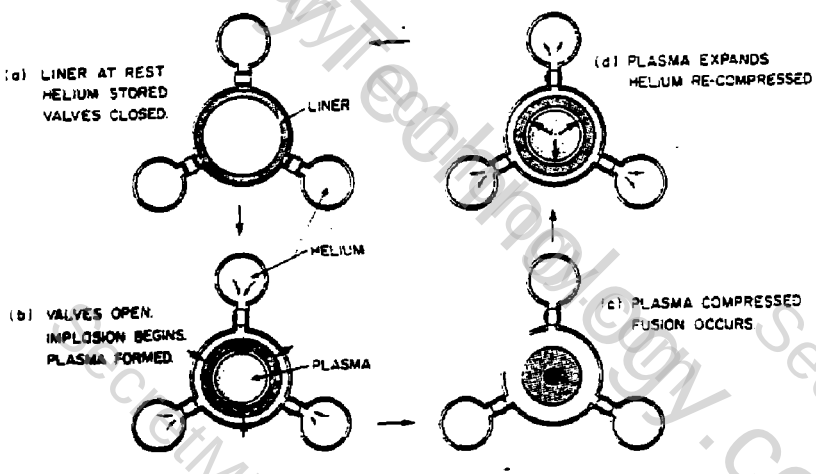

Fig. 1 Linus Reactor Cycle

Hydrodynamically stable compression-expansion cycles are obtained by rotating the liner (which stabilizes the inner surface against Rayleigh-Taylor instability at turnaround) and eliminating the outer free surface by means of a constraining mechanism (the captive liner[4]). A number of arrangements[3,4,5] have been devised for this purpose, one of which is shown in Fig. 2. Here a quasi-cylindrical collapsing shell is formed by a number of long interleaved members which can slide into one another, while the axis of the shell is maintained fixed by means of a system of connecting rods. Driven by helium at ~2000 psi such a mechanism could implode a rotating liquid lithium liner with a mean inner surface velocity of $\sim 10^7$ cm. sec^{-1}. This relatively slow velocity requires that the plasma be well confined, and an elongated compact torus configuration is required, as shown in Fig. 3. The configuration may or may not have a toroidal field for stability. The solid end walls contain the liquid lithium, and also serve to take the end pressure of the plasma, which allows an initial plasma with average $\beta > 0.5$. When compressed radially, $\langle\beta\rangle$ falls until it reaches a value of 0.5, after which the plasma contracts axially while maintaining $\langle\beta\rangle$ constant.

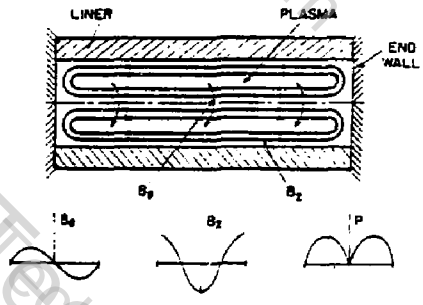

Fig. 2 (left) Captive liner mechanism

Fig. 3 (above) Compact toroidal plasma inside liner

The principal loss mechanism during a cycle arises from the resistive penetration of the confining magnetic field into the inner surface of the liner. As the system initial radius R is increased, the α-particle energy increases faster than the resistive loss, so a self-sustaining cycle is always possible if the system is made large enough. Scaling laws derived elsewhere[5] show that the minimum radius is related to the principal variables as follows:

$$R \propto \langle\beta\rangle^{-4/3} (\epsilon p)^{\frac{1}{3}} \eta^{\frac{1}{3}} \rho^{\frac{-1}{6}} (l_{m\alpha})^{-\frac{1}{2}}$$

where p is the driving pressure, ε the hydraulic efficiency of the system, η the resistivity and ρ the density of the liner, and α the radial compression ratio. Although here it seems that R is quite insensitive to α, if $\alpha > 10$ the increase in η due to heating of the liner, and the decrease in ε due to wave motion and compressibility in the liner, result in a rapid increase in R. Using reasonable values of the main parameters, the self-sustaining cycle requires $R \geq 2m$.

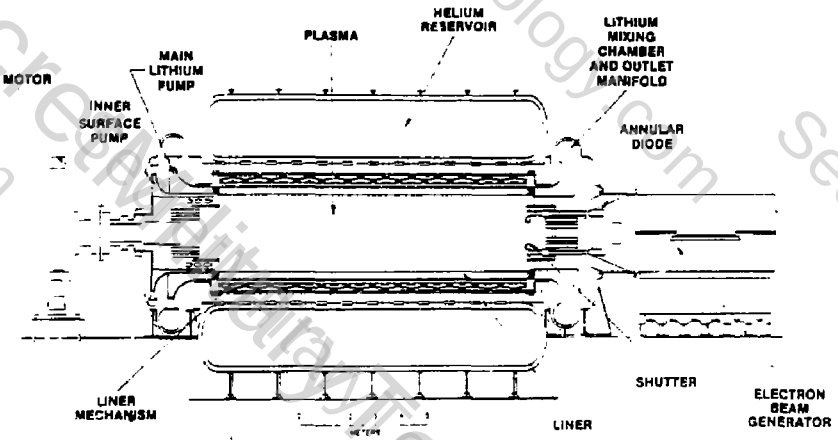

Fig. 4 Linus Reactor

A conceptual reactor on these principles is shown in Fig. 4 . The initial plasma is created inside the liner by means of a rotating relativistic electron beam, as described elsewhere[5]. The initial D-T fuel charge is injected in supersonic jets from injectors in the end plugs directed so as to avoid the liquid surface of the liner. The electron beam is injected through an annular slit in one end, which is closed by a shutter as the liquid liner implodes. The lithium is circulated through the reactor in the axial direction by means of two concentric pumps: the inner surface pump replaces the hot inner surface between cycles, and by introducing a cool lithium stream, condenses the lithium vapor and the previous fuel charge. This pumping requirement limits the repetition rate to ~ 2Hz. The main body of the lithium is circulated more slowly, and is completely replaced after about ten reactor cycles.

The principal physical and technical characteristics of this system are given in Table I. A more complete description of the reactor can be found in Ref. 5.

Table 1. Linus Point Design

Liner length: 10 m	Lithium: 2.6 tonnes. m^{-1}
Initial inner radius: 2 m	Steel shell: 25 tonnes. m^{-1}
Driving pressure: 2000 psi	Fluid rotation: 2.5 rpm
Implosion time: 24 msec	Reaction Time: 0.85 msec

	Initial	Compressed
Plasma radius	200 cm	22 cm
Central density	$9.3 \times 10^{14} cm^{-3}$	1.1×10^{17} cm^{-3}
Temperature	635 eV	15 keV
Magnetic field	6.9 kG	300 kG
$< \beta^2 >$	0.6	0.375
Energy (plasma + field)	30 MJ	1016 MJ

E-beam energy/cycle	60 MJ	Gross electricpower	844 MW
Initial plasma energy	30 MJ	E-beam power	141 MW
Compressed plasma energy	1016 MJ	Motor power	13 MW
Nuclear energy (22.4 MeV/DT)	1206 MJ	Power to b.o.p.	50 MW
Repetition rate	2 Hz	Net electric power	640 MW
Gross thermal power	2532 MW	Mass of reactor	3500 tonnes

Note that the reactor operates with Q~1: this is made possible by the efficient energy recovery in the mechanical cycle. Since the fractional burnup is small, helium accumulation in the plasma is no problem. Because of the size, and the short timescale, plasma loss during a cycle should be negligible, even allowing for anomalous transport. Also, because of the short timescale and the high field, contamination by lithium vapor should be confined to the edge of the plasma.

Probably the most significant feature of this concept is that, apart from the electron beam generator and the pump driving motor, there are no electrical components in the reactor. The electron beam sets up both the plasma and the confining magnetic field and the latter is maintained by skin currents in the liner, making any permanent field coils unnecessary. The main shortcoming of the concept is that the size of the reactor, determined by the conditions for a self-sustaining cycle, is rather large. The size is particularly sensitive to β, and to obtain the figure given above, a rather high β has been assumed. Note that the electron beam generator shown in Fig. 4 is based upon a conceptual inductive storage system: a conventional capacitor-powered generator would be substantially larger.

1. A.E. Robson and P.J. Turchi, Proc. 3rd Topical Conference on Pulsed High Beta Plasmas, Culham UK, 9-12 Sept. 1975, p. 477.
2. P.J. Turchi and A.E. Robson, Proc. 6th Symposium in Engineering Problems of Fusion Research, San Diego, 18-21 Nov. 1975, p. 983.
3. D.L. Book et al., Plasma Physics and Controlled Nuclear Fusion Research 1976, IAEA, Vienna 1977, Vol. III, p. 507.
4. R.L. Burton et al., Proc. 7th Symposium on Engineering Problems of Fusion Research, Knoxville, 25-28 Oct. 1977, Vol. 1, p. 225.
5. A.E. Robson, 2nd Int. Conf. on Megagauss Magnetic Field Generation and Related Topics, Washington, D.C., 29 May - 1 June 1979.
6. J. D. Sethian, this conference.

PRELIMINARY STUDIES OF SPHEROMAK REACTORS

M. Katsurai* and M. Yamada, Plasma Physics Laboratory, Princeton University, Princeton, New Jersey 08544 (*On leave from Dept. of Electronic Engineering, University of Tokyo, Tokyo, Japan)

1. Introduction. In the spheromak reactor, a toroidal fusion plasma is confined by its own internal (self-generated) magnetic field and the vertical-field B_t which is produced by coils not linking the plasma. Among various kinds of spheromak configurations, an oblate-shaped plasma configuration with a center hole called "Oblimak", has been shown to provide better MHD stability and higher attainable beta value than the classical spherical spheromak [1] [2]. In this paper, we derived approximate functional relations between various spheromak plasma parameters, based on a simplified energy principle of circuit theory and using these relationships, have carried out preliminary studies of conceptual spheromak reactor with a stationary plasma as well as with a moving plasma produced by the cormak type formation scheme employed in the S-1 experiment at PPPL. [3]

2. Approximate Analytical Treatment of the Spheromak Configuration. In the framework of electric circuit theories, the spheromak confinement system is regarded as a kind of inductance circuit, where the spheromak plasma corresponds to a single current loop immersed in the magnetic field produced by the external coils, as shown in Fig. 1. The energy function of this system is given by

$$W = \frac{1}{2} L_0 I_0^2 - M I_0 I_t + \frac{1}{2} L_t I_t^2 + \frac{1}{2} L_p I_p^2 + V_p p \qquad (1)$$

where L and M are the self and mutual inductances; and V_p and p are the volume and the pressure of the plasma, respectively.

The spheromak configurations are characterized by the following two conditions (R: the major radius, a: minor radius):

$$\left(\frac{\partial W}{\partial R}\right)_{I_0,\ I_t,\ I_p,\ p} = 0 \quad , \qquad \left(\frac{\partial W}{\partial a}\right)_{I_0,\ I_t,\ I_p,\ p} = 0 \quad . \qquad (2)$$

In the low-β limit, where effects of plasma pressure is neglected, the following relationships are derived [4]:

$$B_t = \frac{\mu_0}{4\pi} \frac{I_t}{R} \left\{ \ell n \frac{8R}{a} - 1 \right\} \quad , \quad I_p = 1.9 \ \frac{R}{a} I_t \quad . \qquad (3)$$

3. Adiabatic Compression. For the formation and heating-up of the reactor grade spheromak plasmas, the adiabatic compression scheme is one of key factors. During the compression, the toroidal and poloidal fluxes have to be conserved resulting in the conservation of both the average safety factor and the aspect ratio of the plasma. Considering further the equation of adiabaticity $T_p V_p^{2/3} = \text{const}$, where T_p is the plasma temperature, the following scalings for various quantities are obtained:

$$T_p \propto R^{-2}, \ B_{to} \propto B_t \propto R^{-2}, \ I_p \propto I_t \propto R^{-1}, \ P_M (\equiv W_M / \tau_M) \propto R^{-3} \quad .$$

P_M is the input power required for the magnetic flux supply, W_M is the magnetic energy inside the plasma and τ_M is the magnetic diffusion time.

4. Reactor Studies. Based upon the above approximate analytical solutions, studies are made on the spheromak reactors. When the aspect ratio is assumed to be in the range of about 1.7 to 4, the relation $B_{to} \sim 2.1\ B_e$ is obtained where B_{to} is the toroidal magnetic field at the center and B_e is the magnetic field at the outer-edge of the plasma as shown in Fig. 2. The location of the semi-spherical first wall is specified by a_w and $a_w = 1.5\ a$ is assumed. Three types of reactors are investigated: 1) DT reactor with TCT (two-component type) operation with a fusion gain Q_F of 1.7; 2) ignited DT reactor and, 3) ignited catalyzed-type DD (Cat-D) reactor. Spatially uniform temperature and density are assumed.

Table 1 lists the main parameters for different conceptual designs of a spheromak reactor with a stationary plasma. A total wall loading of 4 MW/m^2 and the center beta value $\langle\beta_o\rangle = 0.045$ are assumed. The ourer-edge magnetic field is about 4T for DT ignited reactors, which is about half the value for tokamaks. If this field is given rise to ~8T, the required energy confinement time is reduced by a factor of ~4, however, the wall loading is increased by a intolerable factor of ~16. In these stationary spheromaks, the wall loading is found to be a major constraint against increasing the fusion power density and decreasing the required energy confinement time.

5. Structural problems of the spheromak reactor. Various methods have been proposed to produce the spheromak plasma in the reaction chamber. However, they usually require installations of various plasma formation components such as coils, conductors, and sometimes electrodes in the space between the plasma and the blanket, which are used only to produce the spheromak plasma at the start-up phase. The installations of such formation components give rise to numerous difficult technological problems associated with their radiation shielding and cooling, and also result in the deterioration of the neutron economy in the blanket system caused by the neutron absorption by them. Therefore, it is highly recommended that those components are isolated from the reactor chamber so that the direct bombardments of radiation and neutrons to them are avoided. This requirement can be fulfilled by applying the configuration where the production chamber is separated spatially, and the spheromak initially produced by a non-reacting plasma in the former is injected or moved into the latter followed by the fuel supply and further heating. Examples of schematic structure are presented in Fig. 2, where spheromak plasma is injected or carried into the reaction chamber by specially arranged pinch gun (a), or the cormak type exciters (b) [3]. In addition, if the concept of the merging of spheromaks are proved practical, its application is very attractive because it enables relatively small exciter with small apperture to be used to feed a larger spheromak in the reaction chamber. Successive injection of plural of spheromaks will be able to produce one large sphermak in the chamber by this method as illustrated in Fig. 3.

6. Moving Spheromak Reactor. The spheromak plasma, fed specially in the cylindrical reaction chamber, can be moved along the center axis during the fusion reaction process, which enables us to reduce effective wall loading. An example of the configuration is shown in Fig. 3 where the plasma moves inwards according to the numbers (1) to (4), in a continuously repeating cycle. An example of the operation, whose plasma parameters for (1) to (4) are listed in Table 2, is explained in [4].

Useful discussions with Drs. H. P. Furth, D. L. Jassby, H. Maeda, M. Okabayashi, R. E. Olson, A. M. M. Todd and S. Yoshikawa are gratefully acknowledged. This work supported by US Department of Energy Contract No. EY-76-C-02-3073.

[1] Bussac, M. N., et al., Plasma Physics and Controlled Nuclear Fusion Research (Proc. 7th Int. Conf., Innsbruck, 1978) IAEA.

[2] Okabayashi, M., and Todd, A.M.M., in this proceedings.

[3] Yamada, M., et al., Bull. Am. Phys. Soc. 24 (1979) 8; also proceedings of this conference.

[4] Katsurai, M., and Yamada, M., to be published.

FIGURE CAPTIONS

Fig. 1. Circuit model for the spheromak configuration

Fig. 2. Examples of conceptual methods to feed spheromak plasma in the reactor chamber. Initial spheromak is produced by the pinch gun (a) and, the cormak type excitors (b).

Fig. 3. Conceptual design of the spheromak reactor with moving plasma and the cormak type excitor.

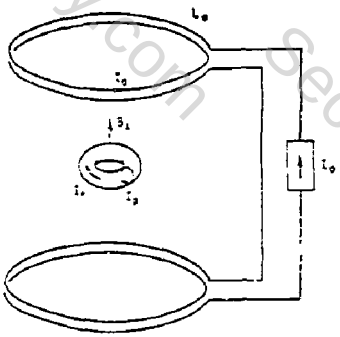

Fig. 1

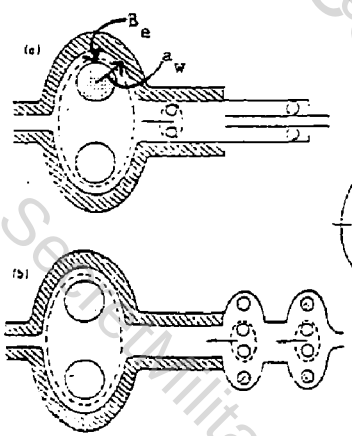

Fig. 2

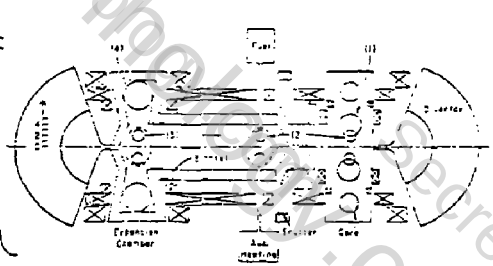

Fig. 3

TABLE 1

Type of Fusion	ST			Cat. DD	
Type of Operation	TCT (Q=1.7)	ICW		ICW	
a Minor radius (m)	0.5	1	1.5	1.5	2
R Major radius (m)	1	2	3	3	4
P_c Total output power (GW)	0.12	0.47	1.1	1.1	1.9
P_w Total wall loading (MW/m^2)	4	4	4	4	4
B_t Vertical magnetic field (T)	1.6	1.9	1.7	4.6	4.4
B_{to} Toroidal magnetic field at center(T)	6.8	8.2	7.4	20	19
$\langle\beta_o\rangle$ Center beta	0.045	0.045	0.045	0.045	0.045
T Plasma temp.(keV)	7	15	15	35	35
n_e Electron density ($\times 10^{14}cm^{-3}$)	1.9	2.6	2.1	6.5	5.6
τ_E Required energy confinement time (sec)	0.053	1.2	1.4	5.4	8.2
$(n_o\tau_E)_o$ (cm^{-3} sec 10^{14})	0.1	3	3	35	35
τ_M Magnetic diffusion time (sec)	46	580	1,300	4,700	8,300
W_M Internal magnetic energy (MJ)	50	580	1.6×10^3	1.2×10^4	2.4×10^4
I_t Toroidal current (MA)	8.9	27	29	79	98
I_p Poloidal current (MA)	34	82	110	300	370

TABLE 2

Phase No. (Plasma)	(Flux core)	(2) (M or M_o)		(3) (D-T)	(4)
Minor radius a(m) a	(1.6)	2.0	1.6	1.6	4.0
Major radius R(m)	(10)	4.0	2.6	3.6	8.0
Vertical field B_t(T)		0.75	3.0	1.3	0.281
Center toroidal field B_{to}(T)	(3.5)	3.2	13.0	5.6	0.34
Total poloidal flux $\langle\beta_p\rangle$ (W_b)	(240)	72	72	31	31
Toroidal flux $\langle\beta_t\rangle$ (W_b)	(20)	11	11	4.8	4.8
Poloidal current I_p(MA)	(130)	65	120	55	14
Toroidal current I_t(MA)	(10)	27	34	14	3.5
Internal magnetic energy W (MJ)	(total magnetic energy) (1400)	750	1,500	280	65
Total wall load. area P_w (MW/m^2)			25	0.98	
Output power P_o (W)			3,000	91	
(Average value)			$\overline{P_w}$ = 1 MW/m^2 $\overline{P_n}$ = 400 W		

THE ALL PLASMA SPHEROMAK: THE PLASMAK

P. Koloc and J. Ogden, Prometheus II, Ltd., Bx 222, College Park, Md. 20740
(301) 434-7317

There has been an evolutionary pattern established in magnetic fusion concepts. The flow in ideas follows three directions. By extrapolating this evolutionary movement, we have anticipated the concept called Spheromak and have predicted the omega of this evolution which is called PLASMAK, or all Plasma Spheromak. The evolutionary directions are from open systems to closed systems, from zero or low dimensional compression schemes to three dimensional compression, and finally from plasma configurations without any self confining currents to a plasma configuration which is completely self confined except for the mechanical pressure necessary to maintain the vertical field and hoop stress. The Stellarator represents a closed configuration requiring a very complex array of external confinement coils. The Tokamak allows vast improvement in plasma parameters, lower aspect ratio, and ohmic heating from plasma confining toroidal currents. ATC compression ratios of ~ 1 may be possible. Nevertheless, the plasma is imprisoned by heavy poloidal coils and a vacuum wall.

The Spheromak enjoys greater stability and obtains higher effective betas, simply expressed as higher fuel amount per unit external confining pressure. This comes about due to the poloidal plasma currents which, in addition to the vertical field, exert a second confining force on the plasma torus. Spheromaks have higher interior magnetic energy than at the separatrix or vertical field current shell. The term used to describe this advantage is Pressure Leverage. Unfortunately, in Tokamaks this second confining force is wasted on the poloidal windings and is a source for engineering problems. See Fig. 1.

Higher ATC compression ratios for Spheromaks are allowed because of the lack of axial obstructions. Energy scales as the square of the linear compression ratio c, (c^2), as it does in Tokamaks; this limits the utility of large compressions. Another consideration limiting very large compressions is the necessity of a tightly fitting shell to maintain stability.

This brings us to the Plasmak, or all Plasma Spheromak. The Plasmak represents the final step in reducing the dependence on external confining coils and for improving compressibility. In the Plasmak, the confining currents are all embedded in plasma with the fully ionizing energetic currents in the outermost mantle producing the vertical field. The equilibrium force arises from the ordinary gas pressure. See Fig. 2.

The Plasmak is fully compressible. As in Spheromak, there are no axial obstructions. The currents are energetic, allowing for high conductivity contributing to ideal MHD stability. Utilizing high voltage or EMF starting formation schemes results in very compact Plasmaks with intensive currents. In the Plasma Kernel (see Fig. 2 for nomenclature) the current densities result in considerable ohmic heating while the L/R times of the uncompressed (higher inductance) Plasmaks is > 1 second. The tightly fitting mantle is another prerequisite for ideal stability.

Compression is achieved by simply increasing the fluid pressure of the

surrounding gas blanket. The first advantage is that the upper bound on mechanical compression methods is higher than magnetic techniques. The second advantage is that the mantle is compressed along with the internal kernel, thereby maintaining a tightly fitting shell and ideal MHD stability throughout compression. The third advantage relates the significantly lower amounts of energy needed to compress a Plasmak as opposed to Tokamaks, or rigid shell Spheromaks where the magnetic energy varies as the compression ratio squared (c^2). In Plasmak, the energy is proportional to the compression ratio (c). The magnetized volume varying as the compression ratio inverse cube (c^{-3}) is responsible for this advantage.

In general, formation techniques can include a technique in which the Plasmak is produced through MHD effects initiated by a helical current stroke in a high density gas. Such a formation technique has been proposed to the US DOE and is currently under review. This particular approach sets up the Plasma Kernel and Mantle simultaneously with high density energetic currents and assumes an ideal MHD configuration from the outset. This technique relates to physical parameter regimes and phenomena not familiar to most fusion physicists, and will not be discussed here.

Another class of formation techniques utilizes a step by step formation and assembly of the Plasmak. A three step scenario includes ring formation followed by capture and injection of energetic currents. The third final step would be formation of the mantle over its external vacuum magnetic field. One common technique for ring formation being currently pursued is the plasma gun. Even the S-1 Spheromak can be considered a plasma gun. This gun differs from those described by LLL and LASL in that it utilizes an inductive startup and it has a disc shape rather than conical or cylindrical shape. Fig. 3 demonstrates this scenario. Incidently, the formation technique of G. Goldenbaum of the University of Maryland is also amenable to gun conversion since the magnetized plasma Kernel can be ejected through a hollow electrode at one end.

Compression, ignition, and energy exchange can take place in a separate and remote compartment. This is true to a limited extent for Spheromaks. Convenience of moving Plasmaks by EM or fluid flow is assured since lifetimes for uncompressed Plasmaks are on the order of seconds. An exciting engineering feature of this fusion furnace in electric power generating application is that the entire fusion and magnetic energy less neutrons can be dissipated in the gas blanket without affecting the walls. This blanket heated to tens of eV can be fed into inductive MHD generators achieving electrical conversion efficiencies of about 85%. Such efficiencies obtain Q values on the order of one hundred. Reduced wall loading is also achieved by moving radiating Plasmaks and Spheromaks. But less direct energy conversion schemes will not be as efficient.

High effective Betas, Pressure Leverage, favorable energy compression scaling ratios, and a technique called SCH or Self Compression Heating along with high Q all combine in the Plasmak to make this approach by far the most viable vehicle to burn exotic fuels. See Fig. 4 and Table 1.

Self Compression Heating (SCH) is the beneficial effect that occurs when a Plasmak has been gas compressed to ignition in a tightly fitting pressure chamber. Fusion energy driven Bremsstrahlung and alphas radiated by the kernel plasma thermalize the surrounding high density cold compression blanket. The subsequent pressure increase of the fusion thermalized blanket further drives

the adiabatic compression of the kernel fuel increasing its temperature, density, and reaction rate. This tool is most effective for higher temperature fuel cycles, i.e., P-B. SCH is not critical for the success of Plasmak furnaces: in fact, careful application of SCH to DT fueled devices is necessary due to the risk of runaway reactions. SCH also improves Q, the energy efficiency factor.

In addition to the proposed work by Spheromak Inc., a subsidiary of Prometheus II, Ltd., the Westinghouse Fusion Power Systems Division is planning Plasmak fusion power generating studies in early 1980. The enthusiasm for this concept is largely due to its engineering simplicity and design points. By proceeding directly with the proposed Plasmak scheme of Spheromak, Inc., the development of a compact fusion device could be completed within five years. Spheromak Inc. is fully ready to cooperate with various interests to develop Plasmak fusion furnaces and power generators. The implementation of Plasmak development requires exceptional administrative and executive action.

REFERENCES EXCLUDED FOR LACK OF SPACE

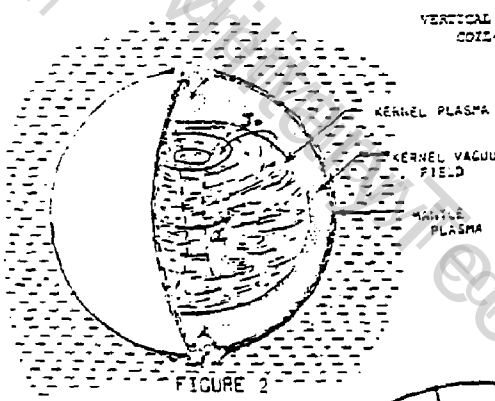

FIGURE 2
PLASMAK

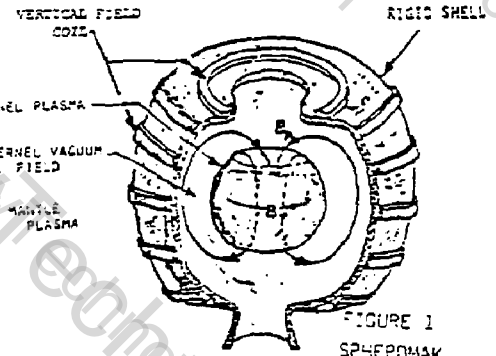

FIGURE 1
SPHEROMAK

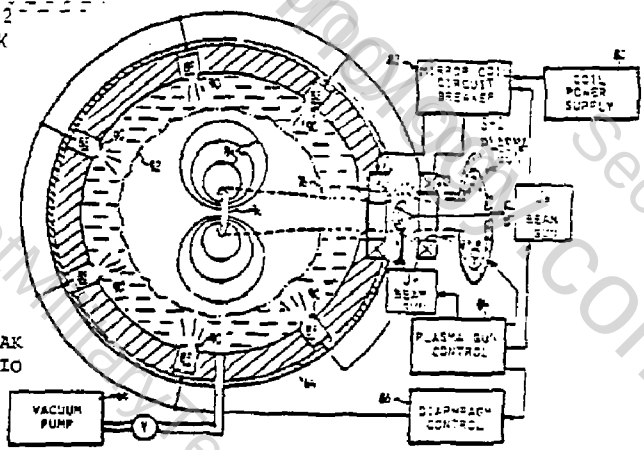

FIGURE 3
THREE STEP PLASMAK FORMATION SCENARIO

FIGURE 4 ELECTRICITY FROM PLASMAK

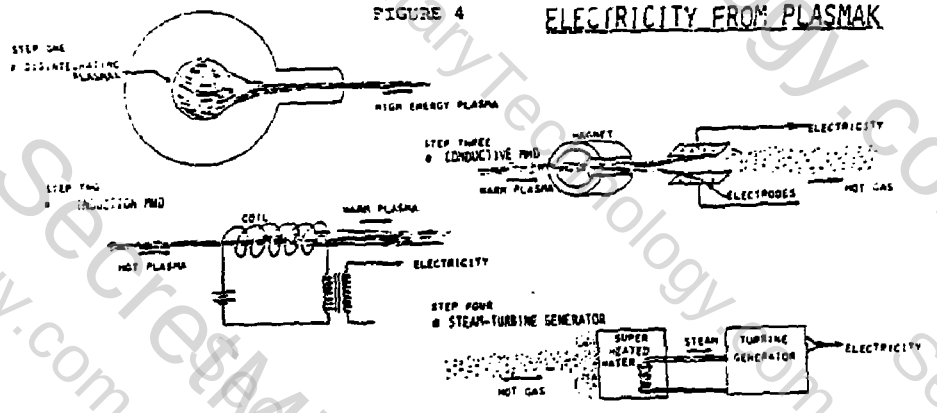

EXPECTED PLASMA PARAMETERS COMPRESSION EXPERIMENTS

TABLE 1	9EF Experiment, D-T		Furnace, D-T		P-211 Furnace	
	Before Compression	After Compression c = 6.69	Before	After (c = 5)	Before	After c = 12.6
Major radius R (cm)	17.7	2.65	38.2	7.63	38.2	3.03
Minor radius a (cm)	8.86	1.32	19.1	3.82	19.1	1.52
Plasma volume V (cc)	27.4 K	91.7	274 K	2.2 K	274 K	139
B (at Mantle (atm)	1	2 K	2	1.25 K	2	50 K
B (at Mantle (KG)	5	226	7.1	178	7.1	1.13 K
B (at kernel axis (KG)	20.3	856	28.7	686	27.9	2.15 K
I (Plasma amp	.57*	3.83**	1.74*	8.71***	1.74*	22 K
Inductance L (uH)	.611	.091	1.32	.263	1.32	.105
β	.019	.128	.021	.104	.076	.781
τE (sec)	.2	8.94	.27	6.75	1.27	150
τi (sec)	.2	8.94	.27	6.75	1.27	200
n (cc	1 E15	2.99 E17	1.6 E15	2 E17	1.26 E15	2.51 E19
Magnetic Energy E_M(*10^6J)	.1	.67	2	10	2	25
Radiation loss time τ_{B_r}	.804	.018	.584	.023	2.14	.013
τBT (sec (sec)	.348	643	.103	324	.383	97.6 K
Rad density P_{B_r} (w/cc)	.060	35.7 K	.177	15.9 K	.179	7700 K
Conductivity (*10^6mho/cm)	6.1	106	2.5	30.6	1.3	166
Mag. dissipation time τ_B(sec)	2.07	.8	4	1.92	.66	0.55
Ohmic heating P_Ω (w/cc)	1.76	9.07 K	1.83	2.37 K	11	331 K
Plasma diff time τ_D (sec)	121	7.04	216	20.8	29.2	2.37
Heat time τ(τEFUS),τ(sec)	.028	.0026	.041	.029	.035	.0013
Reactivity <σv>		2.35 E-28		3.7 E-29		8.3 E-28
D-T FUS Heat P_{FUS} *** (Kw/cc)		263		18.5		78.4 K
D-T Energy E_{FUS} (*10^6J)		19.3		309		60.1
Fusion Power (*10^6w)		120		203		10.8 K
Burn time E_{FUS} / P_{FUS} (sec)		.160		1.52		.006
n (cc		2.41 E17		3.85 E17		1.38 E18
η (efficiency)		28.9		30.9		2.4

* 2 MeV runaway electron currents
** 13 MeV
*** 10 MeV
+ 25 MeV
- excludes energy flux returned through self compression heating
excludes neutron energy flux

NEUTRAL BEAM SUSTAINED, FIELD-REVERSED MIRROR REACTORS*

G. A. Carlson, Lawrence Livermore Laboratory, Livermore, California 94550
K. R. Schultz, General Atomic Company, San Diego, California 92024
A. C. Smith, Jr., Pacific Gas and Electric Company, San Francisco, California 94106

We have carried out conceptual design studies for neutral beam sustained, field-reversed mirror reactors. The field-reversed mirror has a compact toroidal plasma geometry bounded by closed poloidal magnetic field lines generated by an azimuthal diamagnetic plasma current in a nearly uniform background magnetic field. The closed poloidal field structure has major radius R and minor radius a. The principal hypotheses of the FRM plasma are as follows:

- Equilibrium with weak or zero toroidal field, and therefore $\beta \approx 1$.
- Magnetohydrodynamic (MHD) stability achieved by finite ion Larmor radius, $S \equiv a/\rho_i \approx 5$, combined with low aspect ratio, $R/a \approx 2$.
- Plasma positioning by weak mirrors.
- Plasma confinement controlled by cross-field transport.
- Steady state plasma density, energy, and current maintained by neutral beam injection.

These hypotheses will be tested in the ongoing Beta II experiment at LLL. The objectives of Beta II are startup of a field-reversed plasma, confinement in a magnetic well, and steady state sustenance by neutral beam injection. For our reactor studies, we have assumed the validity of the FRM plasma hypotheses, and have calculated the characteristics of the plasma using an analytical model described in Ref. 1.

Our reactor designs have included a multicell commercial reactor and a single cell pilot reactor. The multicell reactor[1] has a linear arrangement of 11 cells, each containing a neutral beam sustained, field-reversed plasma. Advantages of the linear multicell approach include: more uniform wall loading and better utilization of background magnetic field.

The pilot reactor design[2] was sponsored by the Electric Power Research Institute and was carried out jointly by LLL, General Atomic Company, and Pacific Gas and Electric Company. Net power production was specified to be the primary objective of the pilot reactor. Another objective was the use of near-term technhnology in order to permit construction of the pilot plant in the late 1980's, if the present experimental program on field-reversed mirrors is successful. Following the operation of the pilot plant, we would envisage the rapid development of multicell commercial reactors, each cell of which would contain a field-reversed plasma identical to that in the pilot plant.

*This work was performed for the Electric Power Research Institute under Contract No. RP922 and under the auspices of the U.S. Department of Energy Contract No. W-7405-ENG-48 with Lawrence Livermore Laboratory.

The FRM pilot plant is shown in Fig. 1. The field-reversed DT plasma is at the center of the reactor. A cylindrical blanket and shield surround the plasma. The blanket is helium-cooled and contains lithium oxide for the breeding of tritium fuel. Surrounding the blanket and shield is a set of niobium-titanium superconducting magnets which provide the required background magnetic field. Neutral beam injectors fuel and energetically sustain the plasma. The large tanks at the ends of the reactor house direct energy converters and vacuum pumping systems for the plasma end leakage. Also housed in one of the tanks is a coaxial plasma gun for plasma startup.

The performance of the field-reversed plasma depends most strongly on the parameter S, the ratio of plasma minor radius a to the ion gyroradius ρ_i. Stability of the plasma is believed to require that S be a small number, probably 10 or less. We have considered both S = 5 and S = 7, and have sized the reactor to accommodate either plasma. The S = 5 plasma produces 22 MW of fusion power and requires 4.4 MW of neutral beam injection power; so Q = 5. The S = 7 plasma produces 42 MW of fusion plasma and requires 3.2 MW of neutral beam injection power; so Q = 13.

Several ways of forming field-reversed plasma rings are being considered for FRM startup. The startup scenario chosen for this design is the use of a magnetized, coaxial plasma gun, similar to the one now being tested on the Beta II experiment at LLL. A ring-shaped plasma is formed and axially accelerated by discharge current flowing radially across the anode-cathode gap. Beyond the end of the gun the plasma passes through a cusp-shaped magnetic field and emerges - with "captured flux" - as an annular plasma confined by an axially field-reversed, closed magnetic field. We designed the pilot reactor gun based on the Beta II gun and preliminary scaling laws. A unique feature of the pilot reactor gun is the use of a hollow cathode of sufficient radius to permit uninhibited passage of the escaping plasma stream to the direct converters.

The neutral beam injector for the FRM pilot reactor must continuously deliver 11 A of 200 keV deuterium and 11 A of 200 keV tritium. (These are the requirements for the S = 5 plasma; the requirements for S = 7 are somewhat less.) In this study we designed an injector based on negative ions that are directly extracted from a source, similar in principal to that under development at the Brookhaven National Laboratory. The ion source is held at a -200 kV potential. The negative ions, extracted from the source, travel to the accel grids via a sector magnet. The sector magnet separates the negative ions from electrons and deflects the ion beam out of the plume of neutral gas streaming out of the ion source. Subsequently the beam is accelerated and made to pass through a cesium vapor stripping cell, where about 60% of the negative ions are stripped of their extra electrons to become neutrals. A percentage of the energy carried by the un-neutralized fraction of the beam which leaves the stripper is recovered via a thermal beam dump at ground potential. Based on an analysis of all the power needs of such an injector, we estimate its efficiency to be 50%, not including the thermal recovery of the beam dump ions.

The magnet system for the FRM pilot plant consists of a pair of superconducting solenoidal magnets and a set of four superconducting saddle coils. The overall diameter of the coil set is 7.5 m and the overall length is 3.5 m. The solenoidal magnets provide a nearly uniform background magnetic field parallel to the axis of the reactor. The background magnetic field strength is 4.8 T for the S = 5 plasma and 4.6 T for the S = 7 plasma. The solenoidal coils also provide a shallow axial magnetic well for plasma centering. The need for a radial magnetic well is not presently clear, but in this study we assumed that it is necessary for plasma stability. The radial well is produced by the saddle coils.

The FRM plasma particles, although confined in a toroidal, closed magnetic field region, diffuse to open field lines and escape from the ends of the reactor into the direct conversion/vacuum pumping tanks. Half of the particles exit at each end. At the end of each tank is a simple one-stage, immersed-grid direct converter. The plasma first passes through a tenuous grounded grid, then through a negative grid which reflects the primary electrons. The ions are then decelerated by a collector plate held at a positive potential. The direct recovery efficiency of this direct converter is estimated to be about 50%. The collector plate for the direct converter is convectively cooled to remove the heat deposited by the impacted ions. For the pilot plant design, we have assumed that the heat will be removed at a thermodynamically uninteresting temperature and therefore do not route it to the thermal conversion system.

In steady state, the ions collected in the direct converter will reflux as gas and must be vacuum-pumped to maintain an operating pressure of about 5×10^{-6} torr. The pumping is done by an array of chevron-baffled liquid helium-cooled cryopanels mounted on the side walls of the direct conversion/vacuum pumping tanks. The total area of cryopanels is double the active area so that half of the system can be defrosted and degassed while the other half is actively pumping. Reclaimed deuterium and tritium from the cryopanels are recycled to the neutral beam injectors.

Neutron moderation and tritium breeding takes place in the cylindrical shell blanket constructed of Inconel 718. The tritium breeding material is lithium oxide and the blanket coolant is helium. The local blanket energy multiplication is 1.21 and the average multiplication, accounting for beam port and end losses, is 1.14.

The blanket consists of a single large module which may be removed and replaced without cutting and welding. The module is clamped in a frame made by prestressing the biological shielding vault in which the reactor is placed. The clamping force is generated by an inflatable cushion interposed between the module and the frame. When the cushion is inflated it closes all-metal knife seals to seal the central vacuum region.

We calculated the overall performance of the FRM pilot reactor for two cases: the smaller, S = 5 plasma and the larger, S = 7 plasma. The pilot reactor with the smaller plasma is just barely a net power producer: 90% of the 11.6 MW gross electric power must be recirculated to operate the reactor, and the net electric power is only 1.2 MW. Although marginal, the pilot reactor with the smaller plasma does satisfy the net electric power criterion. The larger plasma results in much more attractive performance: 46% of the 19.8 MW gross electric power is recirculated to operate the reactor, and the net electric power is 10.7 MW. Further improvements in performance would be realized in a multicell commercial reactor.

1. G. A. Carlson, W. C. Condit, R. S. Devoto, J. M. Fink, J. D. Hanson, W. F. Neef, and A. C. Smith, Jr., Conceptual Design of the Field-Reversed Mirror Reactor, LLL report UCRL-52467, May 1978.

2 G. A. Carlson, K. R. Schultz, and A. C. Smith, Jr., Definition and Conceptual Design of a Small Fusion Reactor, EPRI Interim Report ER-1045, April 1979, also Final Report in press.

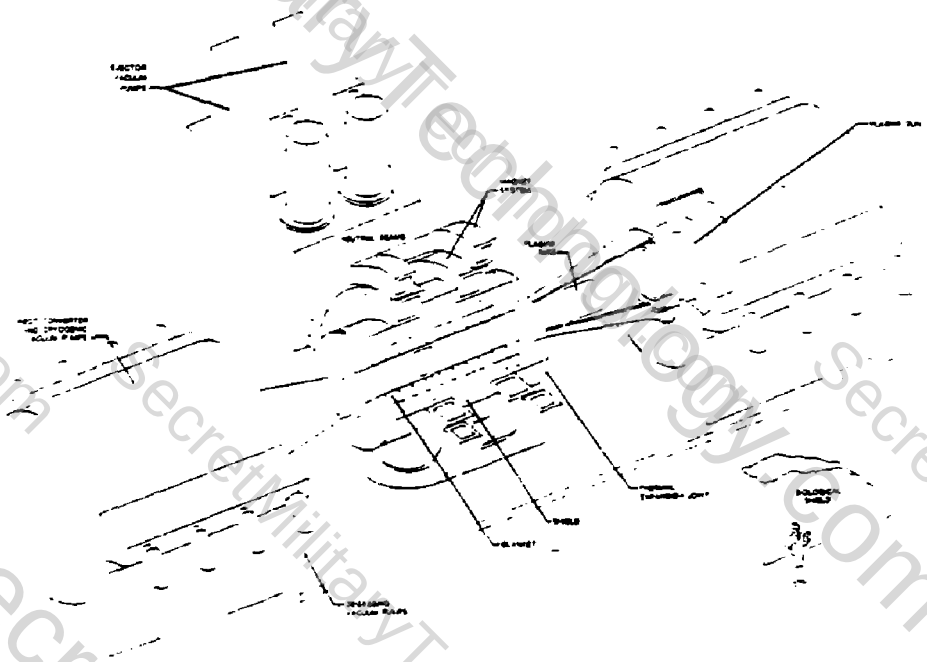

Fig. 1. Single Cell FRM Pilot Reactor

THE MOVING-RING FIELD-REVERSED MIRROR REACTOR CONCEPT*

A. C. Smith, Jr., Pacific Gas and Electric Company, San Francisco, CA 94106
G. A. Carlson, Lawrence Livermore Laboratory, Livermore, CA 94550
H. H. Fleischmann, Cornell University, Ithaca, NY 14853
T. Kammash, University of Michigan, Ann Arbor, MI 48109
K. R. Schultz, General Atomic Company, San Diego, CA 92024
D. M. Woodall, University of New Mexico, Albuquerque, NM 87106

The Moving-Ring Field-Reversed Mirror Reactor (MRFRMR) concept envisions production of electric power by burning magnetically field-reversed rings of fusion fuel which are translated continuously down the bore of a straight, cylindrical reactor burner chamber. Our interest in this reactor scheme arises from its potential design simplicity and the hope that it might be piloted in small size (50-100 MW(e)). This reactor has been evaluated only on a preliminary basis thusfar and much of the following discussion is founded on the results of that first evaluation[1]. We are currently performing a more detailed and thorough design study of this concept*.

The principle features of the reactor's burner section are shown schematically in Figure 1. The reactor is cylindrically-symmetric and consists of three in-line sections: a plasma ring generator, a central burner section, and a spent-ring exhaust section. The preliminary scoping study mentioned above concentrated chiefly on the burner section of the reactor.

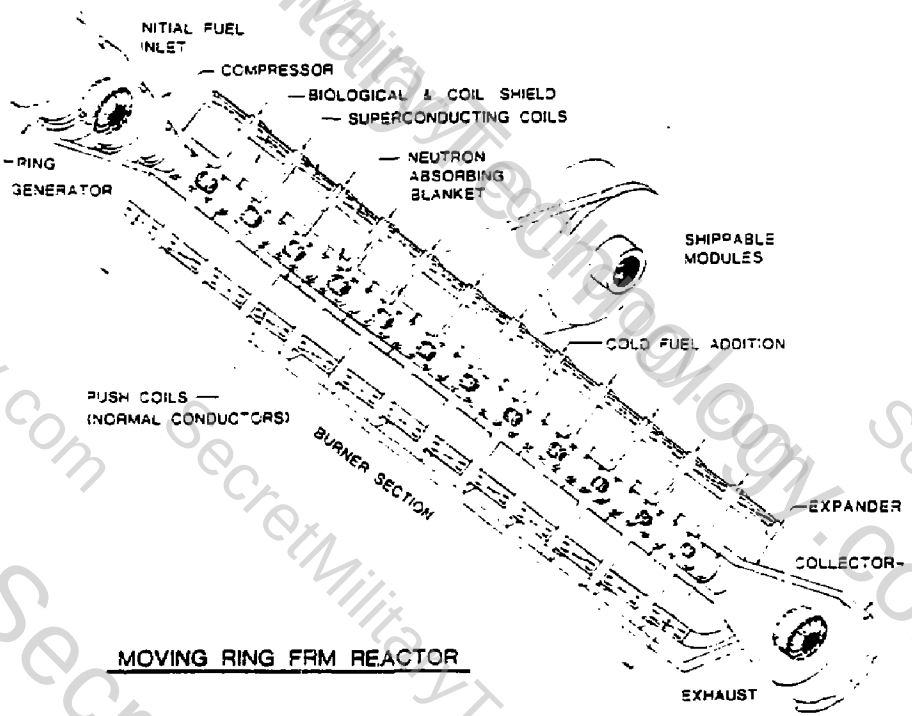

Figure 1

General Reactor Overview: A pulsed start-up mechanism (such as an intense charged particle beam source or a coaxial plasma gun) could generate a field-reversed plasma ring in the relatively low magnetic field just beyond the end of the burner chamber ("Ring Generator" section of Figure 1). A local "moving mirror" (provided by sequentially energizing "push coils" located near the wall of the reactor) then rapidly forces the plasma ring into the high solenoidal magnetic field of the burner section. Certain start-up approaches, such as the coaxial plasma gun currently being tested on the Beta II device at LLL, may provide the plasma ring with adequate axial kinetic energy to drive the ring into the high field region without the use of auxilliary coils. The ring may therefore be compressed and heated to initial burn temperatures in a manner that is potentially efficient. Also, the pulsed start-up mechanism and transient nature of the rings' lifetimes in the reactor may easily permit imbedding a toroidal magnetic field in the plasma, should plasma stability or other considerations require it.

Once the plasma ring has been brought to initial burn temperature, it is transported through the "burner section" of the reactor, possibly by the peristaltic action of an array of sequentially-energized local "moving mirror" coils positioned just inside the first wall. These pulsed coils would probably be constructed from aluminum or copper. The burner chamber consists of a linear string of identical cylindrical modules. Each module is itself a set of nested cylindrical components consisting of the first wall, the tritium breeding blanket, the biological and magnet coil shield, and the superconducting magnet coils providing the axial solenoidal guide field.

As discussed below, the ring may be refuelled during its transit of the burner section with cold plasma (either as pellets or via low-energy plasma guns) such that the power produced by the plasma ring is held nearly constant. Without energetic beam injection, the confinement will be sustained by the internal plasma currents driven by the ring's magnetic self-inductance. For fusion rings of interest, classical magnetic diffusion times can be of the order of tens of seconds, considerably longer than the 0.2 - 1 s plasma burn times envisioned so far. Also, absence of energetic beams in the burner chamber means that only relatively small-bore penetrations in the first wall, blanket, and shield may be required for refueling, considerably simplifying the overall reactor design.

An attractive engineering design feature arising from the pulsed plasma operation in the MRFRMR is the possible elimination of multipole fields to provide radial stabilization of the rings in the mirror field. If successful, this approach would use an electrically conducting first wall to center the rings radially in the burner section through the action of the eddy currents induced in the wall as the rings move with adequate speed down the axis of the device. Elimination of multipole fields may also have advantages in terms of overall plasma confinement. Theoretical work is currently underway to explore this possible means of ring stabilization.

Depending on the fuel composition and purpose of the reactor, heat can be extracted from the tritium-breeding blanket and the radiation shield and used in a conventional steam cycle. When the plasma burn is nearly quenched (due to the cooling effect on the plasma by cold-ion refueling), the plasma rings may be exhausted out the expansion end of the device into magnetic and electrostatic energy recovery units. The linear arrangement of the reactor also offers a built-in divertor-like action, since particles which have diffused out of the burning plasma rings in the reactor will probably flow out both ends of the device into direct converters along the open, axial solenoidal field lines. Although the MRFRMR plasma burns are, individually

speaking, transient events, we believe that fluctuations in the reactor wall heat load can be minimized by appropriate choices of inter-ring spacing and ring axial speed.

Pulsed Plasma Burn Calculations: To date, most of the work on the MRFRMR has centered on studying the characteristics of pulsed burns of DT plasmas. The details of the current 0-D Fokker-Planck plasma modelling analysis have been given elsewhere[2]. Where possible, ongoing plasma equilibrium and stability studies will be incorporated to improve the burn model assumptions on plasma density profiles, diffusion processes, heat transfer, and permissible plasma size. Although the plasma burn model is still under development, some preliminary results illustrate what we might expect during the transient burn of a field-reversed plasma ring heated to initial temperatures $T_i(t=0) = 75keV = 2T_e(t=0)$. The confining guide field is 65 kG and S, the number of average ion gyroradii which fit across the ring's minor radius, is chosen S(t=0) = 10. (The implication that the plasma is stable in the range of S = 10 - 12 may well be an optimistic presumption). Two cases are considered: (A) a plasma which proceeds to burn in a constant magnetic field with no external fuel addition to influence the burn characteristics and (B) a plasma with identical initial conditions but where low energy ions (3 keV deuterons, 5 keV tritons) are added during the burn at a rate such that the total radiated power is held nearly constant. Burn characteristics for cases (A) and (B) are plotted in Figures 2 - 4.

Adding no cold fuel to the plasma causes the ring radiated power to drop from 49 MW to less than 10 MW in 0.5 s (Figure 2). Adding cold plasma fuel under the conditions of case (B) shows the ring radiated power of ≃ 49 MW is sustained for about 0.35 s before dropping rapidly to zero.

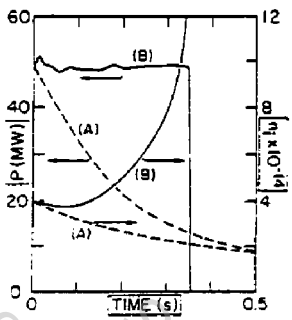

Figure 2

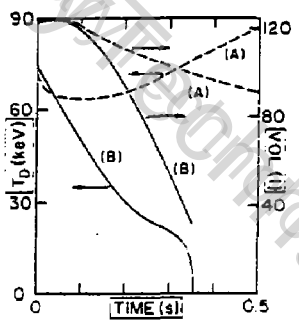

Figure 3

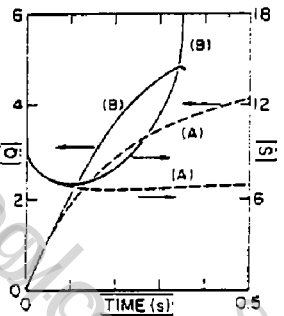

Figure 4

The reasons for this disparate behavior are summarized in Figures 2 - 4. As shown in Figure 3, withholding cold fuel leads to a brief drop in fuel temperature due to heat conduction followed by a rise as alpha particle heating takes effect. Also, as particles are lost via diffusion, the ring volume drops to maintain pressure equilibrium with the external confining field. As shown in Figures 2 and 3, the combined effect of decreasing fuel ion density and plasma volume results in a net drop in ring power by about a factor of 5 at the end of 0.5 s. On the other hand, adding "cold" fuel to the burning plasma brings a dramatic drop in ion temperatures--from 75 keV at t = 0 to about 8 keV at t = 0.35 s. While such a drop in ion temperature greatly reduces $\langle\sigma v\rangle$ for the DT reactions, the ion density has been increased via the cold fuel addition by nearly a factor of 3 in 0.35 s to

maintain constant ring power. As seen in Figure 4, after 0.35 s the Q of the plasma to which cold fuel is added exceeds that of the no fuel addition case by about 30%. Also, the S-value of the rings with no cold fuel added eventually hovers around S = 7, while the cold-fuel-addition case shows a dramatic rise in S near the end of the burn. Plasma stability considerations may dictate whether such a plasma parameter regime is tenable.

This sample, preliminary calculation illustrates some general features which may strongly influence reactor design. Because of the trade-off between ion temperature and density in a fixed confining field, optimal plasma Q values lie in the range of 75 - 150 keV under current assumptions. Both total power per ring and plasma performance are critically sensitive to plasma size: beginning the case (B) plasma burn with an S(t=0) = 12 leads to ignition, while decreasing the initial value of S to 8 gives a Q of only 2.3 and a burn time of 0.17 s. A practical pilot plant design with commercial upgrade potential will probably require plasma Q values in excess of 15.

Preliminary Reactor Study (1978)[1]: The preliminary design mentioned above for the MRFRM called for a reactor burner chamber 12 m long, a first wall radius of 32 cm, and blanket/shield thickness of 137 cm. The guide field of 65 kG was provided by superconducting coils located just outside the shield. Plasma fuel ion/electron temperatures were presumed to be 75/37.5 keV at the start of the burn and stability concerns limited us to burns in which $S(t) \leq 5$. The plasma ring major radius ranged from 9.6 cm to 6.6 cm during the burn. Plasma refueling was accomplished by laser-accelerated DT pellets. Heat conduction from the field-reversed rings was neglected in this work under the assumption that the diffusing plasma escaping from the closed-field confinement is rapidly lost. Also, to achieve a plasma Q value nearly equal to that of the beam-driven FRM[3] ($Q \simeq 5.5$), it was necessary in the preliminary study to assume that the particle confinement was three times better than that needed for the FRM. The plasma rings produced 10.6 MWt/ring with a burn time of 0.32 s. The rings moved down the axis of the 2 cm thick aluminum first wall at a speed of 40 m/s to achieve radial focusing with minimal dissipative wall drag ($\lesssim$ 10 kJ/m per ring). Heat was recovered from the 40 cm thick Li_7Pb_2 breeding blanket and the 97 cm thick stainless steel/B_4C shield by circulating helium in a gas turbine cycle. A plant energy balance showed a net electric power production of 1.25 - 4.75 MW(e) per ring, depending on the efficiencies possible for the magnetic compression and ring energy recovery processes.

Continuing Reactor Design Work: Work is continuing on the MRFRMR to re-evaluate the design issues bearing most directly on reactor performance. The goal of the study is to identify (where possible) the physics and technology issues and conditions which will lead to a pilot reactor which scales to an economically commercial plant.

[1]A. C. Smith, Jr., et al., Preliminary Conceptual Design of the Moving Ring Field-Reversed Mirror Reactor, Pacific Gas & Electric Company Report 78FUS-1 (1978).

[2]T. Chu and A. C. Smith, Jr., RFOT: A Fokker-Planck Code for Pulsed Fusion Plasma Analysis, Lawrence Livermore Laboratory Report (in press).

[3]G. A. Carlson, et al., Conceptual Design of the Field-Reversed Mirror Reactor, LLL Report UCRL-52467, May, 1978.

*This work is being performed for the Electric Power Research Institute under contract No. RP922.

PRELIMINARY REACTOR IMPLICATIONS OF COMPACT TORI: HOW SMALL IS COMPACT?

R. A. Krakowski and R. L. Hagenson, University of California, Los Alamos Scientific Laboratory, Los Alamos, New Mexico 87545

I. INTRODUCTION

The generic name "compact torus" (CT) is applied to the general class of toroidal plasma configurations in which no magnetic coils or material walls extend through the torus. Figure 1 schematically summarizes the "family tree" of CT configurations that have been subjected either to theoretical or experimental examination. Two branches to the CT family of closed-field plasmoids are evident. Ongoing reactor studies at LASL have focused primarily onto the left-hand branch depicted in Fig. 1, with an emphasis being placed upon field-reversed theta pinch (FRΘP) as a means to form, heat and confine a CT plasmoid in a reactor context. Both the spheromac and the FRΘP configurations are assumed to require an electrically conducting wall to provide equilibrium and stability. The purpose of this paper is to present parametrically and by means of a simple analytic model the reactor implications of a FRΘP; an electrically conducting shell is presumed necessary for equilibrium and stability. The question of minimum power and size for this specific CT configuration is addressed.

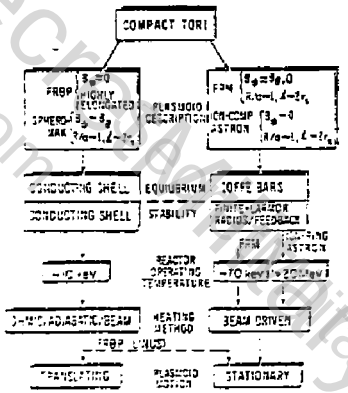

Figure 1
Schematic summary of compact torus plasma configurations.

II. MODEL

A. GENERAL CONSIDERATIONS

Figure 2 depicts the CT model and pertinent notation that form the basis for this analysis. Experimental evidence indicates[1] decreased confinement times as r_c/r_s increases beyond ~ 2 and the plasma becomes overcompressed. The experimental parameters $r_c/r_s \sim 2$ and $\ell/r_s \sim 7$, along with analytic equilibrium constraints, are used to guide this study. As is observed in experiments, the FRΘP plasmoid is assumed to contain little or no toroidal field. The question of plasmoid formation and heating is not addressed here, although these processes would occur in an ex-reactor system by means of slow implosion, adiabatic heating, the application of energetic particle beams, and/or ohmic dissipation.

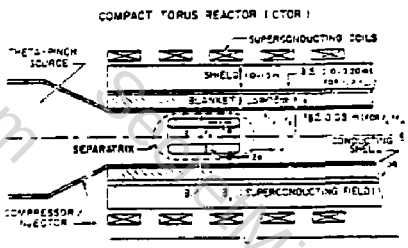

Figure 2
Schematic layout of Compact Torus Reactor (CTOR) based on FRΘP. Conducting shell is shown located either at first wall or outside of blanket.

Given the formation, heating, and translation of the FRCP plasmoid, how best can useful fusion energy be obtained from a shell-stabilized configuration, and in which way does this constraint affect the projected reactor size and power level if realistic engineering constraints are applied? In short, how small is compact?

8. ROLE AND LOCATION OF CONDUCTING SHELL

A central thesis of this study is the presumption that a passive, electrically conducting shell provides both equilibrium and stability and that r_c/r_s must be < 2 for this to occur. The heated and ignited plasmoid of length ℓ enters the linear burn chamber of length L and radius r_w at a velocity $v = L/\tau_s$ that is compatible with the electrical skin time, τ_s, of the conducting shell positioned at radius $r_c > r_w$. Translation of the plasmoid inside this flux-conserving shell increases the stationary magnetic field (provided by external superconducting magnets, Fig. 2), as magnetic flux is constricted to a smaller volume between the separatrix and the shell. That part of the plasma pressure supported by the conducting shell results in ohmic dissipation within shell which must be extracted from the translational energy of the plasmoid. This energy loss may be significant and generally points to the use of a room-temperature shell located outside a blanket of thickness Δb.

As the plasmoid is translated to the burn chamber, the flux within the shell, provided initially by the external superconducting coils, is conserved. A characteristic time, τ_s, for flux penetration into the shell of resistivity η can be derived on the basis of this flux conservation

$$\tau_s = \frac{\mu_o}{2\eta}\frac{\delta}{r_c}\left(r_w^2 - r_s^2\right) \quad . \tag{1}$$

This expression is based upon an allowable flux loss as determined by the limit when the plasmoid would contact the first wall. Placement of the shell at the first wall (i.e., $r_c = r_w$) will require that the shell thickness, δ, be less than ~ 0.05 m for neutronic reasons; additionally, η will be increased because of the higher operating temperature at a first-wall location. Generally, τ_s is computed to be 3–4 times longer if the shell is positioned outside the blanket, inspite of the higher value of $r_c = r_w + \Delta b$. Even when located outside the blanket, the shell thickness should present a cross-sectional area that is appreciably smaller than the crucial area from which flux is being displaced (i.e., $\pi(r_w^2 - r_s^2)$). Furthermore, the ohmic power dissipated in the shell, P_{OHM}, when expressed relative to the alpha-particle power, P_α, is given by

$$P_\alpha/P_{OHM} = 8.6(10)^{16}\,\frac{\delta}{\eta}\,\frac{r_c^3}{r_s^2}\,\frac{\langle\sigma v\rangle}{T^2}\,B_i^2 \quad , \tag{2}$$

where B_i is the compressed magnetic field within the shell. For typical reactor parameters (r_w = 1.0 m, Δb = 0.5 m, B_i = 5 T), this ratio decreases from ~ 60 for an ex-blanket shell (δ = 0.1 m) to ~ 4 (δ = 0.05 m) for a first-wall shell, again giving impetus to shell placement outside the blanket. Lastly, the ohmic dissipation occuring within the shell must be provided either by the kinetic or the fusion (i.e., directly converted alpha-particle energy) powers associated with the translating, burning plasmoid. For a first-wall shell, the required translational power can be considerable, and the plasma expansion required to channel directly the alpha-particle energy to supply this ohmic loss would be prohibitively large. On the basis of these

arguments, the stabilizing conducting shell should be located at a radius $r_c = r_w + \Delta b$, where Δb is expected to be ~ 0.5 m. In order to provide the necessary stabilization of a plasmoid of length $\ell = 7\, r_s$, the translational velocity must be $v = \ell/\tau_s$, again with $r_c/r_s = 2$. As will be seen, these simple constraints play an important role in establishing the minimum size and power of the CT reactor.

C. CONSTRAINTS IMPOSED BY NEUTRON WALL LOADING AND TOTAL POWER

The fusion neutron wall loading, $L_w(W/m^2)$, and a Lawson-like criterion, $n\tau_B$ (s/m^3), at this level of analysis represent important indicators of system performance. The analytic CT equilibrium relationships predict that 87% of the plasmoid volume within the separatrix radius, r_s, would be filled with $\beta = 1$ plasma. The fraction of the burn chamber that is filled with plasma (i.e., the duty factor), is easily shown to equal τ_s/τ_I, where $1/\tau_I$ is the plasmoid injection rate. Recalling that the burn time, $\tau_s = \tau_s(L/\ell)$, the following expression for L_w results

$$\frac{9.02\, L_w\, \tau_I}{(n\tau_B)^2 \langle\sigma v\rangle E_N} = \frac{r_s^2}{r_w}\frac{\tau_s}{\tau_B^2} = \frac{r_s^4}{2r_s - \Delta b}\frac{(\ell/r_s)^2}{L^2\tau_s} \quad , \tag{3}$$

where mks units are used, E_N is the fusion neutron energy, $r_w = r_c - \Delta b$, $r_c/r_s = 2$, $\ell/r_s = 7$, and τ_s (Eq. (1)) can similarly be expressed in terms of r_s. With the exception of τ_I, the left-hand-side of Eq. (3) represents a constant that is chosen on the basis of confinement physics, $n\tau_B$, and desired system performance, L_w. The total system thermal power, $P_{TH}(Wt)$ equals $2\pi r_w L\, L_w M$, where the multiplication M is typically ~ 1.42 (20 MeV/fusion). For a given wall loading and $n\tau_B$ value, therefore, P_{TH} can be evaluated as a function of system dimensions (i.e., r_s and L).

An additional and important constraint is imposed by the allowable thermal cycle, $\Delta T(K)$, experienced by the first wall. The thermal heat flux at the structural first wall is expected to originate primarily from Bremsstrahlung radiation, in that particle losses should be directed out of the burn chamber along open field lines in the region from radius r_s to r_w. If $k(W/mK)$, $\rho(kg/m^3)$ and $c_p(J/kg\ K)$ are, respectively, the thermal conductivity, density, and heat capacity of the first-wall material, the temperature rise for a "thermally thick" first wall that is irradiated solely by Bremsstrahlung leads to the additional constraint

$$\frac{\Delta T \sqrt{c_p k \rho}}{2.63(10)^{-37}\,(n\tau_B)^2 T^{1/2}} = \frac{r_s^2}{r_w}\left[\frac{\ell}{L}\right]^2 \frac{1}{\tau_s^{3/2}} = \frac{r_s^4}{2r_s - \Delta b}\frac{(\ell/r_s)^2}{L^2\tau_s^{3/2}} \quad , \tag{4}$$

where T(keV) is the average plasmoid temperature, and the thermal irradiation time experience by any given section of first wall is taken as τ_s.

III. RESULTS

Typical results are illustrated on Fig. 3, which shows the dependence of P_{TH}, L, and τ_s on the separatrix radius for the fixed parameters indicated. A minimum total power is shown for this case where the duty factor, $f_\ell = \tau_s/\tau_I$, has been fixed at 0.1 and $n\tau_B = 5(10)^{21}$ s/m^2 (i.e., a fuel burnup fraction $f_B = 0.22$). The reactor power initially decreases with increased r_s because of the increased τ_s and correspondingly decrease in required translational

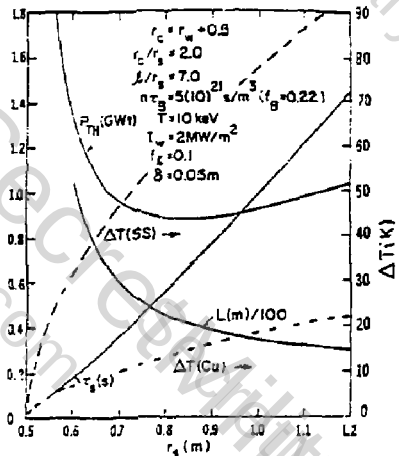

Figure 3
Dependence of total power, P_{TH}, length of burn chamber, L, and shell skin time, τ_s, on plasmoid separatrix radius, r_s, for the fixed parameters indicated.

velocity; an increased reactor length results. As r_s increases beyond the power minimum at 0.83 m, the power increases because of the increased plasma cross-sectional area. Only the magnitude but not the position of the minimum power indicated on Fig. 3 depends on the choice of fixed parameters, Eq. (3) providing the appropriate scaling relationship. Specifically, combining Eq. (3) with $P_{TH} = 2\pi r_w L L_w M$ gives the following explicit form for the power curve depicted on Fig. 3.

$$P_{TH}(Wt) = 8.78\, M L_w^{1/2} \langle\sigma v\rangle^{1/2} (n/\delta)\, \Delta b^{3/2} (n\tau_B) f_\ell^{1/2} \frac{(1-x)^{1/2}}{x^{3/2}[(1-x)^2 - 1/4]} \quad , \quad (5)$$

where $x = \Delta b/r_c = \Delta b/2r_s$. Equation (5) shows the expected minimum at $x = 0.3$ (i.e., $r_s = 0.83$ for $\Delta b = 0.5$ m). For T = 10 keV, M = 1.42 and $n = 2(10)^{-8}$ ohm m (Cu at 300 K), the minimum power equals

$$P_{TH}(Wt) = 5.54(10)^{-17} L_w^{1/2} \Delta b^{3/2} f_\ell^{1/2} (n\tau_B)/\delta \quad , \quad (6)$$

which illustrates explicity the CTOR minimum-power scaling. Because of the direct coupling of plasma performance with the ex-blanket shell, Δb plays a prominent role in establishing the minimum power. Furthermore, contrary to intuition, the minimized total power varies weakly as the square root of the first-wall neutron wall loading. For the minimum power shown on Fig. 3, the following system characteristics are predicted: P_{TH} = 880 MWt, L = 42 m, r_s = 0.83 m, ℓ = 5.8 m, r_w = 1.2 m, r_c = 1.7 m, τ_s = 0.6 s, τ_B = 4.5 s, τ_L = 6.2 s (f_ℓ fixed at 0.1), v = 9.4 m/s (34 km/h), n = $1.1(10)^{21}$ m^{-3}, B_i = 3 T, $P_{TH}/\pi r_c^2 L$ = 2.4 MW/m^3.

The temperature-rise constraint given by Eq. (4) is expressed below in explicit form

$$\Delta T = 8.33(10)^{-28} \left[\frac{(1-x^2)-1/4}{x}\right]^{1/2} \left(\frac{\delta \Delta b}{c_p \rho k \eta}\right)^{1/2} \frac{L_w}{(\langle\sigma v\rangle/T^{1/2}) f_\ell} \quad , \quad (7)$$

which predicts ΔT = 14.2 K at the minimum-power point for a first wall with thermophysical properties of copper. Equation (7) has been plotted on Fig. 3 for rst walls with both stainless-steel and copper thermophysical properties. Application of the thermal cycle constraint, $\Delta T \leq 30$ K, requires that τ_B to be adjusted to ~ 3.2 s and f_ℓ correspondingly be reduced to ~ .05,

resulting in an optimum (i.e., minimized) reactor power of 600 MWt with L = 30 m, again for a first wall with thermophysical properties similar to copper. Stainless steel represents an extreme relative to the assumed copper-like first-wall properties, representing an increase in ΔT by a factor of $\sqrt{(kc_p\rho)_{Cu}/(kc_p\rho)_{SS}} = 4.4$. It is emphasized that the methods used to estimate the thermal-cycle constraint are highly approximate, and considerably more analysis of this important and often neglected problem is warranted.

IV. CONCLUSIONS

The application of simplified but realistic engineering constraints to the special class of wall-stabilized FRCP configurations leads to reactor systems that may be as small as ~ 30 m in length and generating a total thermal power of the order of 500 MWt. Decreased size and power for a given $n\tau_E$ will be accompanied by decreased performance indicators, as reflected in this study by L_z and the allowable ΔT. It should be noted that this analysis is based upon fixing the duty factor, $f_\ell = \tau_s/\tau_T$. Other approaches which treat τ_T rather than f_ℓ as a parameter give somewhat different optima, but the basic conclusions and results embodied in Fig. 3 are not significantly altered. The results of this simple scoping calculation will be used to guide a more detailed modeling of important issues related to plasmoid injection, plasma transport/equilibrium/stability, burn dynamics, transient response of the the first wall and conducting shell, and overall system energy balance.

REFERENCES

1. LASL CTR-Division Staff, "Proposal for FRX-C and Multiple-Cell Compact Torus Experiments," Los Alamos Scientific Laboratory report, LA-8045-P (1979).

2. R. K. Linford, D. A. Platts, and F. G. Sherwood, "Field-Reversed Experiment (Compiled by K. S. Thomas and G. A. Sawyer)," Los Alamos Scientific Laboratory report LA-7474-PR (1979).

TRACT: A SMALL FUSION REACTOR BASED ON A COMPACT TORUS PLASMA

H.J. Willenberg, A.L. Hoffman, L.C. Steinhauer and P.H. Rose
Mathematical Sciences Northwest, Inc.; Bellevue, Washington 98009

A compact torus formed by triggered reconnection and adiabatic compression of a reversed-field theta-pinch plasma can provide the basis for fusion power reactors which are small, relatively easy to fabricate and maintain, and which promise high power gain with modest recirculating power requirements. A new reactor concept, designated TRACT (Triggered Reconnection, Adiabatically Compressed Torus), has been developed based on such a confinement scheme. The TRACT plasma is produced in a linear solenoid by a staged process involving plasma formation in a reversed bias field, introduction of forward flux by external solenoidal shock coils, triggered reconnection of the magnetic field lines resulting in rapid axial compression and heating of the resultant plasma torus and, finally, some adiabatic compression of the plasma by additional forward flux. Plasmas formed in this manner have been experimentally observed to be stable for at least 100 Alfven times.[1]

For plasma major radii of 7 cm or more, the confinement time based on classical particle diffusion across the separatrix exceeds one second. Allowing for anomalous transport across the separatrix to establish a quasi-steady state balance with axial transport processes leads to a confinement time which is about a factor of 30 smaller than classical. Based on this hybrid confinement model, a 15 keV compact torus with a major radius of 24 cm and aspect ratio of 3.9, confined by an external field of 7 Tesla, has a plasma confinement time of 0.5 sec. Such a plasma would generate 225 MJ of neutron energy in 0.5 sec. A TRACT reactor based on this plasma with a repetition rate of one Hertz is capable of generating 90 megawatts of net electrical power.

A conceptual TRACT reactor design is illustrated in Figure 1. The complete reactor vessel, including the blanket, shield, and magnets, is 9 meters high and 3.5 meters in diameter. The plasma chamber is five meters long with a one meter bore. A steady 7 Tesla axial field is maintained with a superconducting solenoid located outside the blanket. This field is disturbed briefly by a normal coil located near the first wall during plasma formation. Prior to each pulse, deuterium-tritium gas is injected axially through a screen nozzle. The normal coil is activated in the opposite polarity to the superconductor to establish a reverse bias field in the plasma chamber. After preionization, the plasma is heated to ignition by a four stage process occurring during the second quarter cycle of the normal coil. First, a rapid drop in the normal coil current causes radial shock compression of the plasma and reversal of the magnetic field. Magnetic field line reconnection is delayed with a magnetic cusp at each end while the plasma is compressed. When sufficient forward flux has been introduced, the cusp current is reversed, resulting in a mirror field which rapidly triggers field line reconnection. This triggered reconnection causes the plasma to contract axially to a configuration with a much less elongated torus. As the normal coil current reduces to zero, the plasma is then adiabatically compressed to ignition temperature. During burn the plasma is confined wholly by the superconducting field. Fusion product heating raises the temperature to 15 keV during burn.

The axial contraction results in a compact torus with a high fill factor x, defined as the ratio of the separatrix radius to the first wall radius.

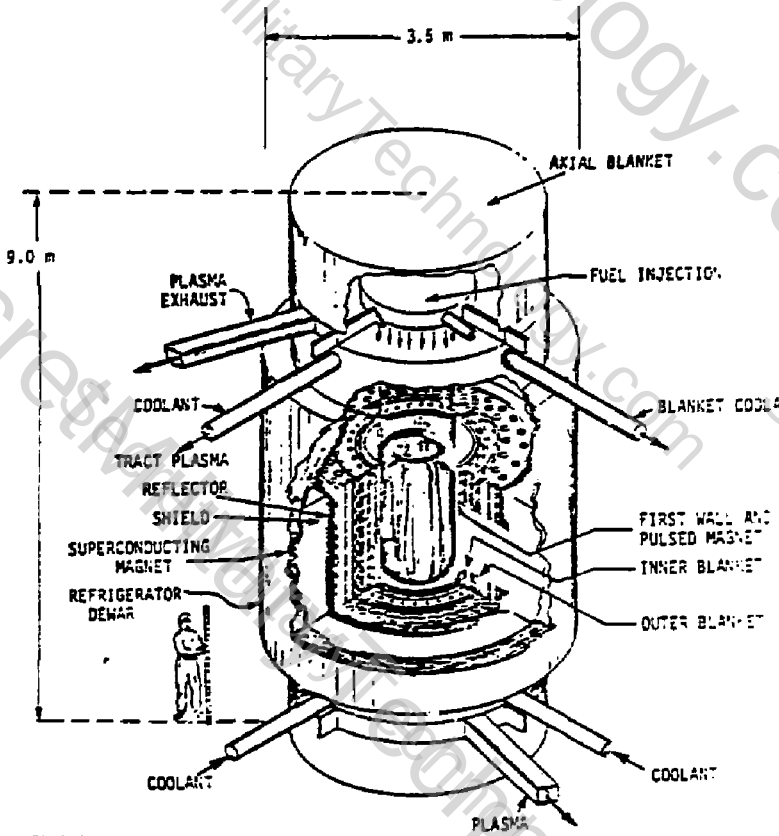

Figure 1. A 90 MWe TRACT Fusion Reactor

fill factors approaching one ($r_s \rightarrow r_w$) have been observed.[1] No signs of instability have been observed for the circuit decay time of the confining magnet as long as the fill factor remains above a critical value which depends on the initial pressure, and is in the range x = 0.3-0.4.

The rapid axial contraction and magnetic field reconnection generates irreversible heating of the plasma, so that the contracted torus is hotter than if the process were adiabatic. Thus, the plasma has been heated by two nonadiabatic processes: radial shock heating of the conventional theta pinch type, and axial compression heating from the reconnection process. The more the plasma is heated by axial compression, the less is required from purely radial processes. This relationship is illustrated in Figure 2, where the axial heating is described by the ratio, g, of the temperature after reconnection to that immediately before reconnection. The higher the value of g, the more heating is achieved by axial processes and the less is required of radial processes. This translates to more relaxed requirements on the azimuthal electric field E_θ at the first wall for shock heating. Figure

2 shows the electric field required to achieve 6 keV at final fill factor X_f for a range of axial temperature gains. X_1 is the fill factor after reconnection. If the critical fill factor $X_f = 0.3$, then $E_\theta < 0.5$ kV/cm for very modest temperature gains, $g \approx 1.5$-2.0. If the critical fill factor is $X_f = 0.5$, then $g \geq 10$ is required for $E_\theta = 0.5$ kV/cm.

The normal coil is supplied by two separate power supplies: the slow field reversal and adiabatic compression is provided by an 85 MJ fast-discharging homopolar generator, and the radial shock field is provided by a 10 MJ capacitor bank. The first wall is made of alumina to allow the fast-rising field to penetrate. The blanket concept chosen for the reference design consists of lithium lead plates cooled by boiling water flowing axially in stainless steel tubes. The radial blanket is divided into two zones: the inner blanket zone must be replaced periodically because of radiation damage, and the outer zone lasts the lifetime of the reactor. A 0.60 meter thick shield of boron carbide and stainless steel protects the superconducting coil from radiation. The entire vessel is enclosed in a vacuum chamber which can be ten meters high and seven meters in diameter. The plasma chamber is vacuum pumped continuously through penetrations at the ends.

The small size and simple geometry of the TRACT reactor provides a great advantage for reactor maintenance. The reactor vessel is small enough to stand vertically. There are no radial penetrations into the plasma chamber or inner blanket, so there are no restrictions to vertical movement during component maintenance. Since the first wall, normal coil, and inner blanket zone are free to move axially and are small, no remote cutting must be performed to prepare these components for removal and replacement by an overhead crane. These features will greatly decrease the time required for blanket/first wall replacement compared to other fusion reactor concepts.

The recirculating power requirements for an ignited TRACT reactor are low. A 1 m bore, 5 m long plasma chamber is sufficient to produce 278 MJ of thermal energy per pulse, with a blanket multiplication of 1.22. Use of the compound magnet concept limits resistive heating of the magnet to only a small fraction of the duty cycle. With a ten millisecond half-cycle time, which is achievable with fast-discharging homopolar generators, Joule heating losses are 1.9 MJ/pulse. Assuming 95 percent switching efficiency, switching losses in the magnet system account for another 4.2 MJ/pulse. Plasma thermal energy at ignition is 4.5 MJ, which is not recovered in the current design. Other losses, including vacuum and coolant pumping power in the blanket as well as the superconductor, amount to less than 1 MJ/pulse. At 36 percent blanket thermal efficiency, the recirculating power fraction is 11 percent. A reactor with a 50 percent duty factor would thus produce 90 MW of net electric power.

Since the plasma volume scales as r^3, where r is the first wall radius, and the confinement time scales as r^2, the thermal energy output per pulse scales roughly as r^5. A small change in the reactor dimensions can substantially change the power output. The hybrid confinement model described above predicts that an experiment with a 0.52 meter bore would result in energy breakeven, and a fusion power pilot plant which produces net electrical power requires only a 0.70 meter bore. The strong power dependence on size also leads to weak reactor sensitivity to confinement scaling. Figure 3 illustrates the first wall radius required to produce 90 MWe for different confinement times. Particle confinement based on classical radial transport would allow a first

wall radius of 0.39 m. Alcator scaling allows a radius of 0.56 m. Even if the particle confinement time scaled as one-tenth of the Alcator model, the required first wall radius would still be only 0.9 m.

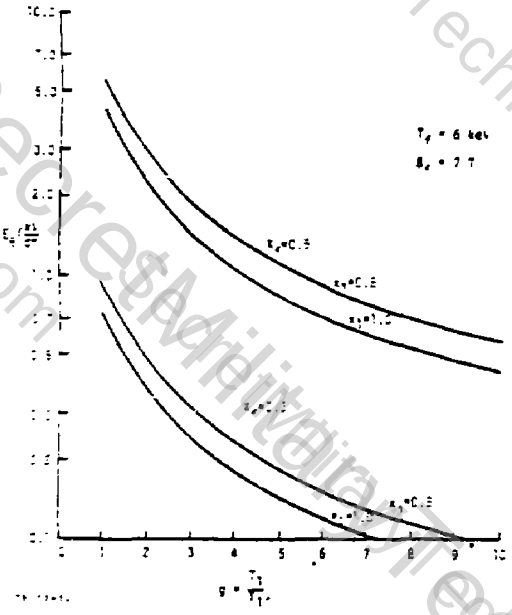

Figure 2. Electric Field Reduction With Axial Compression. Field Required to Achieve $\bar{T}_f = 6$ keV at fill factor X_f with 7 Tesla Magnetic Field. Length Compression Factor = 3. X_1 = radial fill factor immediately after reconnection.

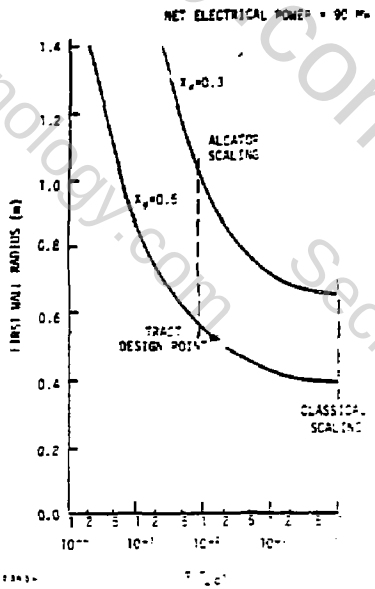

Figure 3. Reactor Size Scaling With Confinement Time. First Wall Radius Required to Achieve 90 MW Net Electrical Power. X_f = radial fill factor at ignition.

REFERENCE

1. A.G. Es'kov et al., "Features of Plasma Heating and Confinement in a Compact Toroidal Configuration," 7th IAEA Conf. on Plasma Physics and Controlled Thermonuclear Research, Innsbruck, 1978.

ACKNOWLEDGEMENT

This work was supported by the Electric Power Research Institute under Contract No. RP-922-4.

US-Japan Joint Symposium on Compact Toruses and Energetic Particle Injection

Attendees

Plasma Physics Group, Faculty of Science
Theoretical Research Center for Nuclear Fusion
Hiroshima University
Higashisenda-machi, Hiroshima, 730
JAPAN

Dr. S. Inoue

Institute of Plasma Physics
Nagoya University
Chikusa-ku, Nagoya, 464
JAPAN

Dr. K. Ikuta
Dr. A. Mohri
Dr. K. Narihara
Dr. Y. Tomita

College of Science and Technology
Nihon University
Chiyoda, Tokyo 101
JAPAN

Dr. Y. Nogi

- -

Bell Telephone Laboratories, Inc.
600 Mountain Avenue
Murray Hill, NJ 07974

Dr. H. Ikezi

Department of Physics
University of California at Irvine
Irvine, CA 92717

Dr. S. Robertson
Dr. N. Rostoker

Attendees

University of California, Los Angeles
Los Angeles, CA 90024

Dr. R. Taylor (Center for Plasma Physics and Fusion Engineering)

Plasma Physics Laboratory
Department of Applied Physics and Nuclear Engineering
Columbia University
New York, NY 10027

Dr. C. K. Chu

Laboratory of Plasma Studies
Cornell University, Upson Hall
Ithaca, NY 14853

Dr. H. Fleischmann (Department of Applied Physics)
Dr. B. Kusse (Department of Applied Physics)
Dr. J. Greenly
Dr. R. Sudan
Dr. A. Reiman

Office of Fusion Energy
Department of Energy
Washington, DC 20545

Dr. J. Clarke
Dr. W. Dove (Division of Applied Plasma Physics)
Dr. T. George
Dr. D. Thomson
Dr. W. Ellis

Grumman Aerospace Corporation
101 College Road, East
Princeton, NJ 08450

Dr. A. Todd

Electric Power Research Institute
3412 Hillview Avenue
Post Office Box 10412
Palo Alto, CA 94304

Dr. D. Paul
Dr. R. Scott

Attendees

General Atomic Company
Post Office Box 81608
San Diego, CA 92138

Dr. T. Ohkawa

Fusion Studies Laboratory
214 Nuclear Engineering Laboratory
University of Illinois
Urbana, IL 61801

Dr. G. Miley

Institute for Advanced Study
Princeton, NJ 08540

Dr. Y.-P. Ho
Dr. M. Rosenbluth
Dr. J. VanDam

Lawrence Livermore Laboratory
Post Office Box 808
Livermore, CA 94550

Dr. S. Auerback
Dr. H. Berk
Dr. G. Carlson
Dr. T. K. Fowler
Dr. J. Hammer
Dr. C. Hartman
Dr. R. Post
Dr. J. Shearer
Dr. W. Turner
Dr. D. Schnack
Dr. A. Shestakov
Dr. D. Anderson

Los Alamos Scientific Laboratory
Post Office Box 1663
Los Alamos, NM 87545

Dr. D. Baker
Dr. D. Barnes
Dr. T. Armstrong
Dr. T. Jarboe
Dr. R. Krakowski
Dr. W. Quinn
Dr. R. Linford
Dr. S. Ortolani
Dr. A. Sherwood
Dr. R. Siemon
Dr. L. Turner

Attendees

Department of Physics and Astronomy
University of Maryland
College Park, MD 20742

Dr. A. DeSilva
Dr. G. Goldenbaum
Dr. Z. An (Southwest Institute of Physics, People's Republic of China)

Department of Physics
Massachusetts Institute of Technology
Cambridge, MA 02139

Dr. A. Janos
Dr. D. Pappas

Mathematical Sciences Northwest, Inc.
Post Office Box 1887
Bellevue, WA 98009

Dr. P. Rose
Dr. L. Steinhauer
Dr. G. Vlases

Max-Planck Institut fur Plasmaphysik
D-8046 Garching
Federal Republic of Germany

Dr. G. Spies

University of Michigan
Department of Nuclear Engineering
145 Cooley Building
Ann Arbor, MI 48105

Dr. T. Kammash
Dr. W. Getty

Plasma Physics Division
Naval Research Laboratory
Washington, DC 20375

Dr. C. Kapetanakos
Dr. J. Finn
Dr. A. Robson
Dr. J. Sethian
Dr. P. Turchi (Code 6770)

Attendees

Jaycor, Inc.
205 South Whiting Street
Alexandria, VA 22015

Dr. E. Scannell

New York University
Courant Institute of Mathematical Sciences
251 Mercer Street
New York, NY 10012

Dr. W. Grossmann
Dr. G. Morikawa

Oak Ridge National Laboratory
Fusion Energy Division
Post Office Box Y
Oak Ridge, TN 37830

Dr. D. Sigmar

The Pennsylvani[illegible]
233 Hammond Bui[illegible]
University Park, [illegible]

Dr. E. Klevans
Dr. T. York

Physics International Company
2700 Merced Street
San Leandro, CA 94577

Dr. V. Bailey
Dr. B. Ecker
Dr. H. Helava

Department of Nuclear Engineering, Room 2524
Pacific Gas and Eelctric Company
77 Beal Street
San Francisco, CA 94106

Dr. A. C. Smith, Jr.

Attendees

Public Service Electric and Gas Company
60 Park Place
Newark, NJ 07101

Dr. B. Jensen

Plasma Physics Laboratory
Princeton University
Post Office Box 451
Princeton, NJ 08544

Dr. A. Boozer
Dr. H. Furth
Dr. M. Gottlieb
Dr. R. Jacobsen
Dr. J. L. Johnson
Dr. M. Katsurai
Dr. S. Jardin
Dr. M. Okabayashi
Dr. F. Perkins, Jr.
Dr. J. Sinnis
Dr. T. Stix
Dr. M. Yamada
Dr. K. Yamazaki
Dr. S. Yoshikawa

University of Washington
Seattle, WA 98195

Dr. F. Ribe
Dr. H. Meuth

Department of Physics
University of Miami
Coral Gables, FL 33134

Dr. D. Wells

Prometheus II, Ltd.
Post Office Box 22
College Park, MD 20740

Dr. P. Koloc
Dr. J. Ogden

Attendees

Society to Advance Fusion Energy
10 Normandy Lane
Scarsdale, NY 10583

Mrs. L. Slaner

Lawrence Berkeley Laboratory
Plasma Physics Program
Berkeley, CA 94720

Dr. B. Feinberg
Dr. M. Levine

Stevens Institute of Technology
Department of Physics
Castle Point Station
Hoboken, NJ 07030

Dr. M. Seidl